

UNIVERSITY OF OKLAHOMA
GRADUATE COLLEGE

DNA BARCODING IDENTIFICATION AND CHEMICAL INVESTIGATION OF
FUNGI

A DISSERTATION
SUBMITTED TO THE GRADUATE FACULTY
in partial fulfillment of the requirements for the
Degree of
DOCTOR OF PHILOSOPHY

By
WENTAO DAI
Norman, Oklahoma
2019

DNA BARCODING IDENTIFICATION AND CHEMICAL INVESTIGATION OF
FUNGI

A DISSERTATION APPROVED FOR THE
DEPARTMENT OF CHEMISTRY AND BIOCHEMISTRY

BY

Dr. Robert H. Cichewicz, Chair

Dr. Adam S. Duerfeldt

Dr. Anne K. Dunn

Dr. Robert L. White

Dr. Si Wu

Acknowledgements

There are many people I would like to acknowledge during the enjoyable and rewarding journey at the University of Oklahoma in the past 5 years. Firstly, I would like to thank my major advisor, Dr. Cichewicz, for giving me the opportunity to work in the natural products drug discovery group. I would never have been able to finish this dissertation without his guidance, advice, encouragement and support.

I would also like to thank my committee members Dr. White, Dr. Duerfeldt, Dr. Wu and Dr. Dunn for their intellectual advice and guidance on both of my research and coursework in the past five years. I would also like to acknowledge Dr. Najjar Fares for all his help for my research. I also want to extend my gratitude to the current and former members of Cichewicz lab: Jarrod, Vicky, Lin, Karen, Adam, Jianlan, Jin Woo, Shengxin, Camille, Andrew, Saikat, Bin, Guojian, Allison, Tiffney, Krysztof, Tylor and other workers in the lab. My research would not have been done without their advice and helps.

I would also like to acknowledge my best friend Yun-Seo Kil for her endless support and encouragement in the past three years. I would also like to thank my parents and sister for their supports and endless love. Finally, I would like to thank my husband Renxing and my lovely son Kevin, they were always there to cheer me up and stood by me through all the time.

Table of Contents

Table of Contents	v
List of Tables	ix
List of Figures	x
Chapter 1: Fungal Natural Products as a Unique Source for Drug Discovery	1
1.1 The importance of natural products in drug discovery	1
1.2 Fungal natural products in drug discovery	3
1.3 DNA barcoding as a tool for fungal identification.....	6
1.4 Fungi as a source of antiparasitic secondary metabolites	7
1.5 Meroterpenoids, selective acetylcholinesterase (AChE) inhibitors from fungi	9
1.6 Prospects for fungal natural product drug discovery	13
Chapter 2: Chapter Overviews.....	15
2.1 Hypothesis.....	15
2.2 Chapter 3. Enhancing Natural Product Discovery Using a Rumsfeldian Matrix to Gauge Fungal Isolate Novelty from DNA-Barcode Data	15
2.3 Chapter 4. Creation and Application of a High-Throughput High-Content Screening Assay for Natural Product Inhibitors of the Human Parasite <i>Trichomonas vaginalis</i>	16
2.4 Chapter 5. Cholinesterase Inhibitory Arisugacins L-Q from a <i>Penicillium</i> sp. Isolate Obtained through a Citizen Science Initiative and their Activities in a Phenotype-Based Zebrafish Assay.....	17
Chapter 3. Enhancing Natural Product Discovery Using a Rumsfeldian Matrix to Gauge Fungal Isolate Novelty from DNA-Barcode Data	18

3.1	Introduction	18
3.2	Results and Discussion.....	21
3.2.1	Conceptual Framework.....	21
3.2.1.1	Unknown Unknowns	23
3.2.1.2	Known-Knowns.....	24
3.2.1.3	Known Unknowns	25
3.2.1.4	Unknown Knowns	26
3.2.2	Sourcing Fungal Isolates through Citizen Science	26
3.2.3	Analyzing the Impact of Insufficiently Identified Fungal Barcodes, Single Direction ITS Region Reads, and Secondary Molecular Taxonomic Marker Gene Data on Generating Genus-Level Taxonomic Assignments	28
3.2.4	Examining the Secondary Metabolome Features in a Candidate Known- Unknown Fungus.....	31
3.3	Conclusion and Future Directions.....	42
3.4	Materials and Methods	42
3.4.1	General Experimental Procedures	42
3.4.2	DNA Extraction and Polymerase Chain Reaction (PCR)	43
3.4.3	Extraction and Isolation of new compounds from the fungus 74E10	44
3.4.4	Preparation of the (<i>S</i>) and (<i>R</i>)-MTPA Mosher Ester Derivatives.....	47
	of 3.11 and 3.12	47
Chapter 4: Creation and Application of a High-Throughput High-Content Screening Assay for Natural Product Inhibitors of the Human Parasite <i>Trichomonas vaginalis</i>		49
4.1	Introduction	49

4.2 Results and Discussion.....	51
4.2.1 Development of an Assay for Detecting <i>T. vaginalis</i> Inhibitors.....	51
4.2.2 Testing Purified Natural Products	54
4.2.3 Testing Fungal Natural Product Extracts	56
4.2.4 Bioassay-Guided Purification and Testing of Natural Products from the <i>Fusarium</i> sp. Isolate B.....	58
4.2.5 Biological Evaluation of Tetramic Acid Derivatives.....	66
4.3 Conclusion and Future Directions	67
4.4 Materials and Methods.....	69
4.4.1 General Experimental.....	69
4.4.2 Culture of Organisms.....	69
4.4.3 Trichomonas Assay	70
4.4.4 Mammalian Cell Cytotoxicity Assay	71
4.4.5 <i>Lactobacillus Acidophilus</i> Viability Assays.....	72
4.4.6 Tetramic Acid Producing Fungal Strains and Fermentation	72
4.4.7 Purification of Tetramic Acid Derivatives	73
4.4.8 Preparation of MTPA Ester	75
4.4.9 Cleavage of the Tetramic Acid Ring and Marfey's Reaction	75
Chapter 5. Cholinesterase Inhibitory Arisugacins L-Q from a <i>Penicillium</i> sp. Isolate Obtained through a Citizen Science Initiative and their Activities in a Phenotype-Based Zebrafish	77
5.1 Introduction.....	77
5.2 Results and Discussion.....	79

5.2.1 Zebrafish-Based Phenotype Screen of Fungal Crude Extract	79
5.2.2 Purification Natural Products from the <i>Penicillium sp.</i> Isolate	80
5.2.3 Testing of Natural Products from the <i>Penicillium sp.</i> Isolate.....	91
5.3 Conclusion and Future Directions.....	94
5.4 Materials and Method.....	96
5.4.1 General Experimental.....	96
5.4.2 Fungal Strain and Fermentation	96
5.4.3 Extraction and Isolation.....	97
5.4.4 Preparation of MTPA Esters.....	98
5.4.5 ECD Calculations of 5.13.....	99
5.4.6 Zebrafish maintenance.....	99
5.4.7 Zebrafish phenotype screen	100
5.4.8 <i>In situ</i> hybridization.....	100
5.4.9 Acetylcholinesterase and butyrylcholinesterase inhibition assays	100
References.....	102
Appendix A: Supporting Data for Chapter 3	115
Appendix Table of Contents	115
Appendix B: Supporting Data for Chapter 4	158
Appendix Table of Contents	158
Appendix C: Supporting Data for Chapter 5	172
Appendix Table of Contents	172
Abbreviations.....	206

List of Tables

Table 3.1. ^1H NMR (400 MHz) Data for Compounds 3.3-3.7	35
Table 3.2. ^{13}C NMR (100 MHz) Data for Compounds 3.1 and 3.3-3.7	36
Table 3.3. ^1H NMR (400 MHz) Data for Compounds 3.8-3.13 in MeOH- d_4	37
Table 3.4. ^{13}C NMR (100 MHz) Data for Compounds 3.2 and 3.8-3.13	38
Table 4.1. ^1H NMR data for compounds 4.4-7 in DMSO- d_6 (δ ppm).....	63
Table 4.2. ^{13}C NMR data for compounds 4.4-4.7 in DMSO- d_6 (100 MHz, δ ppm)	64
Table 4.3. Summary of tetramic acid derivatives: compound source, bioassay results and the corresponding selectivity index value.....	66
Table 5.1. ^1H NMR Data for Compounds 5.4, 5.5, 5.8, 5.12-5.14 (δ ppm).....	88
Table 5.2. ^{13}C NMR Data for Compounds 5.4, 5.5, 5.8, 5.12-5.14 (100 MHz, δ ppm)...	91
Table 5.3. Bioactivity of compounds 5.1-5.14	95

List of Figures

Figure 1.1. Secondary metabolites isolated from plants.....	2
Figure 1.2. Examples of drugs derived from fungi.....	4
Figure 1.3. Examples of secondary metabolites from fungi.....	5
Figure 1.4. Examples of drug for parasites infection.....	8
Figure 1.5. Antiparasitic secondary metabolites from fungi.....	9
Figure 1.6. Structures of territrems.....	11
Figure 1.7. Structures of arisugacins.....	12
Figure 1.8. Structures of terreulactones.....	13
Figure 3.1. Contextual framework of each isolate’s phylogenetic affinity.....	23
Figure 3.2. Map of soil samples received from citizen scientists by the University of Oklahoma Citizen Science Soil Collection Program.....	28
Figure 3.3. Quality control metrics for fungal ITS barcode data associated with the University of Oklahoma Citizen Science Soil Collection Program. Distribution of (A) ITS barcode length and (B) phred scores for sequences in the collection.....	30
Figure 3.4. Structures of fungal metabolites 3.1-3.13	32
Figure 3.5. Key ^1H - ^1H COSY, ^1H - ^{13}C HMBC correlations for compounds 3.1. 3.3-3.7	34
Figure 3.6. Key ^1H - ^1H COSY, ^1H - ^{13}C HMBC correlations for compounds 3.8-3.13	39
Figure 3.7. Key ROESY correlations for compounds 3.8-3.13	40
Figure 3.8. ECD spectra of compounds 3.2 and 3.8-3.13	41
Figure 3.9. Analysis of modified Mosher’s method for 3.11 and 3.12 . $\Delta\delta$ ($\delta_S - \delta_R$) values are shown.....	41

Figure 4.1. A comparison of the traditional resazurin fluorescence assay (red squares) and the newly developed imaging-based assay (green triangles). Using two fields per well, the Operetta’s limit of detection was 1,000 trichomonades per well. The limit of detection is bounded on the lower end by whether a trichomonad appears in an image field. Resazurin assay was unable to detect less than 10,000 organisms per well. 52

Figure 4.2. **A.** Sample field from the Operetta of a fixed and stained (0.5% glutaraldehyde, 2.5 μ M propidium iodide, and 2.5 μ M acridine orange) healthy growing population of trichomonas vaginalis at 17hr. One dead (red) trichomonad can be seen. **B.** Sample screening image from the Operetta showing partial inhibition from a fungal extract at 17hr. 54

Figure 4.3. Nine of 430 pure natural products evaluated for SI_{3T3} values in initial pure compound screening against *T. vaginalis*. Compound sources were diverse and are shown under the compound names. EC_{50} values were determined in *T. vaginalis* and 3T3 mammalian cells to obtain the SI_{3T3} values shown. Notably, 2-bromoascididemin exhibited a SI_{3T3} value of 14.0, which was much higher than any of the other compounds tested. 56

Figure 4.4. Selectivity index of 71 fungal crude extract library hits with activity better than 25 μ M metronidazole..... 58

Figure 4.5. Structures of compounds 4.1-4.9 59

Figure 4.6. **A:** 1H - 1H COSY, HMBC and ROESY correlations of compounds 4.5. **B:** 1H - 1H COSY, HMBC and ROESY correlations of compounds 4.7..... 61

Figure 4.7. CD Spectra of compound 4.5 and 4.7..... 62

Figure 4.8. $\Delta\delta_{S-R}$ values obtained in pyridine- d_5 of the MTPA ester of compound 4.5 .	65
Figure 4.9. Effect of beauversetin on the growth of <i>Trichomonas vaginalis</i> in atmospheres of differing oxygen levels. Numbers shown are calculated from two fields in each well, three replicate wells per condition.....	65
Figure 4.10. Effect of lead compounds from different classes and metronidazole on the growth of <i>Lactobacillus acidophilus</i> grown in an anaerobic atmosphere for 18hr. the tetramic acid beauversetin has no off-target effects, like metronidazole.	67
Figure 5.1. Zebrafish phenotype screen reveals bioactive fungal samples. A. Distribution of assay outcomes from screening of fungal extracts. B. Examples of phenotypes observed include growth arrest (1-3), edema (black arrow), abnormal head (green arrow) and tail (blue arrow) development and undulated notochord (red arrow).	80
Figure 5.2. Zebrafish phenotype screen reveals fungal extracts that impaired motility. Morphological phenotype exhibited by crude extract and representative subfractions that impaired motility comparable to phenotype resulting from treatment with known AChE inhibitor, AZM (1 st , 3 rd panels). DMSO served as negative control. Traces summarizing movement of zebrafish embryos (black dot) in response to external stimulus (represented by a blue line) are shown in panels 2 and 4.	81
Figure 5.3. Structures of compounds 5.1-5.14	82
Figure 5.4. 1H - 1H COSY (blue bold lines) and key HMBC (red arrows) correlations of compounds 5.4-5.5, 5.8, 5.12-5.14	83
Figure 5.5. 3D molecular models of compounds 5.4-5.5, 5.8, 5.12-5.13 showing key ROESY correlations (blue dashed arrows).....	85

Figure 5.6. $\Delta\delta_{S-R}$ values obtained in pyridine- d_5 of the MTPA ester of compounds 5.4 , 5.5 , and 5.12 .	86
Figure 5.7. Comparison of the experimental and calculated ECD spectra of 5.13 .	89
Figure 5.8. 3D molecular models of compound 5.14 showing key ROESY correlations (blue dashed arrows).	90
Figure 5.9. Novel arisugacin compounds show acetylcholinesterase inhibitory activity. A. Phenotypes of 72 hpf embryos that exhibited impaired motility with early compound treatment. B. In situ hybridization for myotome marker, xirp2a (xin actin binding repeat containing 2a), in 72 hpf embryos. Boxed figure is enlargement of the trunk to emphasize abnormalities in myotome (black arrow) structure. C. IC_{50} of new arisugacin analogs were obtained in an in vitro AChE inhibition assay.	92
Figure 5.10. Bioactivity of known arisugacin compounds with no previously reported AChE bioactivity. A. Phenotypes of 72 hpf embryos that exhibited impaired motility with early compound treatment. B. In situ hybridization for xirp2a in 72 hpf embryos. Boxed figure is enlargement of the trunk to emphasize abnormalities in myotome (black arrow) structure. C. IC_{50} of arisugacins C, G and I were obtained in an in vitro AChE inhibition assay.	93

Abstract

Fungi represent a diverse resource in the discovery of new secondary metabolites which have been successfully developed as drugs such as antibiotics, immunosuppressant and stains. However, there are still problems which could potentially restrain the development of fungal natural products drug discovery, such as the confusing taxonomy annotation in NCBI, the deficiency of high capacity screening platforms as well as application of well recognized screening models, and the limited therapeutic diversity. With the aim to discover new fungal secondary metabolites, one efficient approach is to access new biodiversity. In this dissertation, we report the application of this approach in three chapters.

The kingdom Fungi is comprised of highly diverse taxa with an estimated of 2.2 - 3.8 million species on earth, of which only 5% have been described. Morphological characterization and DNA barcoding have served as the major strategies in fungal identification, with the latter considered as the universal tool. One of the growing problems of using DNA barcode data to identify fungi centers on the increasing number of GenBank sequence accessions that fall into the category of “insufficiently identified”. This has important implications for natural product chemical discovery since it is presumed that chemically unexplored fungal species are more likely to serve as sources of new natural products as opposed to well-known organisms whose secondary metabolomes have been thoroughly investigated. In this chapter, we propose a schema for using ITS barcode data to mine GenBank and identify high priority fungal isolates as potential sources of new natural products. In addition, we conducted a chemical analysis

of one high-priority fungal isolate demonstrating that most of its major metabolites were previously unreported natural products.

The sexually transmitted parasite *Trichomonas vaginalis* infects at least 170 million people worldwide and infections are treated with the lone compound metronidazole, a suspected human carcinogen. Reports of resistance to the drug are increasing. Thus, new drug leads are needed with which to treat this and other anaerobic parasites. An assay was developed in order to quantify the growth, viability, and morphology of the *Trichomonas* organism, using the Perkin Elmer Operetta imaging platform. A counter-screen for toxicity was also developed using the normal human cervical cell line Ect1/E6E7 and the Operetta. Screening of a library of 430 pure compounds yielded compounds with selectivity indices (SI) as high as 14. Further screening of our fungal crude extract library and bioassay-guided isolation revealed many promising leads for potent anti-*Trichomonas* compounds that remain safe to human cells. The tetramic acid derivatives rose to the forefront, such as beauversetin (SI = 40), equisetin (SI = 20), and pyrrolocin A (SI = 167). Manipulation of oxygen levels revealed that beauversetin retained activity. An additional test against *Lactobacillus acidophilus*, a beneficial natural flora organism found in the genital tract, was used as a counterscreen. Growth in an anaerobic atmosphere revealed that tetramic acid derivatives like pyrrolocin A behaved like metronidazole and did not disrupt the growth of *L. acidophilus*.

Lastly, zebrafish has been utilized as a model organism for chemical screening to discover novel bioactive compounds. Phenotype-based zebrafish screening of a fungal crude extract library yielded an active fungal extract from a *Penicillium sp.* isolate. Bioassay-guided and chemistry-guided purification led to the identification of fourteen

meroterpenoids including six new and seven known arisugacins and one known terrulactone. Their structures were determined using a combination of NMR and HRESIMS data, as well as the theoretical and experimental ECD spectra, and modified Mosher's method. The purified compounds were tested in zebrafish embryos as well as *in vitro* for acetylcholinesterase inhibition activity. Compound **5.12** produced defects in myotome structure (metameric muscle which is critical for locomotion) *in vivo* and showed the most potent activity with an IC_{50} of 191 nM *in vitro*. This study demonstrates the utility of using zebrafish bioassay-guided sample purification as an effective strategy to rapidly identify bioactive small molecules with therapeutic applications.

Chapter 1: Fungal Natural Products as a Unique Source for Drug

Discovery

1.1 The importance of natural products in drug discovery

Nature has been a source of medicinal metabolites for thousands of years. The history of treatment of disease with natural products (secondary metabolites) can be dated as early as 2600 BC in Mesopotamia. Other civilizations such as Egyptian, Chinese, Indian and Greek also contributed substantially to the development of natural products for the treatment of a variety of diseases.¹⁻²

In addition to the long history of usage, the diverse sources of natural products make natural products even more important in drug discovery. Natural products have been isolated from plants, microorganisms, marine organisms, vertebrates and invertebrates.³⁻⁵ There is no doubt that plants and microorganisms are the major sources. Out of approximately 1 million natural products, 60% are plant derived, and most of the remaining 40% are from microbes.⁶ As early as 2600 BC, the use of plant derived substances as medicine had been documented, while 700 drugs (most were plant origin) were known to be used in Egypt as well as the traditional medicine in China, India and so on.¹⁻² Modern natural products and natural products chemistry began with the isolation of plant derived metabolite morphine in 1803.⁷ This discovery was followed by the isolation of other active metabolites from plants, such as emetine,⁸ strychnine,⁹ atropin,¹⁰ reserpine,¹¹ artemisinin¹² and the most widely used breast cancer drug paclitaxel¹³ (Figure 1.1). Microbial modern natural product was initiated by the discovery of penicillin from fungus *Penicillium notatum* in 1929.¹⁴ Following this discovery, more antibiotics were isolated from microorganisms, such as tetracycline in 1945,¹⁵ chloramphenicol in 1947,¹⁶

and vancomycin in 1953¹⁷. These discoveries played an essential role in saving human life as well as promoting the development of microbial natural products chemistry. In addition to plants and microorganisms, significant contributions to natural products also came from animals and marine organisms. Two successful stories are metabolites teprotide and ω -conotoxin, the former was isolated from snake and used as lead compound for the development of antihypertension drug captopril, the latter was a marine derived metabolite and used to relieve severe and chronic pain.¹⁸⁻¹⁹

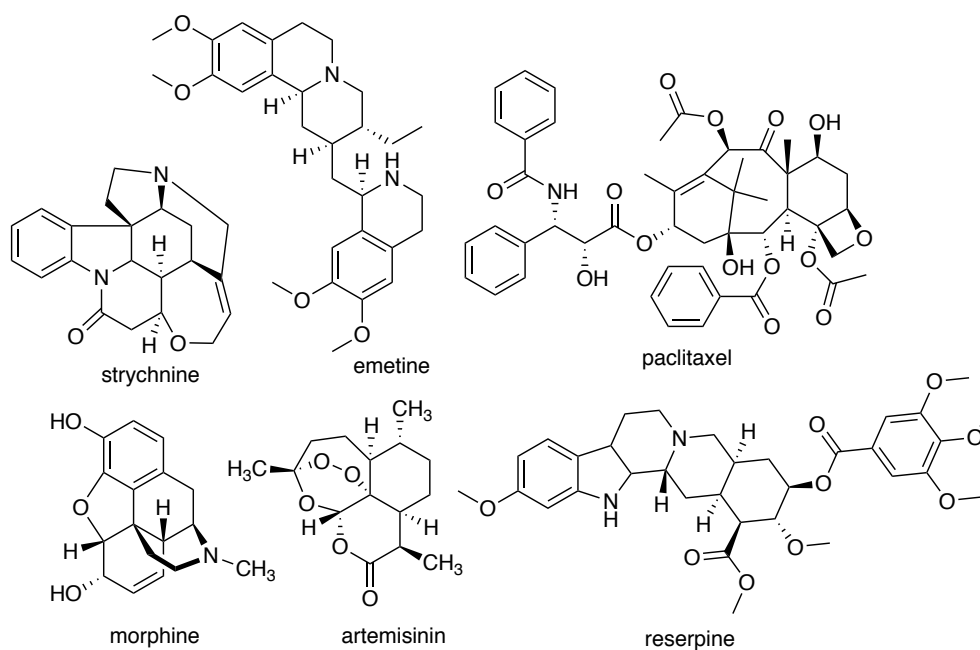


Figure 1.1. Secondary metabolites isolated from plants.

What is more, the excellent chemical diversity and the “naturally active” features of natural products also inspired the discovery of new drugs and drug leads, which led to a complementary approach to synthetic chemistry.²⁰ Diversity-oriented synthesis is a successful strategy for increasing skeletal diversity starting with an active natural

products. Additionally, total synthesis was also applied to natural products for assisting structure elucidation and identification of pharmacophores (e.g., halichondrin).^{2,21}

Between the 1940s to the end of 2014, 49% of the 175 molecules approved anticancer drugs were either natural products or natural product derivatives.²² Among the 74 antihypertensive drugs, approximately 65% were natural products.⁶ A recent review published in *Journal of Natural Products* summarized the percentage of natural products in approved new drugs over the period 1981 to 2014, it showed that 20~50% of new drugs were natural products or natural product based.²² These data support the position that nature has been and will continue to be a major source for drug discovery.

1.2 Fungal natural products in drug discovery

The fungal kingdom is a well-known and valuable source of potential therapeutic compounds. Of the 23,000 microbial derived active metabolites, 42% were from fungi.⁶ The discovery of penicillin was the beginning of fungal natural products,¹⁴ and since then there was a worldwide effort to discover antibiotics from fungi. The β -lactams were one of the successful discoveries, which includes penicillins, cephalosporins, monobactams and carbapenems.²³ Among these antibiotics, mainly penicillins (e.g., amoxicillin, ampicillin), and cephalosporins (e.g., cefalotin, cefuroxime) (Figure 1.2), represented approximately 65% of the world antibiotic market.²⁴ In addition to the outstanding discovery of antibiotics, fungal natural products gained fame for their use as immune-suppressive (e.g., cyclosporine A²⁵), and antifungal agents (e.g., griseofulvin,²⁶ echinocandins²⁷) (Figure 1.2) as well as agricultural fungicides (e.g., strobilurins²⁸).

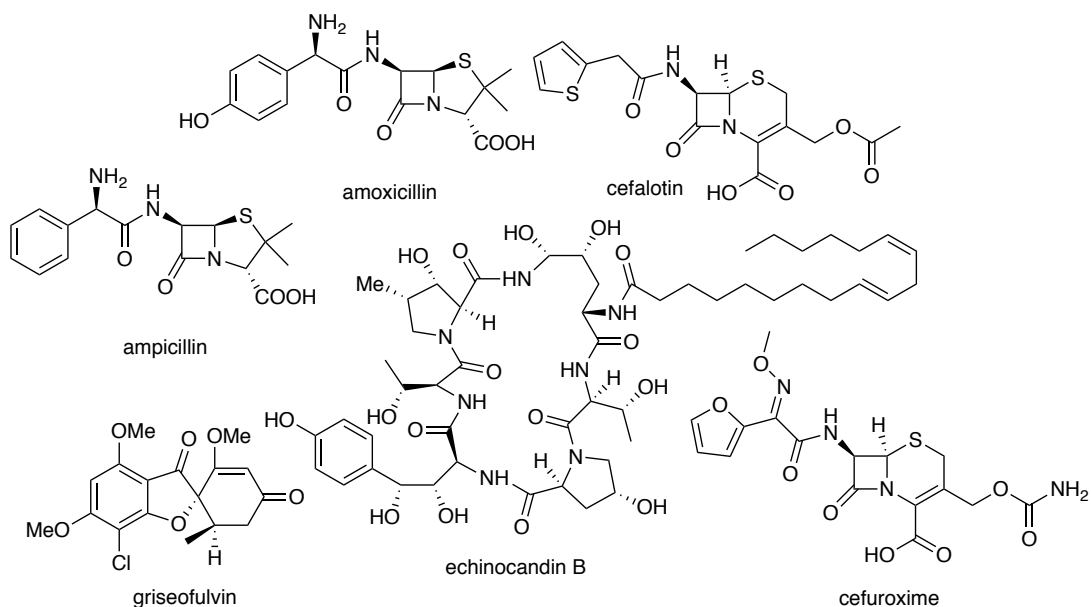


Figure 1.2. Examples of drugs derived from fungi.

Although to date no fungal natural products have been used as anti-cancer drugs clinically, plenty of compounds with documented anticancer activities are being studied and have promise to be potential cancer treatments. For example, fusarisetin A, isolated from *Fusarium* sp., is a potent cancer migration inhibitor for different types of cancer,²⁹⁻³⁰ and ophiobolin A is a potent inducer of glioblastoma cell death by induction of paraptosis (Figure 1.3).³¹ The indole alkaloidal fungal metabolite tryprostatin A isolated from *Aspergillus fumigatus*, is an inhibitor of mitogen activated protein kinase dependent microtubule assembly which leads promoter the cell progression at the mitotic phase,³² and peribysin A is a cell-adhesion inhibitors (Figure 1.3)³³. Fungal natural products have also been investigated for other medical purposes, such as the anti-malarial metabolites pycnidione³⁴ and codinaeopsin,³⁵ anti-tuberculosis compound trichoderin A³⁶ (Figure 1.3).

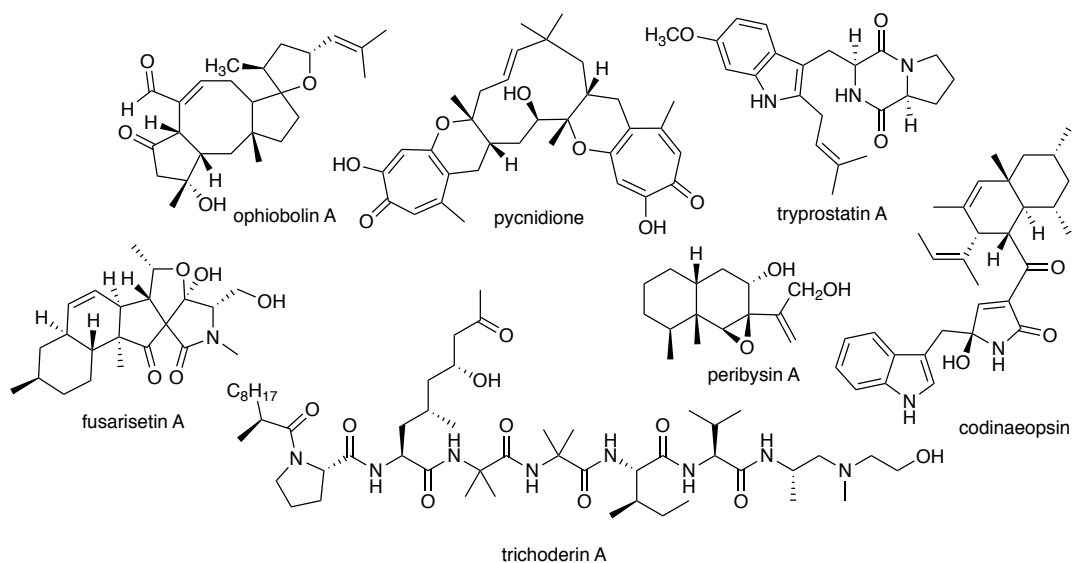


Figure 1.3. Examples of secondary metabolites from fungi.

Besides these chemically and functionally diverse fungal natural products, the extent of fungal diversity is even more remarkable. The fungal kingdom is comprised an estimation of 2.2 to 3.8 million species on earth.³⁷ However, only 5% have been identified so far (16% of them have been cultured) leaving a wide field of potential producers of novel metabolites producers.^{6, 38-39} In addition, the application of synthetic biology to fungal natural products such as manipulating the natural products regulatory gene clusters, heterologous expression and engineering of the biosynthetic enzyme opened another field for novel metabolites production.⁴⁰ The successfully stories include the production of novel metabolite aspyridones by expressing the pathway specific regulator to switch on a silent fungal pathway, the novel dipeptides by co-expressing of non-ribosomal synthetase and prenyltransferase genes in *Aspergillus*.⁴¹⁻⁴²

As the need for new drugs and drug leads is still growing, natural products will continue to be a great source for drug discovery and chemical inspiration. Combining the chemical, functional diversity, the large number of fungal species, and the small fraction

of investigated species with the application of synthetic biology, fungal natural products will continue to play a substantial role in natural products drug discovery for many years to come.

1.3 DNA barcoding as a tool for fungal identification

Traditionally, fungal identification solely relied on the observation of morphological characteristics, such as the fruiting bodies and structures of spore.⁴³ However, the phenotypic approach is not applicable to some cases, including non-sporulation and asexual fungi, high speciose fungi as well as uncultured fungi.⁴⁴⁻⁴⁷ Therefore, alternatives to morphological analyses have been under consideration for a long time. Consequently, a more applicable tool, DNA sequence based approaches have emerged.

DNA sequence based approach, also called DNA barcoding, compares query sequences against sequence database and identify fungi based on sequence similarity. The most commonly used barcodes are the large subunit, small subunit and internal transcribed spacer regions (ITS).⁴⁸ The large subunit evolves slowest and can be used for higher level identification, such as family, order and class, while the ITS region possessing the highest variation and is the most useful barcode for genus and species identification.⁴⁸⁻⁴⁹ In addition, it was found that ITS region have a more than 90% PCR amplification fidelity, about 70% possibility of correct identification as well as the suitable barcode gap, which led it to be the official barcode for fungal identification.⁵⁰⁻⁵¹ However, the ITS region also has limitations and it does not work well for certain genera due to their narrow barcode gaps, such as *Aspergillus* and *Penicillium*.⁵²⁻⁵³ One solution

to this problem is the combination of the ITS region with other protein coding genes. The most commonly used genes are the largest subunit of RNA polymerase (*RPB1*) and second largest subunit of RNA polymerase (*RPB2*),⁵⁴ β -tubulin (*tub2/BenA*)⁵⁵ and the translation elongation factor 1- α (*tef1*)⁵⁶. Among these genes, *tub2/BenA* was recommended as the secondary barcode for *Penicillium* sp.,⁵⁷ while the *tef1* gene was found to have promise to be the universal secondary barcode for fungal identification.⁵⁸ In addition to the aforementioned genes, the mini-chromosome maintenance protein (*MCM7*)⁵⁹ and the partial calmodulin (*CaM*) genes have also showed promise as new barcode markers for fungal identification and was recommended as the secondary barcode for *Aspergillus* sp.⁶⁰

1.4 Fungi as a source of antiparasitic secondary metabolites

Infectious disease caused by parasites is one major threat to human health and causes several million deaths every year.⁶¹ Although most parasites just cause severe discomfort instead of killing the hosts, there are still many deadly parasite infections such as malaria, trypanosomiasis and leishmaniasis.⁶¹ Very few vaccinations have been developed for parasite infections, and many infections still cannot be controlled by currently available treatments.⁶²⁻⁶³ However, most of these drugs have strong side effects (e.g., amphotericin B,⁶⁴ metronidazole,⁶⁵ benznidazole⁶⁶) and in some cases, parasites have already gained resistance (e.g., chloroquine,⁶⁷ sulfadoxine⁶⁸) (Figure 1.4). Moreover, some patients give up on treatments due to the side effects and high cost, which aids in spreading the infections.⁶³ The development of new drugs is needed urgently. But the fact is that investment in antiparasitic drug development is risky for pharmaceutical

companies because parasite infections usually occur in poor countries such as Latin America, Asia and Africa, where many drugs remain unaffordable.⁶³ In addition, parasites share physiological similarity with hosts which makes it hard to develop drugs that are both effective and non-toxic to human.

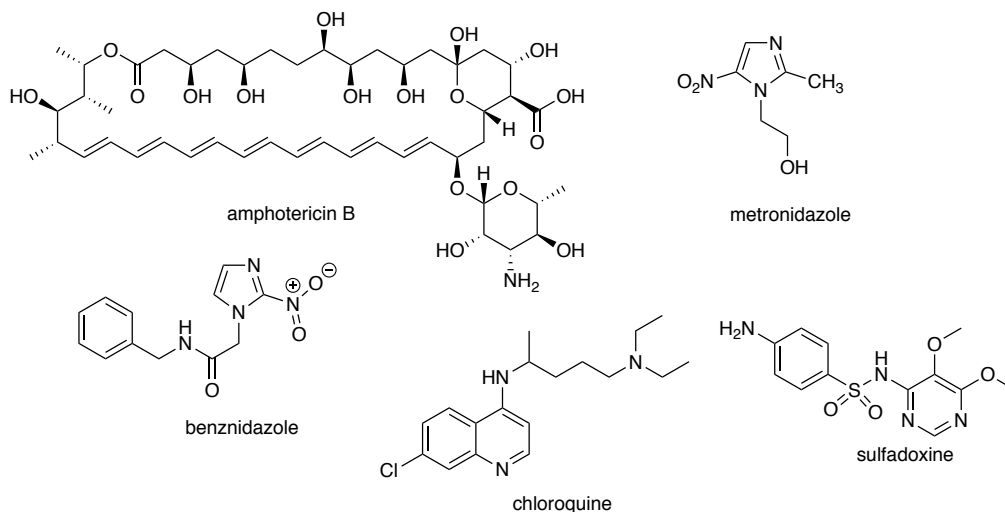


Figure 1.4. Examples of drug for parasites infection.

Fungal secondary metabolites have been an excellent source for treatments of a variety of disease, and some fungi have been used as traditional medicine to treat parasite infections (e.g., the Indian mushroom *Autraeus hygrometricus* is used to treat leishmaniosis). Studies aiming at finding new therapeutics from fungi have been done, and some anti-parasitic secondary metabolites including terpenes (e.g., aurisin A and K,⁶⁹ hypnophilin,⁷⁰ astrakurkurone⁷¹), steroids,⁷² alkaloids (e.g., eurochevalierine,⁷³ hirsutellone F⁷⁴), coumarins,⁷⁵ proteins,⁷⁶ and peptides (e.g., beauvericin,⁷⁷ hirsutellinic acid A⁷⁸) have shown promising activities against various parasites (Figure 1.5). However, considering all the successfully stories for fungal natural products drug

discovery, the diversity of fungal sources as well as the secondary metabolites they produce, these are only the tip of the iceberg. Fungi will be a promising source for anti-parasitic drug discovery, especially with the assistance of the high throughput screening strategy which allows more rapid and efficient identification process.⁷⁹

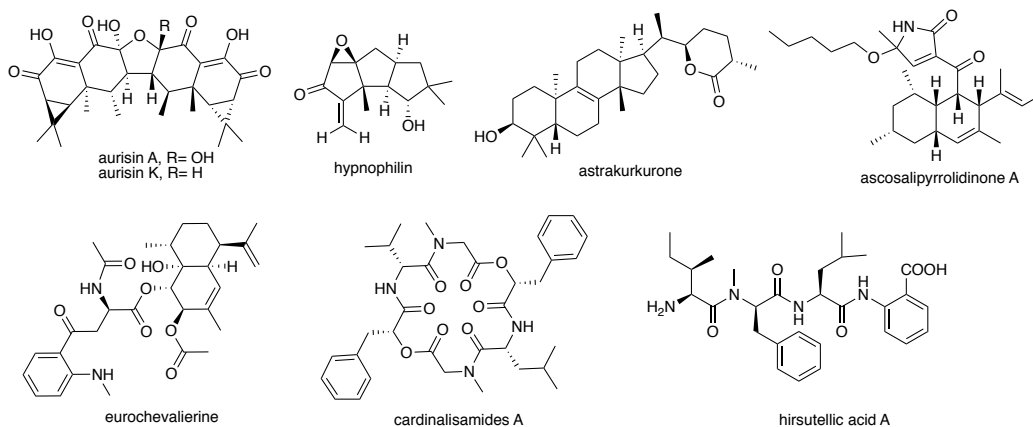


Figure 1.5. Antiparasitic secondary metabolites from fungi.

1.5 Meroterpenoids, selective acetylcholinesterase (AChE) inhibitors from fungi

Meroterpenoids, with diverse structures and important bioactivities, are a class of hybrid natural products that are biosynthetically partially derived in part from terpenoids. They are most often isolated from fungi, and marine organisms, but there are also examples of meroterpenoids isolated from plants, such as tetrahydrocannabinol, isolated from cannabis, and bakuchiol which was isolated from *Psoralea glandulosa* L.⁸⁰ Territrems, arisugacins and terrulactones, mostly containing α -pyrone and triketide-terpenoid, are meroterpenoids that were all isolated from fungi and all showed selective inhibition against AChE with varied potency. AChE is an enzyme which plays a key role in the hydrolysis of the neurotransmitter acetyl choline, and inhibition of AChE has been

reported as a strategy for the treatment of Alzheimer's disease (AD),⁸¹⁻⁸² Parkinson's disease,⁸³ myasthenia gravis,⁸⁴ glaucoma⁸⁵. For examples, there are five medications currently used for AD treatment, four are AChE inhibitors.

The first two compounds in this group (territrem A and territrem B (Figure 1.6), isolated from *Aspergillus terreus* by Ling in 1979, and were found to be the first two tremorgens without nitrogen.⁸⁶ In 1984, the same group reported the isolation of a new analog territrem C (Figure 1.6), which was also a tremorgenic mycotoxin.⁸⁷ Their structures were confirmed by 1D and 2D NMR.⁸⁸ Territrem B was incubated with rat liver microsomes which led to the production of four products MB₁~MB₄, and MB₄ was identical to territrem C.⁸⁹⁻⁹⁰ The inhibition of acetylcholinesterase (AChE) activity of territrem A and territrem B were discovered in 1992,⁹¹ followed by Omura's work that showed they were highly selective AChE inhibitor compared with butyrylcholinesterase (BuChE), with the IC₅₀ in nM range.⁹² Ling's group reported the isolation of territrem A' and territrem B' (Figure 1.6), the structure of territrem B' was confirmed by single crystal x-ray diffractometry, the tremorgenic activity and inhibition effect on AChE of these two molecules were greatly reduced compared to territrem A and territrem B which indicated that the α , β -unsaturated carbonyl is important in the AChE inhibitive activity.⁹³ In order to investigate the structure-activity relationship (SAR) in anti-AChE assay, Peng modified the structure of territrem B by epoxidation and saturation of the C-2 double bond, breaking the pyrone moiety, reduction of C-1 carbonyl and conversion of 4 β -CH₂OH into more hydrophobic and bulky group, to yield five derivatives.⁹⁴ And Peng's study indicated that both the enone and the pyrone moieties play important role in inhibitory activity of AChE.⁹⁴ In 2014, another group reported the

isolation of territrems D and territrems E (Figure 1.6), which also showed strong activity against AChE.⁹⁵

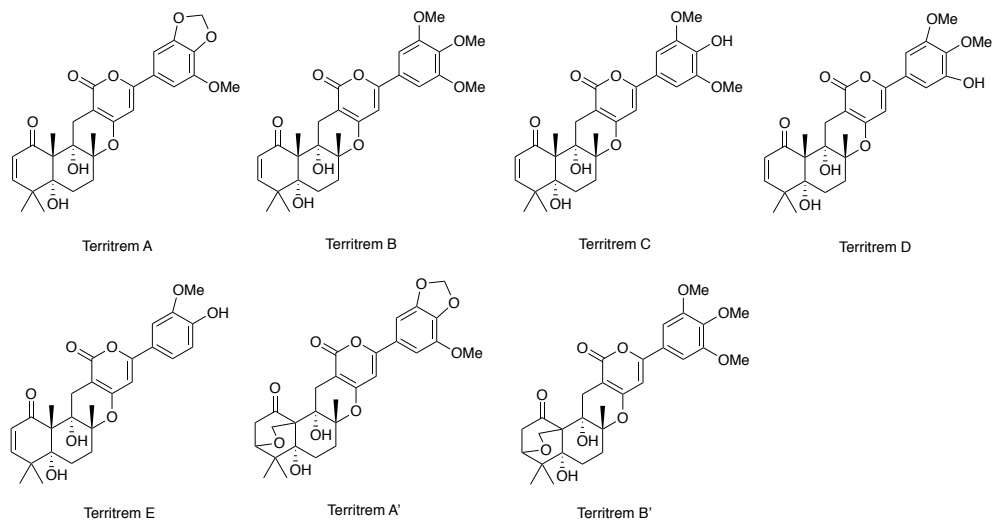


Figure 1.6. Structures of territrems.

Arisugacin (Figure 1.7) was isolated from *Penicillium sp.* FO-4259 together with structurally related compounds territrems B and C, and arisugacin showed even stronger selectivity inhibition of AChE than territrems.⁹² One year later, the same group isolated two more analogs, arisugacin A and B (Figure 1.7) from the same fungal species, and they both showed strong AChE inhibitive activity with arisugacin B slightly less potent.⁹⁶⁻⁹⁷ Fungal strain FO-4259 was treated with UV-light to yield a mutant strain, which lead to the isolation of arisugacin C~H,⁹⁸ the absolute configuration of arisugacin F (Figure 1.7) was determined later by modified Mosher method.⁹⁹ To determine the absolute configuration of arisugacin A and B, Sunazuka did total synthesis of these two molecules, twelve intermediates were evaluated the inhibitory activities against AChE to better understand the SAR of arisugacins, they concluded the α , β -unsaturated carbonyl,

12a-hydroxy group and the E ring substituents were essential for the inhibition of AChE by arisugacins.¹⁰⁰ Sun reported the isolation of arisugacin I and J from fungus *Penicillium sp.* SXH-65, with arisugacin I (Figure 1.7) being the first arisugacins with a linear sesquiterpenoid moiety.¹⁰¹ The cytotoxicity against HL-60, K562 and HeLa cells of arisugacins I and J were tested, both of them did not show any activity.¹⁰¹ Arisugacin K, an epimer of arisugacin E, was isolated by Li from an endophytic fungus *Penicillium echinulatum*, and showed inhibitory activity against *Escherichia coli*.¹⁰² These compounds have not been tested for AChE inhibition.

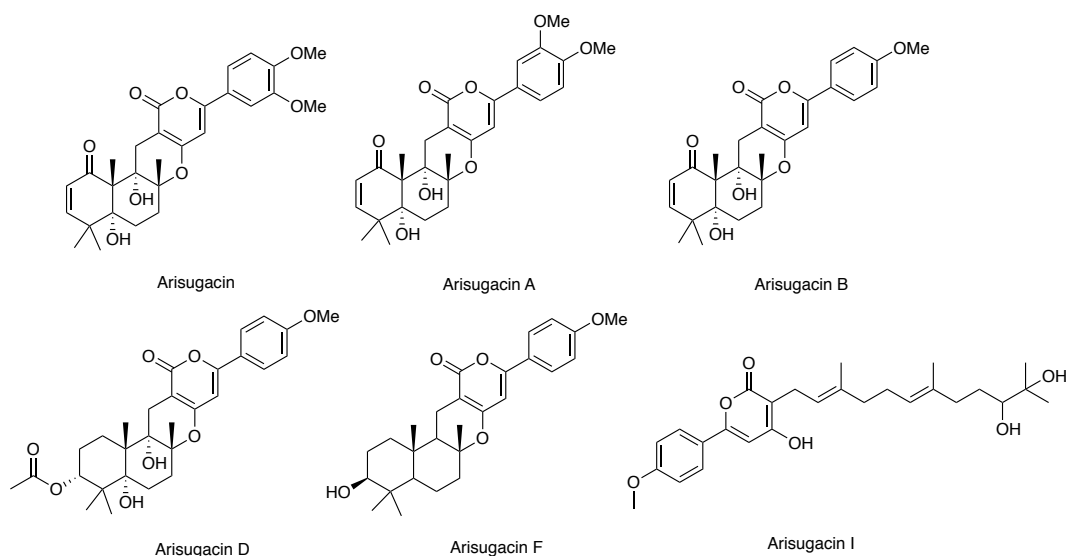


Figure 1.7. Structures of arisugacins.

Terreulactones A~D (Figure 1.8), structurally related compounds to territremes and arisugacins, were isolated from *Aspergillus terreus*.¹⁰³ They showed potent inhibitory activities against AChE with IC_{50} values in range of 0.06-0.42 μ M.¹⁰⁴ Seven-membered lactone type meroterpenoid, isoterreulactone A¹⁰⁵ and 11a-dehydroxyisoterreulactone A⁹⁵ were isolated by Yoo and Nong. The inhibition against AChE of isoterreulactone A

(Figure 1.8) was ten time weaker than terreulactone A, while 11a-dehydroxyisoterreulactone did not show any activity, which was in agreement with previous conclusion that α , β -unsaturated carbonyl and the 11a-OH group are important in the AChE inhibition activity.^{95, 105}

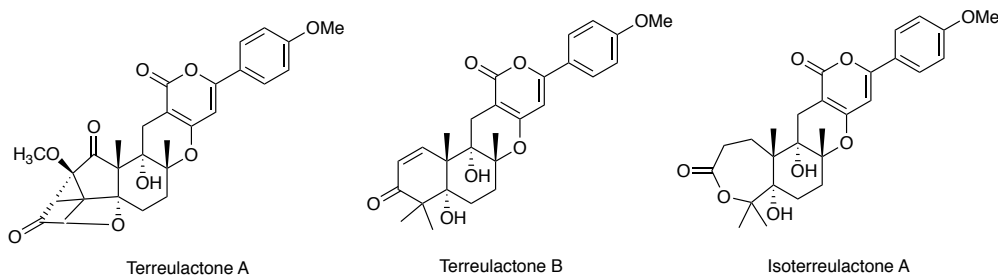


Figure 1.8. Structures of terreulactones.

1.6 Prospects for fungal natural product drug discovery

In the past decade, many pharmaceutical companies have cut down or even abandoned their drug discovery research from natural sources due to their discovery model (quickly and profitably), and the difficulties in discovering drug candidates from natural sources.¹⁰⁶ On the contrary, they shifted to high-throughput screening of synthetic libraries.¹⁰⁷ This led to the declined of new drugs approvals.¹⁰⁶ Despite that, there are still 35% of approved drugs are nature products based.²² In addition, there are enormous natural resources that have not been explored, more than 85% of higher plant species,¹⁰⁸ 99% of bacteria¹⁰⁹ and 95% of fungi⁶. With the development of rapid genome sequencing, culture techniques as well as the development of high-throughput screening, more of these untapped sources will be explored. Moreover, the identification process of natural product drug discovery will be expedited by the development of the analytical techniques

in separation and structure elucidation. What's more, synthetic biology offers a good opportunity for novel natural products discovery. Thus, I believe that natural product drug discovery will continue play a key role in drug discovery.

Chapter 2: Chapter Overviews

2.1 Hypothesis

Estimates of fungal diversity reveals there are more unexplored fungi than those that have been investigated. In addition, fungal derived drugs are currently used in limited therapeutic areas including antibiotics, immunosuppressant, and cholesterol lowering agents. With the aim of discovering new fungal natural products for drug discovery, the hypothesis guiding my research was: **accessing new fungal biodiversity is critical for identifying new bioactive secondary metabolites**. This hypothesis was tested via the following specific aims:

1. Identification of candidate known-unknown fungal isolates (Genbank) from insufficiently described fungi, and the isolation of new compounds from a previously undescribed fungus.
2. Development of a high-throughput high-content screening assay for the human parasite *Trichomonas vaginalis*, discovery of tetramic acid derivatives as potent anti-trichomonas fungal metabolites and the isolation of tetramic acid derivatives.
3. Isolation of new meroterpenoids from a *Penicillium* sp. in the course of phenotype-based zebrafish screening.

2.2 Chapter 3. Enhancing Natural Product Discovery Using a Rumsfeldian Matrix to Gauge Fungal Isolate Novelty from DNA-Barcode Data

The kingdom Fungi is comprised of highly diverse taxa with an estimated of 2.2 - 3.8 million species on earth, of which only 5% have been described so far. Morphological characterization and DNA barcoding have served as the major strategies in fungal

identification, with the latter considered as the universal tool. However, the DNA barcoding approach also suffers from certain weakness. One of the growing problems of is that more and more GenBank sequences accessions fall into the category of “insufficiently identified”. This has important implications for natural product chemical discovery since it is presumed that chemically unexplored fungal species are more likely to serve as sources of new natural products. In this chapter, we propose a schema for using ITS barcode data to mine GenBank and identify high priority fungal isolates as potential sources of new natural products. In addition, we conducted a chemical analysis of one high-priority fungal isolate demonstrating that most of its major metabolites were previously unreported natural products.

2.3 Chapter 4. Creation and Application of a High-Throughput High-Content Screening Assay for Natural Product Inhibitors of the Human Parasite *Trichomonas vaginalis*

In this chapter, a high-throughput high-content screening assay for the human parasite *Trichomonas vaginalis* along with a counter-screen for mammalian cell toxicity using the normal human cervical cell line Ect1/E6E7 were developed. Bioassay-guided purification of one active fungal isolate led to the discovery of a class of molecules, tetramic acid derivatives, which showed potency in the anti-trichomonas assay. This included the natural products equisetin (4.1), pyrrolocin A (4.4), and beauversetin (4.6), which showed tremendous promise as novel chemical leads. The isolation and structure elucidation of these compounds are discussed.

2.4 Chapter 5. Cholinesterase Inhibitory Arisugacins L-Q from a *Penicillium* sp. Isolate Obtained through a Citizen Science Initiative and their Activities in a Phenotype-Based Zebrafish Assay

This chapter explores the use of a phenotype-based zebrafish assay for screening our fungal crude extract library. In addition, we report the isolation and structure elucidation of new compounds, as well as describe their acetylcholinesterase inhibitory activities. In the course of phenotype-based zebrafish screening of fungal crude extract library, one sample was found to impair zebrafish motility. Bioassay-guided purification led to the identification of 14 meroterpenoids including 6 new metabolites, arisugacins L-Q, 7 known arisugacins and 1 known terreulactone. Their structures were elucidated using a combination of NMR and HRESIMS data as well as the theoretical and experimental ECD spectra and modified Mosher's method. The purified compounds were tested in zebrafish embryos as well as *in vitro* for cholinesterase inhibition.

Chapter 3. Enhancing Natural Product Discovery Using a Rumsfeldian Matrix to Gauge Fungal Isolate Novelty from DNA-Barcode Data

This chapter was adapted from a manuscript which is currently being prepared for submission in 2019. The authors are Wentao Dai, Jin Woo Lee, Karen Wendt, Fares Z. Najjar, and Robert H. Cichewicz.

The work presented in this chapter was conducted as follows: Wentao Dai performed DNA barcoding analysis; Jin Woo Lee performed extraction, purification and structure elucidation of compounds 3.1-3.13; Karen Wendt performed the isolation of fungal isolates and large-scale fermentations.

3.1 Introduction

The kingdom Fungi is comprised of highly diverse taxa that have adapted to exploit a wide-range of ecological niches. These organisms exhibit tremendous lifestyle variation and morphological plasticity ranging from single cell yeasts to macroscopic mushrooms.¹¹⁰ The size of fungi also varies considerably from very small (e.g., individual hypha of microscopic fungi can measure as little as ~2-10 μm in diameter) to immense (e.g., the largest organism on Earth is believed to be a clonal *Armillaria ostoyae* located in eastern Oregon, USA, which spans an area covering ~8.9 km^2).¹¹¹ Considered the second largest kingdom of eukaryotic life, fungi play essential roles in the environment, plant and animal health, and human welfare and disease.¹¹²⁻¹¹³ Despite their importance and ubiquity, the true extent of biodiversity within the kingdom Fungi remains unknown with estimates suggesting that perhaps as few as 5% of the world's 2.2 - 3.8 million fungi have been identified.³⁷

As is the case in most fields of taxonomic inquiry, morphological features such as fruiting body characteristics and spore structures have long served as the principal means by which fungi were identified.⁴³ The foundation for these approaches were laid down two and half centuries ago by the likes of Heinrich Anton de Bary, Christian Hendrik Persoon, and Elias Magnus Fries, who were among the first naturalist to apply macroscopic morphological characteristics, as well as qualitative microscopic observations to the systematic classification of fungi.¹¹⁴⁻¹¹⁵ While the field of mycology has adopted many additional tools (e.g., quantitative microscopy, electron microscopy, and others) that have aided in the morphological description and taxonomic classification of fungi,¹¹⁶⁻¹¹⁸ fungal systematics has remained heavily constrained by the limitations that morphological markers imposed on researchers trying to infer evolutionary relationships within the kingdom Fungi. Namely, the taxonomic assessment of fungi using only morphological metrics is complicated by several weaknesses that include (i) problems introduced through the convergent evolution of traits leading to polyphyletic groupings, (ii) the challenges of recognizing and deciphering the remarkable levels of intra- and inter-specific morphological plasticity exhibited by fungi, (iii) an abundance of asexual isolates that present rather indistinct physical features, and (iv) the vagaries of human interpretation introduced during the evaluation of these morphological traits.

Fortunately, the postgenomic era has brought with it a suite of new and powerful molecular tools that have reshaped workflows used to identify fungi and have largely remodeled many fundamental aspects of fungal systematics. Perhaps the most powerful method to emerge is DNA barcoding, which has become a near universally applied tool for fungal identification.¹¹⁰ In general, DNA barcoding is performed by comparing a

fungus-derived DNA sequence against a repository of genomic data (e.g., GenBank) using the Basic Local Alignment Search Tool (BLAST). BLAST results contain both an identity value (sequence similarity) and percent query coverage (the degree to which the query and reference sequences match), which are used in combination to determine the taxonomic affinity of the fungus from which the DNA sequence originated. For fungi, the non-coding internal transcribed spacer (ITS) region is the most commonly employed portion of the fungal genome used for DNA barcoding^{48, 119} and it has been adopted as the official barcode for fungal identification.⁵⁰ Details pertaining to the DNA-barcode-based identification of fungi and best practices for its implementation have been reported.^{112, 120}

While DNA barcoding is an immensely powerful tool, this technique still suffers from certain weaknesses. For example, it has been estimated that nearly 70% of type strains have not been subjected to barcoding rendering them undetectable to sequence-based searches.¹²¹ Moreover, sequence databases are thought to contain substantial numbers of errors (~20% may be misannotated in GenBank).¹²²⁻¹²³ Additional problems have been recognized including non-uniform rates of ITS diversification among fungi, the unintentional introduction of artifacts into barcodes due to sequencing errors, and others.¹²⁴⁻¹²⁵ Whereas the ease and simplicity of ITS barcoding has helped to democratize the process of fungal identification, the sheer number of problematic sequence records entering public databases has created new challenges for investigators.

One of the growing problems of using DNA barcode data to identify fungi centers on the increasing number of GenBank sequences accessions that fall into the category of “insufficiently identified.”^{122-123, 126-127} This term generally refers to fungus-derived

sequence data for which no formal taxonomic assignment was made beyond the sub-kingdom-level resulting in species annotations that include terms such as “*Fungal sp.*,” “*Uncultured Ascomycete*,” “*Ascomycota sp.*,” “*Uncultured Ascomycota*,” “*Uncultured Soil*,” and others. The problems posed by these types of annotations are two-fold: first, the abundance of GenBank entries described using only these terms serves to obscure the real taxonomic identities of fungi, and second, these imprecise labels complicate efforts to mine GeneBank for data supporting a fungal isolate’s phylogenetic novelty. This later point has important implications for natural product chemical discovery since it is presumed that chemically unexplored fungal species are more likely to serve as sources of new natural products as opposed to well-known organisms whose secondary metabolomes have been thoroughly investigated. In this report, we propose a schema for using ITS barcode data to mine GenBank and identify high priority fungal isolates as potential sources of new natural products. In addition, we conducted a chemical analysis of one high-priority fungal isolate demonstrating that most of its major metabolites were previously unreported natural products.

3.2 Results and Discussion

3.2.1 Conceptual Framework

To identify fungal isolates with the highest probabilities of producing new natural products, our group developed a contextual framework for considering each isolate’s phylogenetic affinity (Figure 3.1). Inspiration for the design of this schema originate from a well-known quote given at a press conference by then United States Secretary of Defense Donald Rumsfeld:

“Reports that say that something hasn't happened are always interesting to me, because, as we know, there are known knowns; there are things we know that we know. There are known unknowns. That is to say, there are things that we now know we don't know. But there are also unknown unknowns. There are things we do not know we don't know” – *U.S. Department of Defense News Briefing, February 12, 2002*

While this quote was the subject of significant comedic commentary, the idea behind this concept is thought to have been in circulation for some time and had been used in various manifestations of risk assessment strategies.¹²⁸ Importantly, we believe that this conceptual scaffold can serve as a useful tool for considering the breadth of taxonomic knowledge available about a fungal isolates and help point investigators toward samples that have improved probabilities of yielding new natural products. Specifically, we hypothesize that the secondary metabolomes of many known fungi (known knowns, Figure 3.1) have been characterized partially or completely. In contrast, fungi that are new to the natural products community (known unknowns) may hold promise as the sources of new metabolites. Our experiences have led us to believe that unlike bacteria, the majority of fungi can be grown in the lab with existing methods, but have not yet been observed for one or more reasons unrelated to their respective culturability (e.g., fungal biological diversity far exceeds the mycological community's capacity to culture and describe fungi, certain fungal habitats remain underexplored, low natural propagule abundance, highly localize fungal taxa, and others). Thus, focused

efforts to bring more known-unknown fungi into the lab presents tremendous promise for new natural products discovery.

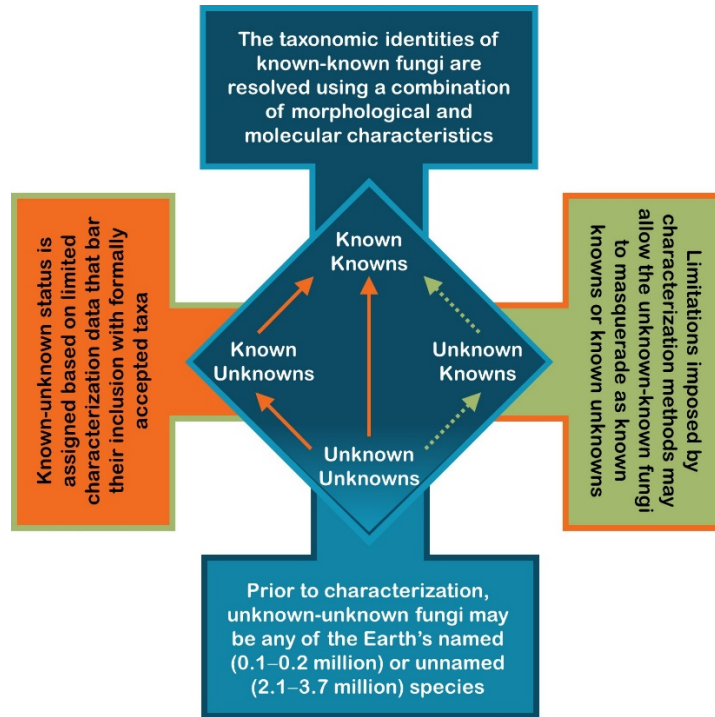


Figure 3.1. Contextual framework of each isolate's phylogenetic affinity.

3.2.1.1 Unknown Unknowns

Under our sorting system, all fungal propagules entering the lab that have yet to be subjected to taxonomic analysis, are considered unknown unknowns. In other words, unknown-unknown fungi optimistically represent the full extent of the hypothesized biodiversity thought to exist within the kingdom Fungi. Current estimates indicate that roughly 0.1–0.2 million fungal taxa have been formally described meaning 2.1–3.6 million fungi have undergone no formal taxonomic analysis. In our view, these numbers imply that if one is interested in seeking yet-to-be described fungal taxa, then most

meaningful attempts to culture fungi from the environment should provide reasonable chances for encountering new taxa as an appreciable fraction of the total number of isolates observed. Once an unknown-unknown fungus has been brought into culture, it is important to subject the isolate to some form of identification that will enable its progression to one of three categories (i.e., known known, unknown known, and known unknown) based on the isolate's proposed taxonomic affinity. In our view, ITS DNA barcoding represents the most practical and effective solution to rapidly evaluate large numbers of fungal isolates. The steep rise in the use of DNA barcoding throughout the mycological community coupled with its cost effectiveness and universal applicability to fungi has made this technique an attractive method, which we have adopted as the standard systematics tool for analyzing fungal isolates.¹²⁹ In the following sections, we describe how DNA barcode data are applied for the provisional assignment of fungi to either known-known or known-unknown status, as well as identify limitations of our system that allow unknown-known fungi to masquerade as known knowns and known unknowns (Figure 3.1).

3.2.1.2 Known-Knowns

The first potential outcome from using ITS DNA-barcode data is that a sequence provides a strong indication that an isolate is a likely representative from a known taxon (a known known). The current consensus is that fungi sharing $\geq 97\%$ ITS barcode sequence identity should be classified as the same taxon.¹³⁰ Although adopting such a rigid cutoff value will invariably result in conflict with the realities of the wide range of sequence variation observed in nature, we agree that this breakpoint provides a good

starting point for initially assessing an isolate's novelty. While we recognize that a DNA barcode alone is insufficient to definitively identify an isolate, we believe that in the context of sifting through thousands of isolates to find candidate fungi that are likely to produce new natural products, a high-quality DNA barcode offers a strong starting point for making a tentative taxonomic assignment that can be later vetted by morphological and/or additional molecular analyses (*vide infra*).

3.2.1.3 Known Unknowns

The second possible outcome is that an isolate presents a weak match to publically available ITS DNA barcode data (<97% sequence similarity). In our terminology, this type of isolate should be tentatively classified as a known unknown (i.e., the DNA barcode data indicate that the isolate represents a new candidate taxon). In our view, isolates falling into this category provide the highest theoretical value for the discovery of new natural products since these fungi are less likely to have been subjected to prior chemical investigation. In addition, we recognize a distinctive sub-group within the known unknowns, which has arisen as a function of the proliferation of metagenomics data entering public databases (e.g., GenBank). Specifically, an isolate may be assigned known-unknown status when it exhibits strong DNA-barcode homology with available ITS sequences, but the sequences are derived from uncultured organisms. There has been a tremendous upsurge of culture-independent microbial surveys occurring the world over covering every major (and many minor) environmental niches. Consequently, it is anticipated that more and more known-unknown fungi will be represented by ITS barcode data long before they enter into culture and are formally described.

3.2.1.4 Unknown Knowns

The third potential outcome for an unknown-unknown fungal isolate is that ITS barcode data will lead to its mistaken assignment as a known known or known unknown. There are several possible ways that unknown knowns can be incorrectly assigned¹²⁴⁻¹²⁵ and some of them are considered here. One of the major challenges of using an ITS-based barcode identification system is that a significant portion of the publically available data are not properly annotated or vetted resulting in sequences that are improperly attributed to an incorrect taxon. Another problem is that not all known fungi, including type strains, have been subjected to ITS sequencing resulting in gaps in our ability to accurately identify fungal isolates. In these situations, fungi may be identified as known unknowns when in fact the isolates represent a formally accepted species. Furthermore, the resolving power of ITS data is not equivalent across all taxonomic groups, which can limit species delineation. Finally, ITS data can be prone to certain technical errors that compromise the accuracy of taxonomic assignments; however, data quality surveillance measure can help to limit the impact of these error types. Unfortunately, most unknown known fungi will remain undetected until additional analysis methods are applied (morphological and/or additional molecular markers).

3.2.2 Sourcing Fungal Isolates through Citizen Science

The University of Oklahoma Citizen Science Soil Collection Program was launched in 2010 to secure chemically-diverse natural products made by fungi for the purpose of identifying bioactive compounds with applications to human and animal health.¹³¹ To date, 5914 of soil samples have been received from citizen scientist located

throughout the United States (Figure 3.2) and data derived from those samples have been made available through our open access data sharing platform on SHAREOK.¹³¹ Our barcoding method focuses on amplifying the non-coding ITS DNA using the ITS1F and ITS4 primers.¹²⁰ This approach provides single-direction nucleotide sequence data for each fungus, which is used to establish an isolate's provisional taxonomic affinity via BLASTN (nucleotide BLAST) with data archived in GenBank. While a DNA barcoding approach imposes certain constraints on the power and precision of the taxonomic assessments that are made, we have found our sequencing procedure to be financially and programmatically optimal since it provides an affordable, high-throughput solution to achieving reasonably high levels of accuracy. Throughput and biological diversity were two key considerations factoring into the development of our pipeline since a functional fungal drug discovery library requires large numbers of taxonomically diverse fungi that afford access to chemically diverse natural products. Based on that vision, our team has prepared 44,000 ITS barcoded isolates from citizen-science-submitted soil samples and we continue to add fungi to the collection at a rate of just under 1,000 isolates per month (e.g., 11,557 fungi were DNA barcoded in 2018). An analysis of the data indicates that our citizen-science-driven efforts are capturing reasonably high level of fungal diversity with at least 630 genera represented in our collection. Moreover, 4,100 (9.3%) of the isolates cannot be readily assigned a genus-level taxonomic affiliation, which suggests that the program is effective at securing fungal “dark matter” that has yet to scientifically described or chemically explored. An analysis of ITS data quality control descriptors revealed that a majority of the ITS data we have generated is composed of reads consisting of >400 base pairs with 90% of the data exhibiting phred scores of 40 or

higher (for reference, a phred score of 40 indicates a 99.99% probability that the bases in ITS sequences were called correctly) (Figure 3.3).

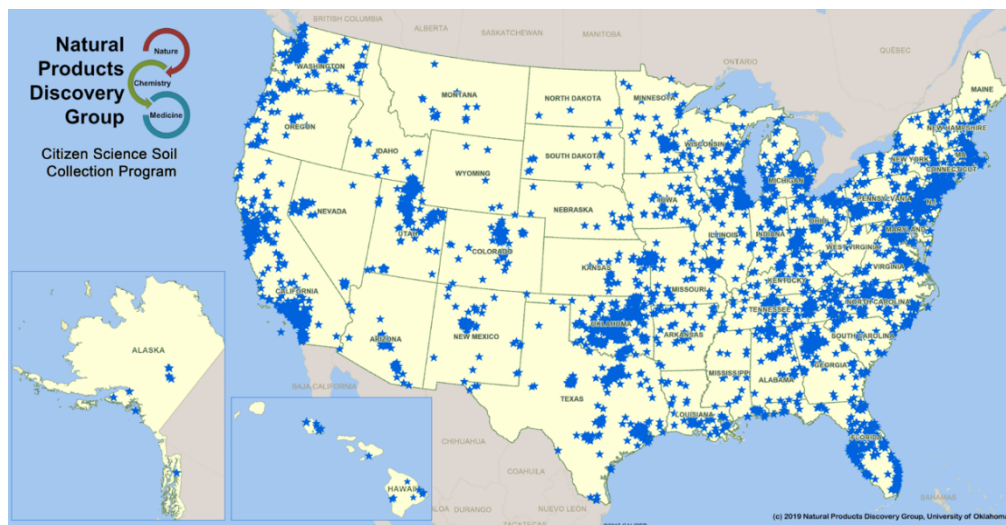


Figure 3.2. Map of soil samples received from citizen scientists by the University of Oklahoma Citizen Science Soil Collection Program.

3.2.3 Analyzing the Impact of Insufficiently Identified Fungal Barcodes, Single Direction ITS Region Reads, and Secondary Molecular Taxonomic Marker Gene Data on Generating Genus-Level Taxonomic Assignments

Informal observations within our group suggested that a substantial number of the fungi in our collection exhibited ITS barcode data with sequence homologies to insufficiently identified fungi (*vide supra*) based on BLASTN comparisons to sequence data archived in GenBank. Therefore, we carried out an experiment to better understand the magnitude of this phenomenon. We began with a random selection of 4,000 fungal isolates prepared between June 2014 and September 2016. It was during this period that our team codified its current fungal ITS DNA barcoding practices. BLASTN analyses were performed and the top 100 most similar GenBank accessions were recorded. To our

surprise, 264 (6.6%) of the isolates exhibited sequence similarity profiles in which at least the top 5 matches were to insufficiently identified fungi (i.e., the top 5 highest probability matches were given as one or a combination of the following terms “*Fungal sp.*,” “*Uncultured Ascomycete*,” “*Ascomycota sp.*,” “*Uncultured Ascomycota*,” and “*Uncultured Soil*”). Further analysis of these results provided a subdivision of these data revealing that 85 isolates (32.2% of insufficiently identified fungi) were labeled primarily as “*Fungal sp.*,” 14 isolates (5.3% of insufficiently identified fungi) were labeled primarily as “*Uncultured Ascomycete*,” 56 isolates (21.2% of insufficiently identified fungi) were labeled primarily as “*Ascomycota sp.*,” 90 isolates (34.1% of insufficiently identified fungi) were labeled primarily as “*Uncultured Ascomycota*,” and 19 isolates (7.2% of insufficiently identified fungi) were labeled primarily as “*Uncultured Soil*.” Further consideration of the reasoning behind the use of these descriptors provided no clear indication for how or why each term was applied; however, it was observed that most of the sources used to generate the DNA sequence data that populated GenBank appeared to consist of sequences derived from metagenome datasets. In our view, these data have several intriguing implications beyond simply complicating ITS-barcode-based identification practices. Namely, the appearance of these types of matches provides a more comprehensive picture of a taxonomic unit’s prevalence in fungal communities, as well as offers an indication of its potential geographical reach.

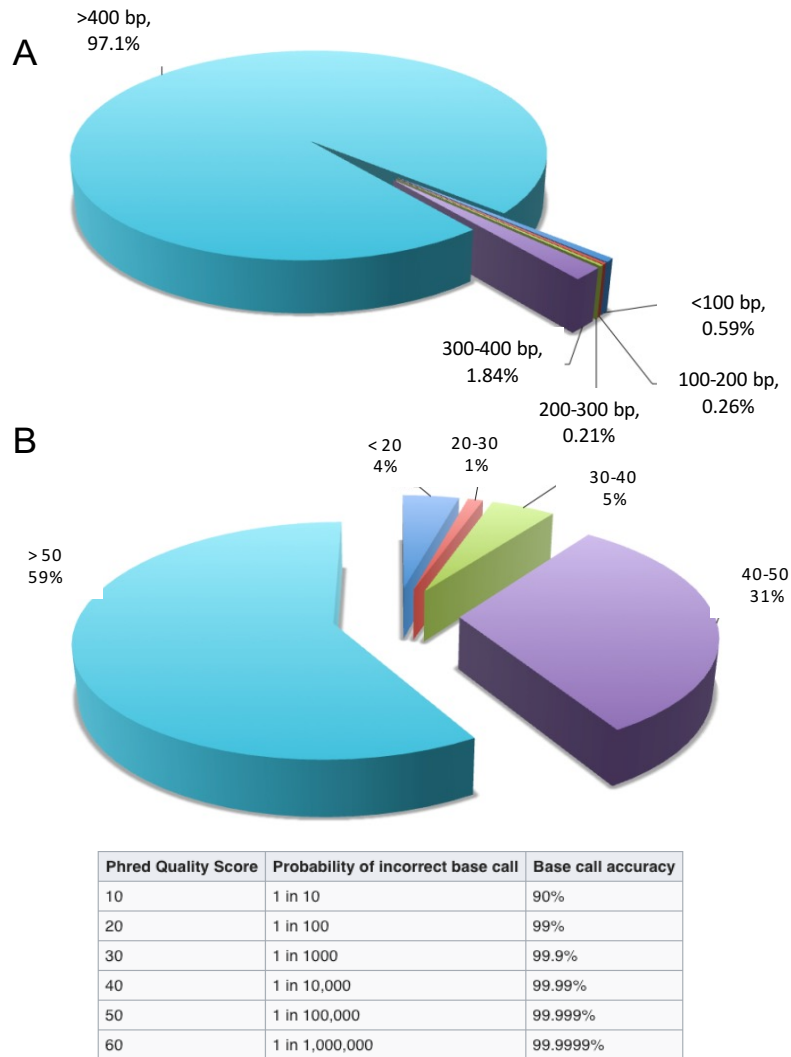


Figure 3.3. Quality control metrics for fungal ITS barcode data associated with the University of Oklahoma Citizen Science Soil Collection Program. Distribution of (A) ITS barcode length and (B) phred scores for sequences in the collection.

The isolates were subjected to a second round of bidirectional sequencing of the ITS region, as well as sequencing of a secondary taxonomic marker gene, *translation elongation factor 1-a (tef1)*.⁵⁶ Published reports have shown that *tef1* has outstanding potential as a secondary fungal DNA barcoding tool that provides excellent taxonomic resolution that complements ITS barcodes.⁵⁸ Further probing the data revealed that 95.1% of the isolates could be assigned with reasonable confidence to a probable genus when all

100 top BLASTN hits were considered (>95% sequence similarity scores). However, 4.9% of the isolates still showed low sequence homology ($\leq 95\%$) to data recorded in GenBank. These results suggest that while our general approach to the ITS barcode identification of isolates is reasonably accurate (10% of fungi were unresolved at the genus level using single direction read data versus 4.9% remaining unresolved using bidirectional ITS sequencing combined with *tefl* sequence data), bidirectional sequencing coupled with employing a secondary molecular taxonomic marker provided increased power for resolving fungal taxonomic affinities. However, when balanced against the differences in cost and time invested, single direction read ITS barcode data are a practical and justifiable starting point for the generation of initial taxonomic descriptors for environmental fungal isolates. Importantly, this simplified approach served as an excellent tool for prioritizing candidate known-unknown fungi for follow-up investigations.

3.2.4 Examining the Secondary Metabolome Features in a Candidate Known-Unknown Fungus

Based on data from our bioinformatics studies, we were highly motivated to explore whether the taxonomically difficult to define isolates could serve as sources of new natural products. While most natural product chemistry studies in our lab are bioassay-driven, we encountered a fortuitous set of circumstances wherein one of the taxonomically ill-defined fungal isolates we had investigated (internal code 74E10) had coincidentally been identified as a hit that inhibited the growth of *Mycobacterium tuberculosis*. Upon fractionation of the crude organic extract from 74E10, the activity had

been lost, but its LC-ESIMS profile suggested it could serve as an interesting candidate for a chemically motivated natural products discovery investigation since only two of its major chemical constituents (**3.1-3.13**) (Figure 3.4) could be readily dereplicated could be readily dereplicated [deoxyphomalone (**3.1**)²¹ and monocerin (**3.2**)^{23,24}]. Barcode data supported the asexual isolate's assignment within the Phaeosphaeriaceae; however, comparisons of its ITS (91% sequence homology to a *Pleosporineae* sp.) and *tefl* (95.3% sequence homology to a *Bipolaris yamadae*) data to GenBank sequences were unable to provide additional taxonomic resolution. Using our terminology (Figure 3.1), this isolate qualified as a known unknown.

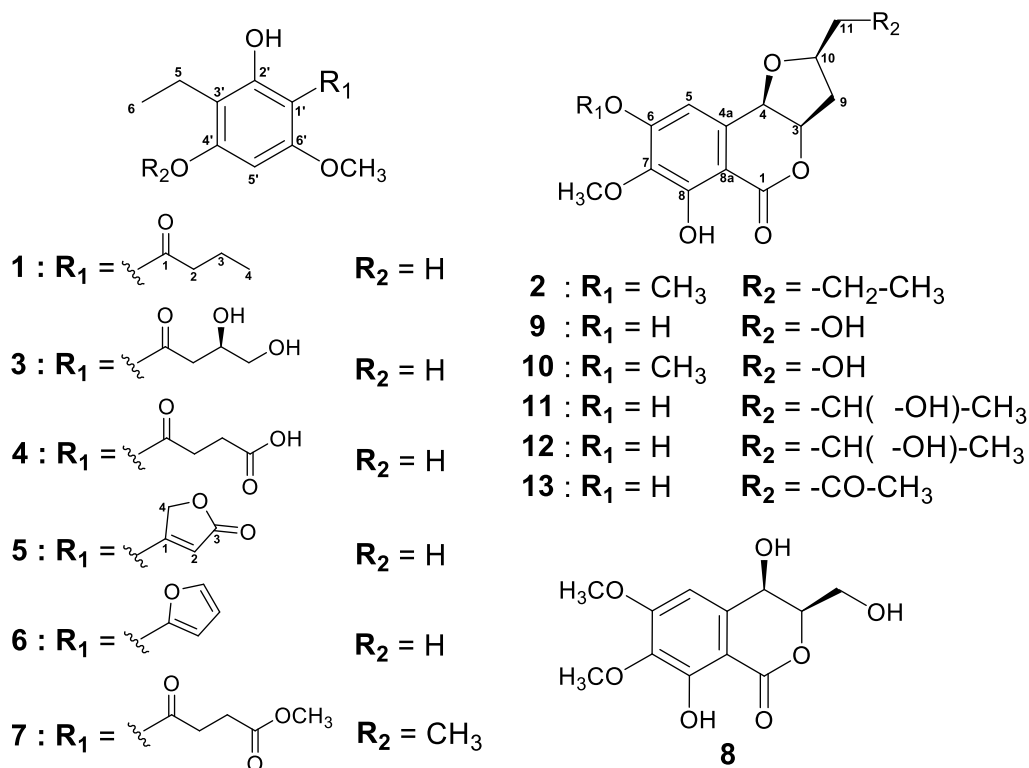


Figure 3.4. Structures of fungal metabolites **3.1-3.13**.

Compound **3.3** was isolated as an amorphous powder. Its molecular formula of $C_{13}H_{18}O_6$ was established by HRESIMS (m/z 293.1007 $[M+Na]^+$), indicating five degrees of unsaturation. The 1H NMR spectra of **3.3** showed signals for an aromatic proton at δ_H 5.97, an methine at δ_H 4.19, an methoxy group at δ_H 3.84, two oxygenated methylenes at δ_H 3.53, four methylene protons at δ_H 3.25, 3.05 and 2.54 (2H) and one methyl group at δ_H 1.03. The ^{13}C NMR and HSQC spectra exhibited 13 carbon signals including characteristic six aromatic carbon signals similar to those of phloroglucinol derivatives such as deoxyphomalone (**3.1**).¹³² The HMBC correlations from the protons of ethyl unit (H-5 and 6) to aromatic carbons (C-2', 3' and 4') revealed this group was attached to C-3' and the HMBC correlations from the methoxy protons to the C-6' in the aromatic ring indicated that the methoxy group was located at C-6' position. In addition, the presence of 3,4-dihydroxy-buta-1-one moiety was confirmed by the 1H - 1H COSY and HMBC correlations, and the weak long-range 1H - ^{13}C HMBC correlations between the aromatic proton and the ketone carbon established this C4 unit was attached to C-4' (Figure 3.5). As a result, the above-mentioned process of the structure elucidation explained that it consisted of C2 (3'-ethyl group), C6 (phloroglucinol) and C4 (1'-butyl group) units. Absolute configuration of C-3 was determined as *R* ($[\alpha]_D^{25} +20$) by comparison with the optical rotation on the basis of the literature reporting (*R*)-3, 4-dihydroxy-1-phenylbutan-1-one ($[\alpha]_D^{25} +41.8$) and its synthetic analogues.¹³³ Therefore, the structure of **3.3** was determined as (3*R*)-3'-ethyl-2',4'-dihydroxy-6'-methoxy-3,4-dihydroxybutyrophenone.

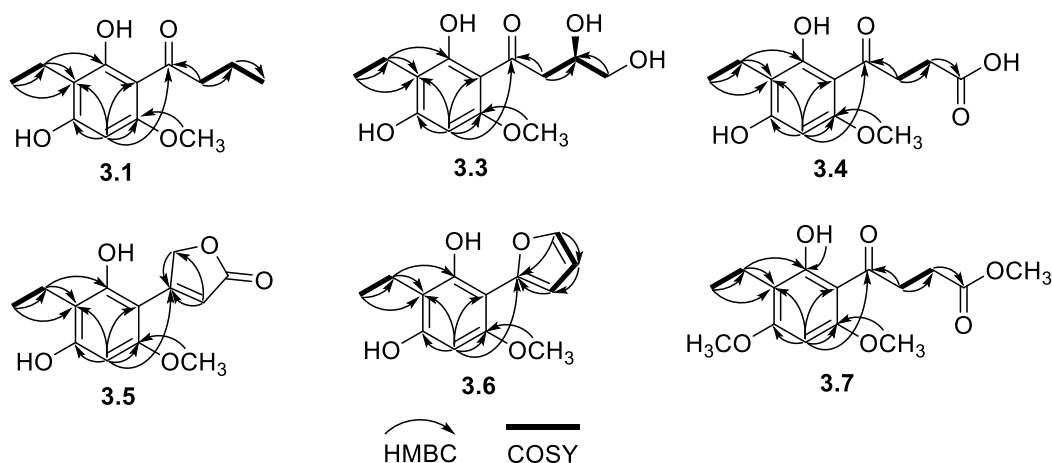


Figure 3.5. Key ¹H-¹H COSY, ¹H-¹³C HMBC correlations for compounds **3.1**, **3.3-3.7**.

Compound **3.4** was obtained as a white amorphous powder. The HRESIMS showed a sodiated molecular ion peak at m/z 291.0850 $[M+Na]^+$ corresponding to molecular formula of $C_{13}H_{16}O_6$, which indicated the presence of six degrees of unsaturation. The ¹H and ¹³C NMR spectra of **3.4** (Table 3.1 and 3.2) suggested that **3.4** shared the C2-C6-C4 skeleton with **3.3**. The ¹³C NMR spectra of **3.4** (Table 3.2) showed signals for a carboxyl group at δ_C 175.9 and an additional methylene carbon at δ_C 28.0 instead of two oxygenated carbons of **3.3**. The HMBC correlations from H-3 to two ketones (C-1 and 4) indicated that a carboxyl group was located at the end of the butanone moiety (Figure 3.5). Thus, the structure of **3.4** was established as 3'-ethyl-2',4'-dihydroxy-6'-methoxy-4-carboxybutyrophenone.

Table 3.1. ¹H NMR (400 MHz) Data for Compounds **3.3-3.7**.

No.	3.3 ^a	3.4 ^a	3.5 ^a	3.6 ^a	3.7 ^b
2a	3.25 (dd, 16.4, 4.4)	3.27 (m)	6.23 (s)	6.56 (d, 3.2)	3.37 (m)
2b	3.05 (dd, 16.4, 8.0)				
3	4.19 (m)	2.60 (m)	-	6.49 (m)	2.67 (m)
4	3.53 (m)	-	4.48 (s)	7.52 (br s)	-
5	2.54 (m)	2.54 (m)	2.77 (m)	2.61 (m)	2.58 (m)
6	1.03 (t, 7.2)	1.02 (t, 7.2)	1.14 (t, 7.2)	1.08 (t, 7.2)	1.06 (t, 7.2)
5'	5.97 (s)	5.97 (s)	6.45 (s)	6.07 (br s)	5.96 (s)
4-OCH ₃	-	-	-	-	3.89 (s)
4'-OCH ₃	-	-	-	-	3.91 (s)
6'-OCH ₃	3.84 (s)	3.84 (s)	3.85 (s)	3.73 (s)	3.92 (s)
2'-OH	-	-	-	-	13.70 (s)

^aObserved in MeOH-*d*₄. ^bObserved in CDCl₃.

Compound **3.5** was obtained as a white amorphous powder. The molecular formula was established to be C₁₃H₁₄O₅ based on HRESIMS (*m/z* 251.0922 [M+H]⁺). Analysis of its NMR spectra revealed that **3.5** carried typical C2-C6 units, but, its C4 unit was a characteristic moiety which was turned out to be an α,β -unsaturated- γ -butyrolactone ring. The HMBC correlations from the protons in the lactone ring to C-1' in the C6 unit, and the two singlet peaks at δ_{H} 6.23 and 4.48 suggested that C2-C6 unit was attached to C-1 in the lactone ring system (Figure 3.5).

Table 3.2. ^{13}C NMR (100 MHz) Data for Compounds **3.1** and **3.3-3.7**.

No.	3.1 ^a	3.3 ^b	3.4 ^b	3.5 ^b	3.6 ^b	3.7 ^a
1	206.1	203.0	202.9	167.0	149.2	203.0
2	46.2	47.7	38.6	107.5	108.6	39.2
3	18.2	68.5	28.0	179.3	110.6	28.4
4	14.0	65.7	175.9	59.8	139.7	173.8
5	15.5	14.9	14.9	15.4	15.7	15.4
6	13.3	12.3	12.3	12.6	12.8	13.4
1'	105.8	104.6	104.2	107.0	99.0	105.4
2'	164.8	164.2	164.0	157.2	156.0	163.4
3'	109.5	110.0	109.9	110.2	110.5	112.1
4'	159.6	162.3	162.2	160.8	153.5	163.2
5'	90.1	89.8	89.7	95.3	91.0	85.7
6'	161.0	161.1	162.2	158.6	155.8	161.5
4-OCH ₃	-	-	-	-	-	51.7
4'-OCH ₃	-	-	-	-	-	55.4
6'-OCH ₃	55.3	54.4	54.4	54.7	54.5	55.3

^aObserved in CDCl₃. ^bObserved in MeOH-*d*₄.

Compound **3.6** was isolated as green oil. Its ^{13}C NMR and HRESIMS data indicated **3.6** had a molecular formula of C₁₃H₁₄O₄ (m/z 235.0974 [M+H]⁺). The ^1H and ^{13}C NMR spectra (Table 3.1 and 3.2) showed characteristic signals for an α -substituted furan ring at δ_{H} 6.49, 6.56 and 7.52, and δ_{C} 149.2, 108.6, 110.6 and 139.7 together with the signals corresponding to the C2-C6 units. Also, ^1H - ^1H COSY correlations between H-2 and H-3 and between H-3 and H-4 suggested that C4 unit formed five membered-ring with a couple of conjugated bonds (Figure 3.5).

Compound **3.7** was obtained as a white amorphous powder. Its molecular formula was determined to be C₁₅H₂₀O₆ from HRESIMS (m/z 319.1161 [M+Na]⁺). The ^1H NMR and ^{13}C NMR data (Table 3.1 and 3.2) were similar to those of deoxyphomalone (**3.1**) except for two additional methoxy group signals. Thus, the structure of **3.7** was determined to be 4,4'-dimethoxy-6-deoxyphomalone.

Table 3.3. ^1H NMR (400 MHz) Data for Compounds **3.8-3.13** in $\text{MeOH-}d_4$.

No.	3.8	3.9	3.10	3.11	3.12	3.13
3	4.51 (m)	5.07 (m)	5.15 (m)	5.09 (br s)	5.08 (br s)	5.07 (br s)
4	4.71 (d, 2.8)	4.63 (d, 2.8)	4.75 (d, 2.8)	4.57 (br s)	4.57 (br s)	4.57 (br s)
5	6.71 (s)	6.50 (s)	6.80 (s)	6.53 (s)	6.53 (s)	6.50 (s)
9a	3.96 (d, 7.0)	2.58 (m)	2.62 (m)	2.68 (m)	2.69 (m)	2.72 (m)
9b	-	2.16 (m)	2.21 (m)	2.10 (m)	2.07 (m)	2.06 (m)
10	-	4.22 (m)	4.25 (m)	4.28 (m)	4.32 (m)	4.51 (br s)
11a	-	3.55 (d, 5.6)	3.58 (d, 5.6)	1.85 (m)	1.71 (m)	2.87 (m)
11b	-	-	-	1.65 (m)	1.69 (m)	2.74 (m)
12	-	-	-	3.86 (m)	3.82 (m)	-
13	-	-	-	1.18 (d, 6.0)	1.18 (d, 6.0)	2.15 (s)
6-OCH ₃	3.95 (s)	-	3.95 (s)	-	-	-
7-OCH ₃	3.80 (s)	3.83 (s)	3.82 (s)	3.86 (s)	3.86 (s)	3.84 (s)

Compound **3.8** was isolated as a white amorphous powder. Its molecular formula was assigned to be $\text{C}_{12}\text{H}_{14}\text{O}_7$ based on the HRESIMS data (m/z 293.0642 $[\text{M}+\text{Na}]^+$), indicating six degrees of unsaturation. The ^1H and ^{13}C NMR spectra of **3.8** (Table 3.3 and 3.4) showed signals for an aromatic ring, two oxymethines, two oxymethylenes, two methoxy groups and a carboxylic carbon at δ_{C} 169.0. Analysis of the NMR data indicated **3.8** had an isochroman-1-one skeleton that was shown in monocerin (**3.2**).¹³⁴⁻¹³⁵ The HMBC and ^1H - ^1H COSY correlations of **3.8** suggested two hydroxyl groups were located at C-4 and 8 and two methoxy groups were assigned as C-6 and 7. Also, a hydroxymethyl group ($-\text{CH}_2\text{-OH}$) was attached to C-3 in the isocoumarin moiety (Figure 3.6). The relative configuration of H-3 and 4 was defined as *cis* conformation by a ROESY experiment (Figure 3.7) and the absolute configuration was determined by using CD analysis. The CD spectrum of (*R*)-(-)-6-hydroxymellein and exserolides, which possess the dihydroisocoumarin moiety like **3.8**, exhibited a negative Cotton effect at 270 nm

equivalent to the $n \rightarrow \pi^*$ band. Since CD spectrum of **3.8** showed a negative Cotton effect at 270 nm, and the absolute configuration of **3.8** was assigned as 3*R*, 4*R* (Figure 3.8).¹³⁶⁻

137

Table 3.4. ¹³C NMR (100 MHz) Data for Compounds **3.2** and **3.8-3.13**.

No.	3.2 ^a	3.8 ^b	3.9 ^b	3.10 ^b	3.11 ^b	3.12 ^b	3.13 ^b
1	167.7	169.0	168.4	168.0	168.3	168.3	168.2
3	81.2	82.2	81.1	81.3	81.5	81.6	81.5
4	74.4	64.0	74.7	74.6	74.3	74.2	74.4
4a	131.1	137.4	131.5	131.8	131.6	131.7	131.4
5	104.3	102.9	109.7	104.7	108.9	109.0	109.1
6	158.6	158.8	158.7	158.7	157.0	157.2	157.4
7	137.2	136.2	135.7	136.7	135.4	135.5	135.6
8	156.2	155.3	156.1	155.5	156.1	156.1	156.1
8a	102.0	101.8	99.0	101.6	99.8	99.7	99.6
9	38.9	60.3	35.3	35.2	38.7	39.1	38.6
10	78.7	-	79.0	79.0	76.2	75.5	74.1
11	38.0	-	64.2	64.1	44.9	45.3	49.3
12	19.1	-	-	-	64.9	64.4	207.7
13	13.9	-	-	-	21.9	22.8	29.0
6-OCH ₃	56.2	55.4	-	55.4	-	-	-
7-OCH ₃	60.0	59.5	59.3	59.5	59.4	59.4	59.4

^aObserved in CDCl₃. ^bObserved in MeOH-*d*₄.

Compound **3.9** was obtained as colorless oil. The molecular formula of C₁₃H₁₄O₇ was established by HRESIMS (m/z 305.0644 [M+Na]⁺), indicating seven degrees of unsaturation. The 1D and 2D NMR data suggested the presence of an additional five membered ring that was also found in monocerin (**3.2**). The ROESY correlations between H-4 and H-3, H-3 and H-9 α , and H-9 α and H-10 indicated H-3, H-4, H-9 α and H-10 placed on the same face of the ring system (Figure 3.7). Therefore, the absolute configuration of **3.9** was determined as 3*R*, 4*R* and 10*R* according to its CD spectrum (Figure 3.8), which exhibited a negative Cotton effect at 270 nm, in the same way as **3.8**.

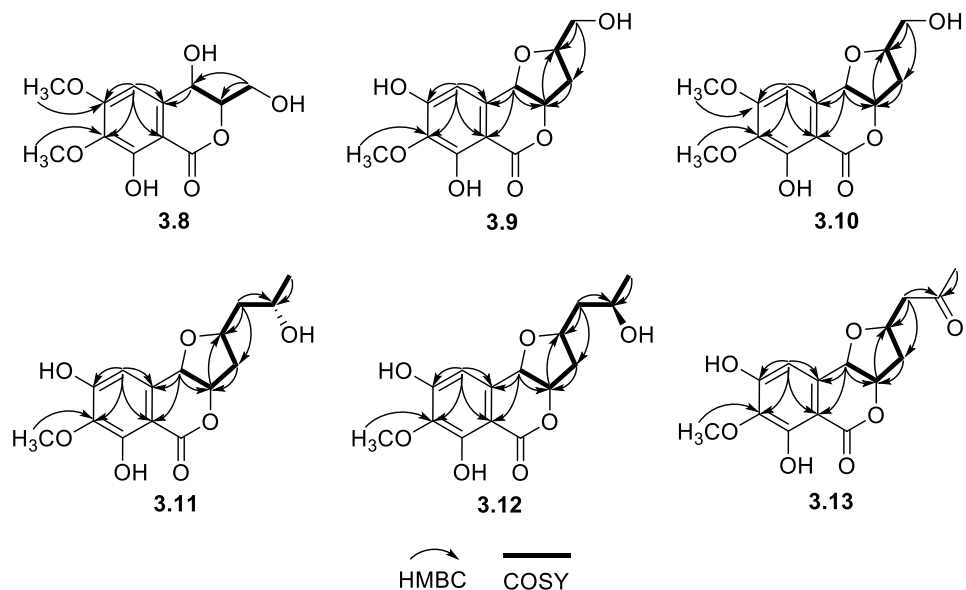


Figure 3.6. Key ^1H - ^1H COSY, ^1H - ^{13}C HMBC correlations for compounds **3.8-3.13**.

Compound **3.10** was isolated as a white amorphous powder and its molecular formula was determined to be $\text{C}_{14}\text{H}_{16}\text{O}_7$ based on the HRESIMS data (m/z 319.0800 $[\text{M}+\text{Na}]^+$). The ^1H and ^{13}C NMR spectra of **3.10** were very similar to those of **3.9** except for the presence of an additional methoxy group. These two methoxy groups were located at C-6 and C-7 like **3.2** by using the HMBC experiment. The absolute configuration of **3.10** was also confirmed as $3R$, $4R$ and $10R$ in the same manner as **3.8**.

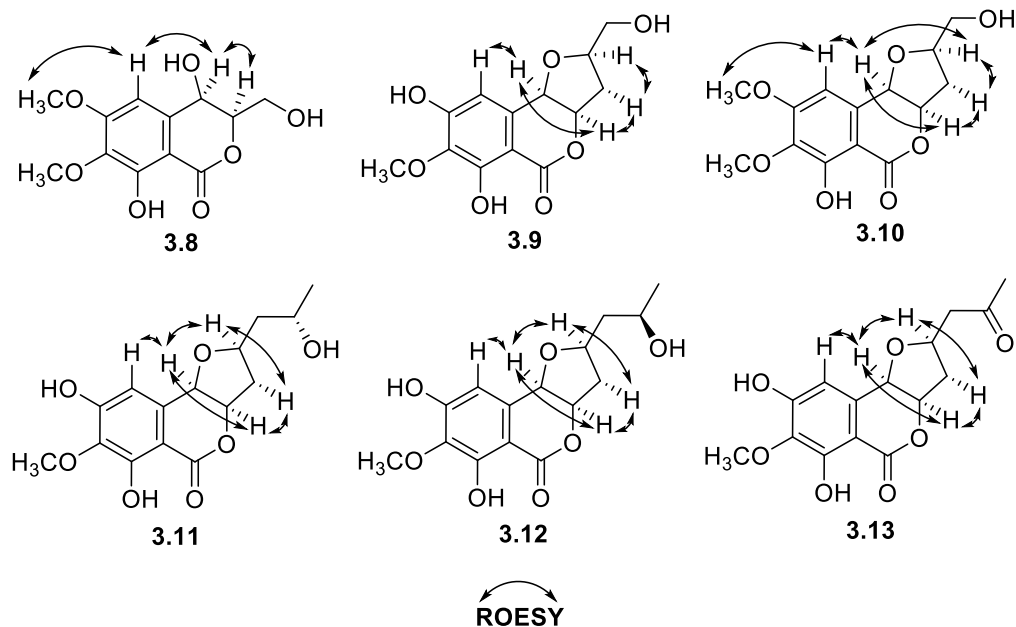


Figure 3.7. Key ROESY correlations for compounds **3.8-3.13**.

Compounds **3.11** and **3.12** were isolated as colorless oil and their molecular formula were the same as $C_{15}H_{18}O_7$ from the HRESIMS data (**3.11**: m/z 333.0957 $[M+Na]^+$, **3.12**: m/z 333.0956 $[M+Na]^+$). The 1D and 2D NMR spectra (Table 3.3 and 3.4) were similar to monocerin (**3.2**) except for the absence of 6-methoxy group and the presence of 12-hydroxy group. The 1D and 2D NMR spectra of **3.11** and **3.12** were nearly identical, other than the ^{13}C NMR resonance of C10-C13, suggesting that they were C12-epimers. In order to confirm, the modified Mosher's method was carried out (Figure 3.9). Thus, the absolute configuration of C-12 of **3.11** was determined as $12S$ and that of **3.12** was $12R$.¹³⁸⁻¹³⁹

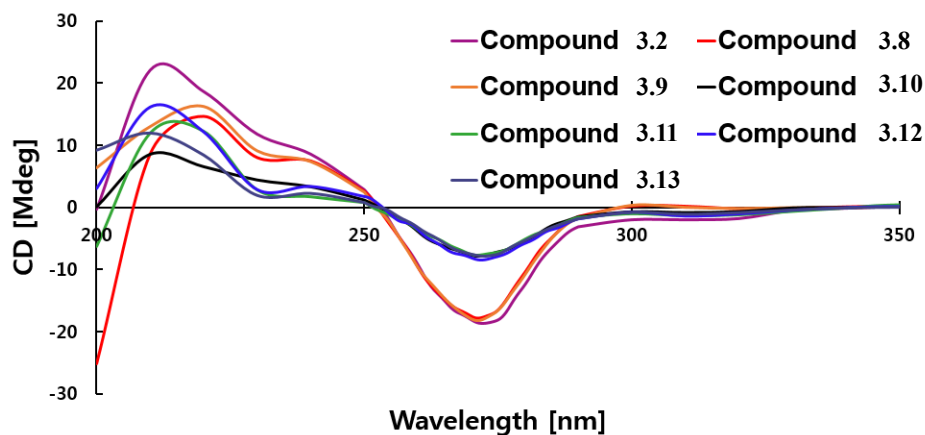


Figure 3.8. ECD spectra of compounds **3.2** and **3.8-3.13**.

Compound **3.13** was obtained as a white amorphous powder. Its HRESIMS data (m/z 331.0800 $[M+Na]^+$), revealed the molecular formula was $C_{15}H_{16}O_7$, indicating eight degree of unsaturation. The 1H and ^{13}C NMR data of **3.13** (Table 3.3 and 3.4) resembled those of **3.11** and **3.12** and the only difference between them was **3.13** had the ketone group (δ_C 207.7) instead of 12-hydroxyl group of **3.11** and **3.12**. The relative and absolute configuration of **3.13** was assigned as $3R$, $4R$ and $10R$ by the ROESY experiment and CD analysis in the above-mentioned way.

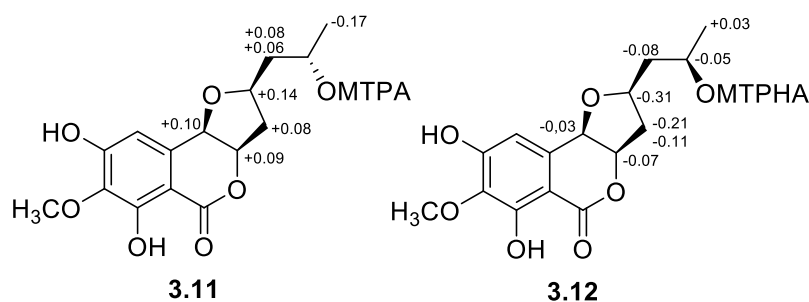


Figure 3.9. Analysis of modified Mosher's method for **3.11** and **3.12**. $\Delta\delta$ ($\delta_S - \delta_R$) values are shown.

3.3 Conclusion and Future Directions

In summary, we proposed a schema for using ITS barcode data to mine GenBank and identify high priority fungal isolates as potential sources of new natural products. On the basis of our study, considering the cost and time invested, single direction read ITS barcode data are a practical and justifiable starting point for the generation of initial taxonomic descriptors for environmental fungal isolates. Importantly, this simplified approach served as an excellent tool for prioritizing candidate known-unknown fungi for follow-up investigations. In addition, we conducted a chemical analysis of one candidate known-unknown fungal isolate and eleven metabolites which were previously unreported have been isolated. This indicated that what we proposed is applicable. In the future, we are going to perform chemical investigation on more candidate known-unknown fungal isolates to testify the schema we proposed. In addition, morphological characterization and other DNA barcoding gene could be used for the identification of those candidate known-unknowns.

3.4 Materials and Methods

3.4.1 General Experimental Procedures

Optical rotation measurements were made on an AUTOPOL[®] III automatic polarimeter. ECD spectra were obtained on a JASCO J-715 circular dichroism spectrometer. The LC-ESIMS analyses were performed on a Shimadzu UFLC system with a quadrupole mass spectrometer using a Phenomenex Kinetex C₁₈ column (3.0 mm × 75 mm, 2.6 μm) and MeCN-H₂O (0.1% HCOOH) gradient solvent system. HRESIMS spectra were measured using an Agilent 6538 Ultra High Definition (UHD) Accurate-

Mass Q-TOF system. NMR spectra were obtained on Varian spectrometers (500 MHz for ^1H and 100 MHz for ^{13}C) using $\text{MeOD-}d_4$ and CDCl_3-d as solvent. The preparative HPLC system was equipped with SCL-10A VP pumps and system controller and a Gemini 5 μm C_{18} column (110 \AA , 250 \times 21.2 mm). The semi-preparative HPLC were performed using Waters 1525 binary pumps coupled with Waters 2998 photodiode array detectors and Gemini 5 μm C_{18} columns (110 \AA , 250 \times 10 mm). PCR was performed using a Lightcycler[®] 480 Real-Time PCR and a PTC-200 Peltier Thermal Cycler instrument. All solvents were of ACS grade or better.

3.4.2 DNA Extraction and Polymerase Chain Reaction (PCR)

A total of 4000 isolates from our Citizen Science Soil Collection Program were cultured on the Czapek Ivermectin Agar (CZI), then subjected to DNA extraction and PCR. DNA extraction were carried out by mixing mycelium with magnetic beads in PBS solution (200 μL), then blended for 5 min, the supernatant is the DNA solution. PCR were done by using the primer ITS1F (20 μM) and primer ITS4 (20 μM) to amplify the nuclear ribosomal internal transcribed spacer (ITS). The cycling parameters for PCR were 40 cycles of 1min at 95°C, 1min at 50°C, 1 min at 72°C. PCR products were sequenced reversely and all the sequence data were queried against GenBank using Basic Local Alignment Search Tool (BLAST). Second round PCR were done for forwardly sequence in order to generate longer sequences for fungal identification. Isolates were cultured in Malt Extract Broth (MEB), then subjected to DNA extraction by using the PowerLyzer Powersoil DNA Isolation Kit. The primers and the cycling parameters used are aforementioned the same. The primers used for *tefl* PCR were EF1 1018F and EF1

1620R. And the cycling parameters were : 1. 94°C - 2 min, 2. 66°C - 56°C touchdown (9 cycles), 3. 94°C -30 second, 4. 56°C - 1 min, 5. 72°C - 1 min, 6. Repeat 3-5 for 36 cycles, 7. 72°C - 10 min, 8. 4°C on hold.¹¹²

3.4.3 Extraction and Isolation of new compounds from the fungus 74E10

The fungus was cultured on a solid medium composed of Cheerios with 0.3% sucrose solution with 0.005% chloramphenicol for four weeks at room temperature (25°C).¹⁴⁰ The fungal cultures were extracted with EtOAc (3×2L) at room temperature, and the EtOAc solution was evaporated *in vacuo* to obtain the crude extract (Fraction A, 26 g). Fraction A was separated by silica gel vacuum column chromatography getting fraction B (Dichloromethane 100%), fraction C (Dichloromethane/MeOH = 10/1) and fraction D (MeOH 100%). Fraction C was also fractionated by HP20ss column chromatography obtaining five fractions, E (30% MeOH), F (50% MeOH), G (70% MeOH), H (90% MeOH) and I (100% MeOH). Fraction E was separated into five sub-fractions (E1-5) by preparative HPLC (C₁₈, 25 to 60% MeCN/H₂O in 15 min, flow rate: 10 mL/min) and subfraction E2 was further subjected to semi-preparative HPLC (C₁₈, MeCN:H₂O = 20:80, flow rate: 4 mL/min) to yield **3.8** (4 mg, *t_R* = 8 min). Fraction F was also separated into eight subfractions (F1-8) by preparative HPLC (C₁₈, 35 to 70% MeCN/H₂O in 15 min, flow rate: 10 mL/min) and subfractions F3, F6 and F7 looked like a pure compound and they were turned out to be **3.3** (25 mg), **3.4** (240 mg) and **3.6** (10 mg), respectively. Compounds **3.5** (1.5 mg, *t_R* = 11 min) and **3.9** (2 mg, *t_R* = 8 min) were purified from subfraction F1 by semi-preparative HPLC (C₁₈, MeCN:H₂O = 25:75, flow rate: 4 mL/min), and compounds **3.10** (2 mg, *t_R* = 10 min), **3.11** (10 mg, *t_R* = 11 min) and

3.12 (2 mg, $t_R = 12$ min) were also isolated from subfraction F2 by semi-preparative HPLC (C_{18} , MeCN:H₂O = 25:75, flow rate: 4 mL/min). Subfraction F was processed by semi-preparative HPLC (C_{18} , MeCN:H₂O = 30:70, flow rate: 4 mL/min) to get **3.13** (3 mg, $t_R = 8$ min), and **3.2** (10 mg, $t_R = 10$ min) was purified from fraction H by semi-preparative HPLC (C_{18} , MeCN:H₂O = 60:40, flow rate: 4 mL/min). Fraction B was also fractionated into five fractions (J-N) by HP20ss column chromatography in the above-mentioned way. Fraction M (90% MeOH) was further subjected to preparative HPLC (C_{18} , 75 to 100% MeCN/H₂O in 15 min, flow rate: 10 mL/min) getting two subfractions (M1 and M2), and **3.7** (7 mg, $t_R = 10$ min) and **3.1** (1 mg, $t_R = 11$ min) were isolated from subfraction M2 by semi-preparative HPLC (C_{18} , MeCN:H₂O = 70:30, flow rate: 4 mL/min).

Deoxyphomalone (3.1): white amorphous powder; ¹³C NMR (100 MHz, CDCl₃), see Table 4; ESIMS m/z 239 [M+H]⁺.

Monocerin (3.2): white amorphous powder; $[\alpha]_D^{25} +40.0$ (c 0.1, MeOH); CD (MeOH) λ_{max} ($\Delta\epsilon$) 213 (+24.4), 270 (-18.1) nm; ¹³C NMR (100 MHz, CDCl₃), see Table 6; ESIMS m/z 309 [M+H]⁺.

Compound 3.3: white amorphous powder; $[\alpha]_D^{25} +16$ (c 0.1, MeOH); UV (MeOH) λ_{max} ($\log \epsilon$) 228 (8.7), 290 (6.6) nm; ¹H NMR (400 MHz, MeOH-*d*₄) and ¹³C NMR (100 MHz, MeOH-*d*₄), see Table 3 and 4; HRESIMS m/z 293.1007 [M+Na]⁺ (calcd for C₁₃H₁₈NaO₆, 293.0996).

Compound 3.4: white amorphous powder; UV (MeOH) λ_{max} ($\log \epsilon$) 232 (2.0), 293 (2.8) nm; ¹H NMR (400 MHz, MeOH-*d*₄) and ¹³C NMR (100 MHz, MeOH-*d*₄), see Table 3 and 4; HRESIMS m/z 291.0850 [M+Na]⁺ (calcd for C₁₃H₁₆NaO₆, 291.0839).

Compound 3.5: white amorphous powder; UV (MeOH) λ_{max} (log ϵ) 202 (8.0), 221 (5.5), 254 (6.5), 296 (2.2) nm; ^1H NMR (400 MHz, MeOH- d_4) and ^{13}C NMR (100 MHz, MeOH- d_4), see Table 3 and 4; HRESIMS m/z 251.0922 $[\text{M}+\text{H}]^+$ (calcd for $\text{C}_{13}\text{H}_{15}\text{O}_5$, 251.0914).

Compound 3.6: green oil; UV (MeOH) λ_{max} (log ϵ) 230 (2.1), 276 (1.6) nm; ^1H NMR (400 MHz, MeOH- d_4) and ^{13}C NMR (100 MHz, MeOH- d_4), see Table 3 and 4; HRESIMS m/z 235.0974 $[\text{M}+\text{H}]^+$ (calcd for $\text{C}_{13}\text{H}_{15}\text{O}_4$, 235.0965).

Compound 3.7: white amorphous powder; UV (MeOH) λ_{max} (log ϵ) 236 (1.6), 291 (3.1) nm; ^1H NMR (400 MHz, CDCl_3) and ^{13}C NMR (100 MHz, CDCl_3), see Table 3 and 4; HRESIMS m/z 319.1161 $[\text{M}+\text{Na}]^+$ (calcd for $\text{C}_{15}\text{H}_{20}\text{NaO}_6$, 319.1152).

Compound 3.8: white amorphous powder; $[\alpha]_{\text{D}}^{25}$ -18.0 (c 0.1, MeOH); UV (MeOH) λ_{max} (log ϵ) 219 (7.0), 231 sh (5.7), 274 (4.5), 308 sh (1.3) nm; CD (MeOH) λ_{max} ($\Delta\epsilon$) 213 (+11.1), 271 (-17.8) nm; ^1H NMR (400 MHz, MeOH- d_4) and ^{13}C NMR (100 MHz, MeOH- d_4), see Table 5 and 6; HRESIMS m/z 293.0642 $[\text{M}+\text{Na}]^+$ (calcd for $\text{C}_{12}\text{H}_{14}\text{NaO}_7$, 293.0632).

Compound 3.9: colorless oil; $[\alpha]_{\text{D}}^{25}$ +30.0 (c 0.1, MeOH); UV (MeOH) λ_{max} (log ϵ) 219 (6.6), 231 sh (5.2), 273 (3.7), 308 sh (1.6) nm; CD (MeOH) λ_{max} ($\Delta\epsilon$) 213 (+11.8), 271 (-18.2) nm; ^1H NMR (400 MHz, MeOH- d_4) and ^{13}C NMR (100 MHz, MeOH- d_4), see Table 5 and 6; HRESIMS m/z 305.0644 $[\text{M}+\text{Na}]^+$ (calcd for $\text{C}_{13}\text{H}_{14}\text{NaO}_7$, 305.0632).

Compound 3.10: white amorphous powder; $[\alpha]_{\text{D}}^{25}$ +24.0 (c 0.1, MeOH); UV (MeOH) λ_{max} (log ϵ) 221 (5.8), 230 sh (5.0), 273 (3.8), 308 sh (1.5) nm; CD (MeOH) λ_{max} ($\Delta\epsilon$) 213 (+9.6), 271 (-7.8) nm; ^1H NMR (400 MHz, MeOH- d_4) and ^{13}C NMR (100 MHz,

MeOH-*d*₄), see Table 5 and 6; HRESIMS *m/z* 319.0800 [M+Na]⁺ (calcd for C₁₄H₁₆NaO₇, 319.0788).

Compound 3.11: colorless oil; [α]_D²⁵ +22.0 (*c* 0.1, MeOH); UV (MeOH) λ_{max} (log ε) 221 (5.4), 231 sh (4.7), 273 (3.8), 308 sh (1.7) nm; CD (MeOH) λ_{max} (Δε) 213 (+14.1), 271 (-7.6) nm; ¹H NMR (400 MHz, MeOH-*d*₄) and ¹³C NMR (100 MHz, MeOH-*d*₄), see Table 5 and 6; HRESIMS *m/z* 333.0957 [M+Na]⁺ (calcd for C₁₅H₁₈NaO₇, 333.0945).

Compound 3.12: colorless oil; [α]_D²⁵ +40.0 (*c* 0.1, MeOH); UV (MeOH) λ_{max} (log ε) 221 (4.3), 231 sh (3.5), 273 (2.3), 308 sh (1.1) nm; CD (MeOH) λ_{max} (Δε) 213 (+17.9), 271 (-8.4) nm; ¹H NMR (400 MHz, MeOH-*d*₄) and ¹³C NMR (100 MHz, MeOH-*d*₄), see Table 5 and 6; HRESIMS *m/z* 333.0956 [M+Na]⁺ (calcd for C₁₅H₁₈NaO₇, 333.0945).

Compound 3.13: white amorphous powder; [α]_D²⁵ +22.0 (*c* 0.1, MeOH); UV (MeOH) λ_{max} (log ε) 221 (2.8), 231 sh (3.5), 273 (2.0), 308 sh (0.9) nm; CD (MeOH) λ_{max} (Δε) 213 (+13.5), 271 (-7.7) nm; ¹H NMR (400 MHz, MeOH-*d*₄) and ¹³C NMR (100 MHz, MeOH-*d*₄), see Table 5 and 6; HRESIMS *m/z* 331.0800 [M+Na]⁺ (calcd for C₁₅H₁₆NaO₇, 331.0788).

3.4.4 Preparation of the (*S*) and (*R*)-MTPA Mosher Ester Derivatives

of 3.11 and 3.12

Compounds **3.11** and **3.12** (each 0.5 mg) were dissolved in pyridine-*d*₅ (each 1 mL) with a small amount of 4-(dimethylamino)-pyridine (DMAP) and were transferred into NMR tubes. (*S*)-(+)-*α*-methoxy-*α*-(trifluoromethyl)-phenylacetyl (MTPA) chloride (10 μL) were added into the NMR tubes under a N₂ gas stream, and then the NMR tubes were shaken to make sure the samples were mixed. The NMR tubes were placed in a

water bath for 6 h (40°C), which afforded (*R*)-MTPA ester derivatives (*S*)-MTPA ester derivatives were also yielded in the same way as the procedure mentioned above, using (*R*)-(-)-MTPA chloride. The ¹H and ¹H-¹H COSY spectra were directly obtained from the MTPA ester derivatives of **3.11** and **3.12**.

(*R*)-MTPA ester of 3.11: ¹H NMR (500 MHz, pyridine-*d*₅) : δ_H 5.44 (1H, br s, H-12), 5.21 (1H, br s, H-3), 4.76 (1H, s, H-4), 4.16 (1H, br s, H-10), 2.53 (1H, m, H-9), 2.16 (1H, m, H-9), 2.13 (1H, m, H-11), 1.81 (1H, m, H-11), 1.31 (3H, br s, H-13).

(*S*)-MTPA ester of 3.11: ¹H NMR (500 MHz, pyridine-*d*₅) : δ_H 5.45 (1H, br s, H-12), 5.30 (1H, br s, H-3), 4.87 (1H, s, H-4), 4.31 (1H, br s, H-10), 2.63 (1H, m, H-9), 2.15 (1H, m, H-9), 2.12 (1H, m, H-11), 1.79 (1H, m, H-11), 1.15 (3H, br s, H-13).

(*R*)-MTPA ester of 3.12: ¹H NMR (500 MHz, pyridine-*d*₅) : δ_H 5.40 (1H, br s, H-12), 5.26 (1H, br s, H-3), 4.94 (1H, s, H-4), 4.39 (1H, br s, H-10), 2.58 (1H, m, H-9), 2.08 (1H, m, H-9), 1.90 (2H, m, H-11), 1.14 (3H, br s, H-13).

(*S*)-MTPA ester of 3.12: ¹H NMR (500 MHz, pyridine-*d*₅) : δ_H 5.35 (1H, br s, H-12), 5.23 (1H, br s, H-3), 4.87 (1H, s, H-4), 4.08 (1H, br s, H-10), 2.37 (1H, m, H-9), 1.97 (1H, m, H-9), 1.82 (2H, m, H-11), 1.17 (3H, br s, H-13).

Chapter 4: Creation and Application of a High-Throughput High-Content Screening Assay for Natural Product Inhibitors of the Human Parasite *Trichomonas vaginalis*

This chapter was adapted from a manuscript which has been submitted to ACS Infectious Disease. The authors are Jarrod King, Adam C. Carter, Wentao Dai, Jin Woo Lee, Yun-Seo Kil, Lin Du, Sara K. Helff, Brandt Huddle, Andrew N. Miller and Robert H. Cichewicz.

The work presented in this chapter was conducted as follows: Jarrod King conducted the assay development and bioassay; Wentao Dai, Jin Woo Lee, Yun-Seo Kil and Lin Du performed extractions, purifications and structure elucidation of all the tetramic acid derivatives 4.1-4.9.

4.1 Introduction

Trichomonas vaginalis is the most frequently encountered sexually-transmitted parasite in the United States.¹⁴¹ Those infected by the parasite exhibit an increased risk for (i) HIV infection, (ii) development of cervical cancer, and (iii) infertility, as well as (iv) adverse pregnancy outcomes including (iv) miscarriage and (v) low-preterm birth weight.¹⁴² Current clinical treatment options are limited to antiprotozoal nitroimidazoles (i.e., metronidazole and tinidazole), which still offer appreciably high levels of clinical efficacy (>90% of patients are cleared of the infection after a single course of treatment)¹⁴³⁻¹⁴⁵. However, concerns have arisen that in addition to several noted side effects (e.g., nausea, vomiting, and others), the nitroimidazoles may possess carcinogenic and mutagenic properties.¹⁴⁶⁻¹⁴⁷ This has led to worry about nitroimidazole treatment

during pregnancy, as well as some apprehension about their use in the general population.¹⁴⁶ A rather troubling problem, which came to light based on surveillance data collected from patients infected with *T. vaginalis* receiving standard courses of nitroimidazole treatment, is the high rate of infection recurrence (5-31% in women).¹⁴⁵ While a portion of disease recurrence is attributable to further contact with untreated sexual partners, data suggest that a portion of *T. vaginalis* cases have the capacity to develop into persistent infection states, which raises concerns about the clinical limitations of nitroimidazole therapies.¹⁴⁸ Even more concerning, nitroimidazole resistance has been detected in up to 9.6% of clinical *T. vaginalis* isolates raising concerns that nitroimidazoles might become clinically less effective.¹⁴⁹⁻¹⁵⁰ Considering the noted safety concerns and troubling clinical observations, there is a need for new disease management options that extend beyond the nitroimidazoles for treating *T. vaginalis* infections.

An examination of the research literature has revealed surprisingly sparse information concerning efforts to identify new classes of antiprotozoal molecules active against *T. vaginalis* with only a small fraction of those endeavors dealing with natural products.¹⁵¹⁻¹⁵² A handful of prior studies had focused exclusively on testing plant extracts,¹⁵³⁻¹⁵⁶ but revealed little about the molecules responsible for their inhibitory effects. In a few instances, chemically-driven investigations of plant extracts have yielded a handful of secondary metabolites possessing activity against *T. vaginalis* including berberine,¹⁵⁷ (-)-usnic acid,¹⁵⁸ emodin,¹⁵⁹ hamycin,¹⁶⁰ hederagin,¹⁶¹ and mulinolic acid;¹⁶² however, these compounds suffer from poor potency and lack selectivity compared to metronidazole. Although the limited scope of reports pertaining to the discovery of new

leads to fight *T. vaginalis* infections is worrisome, it also signals the potential that may exist to identify new bioactive compounds for development into clinically useful agents. This expectation is reasonable, especially for natural products, which have long served as an outstanding resource for the discovery of new antiinfectious agents¹⁶³ including the topmost antiparasitic compounds in current clinical use (e.g., avermectins, artemisinin, and more).¹⁶³⁻¹⁶⁴

Aside from the scarcity of natural-product-focused drug discovery efforts focused on inhibition of *T. vaginalis*, there are relatively few reports of vetted assay methods that are amendable to the systematic screening and identification of compounds that inhibit this unique parasite. Most of the reported methods had employed microscopy-based approaches for cell enumeration¹⁶⁵ or used metabolically-activated dyes such as resazurin as indicators of parasite viability.¹⁶⁶⁻¹⁶⁷ With this in mind, we set about developing an assay system that was (i) able to robustly identify antitrichomonal compounds, (ii) amenable to high-throughput sample testing, (iii) could accurately distinguish between complete versus partial inhibition of the *T. vaginalis*, and (iv) could be used on a wide variety of sample types including pure compounds and natural product extracts. Herein we report the results of our assay development program, as well as describe new natural product scaffolds that exhibit promising inhibitory activities against *T. vaginalis*.

4.2 Results and Discussion

4.2.1 Development of an Assay for Detecting *T. vaginalis* Inhibitors

Resazurin-based colorimetric assays are widely used in bioactive compound screening campaigns to identify substances that inhibit cell viability and proliferation under aerobic and anaerobic conditions.¹⁶⁸ This dye and its water soluble salts are readily

reduced by NADH to yield the red, fluorescent product resorufin. Despite its reported use for detecting *T. vaginalis* inhibitors, we were surprised to discover that, in our hands, this reagent was rather insensitive for the detection of low numbers of viable cells. We observed that under anaerobic assay conditions, a population of ~10,000 trichomonads per well in a 96-well microtiter plate was needed as a threshold to consistently signal a positive response for the presence of live *T. vaginalis*. Given that we established an inoculum of 40,000 trichomonads per well as an optimal starting point for assays, it meant that compounds affording modest (~75%) parasite-kill rates would be indistinguishable from more potent and potentially better agents (Figure 4.1). Therefore, we set about designing a new assay system that was more sensitive, as well as able to handle a wide-range of complex test substances (e.g., pure compounds and extracts containing colored or fluorescing natural products).

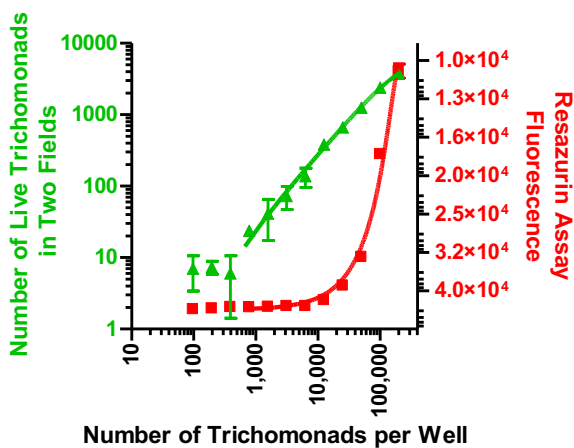


Figure 4.1. A comparison of the traditional resazurin fluorescence assay (red squares) and the newly developed imaging-based assay (green triangles). Using two fields per well, the Operetta's limit of detection was 1,000 trichomonades per well. The limit of detection is bounded on the lower end by whether a trichomonad appears in an image field. Resazurin assay was unable to detect less than 10,000 organisms per well.

One method deemed to be a promising alternative to the resazurin assay was high-content imaging.¹⁶⁹ We speculated that this approach would offer a more responsive tool for evaluating the live/dead-status of virtually every trichomonad within a sample population. However, we quickly recognized that live trichomonads were not compatible with imaging-based detection methods; the rapid movements of the flagellated parasites cause each cell to severely blur even with reasonably fast exposure times (10 ms). Accordingly, we identified a method to fix the trichomonads with glutaraldehyde followed by the application of a dual cell-staining system consisting of acridine orange (cell-permeable DNA stain) and propidium iodide (DNA stain that is not permeant to live cells) for live/dead determination (Figure 4.2). Initial tests conducted using the Operetta (PerkinElmer) high-content imaging system revealed that this assay was capable of detecting as few as one live or dead trophozoite per image field and was robust (*Z*-factor of 0.92). Moreover, this type of detection system was amenable to high-throughput screening of *T. vaginalis* viability, especially with UV/Vis-active natural products since the stored image files (i.e., two image fields recorded per well) could be manually inspected to identify potential false-positive and false-negative results.

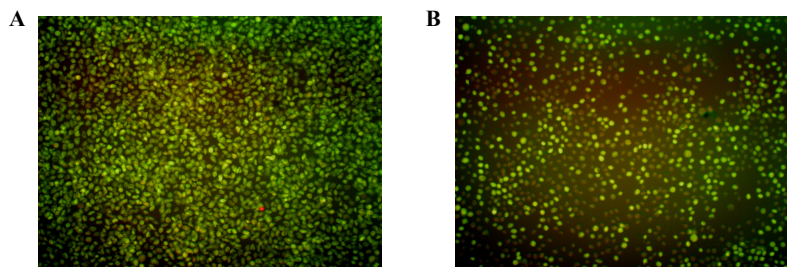


Figure 4.2. **A.** Sample field from the Operetta of a fixed and stained (0.5% glutaraldehyde, 2.5 μ M propidium iodide, and 2.5 μ M acridine orange) healthy growing population of trichomonas vaginalis at 17hr. One dead (red) trichomonad can be seen. **B.** Sample screening image from the Operetta showing partial inhibition from a fungal extract at 17hr.

4.2.2 Testing Purified Natural Products

To examine the probative capabilities of the new *T. vaginalis* imaging-based assay, a focused library of chemically diverse natural products was tested. The compound library consisted of 430 metabolites sourced by our research team from marine organisms, plants, bacteria, and fungi. An initial high-dose concentration (100 μ M) was chosen so as to afford the opportunity to evaluate several challenging screening scenarios, especially those involving potential false-positives brought about by compound precipitation and UV/Vis-interference. The imaging-based assay proved invaluable since all the data files for potential hits (i.e., compounds that provided inhibition exceeding that afforded by 25 μ M metronidazole) were immediately available for inspection to confirm that the number of live trichomonads had been reduced. This test revealed that 64 of the natural products we tested exhibited activities that were equal to or better than the positive control. The large number of active samples was not unexpected since our pure compound library largely contained bioactive substances that had previously demonstrated cytotoxicity toward mammalian cells and/or inhibited the proliferation of microorganisms. To refine

the list of natural products further, the hit compounds were screened at 25 μM , which resulted in a subset of 9 compounds that exhibited activities comparable to 25 μM metronidazole. These results also reinforced the need for a mammalian cell-based cytotoxicity counter screen to aid in the elimination of undesirable non-specific cellular toxins. Accordingly, the 9 hits were subsequently tested over a wide-range of concentrations extending two-orders of magnitude (0.25-25 μM) against both *T. vaginalis* and a normal mouse fibroblast (NIH/3T3) cell line. With these data in hand, the EC_{50} values for all compounds against both the parasite and mammalian cells were estimated. The EC_{50} values were used to calculate a selectivity index (SI) value [$\text{SI}_{3\text{T}3} = (\text{EC}_{50} \text{ for } 3\text{T}3 \text{ cells})/(\text{EC}_{50} \text{ for } T. \text{ vaginalis})$] for each of the bioactive substances (Figure 4.3). While the SI values revealed that most of the pure natural products were equipotent inhibitors of trichomonads and mammalian cells, one noted exception was 2-bromoascididemine, which exhibited modest selectivity ($\text{SI}_{3\text{T}3} = 14$). Thus, we established that the new assay was amendable to the testing of structurally diverse natural products across a wide range of concentrations; furthermore, it could reveal each substance's ability to selectively inhibit the target parasite.

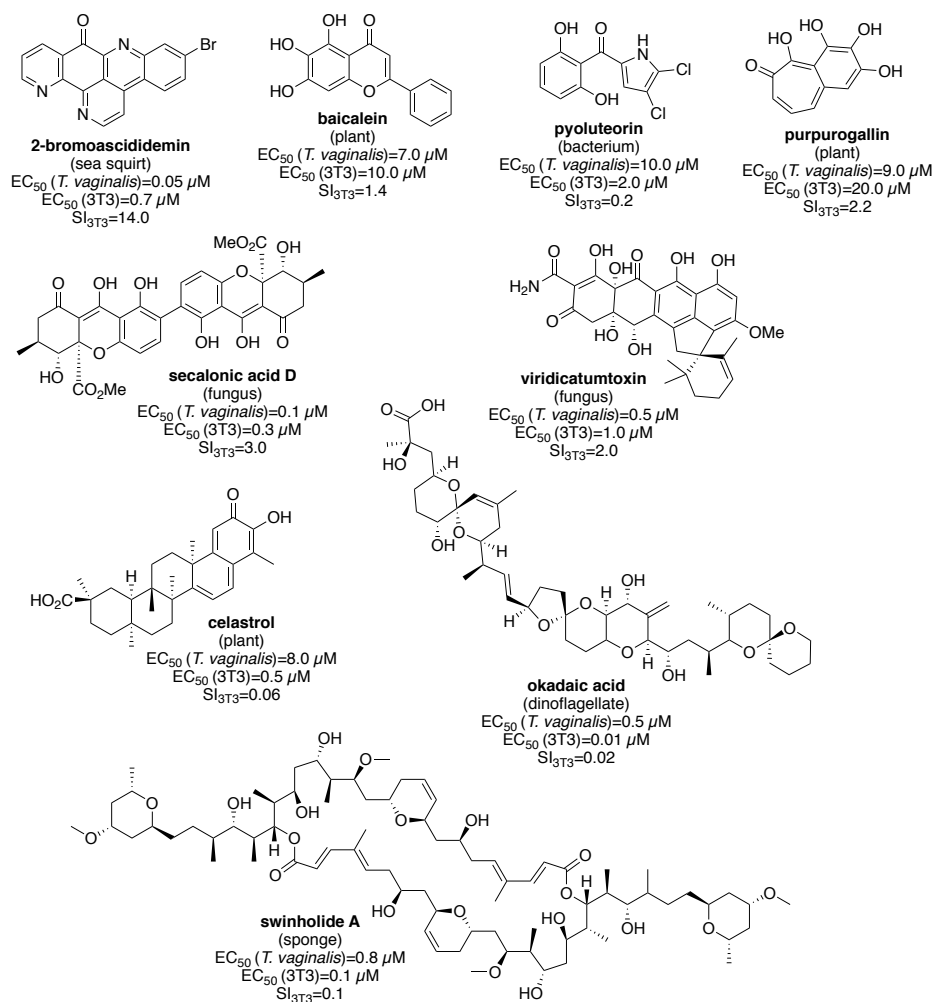


Figure 4.3. Nine of 430 pure natural products evaluated for SI_{3T3} values in initial pure compound screening against *T. vaginalis*. Compound sources were diverse and are shown under the compound names. EC₅₀ values were determined in *T. vaginalis* and 3T3 mammalian cells to obtain the SI_{3T3} values shown. Notably, 2-bromoascididemin exhibited a SI_{3T3} value of 14.0, which was much higher than any of the other compounds tested.

4.2.3 Testing Fungal Natural Product Extracts

The University of Oklahoma, Natural Products Discovery Group has generated a library of over 50,000 fungal extracts. Each extract consists of the organic residue obtained after a fungal isolate was cultured in small scale for 3 weeks on Cheerios breakfast cereal, extracted with ethyl acetate, and partitioned against water. For testing

purposes, a subset of 1,748 samples was selected for examination in the high-content-imaging assay system. For the first stage of testing, we determined that it was most efficient to screen extracts in duplicate at a single concentration (15 $\mu\text{g}/\text{mL}$). This provided 111 ‘hits’ that inhibited the viability of *T. vaginalis* at levels equal to or better than the inhibition achieved using 25 μM metronidazole. These ‘hit’ extracts were subjected to a second stage of testing over a range of concentrations (0.15-15 $\mu\text{g}/\text{mL}$), which yielded 71 samples that retained potent activity and generated sigmoidal concentration-response curves. During this period in the assay development process, we considered the value of introducing a second mammalian cell selectivity evaluation since fibroblasts cells, although capable of vigorous *in vitro* growth that made them simple to test, might not offer the level of cytotoxin sensitivity or cellular properties typically found at the site of *T. vaginalis* infections. Thus, Ect1/E6E7 normal-type cervical cells were chosen to provide a second point of reference during selectivity testing. Accordingly, the EC_{50} values for each extract’s parasite-inhibitory activity, as well as its cytotoxic effects toward Ect1/E6E7 cells were determined and the data were plotted as illustrated in Figure 4.4. This data visualization method provided a simple graphical tool to identify samples that offered the best selectivity for inhibiting parasites, yet exhibited limited toxicity toward mammalian cells. Thus, we proceeded to prioritize samples appearing in the upper right quadrant of the graph since those samples offered the best starting points for new bioactive compound discovery.

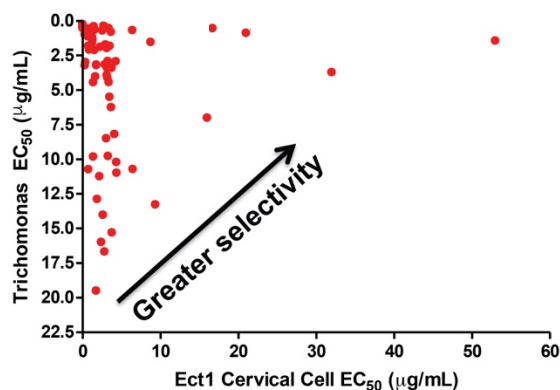


Figure 4.4. Selectivity index of 71 fungal crude extract library hits with activity better than 25 μM metronidazole.

4.2.4 Bioassay-Guided Purification and Testing of Natural Products from the *Fusarium* sp. Isolate B

A crude extract prepared from the *Fusarium* sp. isolate was subjected to bioassay-guided fractionation using silica gel vacuum liquid chromatography (VLC), HP20SS VLC, and C_{18} HPLC to afford the compound equisetin (**4.1**) (Figure 4.5). In the process of obtaining **4.1**, 5'-epiequisetin (**4.2**) (Figure 4.5) was also purified from the extract since its LC-ESIMS data had provided evidence that it was a likely structural analog of the bioactive constituent. The purified compounds were identified by comparison of their ^1H and ^{13}C NMR spectra and HRESIMS data to published values.¹⁷⁰ The absolute configurations of the tetramic acid protons of both compounds were determined using a previously described oxidative bond-cleavage and LC-ESIMS analysis methodology.¹⁷¹⁻
¹⁷² Testing of the purified compound immediately revealed a stark difference in their respective antitrichomonal activities; whereas **4.1** exhibited rather potent inhibitory effects ($\text{EC}_{50} = 3 \mu\text{M}$) with good selectivity ($\text{SI} = 33$), **4.2** was inactive at a concentration

as high as 25 μM . An examination of both metabolites revealed that the remarkable difference in their biological activities could be traced to the inversion of single stereocenter ($5'S$ in **4.1** and $5'R$ in **4.2**). Taking these data into consideration, as well as considering the fact that **4.1** was non-toxic to *L. acidophilus* at concentrations up to 50 μM (Table 4.3), there was ample reason to believe that further exploration of this unique class of natural products had the potential to provide additional bioactive analogs.

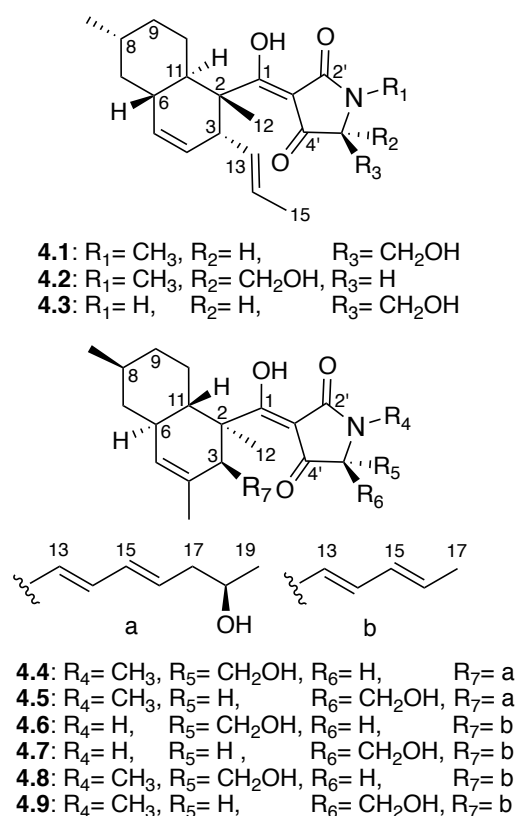


Figure 4.5. Structures of compounds **4.1-4.9**.

To facilitate the identification of other natural products containing a tetramate linked to a *trans*-decalin system, we turned to our extensive library of fungal isolates and their associated chemical data. This family of natural products has been reported from a

taxonomically diverse assemblage of fungi^{171, 173-177} and our records revealed that we had previously encountered these compounds from several fungal isolates in our collection. After considering the range of metabolites anticipated from each candidate isolate, a list of four fungi was chosen to serve as the subjects of chemically-guided targeted isolation process: (i) *Fusarium* sp. isolate C, (ii) *Penicillium* sp., (iii) *Alternaria* sp., (iv) *Phoma* sp. P34E5. Those efforts led to the purification of seven additional tetramic acid derivatives trichosetin (**4.3**)¹⁷⁵, pyrrolocin A (**4.4**),¹⁷¹ 5'-epipyrrolocin A (**4.5**) (new), beauversetin (**4.6**),¹⁷⁶ 5'-epibeauversetin (**4.7**) (new), phomasetin (**4.8**),¹⁷⁷ and 5'-epiphomasetin (**4.9**)¹⁷⁷ (Figure 4.5 and Table 4.3). Whereas the previously reported tetramic acid metabolites were identified based on comparisons of their mass spectrometry and spectroscopy data to published data, the new analogues became the foci of structure determination efforts.

Compound **4.5** (purified from the *Penicillium* sp. isolate) was obtained as a pale yellow solid. Its molecular formula was deduced from HRESIMS data to be C₂₇H₃₉NO₅ ([M-H]⁻ ions at m/z 456.2747, calcd for 456.2747). The ¹H (Table 4.1) and ¹³C (Table 4.2) NMR data revealed the presence of eight olefinic carbons, an oxygenated methylene, an oxygenated methine, and five methyl groups. Comparison of the 1D NMR data of **4.5** with compound **4.4** (isolated from the same fungus) indicated that the only noteworthy difference in the ¹³C NMR data for these two molecules was the carbon spin resonating at δ_C 68.1 in compound **4.4** now appeared at δ_C 67.4 in metabolite **4.5**. Combining this information with the bond-line structure established for **4.5** (based on analyses of its ¹H-¹H COSY, HSQC, and HMBC data summarized in Figure 4.4), it was proposed that the new natural product was the 5'-epimer of **4.4**.

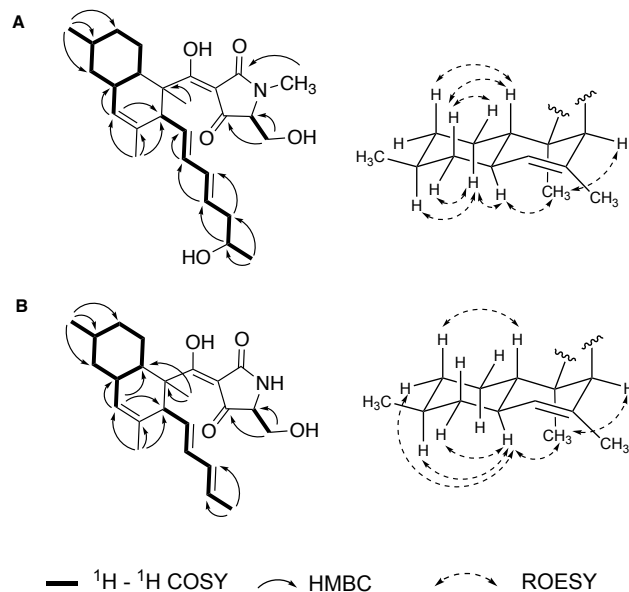


Figure 4.6. A: $^1\text{H} - ^1\text{H}$ COSY, HMBC and ROESY correlations of compounds **4.5**. B: $^1\text{H} - ^1\text{H}$ COSY, HMBC and ROESY correlations of compounds **4.7**.

Upon probing the stereochemical properties of compound **4.5**, the relative configuration of the decalin system was affirmed based on $^1\text{H} - ^1\text{H}$ ROESY correlations detected between the following sets of protons: Me-12 \leftrightarrow H-6 and H-3; H-10a \leftrightarrow H-6, H-7b, and H-8; as well as H-7a \leftrightarrow H-10b and H-11 (Figure 4.6A). The absolute configuration of this moiety was determined by comparing its CD spectrum with data obtained for similar metabolites. Specifically, the positive Cotton effects at 234 and 291 nm indicated that the absolute configuration of the decalin-ring portion of this structure was $2R,3S,6R,8S,11S$ (Figure 4.7).¹⁷¹ The absolute configuration of the hydroxy group on the olefinic side chain was determined as $18R$ by using the modified Mosher reaction (Figure 4.8).^{138, 171} The absolute configuration of C-5' was determined by oxidative bond cleavage of the tetramic acid ring followed by acid hydrolysis to yield *N*-Me-serine.¹⁷¹⁻¹⁷² Marfey derivatization of the *N*-Me-serine was performed and the product was analyzed by LC-ESIMS together with the derivatized hydrolytic products generated from *N*-Me-L

and D-serine standards. *N*-Me-D-serine was made by racemization of commercially available *N*-Me-L-serine using acetic acid and salicylaldehyde as described previously.¹⁷⁸⁻¹⁷⁹ The resulting amino acid residue was determined to be *N*-Me-L-serine, thus, the absolute configuration of **4.5** was assigned as 2*R*, 3*S*, 6*R*, 8*S*, 11*S*, 18*R*, 5'*S*.

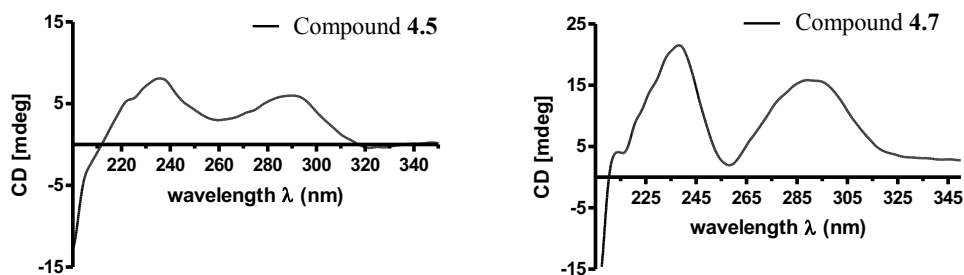


Figure 4.7. CD Spectra of compound **4.5** and **4.7**.

Compound **4.7** was purified as a pale yellow solid. Its molecular formula was deduced as $C_{24}H_{33}NO_4$ based on HRESIMS data. The 1H NMR spectrum of **4.7** (Table 4.1) showed thirty-one proton signals including five aromatic protons and four methyl spins. The ^{13}C NMR spectrum (Table 4.2) contained twenty-four carbon spins, which were later classified according to their multiplicities using HSQC. Those data indicated that **4.7** was structurally similar to **4.5**. Based on 2D NMR (1H - 1H COSY, HSQC, and HMBC) data (Figure 4.6B), the bond-line structure of **4.7** was confirmed to be the same as metabolite **4.6**, which indicated that two compounds were likely to be another set of 5' epimers.

Table 4.1. ¹H NMR data for compounds **4.4-7** in DMSO-d₆ (δ ppm).

No.	δ_{H} (J in Hz)			
	4.4 ^a	4.5 ^a	4.6 ^b	4.7 ^b
3	3.13, m	3.25, m	3.20, m	3.21, m
5	5.19, s	5.17, s	5.19, s	5.17, s
6	1.76, m	1.78, m	1.79, m	1.78, m
7	0.82, m	0.81, m	0.80, m	0.80, m
	1.79, m	1.77, m	1.77, m	1.77, m
8	1.49, m	1.48, m	1.48, m	1.48, m
9	1.02, m	1.00, m	1.01, m	0.97, m
	1.70, m	1.70, m	1.70, m	1.70, m
10	0.99, m	0.98, m	0.95, m	0.94, m
	1.89, m	1.90, m	1.93, m	1.93, m
11	1.57, m	1.57, m	1.54, m	1.53, m
12	1.33, s	1.36, s	1.33, s	1.35, s
13	5.22, m	5.16, m	5.15, m	5.11, dd (10.4, 14.7)
14	5.71, m	5.79, m	5.72, dd (10.5, 14.7)	5.78, dd (10.5, 14.7)
15	5.88, m	5.82, m	5.90, dd (10.5, 13.7)	5.86, dd (10.5, 13.7)
16	5.50, m	5.46, m	5.50, m	5.46, m
17	2.00, m	1.99, m	1.63, d (6.5)	1.62, d (6.5)
	2.09, m	2.08, m		
18	3.57, m	3.57, m	1.52, s	1.51, s
19	0.98, d (6.0)	0.98, d (6.0)	0.88, d (6.3)	0.88, d (6.3)
20	1.52, s	1.52, s		
21	0.88, d (6.5)	0.88, d (6.5)		
1'			9.25, s	9.05, s
5'	3.75, br s	3.71, m	3.80, br s	3.78, br s
6'	3.81, d (11.0)	3.81, m	3.63, dd (2.1, 11.0)	3.67, dd (2.1, 11.0)
	3.69, m	3.72, m	3.59, m	3.61, m
N-Me	2.92, s	2.91, s	2.92, s	

^aRecorded at 500MHz, ^bRecorded at 400MHz

Table 4.2. ^{13}C NMR data for compounds **4.4-4.7** in $\text{DMSO-}d_6$ (100 MHz, δ ppm)

No.	δ_{C}			
	4.4	4.5	4.6	4.7
1	195.9	196.5	199.0	199.0
2	49.0	49.6	49.2	49.5
3	49.2	48.6	48.5	48.1
4	131.3	131.9	131.4	131.6
5	126.4	126.1	126.0	125.7
6	39.1	39.2	38.7	38.7
7	42.4	42.5	42.1	42.2
8	33.3	33.4	33.0	33.0
9	35.8	35.9	35.5	35.5
10	28.1	28.1	27.6	27.7
11	39.4	39.9	39.3	39.3
12	14.0	14.2	13.4	13.5
13	130.9	131.4	130.5	130.6
14	132.7	133.0	132.1	132.5
15	131.8	132.0	131.1	131.6
16	130.9	130.5	128.0	127.7
17	42.7	42.8	17.8	17.9
18	66.3	66.3	22.2	22.3
19	23.5	23.5	22.5	22.5
20	22.6	22.7		
21	22.8	22.9		
2'	176.6	175.8	179.2	179.0
3'	100.9	101.6	99.4	99.8
4'	190.9	190.5	190.7	190.6
5'	68.1	67.4	63.2	62.9
6'	58.4	58.6	60.8	60.7
N-Me	27.2	27.3		

The relative configuration of the decalin moiety was deduced as $2R^*,3S^*,6R^*,8S^*,11S^*$ based on the key $^1\text{H-}^1\text{H}$ ROESY correlations between H-3 \leftrightarrow Me-12 and H-6, H-6 \leftrightarrow H-9b, as well as H-11 \leftrightarrow H-7a and H-9a (Figure 4.6B). The positive CD cotton effects of **4.7** at 234 and 289 nm indicated that the absolute configuration of the decalin moiety in **4.7** was the same as what occurred in **4.6** (Figure 4.7). Further analysis of the key ROESY correlations including H-13 and H-15 \leftrightarrow H-13 and Me-17 revealed both exocyclic olefins (Δ^{13} and Δ^{15}) had *trans* geometries. Using the same

oxidative bond cleavage and LC-ESIMS analysis method that had been applied to the tetramic acid moiety in metabolite **4.5**, the absolute configuration of C-5' were determined as *5'R* (**4.6**) and *5'S* (**4.7**), respectively.^{171-172, 180} Thus, the absolute configuration of **4.7** was determined to be *2R, 3S, 6R, 8S, 11S, 5'S*.

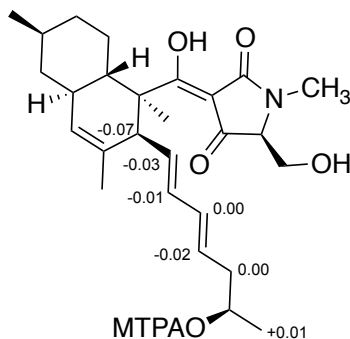


Figure 4.8. $\Delta\delta_{S-R}$ values obtained in pyridine- d_5 of the MTPA ester of compound **4.5**

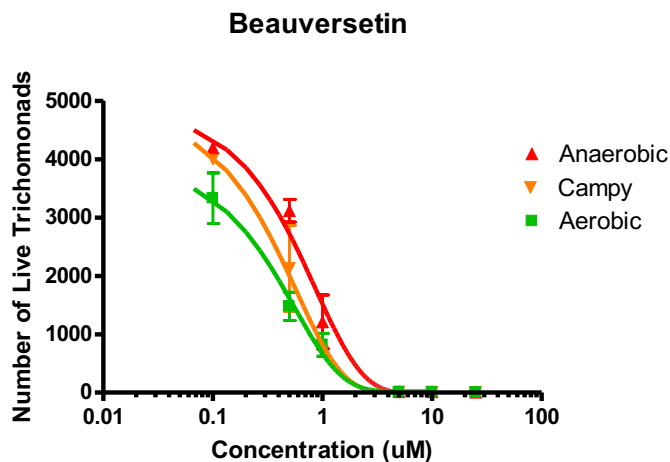


Figure 4.9. Effect of beauversetin on the growth of *Trichomonas vaginalis* in atmospheres of differing oxygen levels. Numbers shown are calculated from two fields in each well, three replicate wells per condition.

Table 4.3. Summary of tetramic acid derivatives: compound source, bioassay results and the corresponding selectivity index value.

Fungal Isolate Code	Isolate Identity from ITS	Compound	Assay (EC ₅₀ Data in μ M)				Selectivity Index Value (SI)		
			<i>T. vaginalis</i>	3T3 Mouse Fibroblast	Ect1 Normal Cervical	<i>L. acidophilus</i>	SI _{3T3}	SI _{Ect1}	SI _{L. acid}
Miller-1	<i>Fusarium</i> sp.	equisetin (4.1)	3.0	100	35	>50	33	12	>17
Cz-3	isolate B	5'-epiequisetin (4.2)	Inactive	nt	nt	nt	nt	nt	nt
Miller-26	<i>Fusarium</i> sp.	trichosetin (4.3)	2.5	30	34	>50	12	14	>20
SEA-3	isolate C								
KY6863 TV8-3	<i>Penicillium</i> sp.	pyrrolocin A (4.4)	0.060	6	10	>50	100	167	>833
		5'-epipyrrolocin A (4.5)	Inactive	nt	nt	nt	nt	nt	nt
Column L5 SEA-1	<i>Alternaria</i> sp.	beauversetin (4.6)	0.80	35	35	>50	44	44	>62
		5'-epibeauversetin (4.7)	Inactive	nt	nt	nt	nt	nt	nt
CA9310 TV8-3	<i>Phoma</i> sp.	phomasetin (4.8)	0.35	10	7	>50	29	20	>142
		5'-epiphomasetin (4.9)	Inactive	nt	nt	nt	nt	nt	nt

nt: not tested

4.2.5 Biological Evaluation of Tetramic Acid Derivatives

The antitrichomonal effects of the tetramic-acid-containing natural products were evaluated revealing an intriguing trend; whereas none of the 5'-epi compounds were active even at 25 μ M. Compounds **4.1**, **4.3**, **4.4**, **4.6** and **4.8** showed good activities with EC₅₀ values at or below single digit micromolar concentrations. The three most potent molecules, **4.4** (EC₅₀=0.060 μ M), **4.6** (EC₅₀=0.80 μ M), and **4.8** (EC₅₀=0.35 μ M) showed strongest activities and were among the most potent *T. vaginalis* inhibitors we had observed to date. To determine if the *Trichomonas*-inhibitory effects of the tetramic acid natural products were affected by the presence of oxygen, metabolite **4.6** was tested under aerobic, microaerophilic, and anaerobic conditions and it maintained potency under all the tested atmospheric conditions (Figure 4.9). Although some tetramic-acid-containing have been reported to possess antibacterial activities,¹⁸¹⁻¹⁸² none of the compounds that inhibited *T. vaginalis* inhibited *L. acidophilus* at 50 μ M (Figure 4.10). The selectivity of the tetramic-acid metabolites for *T. vaginalis* versus mammalian cells also appeared favorable (Table 4.3) with relatively large SI values for compound **4.4** (SI_{3T3}= 100, SI_{Ect1}=167). Based on these data, the tetramic-acid compounds exhibited

many promising characteristics that suggested the potential for further development as inhibitors of *T. vaginalis*.

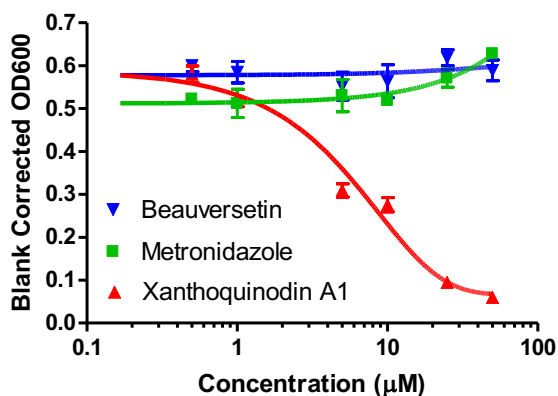


Figure 4.10. Effect of lead compounds from different classes and metronidazole on the growth of *Lactobacillus acidophilus* grown in an anaerobic atmosphere for 18hr. the tetramic acid beauversetin has no off-target effects, like metronidazole.

4.3 Conclusion and Future Directions

A rapid and sensitive assay for *T. vaginalis* was developed and used to screen a variety of substances varying from pure compounds to complex fungal extracts. In screening a portion of our library of fungal extracts, we were able to isolate and identify pure compounds showing selective activity in *T. vaginalis* when counterscreened in Ect1/E6E7 human cells. One promising class of compounds, the tetramic acid derivatives, performed favorably in both of these counterscreens, suggesting that they possess real selectivity in the inhibition of *T. vaginalis*. Compound **4.4** emerged as a rather promising metabolite based on its potent activity against the parasite ($EC_{50} = 0.060 \mu\text{M}$) and limited toxicity against both the human Ect1/E6E7 cervical cell line ($SI = 167$) and *L.*

acidophilus ($EC_{50} >0.060 \mu\text{M}$). Although our testing was limited to 9 tetramic-acid-containing natural products, the data suggested that modifications to the C-3 group of the *trans*-decaline system may provide additional opportunities for generating new analogues that have even further increased potency and selectivity. Further tests are now underway to test the tetramic-acid containing compounds as therapeutic agents against *T. vaginalis* infections.

4.4 Materials and Methods

4.4.1 General Experimental

Optical rotation measurements were made on an AUTOPOL[®] III automatic polarimeter. The LC-ESIMS analyses were performed on a Shimadzu UFLC system with a quadrupole mass spectrometer using a Phenomenex Kinetex C₁₈ column (3.0 mm × 75 mm, 2.6 μm) and MeCN-H₂O (0.1% HCOOH) gradient solvent system. HRESIMS spectra were measured using an Agilent 6538 Ultra High Definition (UHD) Accurate-Mass Q-TOF system. NMR spectra were obtained on Varian spectrometers (400MHz, 500 MHz for ¹H and 100, 125 MHz for ¹³C) using DMSO-*d*₆ (Aldrich) as solvents. HPLC was performed on a Waters System equipped with a 1525 binary HPLC pump coupled to a 2998 PDA detector with a Phenomenex C₁₈ column (21.2 × 250 mm or 10 × 250 mm, 5 μm particle size).

4.4.2 Culture of Organisms

Trichomonas vaginalis Donne (PRA-98) was purchased from the American Type Culture Collection (ATCC, Bethesda, MD). The superior medium for growth of the organism was found to be Keister's Modified TYI-S33 medium¹⁸³ with the pH adjusted to 6.0, the pH optimum for growth of *Trichomonas*. The medium was filter sterilized and aliquots stored frozen for future use. Medium preparation was found to be very particular with regard to ingredients, most especially with the bovine bile component, which was only successful when Sigma B8381 was used, as opposed to other bovine bile products. All assays mentioned in this publication were performed in this medium. Trichomonads were grown in a 37°C incubator in sealed screw cap tubes for propagation and in an air incubator (21% O₂, 0.04% CO₂), candle jar (10% O₂, 5% CO₂), or with BD GasPak EZ Campy (6-16% O₂, 2-10% CO₂) or EZ Anaerobe sachets (<1%

O₂, >13% CO₂) for 96-well plate assays, in order to reduce oxygen levels and add carbon dioxide, a stimulator of *Trichomonas* growth.¹⁸⁴

NIH/3T3 (CRL-1658) mouse fibroblast and Ect1/E6E7 (CRL-2614) normal human ectocervical cell lines were purchased from ATCC. NIH/3T3 cells were maintained in Dulbecco's Modified Eagle's Medium with 5% FetalClone III (Hyclone) and Ect1/E6E7 cells in keratinocyte-serum free medium (K-SFM, GIBCO-BRL 17005-042) or RPMI 1640 medium with 5% FetalClone III and supplemented with EGF (10 ng/mL Novoprotein #C029).

Lactobacillus acidophilus (ATCC 4356) was purchased from ATCC and grown on MRS agar and broth at 37°C under anaerobic conditions provided by BD GasPak EZ Anaerobe sachets.

4.4.3 *Trichomonas* Assay

A 250 µL cryopreserved (5% DMSO in liquid N₂) aliquot of *Trichomonas* was thawed rapidly at 37 deg. C and put into a screw cap tube containing 12 mL of pre-warmed Modified TYI-S33 medium. The sample was incubated for 24 hours at which point robust growth occurred and live trophozoites were counted. A typical count yielded >30X10⁶ cells per tube. Stock cultures were diluted into fresh medium to achieve 40,000 trophozoites per 100 µL of medium in each well of a 96-well plate. Into each well, a pin tool or pipet tip was used to dispense extracts or pure compounds dissolved in dimethyl sulfoxide (DMSO). Care was taken throughout to maintain the anaerobic nature of the medium and rapidity was observed (ideally 30 minutes or less time exposed to normal atmospheric conditions). *Trichomonads* tolerated a DMSO concentration of at least 1%. DMSO and 25 µM metronidazole negative and positive controls were included. The plates were placed in a humidified candle jar, the candle was lit, and the jar was sealed and placed in a 37 degrees' Celsius incubator overnight for a 17-hour

incubation for the candle jar condition. BD GasPak instructions were followed for that condition and plates incubated in either the provided pouch or the BD Anaerobe Container System. After 17 hours, the plates were removed and 100 μ L per well of room temperature *Trichomonas* and *Giardia* assay and fixation (TGAF) solution was added per well. TGAF solution is a PBS based solution we developed that contains 1% glutaraldehyde, 5 μ M propidium iodide, and 5 μ M acridine orange (HCl salt). This solution was found to be stable for many months kept at room temperature and even longer when kept refrigerated. The plates were shaken in a plate reader for thirty seconds to disperse any clumps and placed in the incubator for three hours for staining and fixation to occur. The plates were then quantitatively imaged using the Perkin Elmer Operetta and the Harmony 3.5.1 software package. Quantification involved the software identifying all trophozoites and subtracting live (green only) from dead (green and red) using a propidium iodide threshold of less than 6500 units; this threshold was determined to enable the assessment of membrane integrity and thus live/dead determination.

For comparison, a traditional resazurin based assay using the plate reader was also performed.¹⁶⁷ Known amounts of trichomonads were added to each well and then 10 μ L of a 0.1 mg/mL resazurin stock in PBS was added to each well and incubated for one hour at room temperature in the dark. At 1 hr, plates were shaken and read on a fluorescence plate reader (Tecan Infinite M200) with a 556 nm excitation wavelength and an emission of 590 nm.

4.4.4 Mammalian Cell Cytotoxicity Assay

Mammalian cell assays were performed as described previously¹⁸⁵ and viability determined by MTT assay¹⁸⁶ or by a Calcein AM and Hoechst 33342 live cell area assay on the Operetta. This assay was performed by adding 5 μ L to each well of a 1:5 dilution in PBS of a 40

uM calcein AM and 160 uM Hoechst 33342 DMSO stock, incubating the plate for 30 minutes and reading the plate on the Operetta. Harmony software was used to calculate the live cell area by finding all Hoechst-labeled nuclei and assigns live or dead assessments to each cell based on a threshold of green fluorescence. Live cells are those with esterases still capable of cleaving the AM group from calcein AM, and glow bright green.

4.4.5 *Lactobacillus Acidophilus* Viability Assays

A colony of *L. acidophilus* was taken to 10 mL of MRS broth and vortexed. 100 μ L was added to wells of a 96-well plate. Test compounds in DMSO (0.05% final concentration DMSO) were added to the wells. The plate was read on a microplate reader at 600 nm to establish a baseline value and the plate incubated overnight in a 37 deg. C incubator. After 18 hours, the plate was read again and the baseline value subtracted to generate a change in optical density value.

4.4.6 Tetramic Acid Producing Fungal Strains and Fermentation

Five fungal isolates coded Miller-1 Cz-3, Miller-26 SEA-3, KY6863 TV8-3, Column L5 SEA-1, CA9310 TV8-3, and were identified as *Fusarium* sp. isolate B, *Fusarium* sp. isolate C, *Penicillium* sp., *Alternaria* sp., and *Phoma* sp. respectively based on their ribosomal internal transcribed spacer (ITS) sequence data (GenBank accession numbers MK401898, MK401899, MK401895, MK401896, and MK401897, respectively). Fungal strain Miller-1 Cz-3, Miller-26 SEA-3, KY6863 TV8-3 and CA9310 TV8-3, were fermented on a solid-state medium composed of Cheerios breakfast cereal supplemented with 0.3% sucrose solution for four weeks at room temperature (25°C). Fungal isolate Column L5 SEA-1 was inoculated into 16 L of PDB media

(10 g/L dried mashed potato, 5g/L glucose) supplemented with 2 g/L NaNO₃ and cultured for 9 days on a shaker.

4.4.7 Purification of Tetramic Acid Derivatives

The fungal cultures of Miller-1 Cz-3 were homogenized and extracted three times with EtOAc. The resulting EtOAc extract (25.0 g) was subjected to silica gel vacuum column chromatography (VLC) with elution steps of 1:1 hexane/DCM, DCM, 10:1 DCM/MeOH, and MeOH, yielding four fractions. The 10:1 DCM/MeOH fraction was subjected to HP20SS VLC and eluted with a step gradient of MeOH in water (30%, 50%, 70%, 90% and 100%), yielding five fractions. The 90% MeOH fraction from HP20SS VLC was further fractionated by preparative C18 HPLC (250 mm x 21.2 mm, 5 μm) with a MeCN-H₂O gradient containing 0.1% HCOOH (70:30 to 100:0) to yield compounds **4.1** (56 mg) and **4.2** (18.9 mg).

The fungal cultures of Miller-26 SEA-3 were homogenized and extracted three times with EtOAc. The resulting EtOAc extract (14.0 g) was subjected to silica gel VLC with elution steps of 1:1 hexane/DCM, DCM, 10:1 DCM/MeOH, and MeOH, yielding four fractions. The 10:1 DCM/MeOH fraction was subjected to HP20SS VLC and eluted with a step gradient of MeOH in water (30%, 50%, 70%, 90%, 100%), yielding five fractions. The 70% MeOH fraction from HP20SS VLC was further fractionated by isocratic preparative C₁₈ HPLC (250 mm x 21.2 mm, 5 μm) with MeOH-H₂O (75:25) to yield compound **4.3** (50 mg).

The fungal cultures of KY6863 TV8-3 were homogenized and extracted three times with EtOAc. The resulting EtOAc extract (31.0 g) was subjected to silica gel VLC with elution steps of 1:1 hexane/DCM, DCM, 10:1 DCM/MeOH, and MeOH, yielding four fractions. The 10:1 DCM/MeOH fraction was subjected to HP20SS VLC and eluted with a step gradient of MeOH in water (30%, 50%, 70%, 90%, 100%), yielding five fractions. The 90% MeOH fraction from

HP20SS VLC was further fractionated by preparative C₁₈ HPLC (250 mm x 21.2 mm, 5 μm) with a MeOH-H₂O gradient containing 0.1% HCOOH (85:15 to 100:0) to yield compounds **4.4** (50 mg) and **4.5** (15mg).

epipyrrolocin A (4.5): pale yellow plate; $[\alpha]_D^{20}$ 238 (c 0.1, MeOH); UV (MeOH) λ_{\max} (log ϵ) 238 (2.37), 265 (0.42), 295 (0.77); CD (MeOH) λ_{\max} ($\Delta\epsilon$) 234 (8.1), 291 (6.1); ¹H and ¹³C NMR data, see Tables 2 and 3; HRESIMS m/z 456.2747 [M-H]⁻ (calcd for 456.2747).

Fungal culture broth of Column L5 SEA-1 was partitioned three times with EtOAc to obtain 3.0 g of organic residue. The organic residue was subjected to HP20SS VLC and eluted with a step gradient of MeOG in water (30%, 50%, 70%, 90%, 100%), yielding five fractions. The 90% MeOH fraction was further separated by preparative C₁₈ HPLC (250 mm x 21.2 mm, 5 μm) with a MeOH-H₂O gradient containing 0.1% HCOOH (90:10 to 100:0), yielding a total of six fractions (Fr. 1-6). Fractions 2 and 4 were further purified by isocratic semi-preparative C₁₈ HPLC (250 mm x 10 mm, 5 μm) with MeCN-H₂O containing 0.1% HCOOH (80:20) to yield compounds **4.6** (67mg) and **4.7** (7.5mg).

epibeauversetin (4.7): pale yellow plate; $[\alpha]_D^{20}$ 409 (c 0.17, MeOH); UV (MeOH) λ_{\max} (log ϵ) 236 (4.39), 287 (4.11); CD (MeOH) λ_{\max} ($\Delta\epsilon$) 232 (8.2), 285 (9.8); ¹H and ¹³C NMR data, see Tables 2 and 3; HRESIMS m/z 398.2337, [M-H]⁻ (calcd for C₂₄H₃₂NO₄, 398.2337).

The fungal cultures of CA9310 TV8-3 were homogenized and extracted three times with EtOAc. The resulting EtOAc extract (38.0 g) was subjected to silica gel VLC with elution steps of 1:1 hexane/DCM, DCM, 10:1 DCM/MeOH, and MeOH, yielding four fractions. The 10:1 DCM/MeOH fraction was subjected to HP20SS VLC and eluted with a step gradient of MeOH in water (30%, 50%, 70%, 90%, 100%), yielding five fractions. The 70% MeOH fraction from HP20SS VLC was further fractionated by isocratic preparative C₁₈ HPLC (250 mm x 21.2 mm, 5

μm) with MeOH-H₂O containing 0.1% HCOOH (85:15) to yield compounds **4.8** (140 mg) and **4.9** (4 mg).

4.4.8 Preparation of MTPA Ester

Compound **4.5** (0.5 mg) was dissolved in pyridine-*d*₆ and transferred into clean NMR tubes. The (*R*)- α -methoxy- α -trifluoromethyl-phenylacetyl chloride [(*R*)-MTPA-Cl] (5 μl) was added into sample under an N₂ gas stream. After mixing, it was incubated at 40 °C in a water bath and monitored every 2 hours by ¹H-NMR. ¹H-NMR data of the (*S*)-MTPA ester derivative (500 MHz, pyridine-*d*₅): δ_{H} 6.38 (1H, m, H-14), 6.07 (1H, m, H-15), 5.90 (1H, m, H-16), 5.69 (1H, m, H-13), 3.87 (1H, m, H-12), 2.37 (1H, m, H-17), 2.10 (1H, m, H-17), 1.20 (3H, d, 6.5, CH₃-19).¹³⁸

The same method was used to yield (*R*)-Mosher esters derivative using (*S*)- α -methoxy- α -trifluoromethyl-phenylacetyl chloride [(*S*)-MTPA-Cl].

¹H-NMR data of the (*R*)-MTPA ester derivative (500 MHz, pyridine-*d*₅): δ_{H} 6.39 (1H, m, H-14), 6.07 (1H, m, H-15), 5.92 (1H, m, H-16), 5.72 (1H, m, H-13), 3.94 (1H, m, H-12), 2.37 (1H, m, H-17), 2.10 (1H, m, H-17), 1.19 (3H, d, 6.5, CH₃-19).

4.4.9 Cleavage of the Tetramic Acid Ring and Marfey's Reaction

Sample (20 mg) was dissolved in methanol (0.6 mL) followed by addition of 1 M NaOH (0.075 mL) and a NaOCl solution (available chlorine 10–15%, 0.35 mL). The mixture was stirred at room temperature for 8 h and then it was quenched by 1 M aqueous Na₂SO₂ (3 mL). The mixture was neutralized by addition of 1 M HCl. After removal of the solvent, the residue was diluted with H₂O, and then the resulting mixture was extracted with ethyl acetate. The organic layer was dried in vacuo. The residue was dissolved in 6 M HCl (500 μl) and then

heated at 110°C overnight. The hydrolysate was dried under a stream of N₂ and then treated with 1 M NaHCO₃ (40 µl) and 1% FDAA/acetone (200 µl) at 70°C for 1 h. The reactants were neutralized with 1 M HCl (40 µl), and diluted with MeCN (400 µl) prior to LC-MS analysis. FDAA derivatives of L-Ser/N-Me-L-Ser and D-Ser/N-Me-D-Ser standards were prepared in a similar manner. Aqueous solutions of serine standards (50 mM, 50 µl) were reacted, neutralized, and diluted following the same procedure.¹⁷¹⁻¹⁷²

Chapter 5. Cholinesterase Inhibitory Arisugacins L-Q from a *Penicillium* sp. Isolate Obtained through a Citizen Science Initiative and their Activities in a Phenotype-Based Zebrafish

This chapter was adapted from a manuscript which is currently being prepared for submission in 2019. The authors are Wentao Dai, Imelda T. Sandoval, Shengxin Cai, Kaylee A. Smith, Richard Glenn C. Delacruz, Kevin A. Boyd, Jessica J. Mills, David A. Jones and Robert H. Cichewicz.

The work presented in this chapter was conducted as follows: Imelda T.Sandoval conducted the bioassay, Wentao Dai performed extraction, purifications and structure elucidation of compounds 5.1-5.14.

5.1 Introduction

The cholinesterases are an important class of enzymes that catalyze the hydrolysis of ester bond linkages in choline-containing molecules. This group of enzymes is further subdivided into two major families: acetylcholinesterase (AChE) and butyrylcholinesterase (BuChE) whose names reflect the enhanced rates at which these enzymes hydrolyze acetylcholine (ACh) and butyrylcholine, respectively.¹⁸⁷ Biomedically, acetylcholinesterases play several important roles revolving around their abilities to rapidly hydrolyze ACh (a key neurotransmitter) and thus terminate nerve signal transmission. Consequently, the therapeutic inhibition of AChE using drugs such as donepezil, rivastigmine and galantamine is an effective clinical strategy for symptomatic relief in several types of pathologies including Alzheimer's disease,⁸¹⁻⁸² Parkinson's disease,⁸³ myasthenia gravis,⁸⁴ and glaucoma⁸⁵.

In addition to the treatment of human diseases, AChE inhibitors have found widespread uses as insecticides (e.g., aldicarb, carbofuran), fungicides (e.g., butylate, pebulate) and herbicides (e.g., ferbam, mancozeb).¹⁸⁷ Many types of plant-derived natural products have been identified as AChE inhibitors with additional reports emerging from fungi and marine source suggesting that nature is a valuable resource to mine for AChE inhibitor scaffolds.¹⁸⁸⁻¹⁹⁴ Among the handful of reported fungus-derived natural products that disrupt AChE activity, the territremes, arisugacins, and terreulactones stand out as a structurally distinct group of meroterpenoids that exhibit potent and selective AChE inhibition. To date, 7 territremes,^{86-87, 93, 95} 12 arisugacins,^{92, 97-98, 101-102} and 6 terreulactones^{95, 103, 105} have been reported with the most potent inhibitors exhibiting IC₅₀ values extending into the low nanomolar range.^{92, 104}

Zebrafish have been used as a model organism for phenotype-driven drug discovery since 2000.¹⁹⁵⁻¹⁹⁶ As one of the few groups to investigate chemical libraries in an unbiased phenotype screen, we have shown from previous work that we can utilize zebrafish to assign mechanism of action, in juxtaposition with zebrafish genetics, to a class of compounds with unknown bioactivity.¹⁹⁷ Zebrafish have several desirable characteristics that make them ideal as chemical testing platforms including high fecundity, small-size (amenable to use in microtiter plate formats), and transparent embryos that rapidly develop *ex utero*. This latter point is important because it allows for the visualization and scoring of diverse phenotypes, which can provide critical insights into the mechanistic effects of many chemicals. Compared to simpler cell-based assays, these complex phenotypic cues can help with the early-stage prioritization of hits and provide an additional tool for filtering through subtle, but meaningful differences in how molecules behave in intact organisms. Notably, zebrafish share a high degree of genetic and physiological similarity with humans; approximately 70% of human genes have an orthologue in

zebrafish, enabling drug screening in zebrafish to have direct therapeutic relevance to a host of human diseases.^{196, 198-204}

Given the immense number of mechanistically uncharacterized bioactive compounds produced by fungi, a collaborative effort was launched to assess a pilot-scale set of fungal natural product extracts as a resource for integrating into a zebrafish-focused bioactive compound discovery program. In the course of this study, an extract prepared from a *Penicillium* sp. isolate was found to induce a paralysis phenotype in zebrafish embryos, indicative of central nervous system (CNS) modulators,²⁰⁵ and it was prioritized for further investigation. Bioassay-guided investigation led to the identification of 14 meroterpenoids, including 6 previously undescribed natural products. The purification, structure determination, and biological characterization of the metabolites, including results from the zebrafish-based phenotype screen are described in this report.

5.2 Results and Discussion

5.2.1 Zebrafish-Based Phenotype Screen of Fungal Crude Extract

Studies were performed using a circumscribed set of 384 fungal extracts prepared from fungi secured from the Great Lakes (MI, USA) and soil samples from Lawton (OK, USA) that were obtained through the Citizen Science Soil Collection Program operated out of the University of Oklahoma.¹³¹ Whereas a majority of the extracts had no effect on normal development, 46 samples (12%) resulted in a wide range of viable phenotypes that included growth arrest, head and tail defects, edema, and behavioral abnormalities (Figure 5.1). In addition, 45 crude extracts (12%) were lethal to the embryos (Figure 5.1). To examine this further, a dose curve analysis from 10 to 0.1 $\mu\text{g/ml}$ was performed for 34 samples that caused

death, resulting in 16 extracts that gave specific developmental abnormalities at lower concentrations (Table C2). This demonstrates that embryonic lethality as an assay outcome should not be dismissed, as it can lead to viable phenotypic aberrations upon optimization of experimental conditions such as dosing and time of treatment.

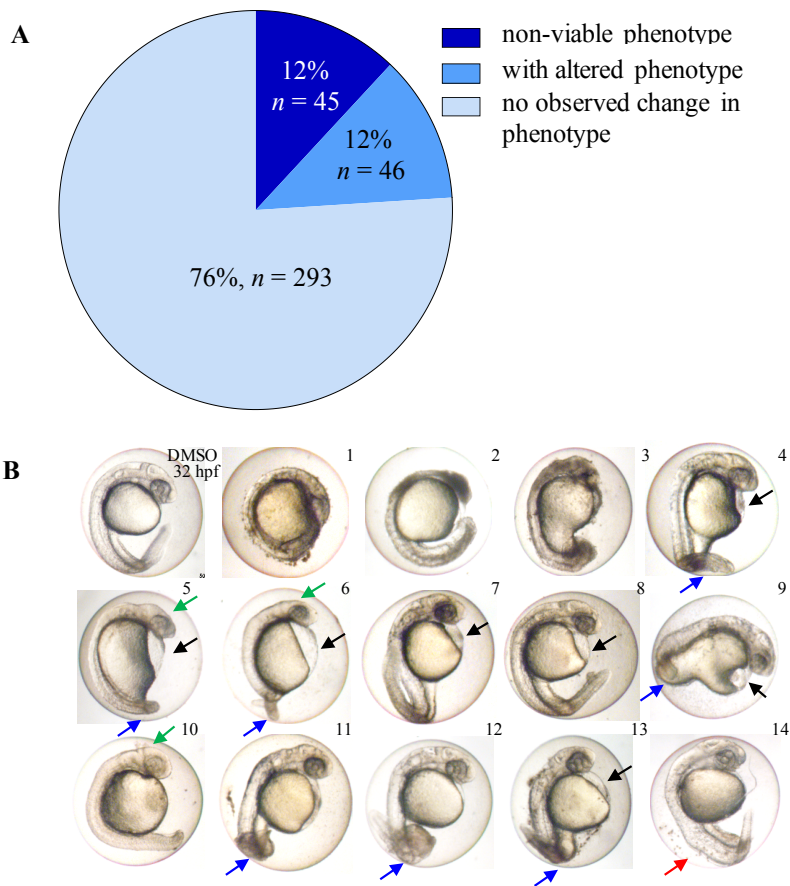


Figure 5.1. Zebrafish phenotype screen reveals bioactive fungal samples. **A.** Distribution of assay outcomes from screening of fungal extracts. **B.** Examples of phenotypes observed include growth arrest (1-3), edema (black arrow), abnormal head (green arrow) and tail (blue arrow) development and undulated notochord (red arrow).

5.2.2 Purification Natural Products from the *Penicillium* sp. Isolate

Fungal extracts that affected motility were prioritized because of its clinical relevance, as this phenotype often indicates perturbation of the CNS.²⁰⁶ We chemically investigated an extract

derived from a *Penicillium sp.* isolate, which induced paralysis as shown by very limited movement of zebrafish embryos when stimulated externally with a tip, similar to phenotype resulting from exposure to azinphos-methyl (AZM), a known AChE inhibitor (Figure 5.2, Figure C1). Further purification of the crude extract, using paralysis as assay readout, revealed fungal metabolites belonging to the arisugacin family of compounds.

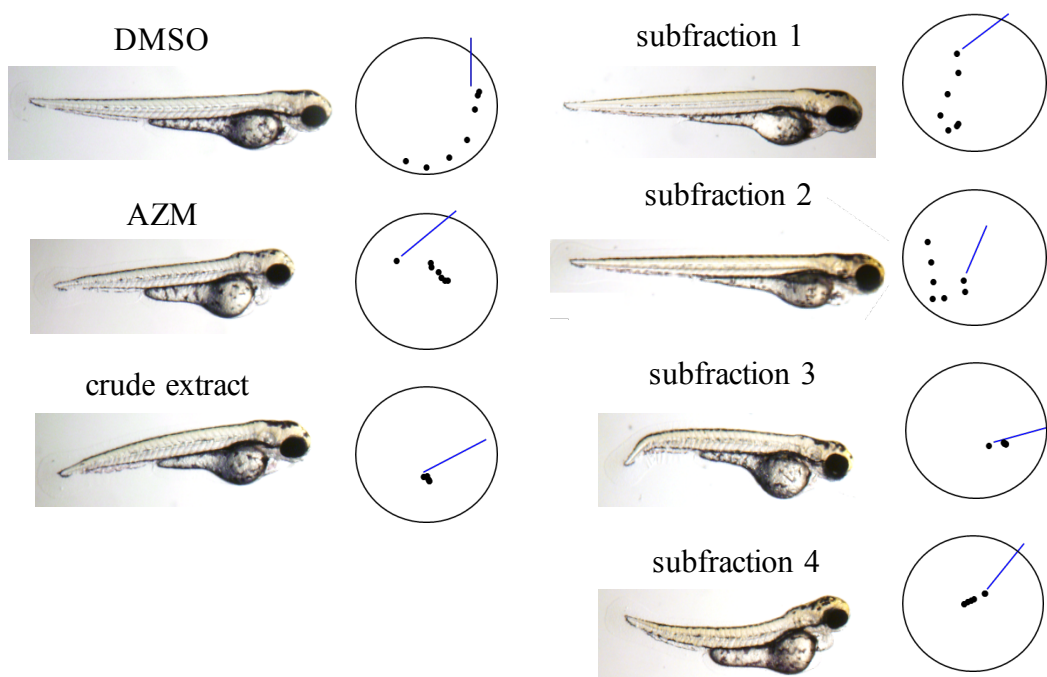


Figure 5.2. Zebrafish phenotype screen reveals fungal extracts that impaired motility. Morphological phenotype exhibited by crude extract and representative subfractions that impaired motility comparable to phenotype resulting from treatment with known AChE inhibitor, AZM (1st, 3rd panels). DMSO served as negative control. Traces summarizing movement of zebrafish embryos (black dot) in response to external stimulus (represented by a blue line) are shown in panels 2 and 4.

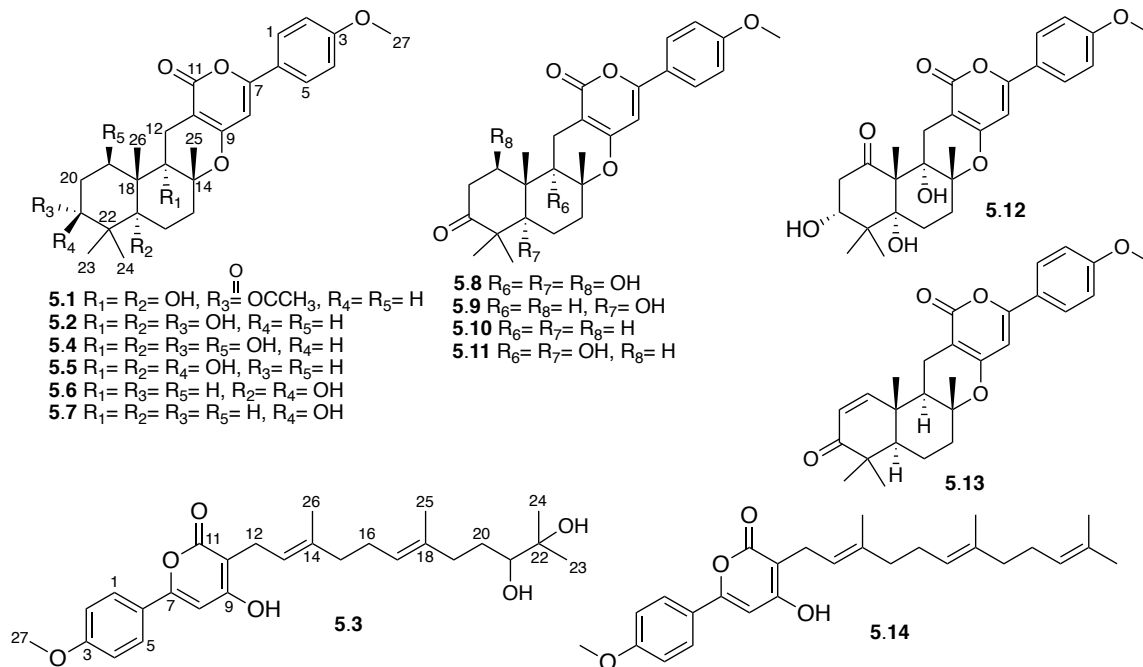


Figure 5.3. Structures of compounds **5.1-5.14**.

For chemical studies, the *Penicillium* sp. isolate was grown on Cheerios breakfast cereal and the resulting mycelial mass was extracted with EtOAc, affording a crude extract that was subjected to bioassay-guided fractionation. This resulted in the purification of metabolites **5.1-5.3**, which were identified as arisugacin D (**5.1**), arisugacin J (**5.2**), and arisugacin I (**5.3**) (Figure 5.3) based on comparisons of their 1H NMR spectra, optical rotation values, and LC-ESIMS data to authentic samples and published data.^{101, 207} Both **5.1** and **5.3** have been reported as selective AChE inhibitors with IC_{50} values of 2.5 μM and 3.5 μM , respectively.²⁰⁷ This initial observation, combined with the impaired motility phenotype from our zebrafish screen, inspired us to further pursue the structure identification of the compounds contained within the bioactive extract because other related structures such as arisugacin A and B, as well as territrem A and B have shown rather high levels of selectivity for AChE with IC_{50} values ranging from 1 – 25.8 nM.²⁰⁸ With LC-ESIMS evidence for the presence of several structurally related metabolites in the

Penicillium sp. extract including several compounds that could not be readily dereplicated, we decided that further investigation of the bioactive components present in this sample was warranted in the hope of securing additional potent bioactive congeners (Figure 5.3).

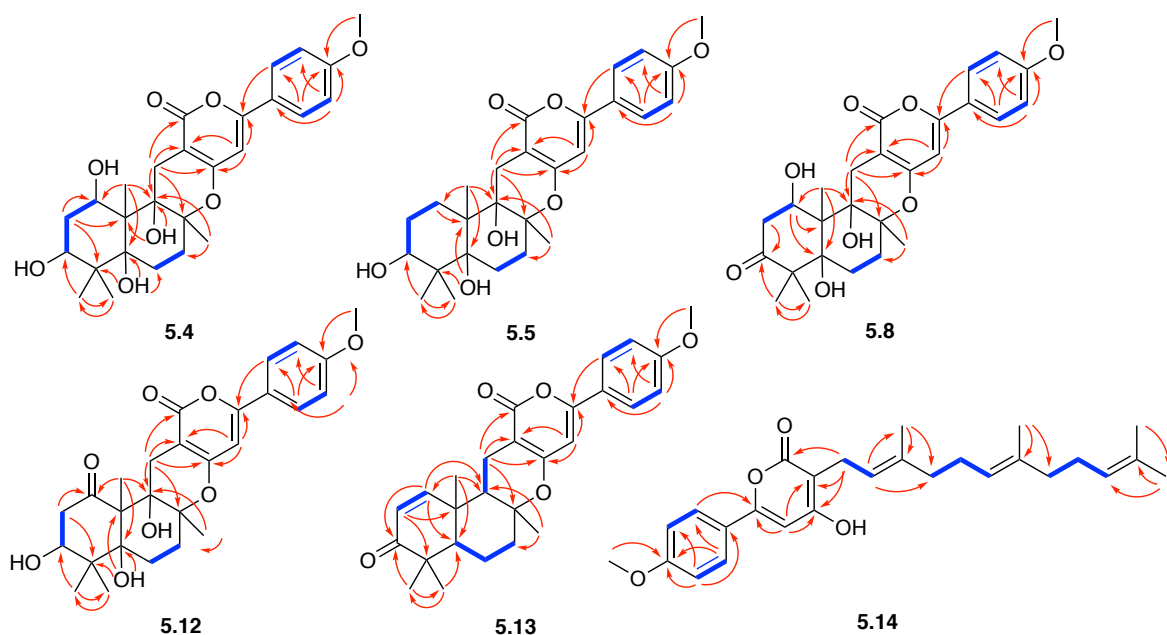


Figure 5.4. ^1H - ^1H COSY (blue bold lines) and key HMBC (red arrows) correlations of compounds **5.4-5.5**, **5.8**, **5.12-5.14**.

Arisugacin L (**5.4**) was obtained as a white amorphous powder and its molecular formula was established as $\text{C}_{27}\text{H}_{34}\text{O}_8$ based on HRESIMS data that featured ions at m/z 487.2341 $[\text{M} + \text{H}]^+$, and 509.2155 $[\text{M} + \text{Na}]^+$. This corresponded to 11 units of unsaturation. An inspection of the ^1H and ^{13}C NMR data for **5.4** (Tables 5.1 and 5.2) revealed that this compound shared many structural features with known metabolite **5.2**.¹⁰¹ Considering that **5.4** contained one additional oxygen atom, further inspection of the data revealed that C-19 in **5.4** was more deshielded (δ_{C} 65.4) suggesting that it was attached to a hydroxy group. Analysis of the HMBC and COSY data

provided substantiation for the structure of the remaining portions of the molecule confirming that **5.4** was a new tetrahydroxy arisugacin (Figure 5.4).

Turning to address the orientation of the stereogenic carbon atoms in **5.4**, ^1H - ^1H ROESY correlation data played a key role in establishing the metabolite's relative configuration (Figure 5.5). Two distinct sets of ROESY correlations were observed arising from the hydrogens occupying opposite faces of the molecule's dodecahydro-1*H*-benzo[*f*]chromene core. Specifically, ROESY correlations among H₃-26 ↔ H₃-24, H₃-25, and H-12 (δ_{H} 2.71); H₃-25 ↔ H-16 (δ_{H} 1.94); and H₃-24 ↔ H-21 provided evidence that those atoms were located on one face of molecule. A second set of ROESY correlations among H₂-12 (δ_{H} 3.14) ↔ H-19 and OH-13, as well as between H₃-23 ↔ OH-17, H-21, and H-16 (δ_{H} 1.73) indicated those atoms occupied the opposite face of the molecule. This left one hydrogen atom, H-21, whose relative orientation remained ambiguous; however, an examination of its splitting pattern (double doublet) and coupling constant data ($J = 2.3$ and 2.8 Hz), indicated this hydrogen occupied an equatorial position. Taking these data into consideration, the relative configuration of **5.4** was assigned to be $13S^*,14R^*,17R^*,18S^*,19R^*,21R^*$, which is similar to several known arisugacin analogues containing three *trans*-fused six-member ring systems.^{101, 104, 207} Using a modified Mosher esterification strategy, C-21 was determined to have an *R* configuration (Figure 5.6), thus, the absolute configuration of **5.4** was determined to be $13S,14R,17R,18S,19R,21R$.

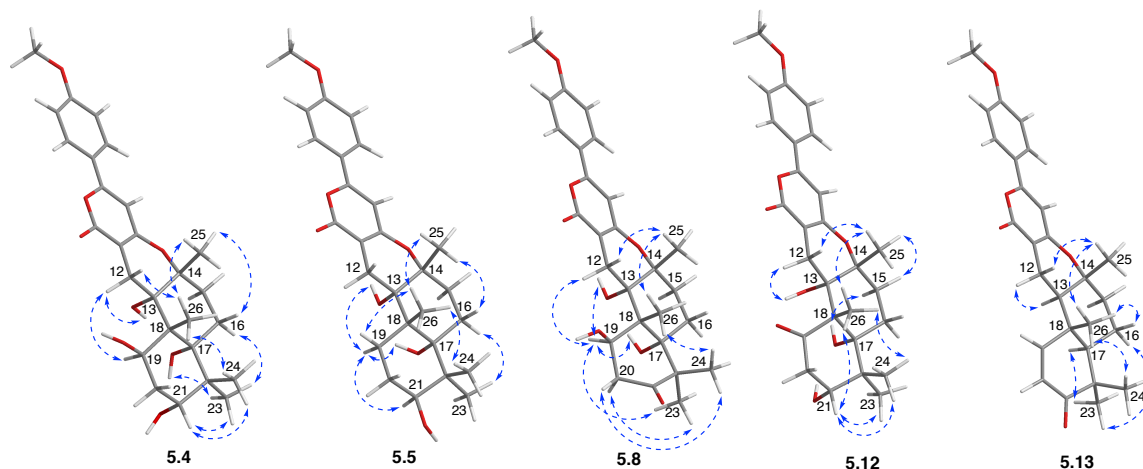


Figure 5.5. 3D molecular models of compounds **5.4-5.5**, **5.8**, **5.12-5.13** showing key ROESY correlations (blue dashed arrows).

Arisugacin M (**5.5**) was obtained as a white amorphous powder. The molecular formula was assigned as $C_{27}H_{34}O_7$ based on its HRESIMS data ($[M+H]^+$ ion at m/z 471.2393; $[M+Na]^+$ ion at m/z 493.2210) indicating 11 units of unsaturation. An analysis of the ^{13}C NMR and HSQC data revealed that the hydroxyl group observed on C-19 in **5.4** was missing in **5.5** and instead, a new methylene signal was present (δ_C 26.2). This conclusion was supported by an analysis of the HMBC and COSY data, which also confirmed the proposed bond-line structure of **5.5** (Figure 5.4).

1H - 1H ROESY correlation data were instrumental for solving the relative configuration of **5.5** (Figure 5.4). Once again, two sets of correlations emerged based on which face of the dodecahydro-1*H*-benzo[*f*]chromene scaffold that the hydrogen atoms occupied. The first series of observed correlations included $H_3-26 \leftrightarrow H_3-25$, H_3-24 , and H-19 (δ_H 1.11), as well as between $H_3-25 \leftrightarrow H-16$ (δ_H 1.87). On the opposite face of **5.5**, ROESY correlations were observed between H-19 (δ_H 2.11) \leftrightarrow OH-13, H-21, and OH-17, as well as $H_3-23 \leftrightarrow H-16$ (δ_H 1.61). These data pointed toward a $13S^*,14R^*,17R^*,18S^*,21S^*$ relative configuration. The absolute

configuration of C-21 was next determined to be *S* by modified Mosher's method (Figure 5.6), thus the overall absolute configuration of **5.5** was assigned as 13*S*, 14*R*, 17*R*, 18*S*, and 21*S*.

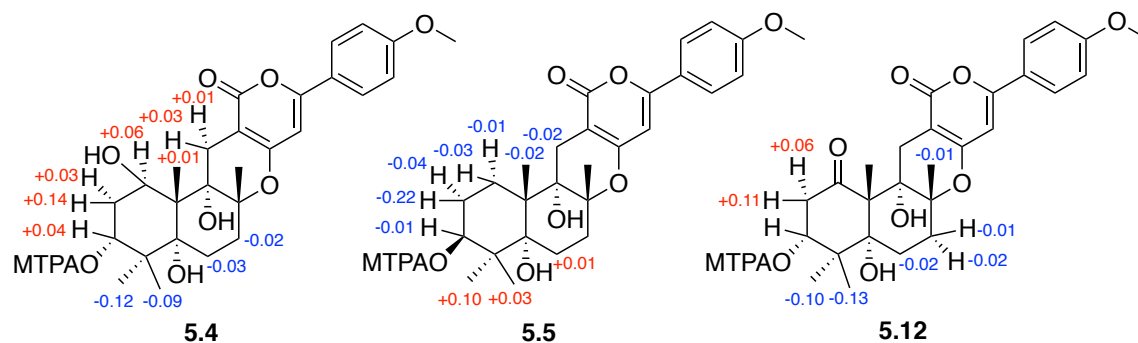


Figure 5.6. $\Delta\delta_{S-R}$ values obtained in pyridine- d_5 of the MTPA ester of compounds **5.4**, **5.5**, and **5.12**.

Arisugacin N (**5.8**) was obtained as a white amorphous powder. The molecular formula was established to be $C_{27}H_{32}O_8$, on the basis of the HRESIMS data ($[M+H]^+$ ion at m/z 485.2165; $[M+Na]^+$ ion at m/z 507.1982). The 1H and ^{13}C NMR data for **5.8** showed substantial similarities to **5.4** except for a new carbonyl signal (δ_C 212.8) representing a ketone that appeared in place of a hydroxymethine (C-21 in **5.4**). Analysis of the 1H - 1H COSY and HMBC correlation data provided confirmation that other than the noted change in C-21, the atom-bond arrangements in **5.8** were the same as those observed for **5.4** (Figure 5.4). Next, 1H - 1H ROESY data [H_3 -26 \leftrightarrow H_3 -24 and H_3 -25; H_3 -24 \leftrightarrow H-20 (δ_H 2.74); H_3 -25 \leftrightarrow H-12 (δ_H 2.65); H-19 \leftrightarrow H-12 (δ_H 2.95), OH-13, OH-17, and H_3 -23; as well as H_3 -23 \leftrightarrow H-20 (δ_H 2.54)] were used to confirm a 13*S**,14*R**,17*R**,18*S**,19*R** relative configuration for **5.8** (Figure 5.5). All attempts to create at C-19 Mosher ester derivative failed, which limited our ability to assign the absolute configuration for **5.8**. However, in view of the consistent configurations observed for the C-13, C-14, C-17, and C-18 stereogenic centers in this metabolite series (**5.1-5.7**), as well as the similar

optical rotation values observed for these metabolites,^{101, 207} we propose that the absolute configuration for **5.8** is likely 13*S*,14*R*,17*R*,18*S*,19*R*.

Arisugacin O (**5.12**) was obtained as a white amorphous powder. HRESIMS provided molecular ions ($[M+H]^+$, $[M+Na]^+$ at m/z 485.2164 and 507.1989, respectively) indicative of the molecular formula $C_{27}H_{32}O_8$. This molecular formula was the same as that for **5.8** and comparisons of their 1H and ^{13}C NMR data (Table 5.1 and 5.2) indicated that the structures of **5.8** and **5.12** were highly similar. A comparative analysis of the HMBC data for **5.8** and **5.12** revealed that the C-19 hydroxymethine in **5.8** was oxidized to a ketone in **5.12** [H_3-26 (δ_H 1.24) \rightarrow C-19 (δ_C 209.6)], while the C-21 ketone in **5.8** now appeared in a reduced state as a hydroxymethine in **5.12** [H_3-23 (δ_H 0.96) \rightarrow C-21 (δ_C 72.4)] (Figure 5.4). The relative configuration of **5.12** was determined to be 13*S**,14*R**,17*R**,18*S**,21*R** based on an analysis of 1H - 1H ROESY correlation data (Figure 5.5). Specifically, ROESY correlations among protons $H_3-26 \leftrightarrow H_3-25$, H_3-24 , and H-21; $H_3-25 \leftrightarrow H-15$ (δ_H 1.60) and H-12 (δ_H 2.72); $H_3-24 \leftrightarrow H-21$; H-12 (δ_H 3.39) \leftrightarrow OH-13; as well as H-15 (δ_H 2.22) \leftrightarrow OH-17 supported a 13*S**,14*R**,17*R**,18*S**,21*R** relative configuration. The absolute configuration of C-21 was determined to be *R* by the modified Mosher's method (Figure 5.6) enabling us to assign the overall absolute configuration of **5.12** as 13*S*, 14*R*, 17*R*, 18*S*, 21*R*.

Table 5.1. ¹HNMR Data for Compounds **5.4**, **5.5**, **5.8**, **5.12-5.14** (δ ppm)

No.	δ_{H} (ppm), mult (J in Hz)						
	5.4 ^{a,d}	5.5 ^{b,d}	5.5 ^{c,e}	5.8 ^{c,d}	5.12 ^{c,d}	5.13 ^{c,d}	5.14 ^{a,d}
1	7.81 d (8.9)	7.54 d (8.9)	7.81, d (8.5)	7.80 d (8.9)	7.81 d (9.0)	7.82 d (9.0)	7.73 d (8.7)
2	7.03 d (8.9)	6.89 d (8.9)	7.04, d (8.5)	7.04 d (8.9)	7.04 d (9.0)	7.04 d (9.0)	7.00 d (8.7)
4	7.03 d (8.9)	6.89 d (8.9)	7.04, d (8.5)	7.04 d (8.9)	7.04 d (9.0)	7.04 d (9.0)	7.00 d (8.7)
5	7.81 d (8.9)	7.54 d (8.9)	7.81, d (8.5)	7.80 d (8.9)	7.81 d (9.0)	7.82 d (9.0)	7.73 d (8.7)
8	6.42 s	5.95 s	6.73, s	6.72 s	6.70 s	6.73 s	6.67 s
12	2.71 d (17.9) 3.14 d (17.9)	2.57 d (17.1) 2.71 d (17.1)	2.19, d (16.7) 2.60, d (16.7)	2.65 d (18.1) 2.95 d (18.1)	2.72 d (17.2) 3.39 d (17.2)	2.31 dd (13.0, 16.8) 2.67 dd (4.5, 16.8)	3.17 d (7.4)
13						1.78 dd (4.5, 13.0)	5.32 dd (6.4, 7.4)
15	1.61 ddd (3.3,5.6 11.5) 2.38 ddd (4.1, 11.5, 15.9)	1.74 m 2.51 ddd (4.8, 10.6, 15.4)	1.57, m 2.28, ddd (2.8, 11.5, 15.0)	1.63 m 2.23 ddd (4.9, 13.4, 15.9)	1.60 ddd (3.4, 6.2, 12.7) 2.22 ddd (3.5, 12.7, 16.2)	1.73 m 2.11 m	1.99 dd (5.5, 8.7)
16	1.73 ddd (3.3, 5.6, 12.3) 1.94 ddd (4.1,12.3 15.9)	1.85 m	1.61, m 1.89, ddd (3.1, 12.7, 15.0)	1.63 m 1.96 ddd (3.5, 12.1, 15.9)	1.74 ddd (3.5, 6.2, 13.4) 1.92 ddd (3.4, 13.4, 16.2)	1.62 m 1.74 m	2.09 m
17						1.86 dd (2.3, 12.5)	5.11 dd (6.1, 7.7)
19	4.91 brd (11.4)	1.44 m 2.39 ddd (3.9, 11.0, 15.5)	1.14, m 2.11, m	4.74 dd (7.2, 7.3)		7.33 d (10.2)	1.94 dd (6.3, 9.4)
20	2.05 m 2.16 ddd (2.8, 11.4, 14.4)	1.70 m 1.91 m	1.58, m	2.54 m 2.74 dd (7.2, 15.2)	2.65 dd (4.3, 16.1) 2.79 dd (9.6,16.1)	5.81 d (10.2)	2.04 m
21	3.66 dd (2.3, 2.8)	4.09 dd (5.2, 11.8)	3.72, dd (8.3, 8.9)		3.94 dd (4.3, 9.6)		5.06 dd (7.7, 7.1)
23	1.10 s	0.98 s	0.91, s	1.10 s	0.96 s	1.09 s	1.61 s
24	1.04 s	1.11 s	0.84, s	0.96 s	1.11 s	1.02 s	1.55 s
25	1.44 s	1.41 s	1.37, s	1.38 s	1.37 s	1.30 s	1.78 s
26	1.19 s	1.18 s	1.07, s	1.10 s	1.24 s	1.10 s	1.57 s
27	3.86 s	3.86 s	3.81, s	3.81 s	3.82 s	3.81 s	3.85 s
OH-13	6.72 brs	-	6.66, brs ^f	6.63 brs ^f	6.44 brs		
OH-17	6.81 brs	5.74 brs	6.08, brs ^f	6.46 brs ^f	6.73 brs		
OH-19	3.63 brs ^f	nd ^g		5.05, brs ^f			
OH-21	5.44 brs ^f	nd	4.19, brs ^f		5.10, brs		

^aObserved in acetone-*d*₆. ^bObserved in CDCl₃. ^cObserved in DMSO-*d*₆. ^dRecorded at 500 MHz. ^eRecorded at 600 MHz. ^fAssignments based on ROESY. ^gnd: not detected.

Arisugacin P (**5.13**) was obtained as a white amorphous powder and its molecular formula was determined to be C₂₇H₃₀O₅ by the analysis of the HRESIMS data including an [M+H]⁺ ion at *m/z* 435.2181 and an [M + Na]⁺ ion at *m/z* 435.2181 requiring 13 units of unsaturation. The HSQC data revealed that in comparison to compounds **5.8** and **5.12**, metabolite **5.13** possessed two new deshielded methine carbon atoms (δ_{C} 157.5 CH and 125.3 CH), which, based on ¹³C NMR (Table 5.2) and HMBC (Figure 5.4) data, were determined to be part of a α , β -unsaturated carbonyl system associated with ketone C-21. Further investigation of the HMBC data revealed that **5.13** was structurally similar to the previously described meroterpenoid, terreulactone B,¹⁰⁴ which had been isolated from an *Aspergillus terreus*. The major difference between these metabolites was that both the C-13 and C-17 hydroxy groups reported in

terreulactone B were missing and instead, metabolite **5.13** featured two new methine spins (δ_C 45.8 and 52.1) (Table 5.2). The relative configuration of **5.13** was determined to be $13S^*,14R^*,17R^*,18S^*$ based on 1H - 1H ROESY correlation data (Figure 5.5). Specifically, correlations among protons $H_3-26 \leftrightarrow H-16$ (δ_H 1.62), H_3-24 , and H_3-25 ; $H_3-25 \leftrightarrow H-12$ (δ_H 2.31); $H_3-23 \leftrightarrow H-17$ and $H-16$ (δ_H 1.74); as well as $H-12$ (δ_H 2.67) \leftrightarrow $H-13$ were instrumental in the assignment of the molecule's configuration. To evaluate the absolute configuration of **5.13**, the experimental and calculated ECD spectra of **5.13** were compared (Figure 5.7). The calculated ECD spectrum displayed Cotton effect that were similar to the experimentally-derived ECD spectrum, supporting a $13S,14R,17R,18S$ absolute configuration for compound **5.13**.

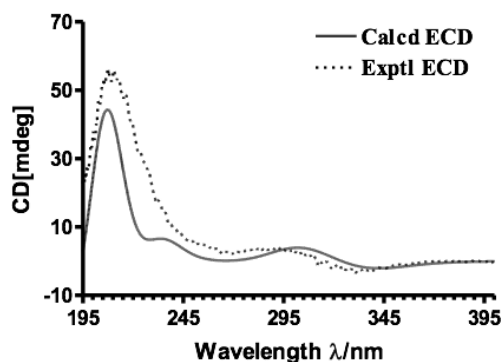


Figure 5.7. Comparison of the experimental and calculated ECD spectra of **5.13**.

Arisugacin Q (**5.14**) was obtained as a white amorphous powder. HRESIMS analysis provided both $[M+H]^+$ (m/z 423.2517) and $[M+Na]^+$ (m/z 445.2341) ions that supported a molecular formula of $C_{27}H_{34}O_4$, requiring 11 units of unsaturation. The 1H , ^{13}C and HSQC NMR experiments (Tables 5.1 and 5.2) provided data for a molecule that largely mirrored compound **5.3**,¹⁰¹ which was the first arisugacin reported to possess a largely linear sesquiterpenoid moiety.

Notable differences in **5.14** compared to **5.3** were the presence of carbon spins attributable to an additional olefinic bond (δ_c 125.4, 131.7) in **5.14**, which coincided with the loss of two oxygen atoms. The ^1H - ^1H COSY correlation data revealed couplings between the H₂-20 (δ_{H} 2.04) and H-21 (δ_{H} 5.06), while HMBC correlations from H-20 \rightarrow C-22, H₃-23 \rightarrow C-21, and H₃-24 \rightarrow C-21, secured the structural assignment for the new portion of the compound. Further investigation using the 2D NMR data (Figure 5.4) helped establish the complete structure of **5.14** (Figure 5.3). The geometry of the two double bonds (Δ^{13} and Δ^{17}) were determined as *E,E* on the basis of ROESY correlations among H₂-12 \leftrightarrow H₃-26, H-13 \leftrightarrow H₂-15, H₂-16 \leftrightarrow H₃-25, and H-17 \leftrightarrow H₂-19 (Figure 5.8).

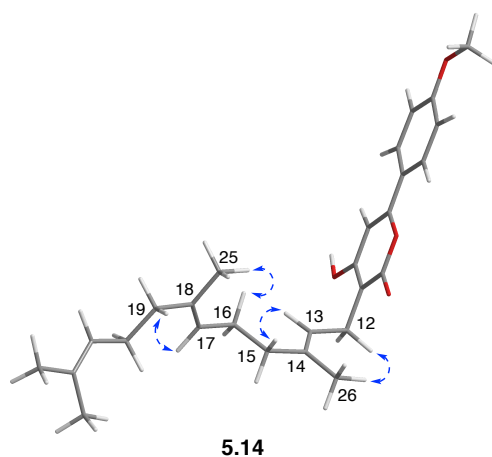


Figure 5.8. 3D molecular models of compound **5.14** showing key ROESY correlations (blue dashed arrows).

In addition to the new compounds, several more metabolites were also observed and subsequently purified yielding the known compounds *epi*-arisugacin E (**5.6**),¹⁰² arisugacin F (**5.7**),²⁰⁷ arisugacin C (**5.9**),⁹⁸ arisugacin G (**5.10**),²⁰⁷ and terreulactone C (**5.11**).¹⁰⁴ The structures of these compounds were determined based on comparisons of ^1H and ^{13}C NMR and HRESIMS data with previously reported data.

Table 5.2. ^{13}C NMR Data for Compounds **5.4**, **5.5**, **5.8**, **5.12-5.14** (100 MHz, δ ppm)

No.	δ_{C} , mult					
	4 ^b	5 ^c	8 ^d	12 ^d	13 ^d	14 ^b
1	127.6 CH	127.2 CH	126.8 CH	126.8 CH	127.0 CH	127.8 CH
2	115.1 CH	114.2 CH	114.5 CH	114.5 CH	114.5 CH	115.3 CH
3	162.4 C	161.8 C	161.1 C	161.0 C	161.2 C	162.4 C
4	115.1 CH	114.2 CH	114.5 CH	114.5 CH	114.5 CH	115.3 CH
5	127.6 CH	127.2 CH	126.8 CH	126.8 CH	127.0 CH	127.8 CH
6	125.4 C	123.6 C	123.6 C	123.6 C	123.4 C	125.7 C
7	158.2 C	158.7 C	157.0 C	157.0 C	157.6 C	158.4 C
8	97.4 CH	96.6 CH	96.6 CH	96.6 CH	96.5 CH	98.4 CH
9	163.4 C	164.1 C	162.4 C	162.4 C	163.1 C	167.5 C
10	99.6 C	96.7 C	97.4 C	97.3 C	97.8 C	102.9 C
11	164.4 C	165.6 C	163.4 C	163.3 C	162.9 C	165.5 C
12	29.9 CH ₂	25.7 CH ₂	27.4 CH ₂	26.7 CH ₂	16.8 CH ₂	23.3 CH ₂
13	77.9 C	77.6 C	76.3 C	75.6 C	45.8 CH	123.4 CH
14	82.4 C	82.2 C	81.4 C	80.8 C	80.5 C	135.4 C
15	29.9 CH ₂	29.5 CH ₂	28.5 CH ₂	28.4 CH ₂	39.2 CH ₂	40.7 CH ₂
16	26.5 CH ₂	26.0 CH ₂	25.3 CH ₂	25.4 CH ₂	19.3 CH ₂	27.4 CH ₂
17	84.7 C	80.1 C	80.7 C	81.5 C	52.1 CH	125.2 CH
18	49.1 C	43.6 C	47.9 C	57.1 C	39.0 C	135.6 C
19	65.4 CH	26.0 CH ₂	67.1 CH	209.6 C	157.5 CH	40.6 CH ₂
20	37.2 CH ₂	27.3 CH ₂	44.7 CH ₂	45.8 CH ₂	125.3 CH	27.6 CH ₂
21	78.9 CH	73.7 CH	212.8 C	72.4 CH	203.5 C	125.4 CH
22	42.2 C	44.5 C	52.8 C	42.9 C	44.0 C	131.7 C
23	23.8 CH ₃	22.8 CH ₃	23.3 CH ₃	20.7 CH ₃	27.3 CH ₃	26.0 CH ₃
24	24.7 CH ₃	18.7 CH ₃	21.7 CH ₃	25.5 CH ₃	21.4 CH ₃	17.9 CH ₃
25	24.8 CH ₃	24.6 CH ₃	23.4 CH ₃	23.5 CH ₃	20.7 CH ₃	16.6 CH ₃
26	17.4 CH ₃	21.0 CH ₃	16.0, CH ₃	18.6 CH ₃	18.1 CH ₃	16.3 CH ₃
27	55.8 CH ₃	55.6 CH ₃	55.4, CH ₃	55.4 CH ₃	55.5 CH ₃	56.0 CH ₃

^aMultiplicities were assigned based on ^1H , ^{13}C and HSQC NMR (^{13}C 100/ ^1H 500 MHz) experiments. ^bObserved in acetone- d_6 . ^cObserved in CDCl_3 . ^dObserved in $\text{DMSO}-d_6$.

5.2.3 Testing of Natural Products from the *Penicillium sp.* Isolate

Following the purification of these compounds, all metabolites were evaluated in zebrafish embryos. New compounds **5.5** and **5.12-5.14** induced paralysis with compound **5.12** being the most active at a test concentration of 1 μM (Table 5.3). Additionally, embryos exposed to compound **5.12** exhibited defects in myotome structure as shown by *in situ* hybridization for *xirp2a*, closely phenocopying embryos treated with the known AChE inhibitors, azinphosmethyl

(APM) and physostigmine (Figure 5.9A and B).^{187, 209} This is consistent with previous reports of AChE inhibition leading to severe abnormalities in muscle development.²⁰⁶ Treatment with the known BuChE inhibitor, tetraisopropyl-pyrophosphoramidate (iso-OMPA), did not result in compromised motility or aberrant myotome development (Figure 5.9A and B).²¹⁰ Using an *in vitro* assay to investigate whether the new arisugacins directly inhibit AChE, we found that compounds **5.5** and **5.12** showed the strongest inhibition, with IC₅₀ values of 3.9 and 0.19 μM, respectively (Table 5.3 and Figure 5.9C). Compounds **5.4** and **5.8** did not impair motility in zebrafish embryos; however, these compounds did inhibit *in vitro* AChE activity, which suggests that certain pharmacological parameters were not met to cause bioactivity *in vivo* (Table 5.3).

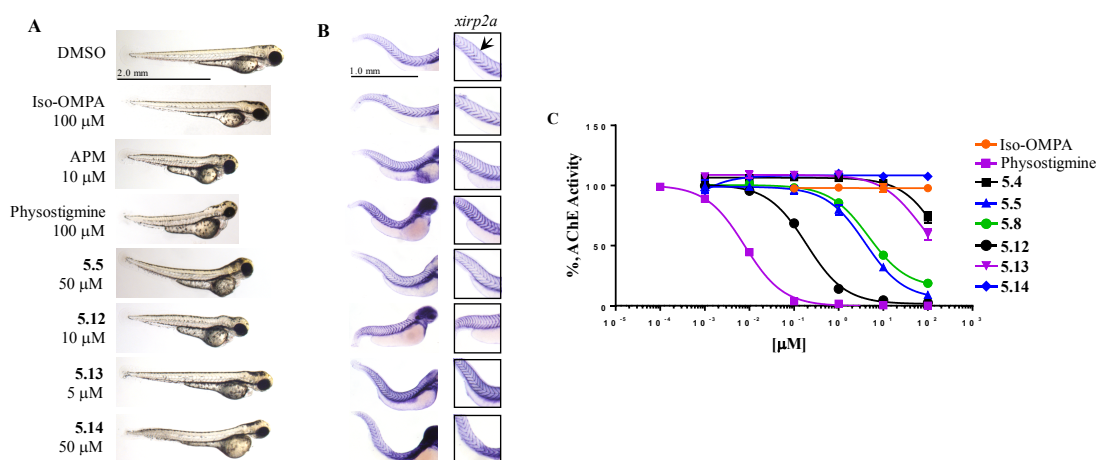


Figure 5.9. Novel arisugacin compounds show acetylcholinesterase inhibitory activity. **A.** Phenotypes of 72 hpf embryos that exhibited impaired motility with early compound treatment. **B.** In situ hybridization for myotome marker, *xirp2a* (xin actin binding repeat containing 2a), in 72 hpf embryos. Boxed figure is enlargement of the trunk to emphasize abnormalities in myotome (black arrow) structure. **C.** IC₅₀ of new arisugacin analogs were obtained in an *in vitro* AChE inhibition assay.

The known compounds **5.1**, **5.3**, **5.9-5.10** produced a paralysis phenotype in zebrafish with compound **5.3** and **5.10** causing myotome structural abnormalities, as well as demonstrating the abilities to inhibit AChE *in vitro* (Figure 5.10, Table 5.3). Both compounds have not been

shown to be biologically active but possess weak AChE inhibitory properties in previous *in vitro* assays.^{101, 207} Compound **5.11**, which has been previously reported to be potent and selective AChE inhibitor did not induce phenotypic changes in the zebrafish (Table 5.3).¹⁰⁴ All compounds showed minimal inhibition of BuChE, however, only compound **5.12** stood out as highly selective towards AChE (Table 5.3).

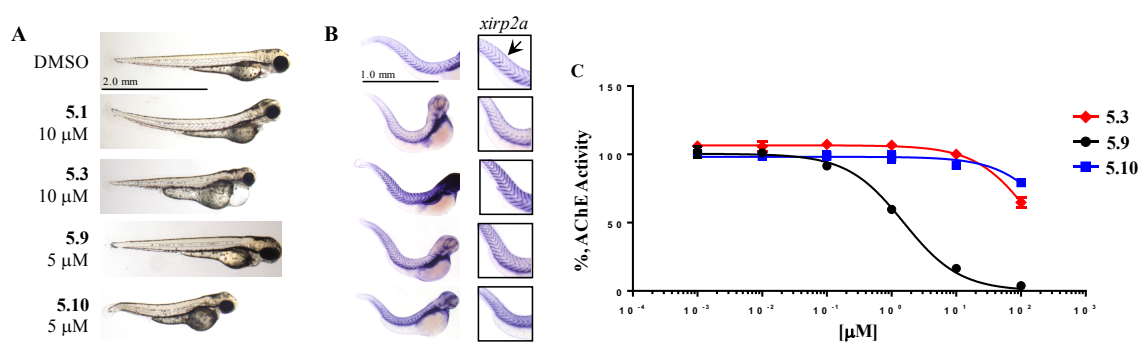


Figure 5.10. Bioactivity of known arisugacin compounds with no previously reported AChE bioactivity. **A.** Phenotypes of 72 hpf embryos that exhibited impaired motility with early compound treatment. **B.** In situ hybridization for *xirp2a* in 72 hpf embryos. Boxed figure is enlargement of the trunk to emphasize abnormalities in myotome (black arrow) structure. **C.** IC₅₀ of arisugacins C, G and I were obtained in an *in vitro* AChE inhibition assay.

There were several compounds that had consistent bioactivity in both phenotype-based zebrafish screen and *in vitro* AChE inhibition assay (Table 5.3). However, there were samples that showed opposite results, for example, compound **5.11** did not affect motility in zebrafish while physostigmine induced phenotype only at 100 μM. Both compounds inhibited AChE *in vitro* at low nanomolar concentrations, which indicates that there are pharmacological properties that need to be addressed for these compounds to be useful as potential therapeutics. AZM, in contrast, caused paralysis in zebrafish embryos at 1 μM but showed weak inhibition of AChE *in vitro*. This is consistent with the mechanism of toxicity of AZM, its conversion to the oxon form

by cytochrome P450 has been found to be responsible for its AChE inhibitory activity, which is not readily apparent in an *in vitro* assay. Lastly, we have observed bioactivity for compounds **5.3** and **5.10** in developing zebrafish embryos, both of which were weakly active in *in vitro* assays. These examples illustrate the unique advantage of using a whole organism-based phenotype screen such as the zebrafish, as it not only provides information about biological activity of small molecules *in vivo*, but insights about their pharmacokinetic and pharmacodynamic characteristics as well. This knowledge is critical in determining and prioritizing lead compounds, and in facilitating drug discovery efforts in general.

5.3 Conclusion and Future Directions

Our findings demonstrate the utility of the zebrafish in rapidly deconvoluting complex mixtures into its active components and elucidating their mechanism of action. From 384 fungal extracts, six new and eight known meroterpenoids were purified from a *Penicillium* sp. isolate. Four of the new compounds (**5.5**, **5.12-5.14**) induced paralysis in zebrafish with compound **5.12** demonstrating potent and selective AChE inhibitory activity under both *in vivo* and *in vitro* conditions. AChE inhibitors have found clinical use for treating various human malignancies that include bladder distention, glaucoma, vascular dementia and symptoms of Alzheimer's Disease (AD). Currently, majority of drugs approved for AD treatment are AChE inhibitors, but the need to develop better therapeutics to address cognitive impairment remains.²¹¹ Our discovery of new arisugacin compounds, some with potent and specific AChE inhibitory activity, would enable further structure-function analyses that could lead to the development of better AChE inhibitors in the clinic.

Table 5.3. Bioactivity of compounds **5.1-5.14**.

Compound	Zebrafish Assay Active Concentration ^a (μM)	AChE Inhibition ^b at 50 μM (%)	BuChE Inhibition ^b at 50 μM (%)	AChE inhibition IC_{50} (μM)
Iso-OMPA ^c	-	1.3	15.1	>100
APM ^d	1	12.2	3.3	nt
Physostigmine ^d	100	99.8	93.2	0.0078
5.1	10	60.1	4.7	nt
5.2	-	83.4	0	nt
5.3	10	34.1	4.7	>100
5.4	-	29.2	0	>100
5.5	50	89.4	4.7	3.9
5.6	-	75.4	7.0	nt
5.7	-	3.0	4.7	nt
5.8	-	83.6	0	4.6
5.9	5	95.1	32.6	1.4
5.10	5	26.9	11.6	>100
5.11	-	96.6	9.3	nt
5.12	1	98.0	0	0.191
5.13	5	40.3	0	66
5.14	50	4.3	0	>100

^a Active concentration refers to the lowest compound concentration where it induces paralysis in zebrafish embryos treated at 7 hpf and evaluated for phenotype at 72 hpf.

A dash (-) signifies no bioactivity *in vivo* at 100 μM or lower.

^b Inhibitory activity against acetylcholinesterase (AChE) and butyrylcholinesterase (BuChE) was determined at sample concentration of 50 μM .

^c BuChE inhibitor. ^d AChE inhibitor. nt-not tested.

Iso-OMPA, APM stand for tetraisopropylpyrophosphamide and azinphosmethyl

5.4 Materials and Method

5.4.1 General Experimental

Optical rotations were measured on a Rudolph Research Autopol[®] III. NMR data were obtained on Varian VNMR spectrometers (500 MHz and 600MHz for ¹H and 2D NMR, 100 MHz for ¹³C). The LC-ESIMS analyses were performed on a Shimadzu UFLC system with a quadrupole mass spectrometer using a Phenomenex Kinetex C₁₈ column (3.0 mm × 75 mm, 2.6 μm) and MeCN-H₂O (0.1% HCOOH) gradient solvent system. Accurate mass data was collected on an Agilent 6538 high-mass-resolution QTOF mass spectrometer. Analytical and Semi-preparative HPLC were performed on a Waters 2998 photodiode array detector, the columns used were Phenomenex Gemini 5 μm C18 column (110Å, 250*4.6 mm, 1 mL/min; 110Å, 250*10 mm, 4 mL/min), Kinetex 5 μm Biphenyl (110Å, 250*4.6mm, 1 mL/min; 110Å, 250*10mm, 4 mL/min). All solvents are of ACS grade or better.

5.4.2 Fungal Strain and Fermentation

The fungal isolate was obtained from a soil sample submitted by a citizen scientist from Lawton, Oklahoma to the University of Oklahoma Citizen Science Soil Collection Program. The isolate was identified as a probable *Penicillium* sp. (most closely associated to *Penicillium oxalicum*) based on analysis of its ribosomal internal transcribed spacer (ITS) sequence data (GenBank accession number MK722362) by comparison to the BLAST database. Fermentation was performed by inoculating fungal mycelia and spores on to a solid-state medium composed of Cheerios[®] breakfast cereal supplemented with a 0.3% sucrose solution. The fungus was grown for four weeks at room temperature (25°C).

5.4.3 Extraction and Isolation

The fungal biomass was extracted with EtOAc ($\times 3$) and the organic solvent was concentrated under vacuum to generate the crude extract (130 g). The crude extract was separated into five fractions (Fr.1-Fr.5) by silica gel vacuum liquid chromatography [eluted with equal volumes of hexane-CH₂Cl₂ (1:1), CH₂Cl₂, CH₂Cl₂-MeOH (10:1, 1:1)] and MeOH. Fr.3 (eluted with 10:1 CH₂Cl₂-MeOH) was subjected to HP20ss vacuum liquid chromatography (eluted with 30%, 50%, 70%, 90%, 100% MeOH in H₂O) to yield five subfractions. The fourth fraction was found active zebrafish assay and it was further separated by semi-preparative HPLC (eluted with 40:60 ACN:H₂O, with 0.1% formic acid in H₂O) yielded compounds **5.1** (1.9 mg), **5.2** (3.7 mg), **5.3** (1.5 mg) **5.4** (4.5 mg), **5.5** (7.9 mg), and **5.6** (2.6 mg). Subfraction 5 (100% MeOH) was further purified by semi-preparative HPLC (70:30 ACN:H₂O with 0.1% HCOOH) to afford compounds **5.7** (2.2 mg), **5.8** (3.7 mg), **5.9** (7.9 mg), **5.10** (10.1 mg), **5.11** (4.0 mg), **5.12** (2.2 mg), **5.13** (1.1 mg), and **5.14** (2.1 mg).

Arisugacin M (5.4): amorphous, white powder; $[\alpha]_D^{20} + 69.3$ (c, 0.225, MeOH); ¹H and ¹³C NMR, see Table 1 and Table 2; HRESIMS $[M+H]^+ m/z$ 487.2341, $[M+Na]^+ m/z$ 509.2155 (calcd for C₂₇H₃₅O₈, 487.2326, C₂₇H₃₄O₈Na, 509.2146).

Arisugacin N (5.5): amorphous, white powder; $[\alpha]_D^{20} + 64.8$ (c, 0.395, MeOH); ¹H and ¹³C NMR, see Table 1 and Table 2; HRESIMS $[M+H]^+ m/z$ 471.2393, $[M+Na]^+ m/z$ 493.2210 (calcd for C₂₇H₃₅O₇, 471.2377 C₂₇H₃₄O₇Na, 493.2197).

Arisugacin O (5.8): amorphous, white powder; $[\alpha]_D^{20} + 64.9$ (c, 0.185, MeOH); ¹H and ¹³C NMR, see Table 1 and Table 2; HRESIMS $[M+H]^+ m/z$ 485.2165, $[M+Na]^+ m/z$ 507.1982 (calcd for C₂₇H₃₃O₈, 485.2170, C₂₇H₃₂O₈Na, 507.1989).

Arisugacin L (5.12): amorphous, white powder; $[\alpha]_D^{20} + 4.5$ (c, 0.11, MeOH); ^1H and ^{13}C NMR, see Table 1 and Table 2; HRESIMS $[\text{M}+\text{H}]^+ m/z$ 485.2164, $[\text{M}+\text{Na}]^+ m/z$ 507.1989 (calcd for $\text{C}_{27}\text{H}_{33}\text{O}_8$, 485.2170, $\text{C}_{27}\text{H}_{32}\text{O}_8\text{Na}$, 507.1989).

Arisugacin P (5.13): amorphous, white powder; $[\alpha]_D^{20} + 100$ (c, 0.05, MeOH); ^1H and ^{13}C NMR, see Table 1 and Table 2; HRESIMS $[\text{M}+\text{H}]^+ m/z$ 435.2181, $[\text{M}+\text{Na}]^+ m/z$ 457.1993 (calcd for $\text{C}_{27}\text{H}_{31}\text{O}_5$, 435.2166, $\text{C}_{27}\text{H}_{30}\text{O}_5\text{Na}$, 457.2064).

Arisugacin Q (5.14): amorphous, white powder; ^1H and ^{13}C NMR, see Table 1 and Table 2; HRESIMS $[\text{M}+\text{H}]^+ m/z$ 423.2517, $[\text{M}+\text{Na}]^+ m/z$ 445.2341 (calcd for $\text{C}_{27}\text{H}_{35}\text{O}_4$, 423.2530, $\text{C}_{27}\text{H}_{34}\text{O}_4\text{Na}$, 445.2349).

5.4.4 Preparation of MTPA Esters

Compound **5.4**, **5.5** and **5.12** (0.2 mg each) were dissolved separately in pyridine (500 μL) and transferred into NMR tubes. 2 μL of (*S*)-*a*-methoxy-*a*-trifluoromethylphenylacetic acid (MTPA) was added to each sample and the reaction mixture monitored every 2 h by ^1H -NMR. (*S*)-MTPA esters were prepared in a similar way using (*R*)-*a*-methoxy-*a*-trifluoromethylphenylacetic acid.

(*R*)-MTPA Ester of 5.4: ^1H NMR (500 MHz, pyridine- d_5) δ 5.49 (H-21), 5.39 (H-19), 4.08 (H-12b), 3.37 (H-12a), 2.88 (H-15b), 1.87 (H-15a), 2.55 (H-20b), 2.55 (H-20a), 2.01 (H-16b), 1.86 (H-16a), 1.54 (H-25), 1.46 (H-26), 1.28 (H-23), 1.19 (H-24); ESIMS m/z 703.35 $[\text{M}+\text{H}]^+$.

(*S*)-MTPA Ester of 5.4: ^1H NMR (500 MHz, pyridine- d_5) δ 5.53 (H-21), 5.45 (H-19), 4.11 (H-12b), 3.38 (H-12a), 2.85 (H-15b), 1.84 (H-15a), 2.69 (H-20b), 2.58 (H-20a), 1.99 (H-16b), 1.84 (H-16a), 1.54 (H-25), 1.47 (H-26), 1.16 (H-23), 1.10 (H-24); ESIMS m/z 703.35 $[\text{M}+\text{H}]^+$.

(R)-MTPA Ester of 5.5: ^1H NMR (500 MHz, pyridine- d_5) δ 6.03 (H-21), 3.09 (H-12b), 2.92 (H-12a), 2.83 (H-15b), 1.96 (H-15a), 2.75 (H-19b), 1.42 (H-19a), 2.18 (H-20b), 2.08 (H-20a), 1.90 (H-16b), 1.86 (H-16a), 1.50 (H-25), 1.23 (H-23), 1.21 (H-26), 1.11 (H-24).

(S)-MTPA Ester of 5.5: ^1H NMR (500 MHz, pyridine- d_5) δ 6.02 (H-21), 3.07 (H-12b), 2.90 (H-12a), 2.84 (H-15b), 1.97 (H-15a), 2.74 (H-19b), 1.39 (H-19a), 2.14 (H-20b), 1.86 (H-20a), 1.90 (H-16b), 1.86 (H-16a), 1.50 (H-25), 1.33 (H-23), 1.19 (H-26), 1.14 (H-24).

(R)-MTPA Ester of 5.12: ^1H NMR (500 MHz, pyridine- d_5) δ 5.96 (H-21), 4.35 (H-12b), 3.24 (H-12a), 3.48 (H-20b), 3.07 (H-20a), 2.81 (H-15b), 1.87 (H-15a), 1.96 (H-16b), 1.94 (H-16a), 1.50 (H-25), 1.45 (H-26), 1.34 (H-23), 1.31 (H-24).

(S)-MTPA Ester of 5.12: ^1H NMR (500 MHz, pyridine- d_5) δ 5.96 (H-21), 4.35 (H-12b), 3.24 (H-12a), 3.59 (H-20b), 3.13 (H-20a), 2.80 (H-15b), 1.85 (H-15a), 1.94 (H-16b), 1.92 (H-16a), 1.49 (H-25), 1.45 (H-26), 1.24 (H-23), 1.19 (H-24).

5.4.5 ECD Calculations of 5.13

Conformational analyses were performed using Spartan'10.²¹² Geometry, frequency and ECD calculations were carried out at the DFT level with Gaussian 09.²¹³ SpecDis 1.60 was used to average single ECD spectra after Boltzmann statistical weighting.²¹⁴

5.4.6 Zebrafish maintenance

Wild-type (WT) *AB/TU Danio rerio* (zebrafish) were maintained as previously described.²¹⁵ Fertilized embryos were collected following natural spawning in 1 \times E3 medium (286 mg/L NaCl, 13 mg/L KCl, 48 mg/L CaCl₂·2H₂O, 40 mg/L MgSO₄, 0.01% methylene blue) and allowed to develop at 28.5 °C.

5.4.7 Zebrafish phenotype screen

Crude fungal extracts were assayed based on our previously reported zebrafish phenotype screen¹⁹⁷. Crude and semi-pure extracts were prepared in dimethyl sulfoxide (DMSO) as 2 mg/ml stocks. Pure fungal compounds were prepared as 10 mM stocks. Azinphos-methyl (APM), tetraisopropyl pyrophosphoramidate (iso-OMPA) and physostigmine were prepared as 100 mM stocks in DMSO. Further dilutions were carried out in DMSO.

5.4.8 *In situ* hybridization

In situ hybridizations were performed as previously described using digoxigenin-labeled riboprobes for *xirp2a* (*xin actin binding repeat containing 2a*)²¹⁶. Embryos were cleared in 2:1 benzyl benzoate/benzyl alcohol solution and documented using an Olympus SZX12/DP71 imaging system (Olympus Corporation, Japan). RNA Reference Sequence deposited in ZFIN (zfin.org) was used in designing the riboprobe.

5.4.9 Acetylcholinesterase and butyrylcholinesterase inhibition assays

AChE inhibition was determined using QuantiChrom™ Acetylcholinesterase Inhibitor Screening Kit following manufacturer's protocol (BioAssay Systems – Hayward, CA). Briefly, test compounds were incubated with AChE from *E. electricus* (Sigma-Aldrich) for 15 min. Absorbance was measured at T= 0 min and T= 15 min after addition of assay buffer containing AChE substrate and 5,5'-dithiobis (2-nitrobenzoic acid) (DTNB). The same kit and protocol were used to measure butyrylcholinesterase inhibition by substituting butyrylcholinesterase from equine serum and s-butrylthiocholine iodide as substrate. Both reagents were purchased from Sigma-Aldrich. Raw absorbance readings were corrected against 'No Enzyme' control and

normalized to 'No Inhibitor' control. Data was plotted and analyzed using Graph Pad Prism v7.02.

References

1. Borchardt, J. K., The beginnings of drug therapy: ancient Mesopotamian medicine. *Drug News and Perspectives* **2002**, *15* (3), 187-192.
2. Cragg, G. M.; Newman, D. J., Natural products: a continuing source of novel drug leads. *Biochimica et Biophysica Acta* **2013**, *1830* (6), 3670-3695.
3. All natural. *Nature Chemical Biology* **2007**, *3* (7), 351.
4. Koehn, F. E.; Carter, G. T., The evolving role of natural products in drug discovery. *Nature Reviews Drug Discovery* **2005**, *4* (3), 206-220.
5. Newman, D. J.; Cragg, G. M.; Snader, K. M., The influence of natural products upon drug discovery. *Natural Product Reports* **2000**, *17* (3), 215-234.
6. Demain, A. L., Importance of microbial natural products and the need to revitalize their discovery. *Journal of Industrial Microbiology and Biotechnology* **2014**, *41* (2), 185-201.
7. Schmitz, R., Friedrich Wilhelm Sertürner and the discovery of morphine. *Pharmacy in History* **1985**, *27* (2), 61-74.
8. DerMarderosian, A.; Beutler, J. A., The review of natural products: the most complete source of natural product information. *Facts and Comparisons*: **2002**.
9. Reif-Acherman, S., The contributions of Henri Victor Regnault in the context of organic chemistry of the first half of the nineteenth century. *Química Nova* **2012**, *35* (2), 438-443.
10. Allen, D. E.; Hatfield, G., Medicinal plants in folk tradition. *Timber Press*: **2004**.
11. Vakil, R. J., A clinical trial of Rauwolfia serpentina in essential hypertension. *British Heart Journal* **1949**, *11* (4), 350.
12. Klayman, D. L.; Lin, A. J.; Acton, N.; Scovill, J. P.; Hoch, J. M.; Milhous, W. K.; Theoharides, A. D.; Dobek, A. S., Isolation of artemisinin (qinghaosu) from *Artemisia annua* growing in the United States. *Journal of Natural Products* **1984**, *47* (4), 715-717.
13. Khanna, C.; Rosenberg, M.; Vail, D. M., A review of paclitaxel and novel formulations including those suitable for use in dogs. *Journal of Veterinary Internal Medicine* **2015**, *29* (4), 1006-1012.
14. Kardos, N.; Demain, A. L., Penicillin: the medicine with the greatest impact on therapeutic outcomes. *Applied Microbiology and Biotechnology* **2011**, *92* (4), 677.
15. Nelson, M. L.; Levy, S. B., The history of the tetracyclines. *Annals of the New York Academy of Sciences* **2011**, *1241* (1), 17-32.
16. Falagas, M. E.; Grammatikos, A. P.; Michalopoulos, A., Potential of old-generation antibiotics to address current need for new antibiotics. *Expert Review of Anti-infective Therapy* **2008**, *6* (5), 593-600.
17. Camb, D., The Killers Within: The deadly rise of drug-resistant bacteria. *Ecologist* **2003**, *33* (5), 61.
18. Ferreira, S., A bradykinin-potentiating factor (BPF) present in the venom of *Bothrops jararaca*. *British Journal of Pharmacology and Chemotherapy* **1965**, *24* (1), 163-169.
19. Bowersox, S. S.; Luther, R., Pharmacotherapeutic potential of *omega*-conotoxin MVIIA (SNX-111), an N-type neuronal calcium channel blocker found in the venom of *Conus magus*. *Toxicon* **1998**, *36* (11), 1651-1658.
20. Siddiqui, A. A.; Iram, F.; Siddiqui, S.; Sahu, K., Role of natural products in drug discovery process. *International Journal of Drug Development and Research* **2014**, *6* (2), 172-204.

21. Seletsky, B. M.; Wang, Y.; Hawkins, L. D.; Palme, M. H.; Habgood, G. J.; DiPietro, L. V.; Towle, M. J.; Salvato, K. A.; Wels, B. F.; Aalfs, K. K., Structurally simplified macrolactone analogues of halichondrin B. *Bioorganic and Medicinal Chemistry Letters* **2004**, *14* (22), 5547-5550.
22. Newman, D. J.; Cragg, G. M., Natural Products as Sources of New Drugs from 1981 to 2014. *Journal of Nature Product* **2016**, *79* (3), 629-661.
23. Penicillins, O., Appropriate prescribing of oral beta-lactam antibiotics. *American Family Physician* **2000**, *62*, 611-620.
24. Elander, R. P., Industrial production of beta-lactam antibiotics. *Applied Microbiol Biotechnol* **2003**, *61* (5-6), 385-392.
25. Kahan, B. D., Cyclosporine. *New England Journal of Medicine* **1989**, *321* (25), 1725-1738.
26. Grove JF, M. J., Mulholland TPC, Rogers MAT, Griseofulvin. Part IV. structure. *Journal of the Chemical Society* **1952**, 3977-3987.
27. Denning, D. W., Echinocandins: a new class of antifungal. *Journal of Antimicrobial Chemotherapy* **2002**, *49* (6), 889-891.
28. Sauter, H.; Steglich, W.; Anke, T., Strobilurins: evolution of a new class of active substances. *Angewandte Chemie International Edition* **1999**, *38* (10), 1328-1349.
29. Jang, J.-H.; Asami, Y.; Jang, J.-P.; Kim, S.-O.; Moon, D. O.; Shin, K.-S.; Hashizume, D.; Muroi, M.; Saito, T.; Oh, H., Fusarisetin A, an acinar morphogenesis inhibitor from a soil fungus, *Fusarium* sp. FN080326. *Journal of the American Chemical Society* **2011**, *133* (18), 6865-6867.
30. Xu, J.; Caro-Diaz, E. J.; Lacoske, M. H.; Hung, C.-I.; Jamora, C.; Theodorakis, E. A., Fusarisetin A: scalable total synthesis and related studies. *Chemical Science* **2012**, *3* (12), 3378-3386.
31. Bury, M.; Girault, A.; Megalizzi, V.; Spiegl-Kreinecker, S.; Mathieu, V.; Berger, W.; Evidente, A.; Kornienko, A.; Gailly, P.; Vandier, C., Ophiobolin A induces paraptosis-like cell death in human glioblastoma cells by decreasing BKCa channel activity. *Cell Death and Disease* **2013**, *4* (3), 561.
32. Usui, T.; Kondoh, M.; Cui, C.-B.; Mayumi, T.; Osada, H., Tryprostatin A, a specific and novel inhibitor of microtubule assembly. *Biochemical Journal* **1998**, *333* (Pt 3), 543.
33. Yamada, T.; Iritani, M.; Minoura, K.; Kawai, K.; Numata, A., Peribysins A–D, potent cell-adhesion inhibitors from a sea hare-derived culture of *Periconia* species. *Organic and Biomolecular Chemistry* **2004**, *2* (14), 2131-2135.
34. Wright, A. D.; Lang-Unnasch, N., Diterpene formamides from the tropical marine sponge *Cymbastela hooperi* and their antimalarial activity in vitro. *Journal of Natural Products* **2009**, *72* (3), 492-495.
35. Kontnik, R.; Clardy, J., Codinaeopsin, an antimalarial fungal polyketide. *Organic Letters* **2008**, *10* (18), 4149-4151.
36. Pruksakorn, P.; Arai, M.; Kotoku, N.; Vilchèze, C.; Baughn, A. D.; Moodley, P.; Jacobs Jr, W. R.; Kobayashi, M., Trichodermins, novel aminolipopeptides from a marine sponge-derived *Trichoderma* sp., are active against dormant mycobacteria. *Bioorganic and Medicinal Chemistry Letters* **2010**, *20* (12), 3658-3663.
37. Hawksworth, D. L.; Lücking, R., Fungal diversity revisited: 2.2 to 3.8 million species. *Microbiology Spectrum* **2017**, *5* (4).
38. Schueffler, A.; Anke, T., Fungal natural products in research and development. *Natural Product Report* **2014**, *31* (10), 1425-1448.

39. Bass, D.; Richards, T. A., Three reasons to re-evaluate fungal diversity ‘on Earth and in the ocean’. *Fungal Biology Reviews* **2011**, *25* (4), 159-164.
40. Mattern, D. J.; Valiante, V.; Unkles, S. E.; Brakhage, A. A., Synthetic biology of fungal natural products. *Frontiers in Microbiology* **2015**, *6*, 775.
41. Bergmann, S.; Schümann, J.; Scherlach, K.; Lange, C.; Brakhage, A. A.; Hertweck, C., Genomics-driven discovery of PKS-NRPS hybrid metabolites from *Aspergillus nidulans*. *Nature Chemical Biology* **2007**, *3* (4), 213.
42. Wunsch, C.; Mundt, K.; Li, S.-M., Targeted production of secondary metabolites by coexpression of non-ribosomal peptide synthetase and prenyltransferase genes in *Aspergillus*. *Applied Microbiology and Biotechnology* **2015**, *99* (10), 4213-4223.
43. Hyde, K. D.; Abd-Elsalam, K.; Cai, L., Morphology: still essential in a molecular world. *Mycotaxon* **2011**, *114* (1), 439-451.
44. Jeewon, R.; Liew, E. C.; Hyde, K. D., Phylogenetic relationships of *Pestalotiopsis* and allied genera inferred from ribosomal DNA sequences and morphological characters. *Molecular Phylogenetics and Evolution* **2002**, *25* (3), 378-392.
45. Promputtha, I.; Jeewon, R.; Lumyong, S.; McKenzie, E. H.; Hyde, K. D., Ribosomal DNA fingerprinting in the identification of non sporulating endophytes from *Magnolia liliifera* (*Magnoliaceae*). *Fungal Diversity* **2005**.
46. Salamanca-Cardona, L.; Keshari, K. R., ¹³C-labeled biochemical probes for the study of cancer metabolism with dynamic nuclear polarization-enhanced magnetic resonance imaging. *Cancer and Metabolism* **2015**, *3*, 9.
47. Tkacz, J. S.; Lange, L., Advances in fungal biotechnology for industry, agriculture, and medicine. *Springer Science and Business Media*: **2004**.
48. Bruns, T. D.; White, T. J.; Taylor, J. W., Fungal molecular systematics. *Annual Review of Ecology and Systematics* **1991**, *22* (1), 525-564.
49. Mitchell, J. I.; Zuccaro, A., Sequences, the environment and fungi. *Mycologist* **2006**, *20* (2), 62-74.
50. Schoch, C. L.; Seifert, K. A.; Huhndorf, S.; Robert, V.; Spouge, J. L.; Levesque, C. A.; Chen, W.; Bolchacova, E.; Voigt, K.; Crous, P. W., Nuclear ribosomal internal transcribed spacer (ITS) region as a universal DNA barcode marker for Fungi. *Proceedings of the National Academy of Sciences* **2012**, *109* (16), 6241-6246.
51. Stielow, J. B.; Levesque, C. A.; Seifert, K. A.; Meyer, W.; Iriny, L., One fungus, which genes? Development and assessment of universal primers for potential secondary fungal DNA barcodes. *Persoonia* **2015**, *35*, 242-263.
52. Tam, E. W.; Chen, J. H.; Lau, E. C.; Ngan, A. H.; Fung, K. S.; Lee, K.-C.; Lam, C.-W.; Yuen, K.-Y.; Lau, S. K.; Woo, P. C., Misidentification of *Aspergillus nomius* and *Aspergillus tamaritii* as *Aspergillus flavus*: characterization by internal transcribed spacer, β -tubulin, and calmodulin gene sequencing, metabolic fingerprinting, and matrix-assisted laser desorption ionization–time of flight mass spectrometry. *Journal of Clinical Microbiology* **2014**, *52* (4), 1153-1160.
53. Seifert, K. A.; Samson, R. A.; Houbraken, J.; Lévesque, C. A.; Moncalvo, J.-M.; Louis-Seize, G.; Hebert, P. D., Prospects for fungus identification using CO1 DNA barcodes, with *Penicillium* as a test case. *Proceedings of the National Academy of Sciences* **2007**, *104* (10), 3901-3906.

54. Liu, Y. J.; Hall, B. D., Body plan evolution of *ascomycetes*, as inferred from an RNA polymerase II phylogeny. *Proceedings of the National Academy of Sciences* **2004**, *101* (13), 4507-4512.
55. Glass, N. L.; Donaldson, G. C., Development of primer sets designed for use with the PCR to amplify conserved genes from filamentous *ascomycetes*. *Applied and Environmental Microbiology* **1995**, *61* (4), 1323-1330.
56. Rehner, S. A.; Buckley, E., A *Beauveria* phylogeny inferred from nuclear ITS and *EF1- α* sequences: evidence for cryptic diversification and links to *Cordyceps teleomorphs*. *Mycologia* **2005**, *97* (1), 84-98.
57. Visagie, C.; Houbraeken, J.; Frisvad, J. C.; Hong, S.-B.; Klaassen, C.; Perrone, G.; Seifert, K.; Varga, J.; Yaguchi, T.; Samson, R., Identification and nomenclature of the genus *Penicillium*. *Studies in Mycology* **2014**, *78*, 343-371.
58. Stielow, J. B.; Levesque, C. A.; Seifert, K. A.; Meyer, W.; Iriny, L.; Smits, D.; Renfurm, R.; Verkley, G.; Groenewald, M.; Chaduli, D., One fungus, which genes? development and assessment of universal primers for potential secondary fungal DNA barcodes. *Persoonia: Molecular Phylogeny and Evolution of Fungi* **2015**, *35*, 242.
59. Kaufman, C. K.; White, R. M.; Zon, L., Chemical genetic screening in the zebrafish embryo. *Nature Protocol* **2009**, *4* (10), 1422-1432.
60. Samson, R. A.; Visagie, C. M.; Houbraeken, J.; Hong, S.-B.; Hubka, V.; Klaassen, C. H.; Perrone, G.; Seifert, K. A.; Susca, A.; Tanney, J. B., Phylogeny, identification and nomenclature of the genus *Aspergillus*. *Studies in Mycology* **2014**, *78*, 141-173.
61. Wink, M., Medicinal plants: a source of anti-parasitic secondary metabolites. *Molecules* **2012**, *17* (11), 12771-12791.
62. Dalton, J.; Mulcahy, G., Parasite vaccines—a reality? *Veterinary Parasitology* **2001**, *98* (1-3), 149-167.
63. Beaumier, C. M.; Gillespie, P. M.; Hotez, P. J.; Bottazzi, M. E., New vaccines for neglected parasitic diseases and dengue. *Translational Research* **2013**, *162* (3), 144-155.
64. Hefnawy, A.; Berg, M.; Dujardin, J.-C.; De Muylder, G., Exploiting knowledge on *Leishmania* drug resistance to support the quest for new drugs. *Trends in Parasitology* **2017**, *33* (3), 162-174.
65. Bradley, W. G.; Karlsson, I.; Rassol, C., Metronidazole neuropathy. *British Medical Journal* **1977**, *2* (6087), 610.
66. Viotti, R.; Vigliano, C.; Lococo, B.; Alvarez, M. G.; Petti, M.; Bertocchi, G.; Armenti, A., Side effects of benzimidazole as treatment in chronic Chagas disease: fears and realities. *Expert Review of Anti-infective Therapy* **2009**, *7* (2), 157-163.
67. Krogstad, D. J.; Gluzman, I. Y.; Kyle, D. E.; Oduola, A.; Martin, S. K.; Milhous, W. K.; Schlesinger, P. H., Efflux of chloroquine from *Plasmodium falciparum*: mechanism of chloroquine resistance. *Science* **1987**, *238* (4831), 1283-1285.
68. Wang, P.; Read, M.; Sims, P. F.; Hyde, J. E., Sulfadoxine resistance in the human malaria parasite *Plasmodium falciparum* is determined by mutations in dihydropteroate synthetase and an additional factor associated with folate utilization. *Molecular Microbiology* **1997**, *23* (5), 979-986.
69. Kanokmedhakul, S.; Lekphrom, R.; Kanokmedhakul, K.; Hahnvajanawong, C.; Bua-Art, S.; Saksirirat, W.; Prabpai, S.; Kongsaree, P., Cytotoxic sesquiterpenes from luminescent mushroom *Neonothopanus nambi*. *Tetrahedron* **2012**, *68* (39), 8261-8266.

70. Souza-Fagundes, E.; Cota, B.; Rosa, L.; Romanha, A.; Corrêa-Oliveira, R.; Rosa, C.; Zani, C.; Teixeira-Carvalho, A.; Martins-Filho, O., *In vitro* activity of hypnophilin from *Lentigin strigosus*: a potential prototype for Chagas disease and leishmaniasis chemotherapy. *Brazilian Journal of Medical and Biological Research* **2010**, *43* (11), 1054-1061.
71. Mallick, S.; Dutta, A.; Chaudhuri, A.; Mukherjee, D.; Dey, S.; Halder, S.; Ghosh, J.; Mukherjee, D.; Sultana, S. S.; Biswas, G., Successful therapy of murine visceral Leishmaniasis with astrakurkurone, a triterpene isolated from the mushroom *Astraeus hygrometricus*, involves the induction of protective cell-mediated immunity and TLR9. *Antimicrobial Agents and Chemotherapy* **2016**, *60* (5), 2696-2708.
72. Leliebre-Lara, V.; Monzote Fidalgo, L.; Pferschy-Wenzig, E.-M.; Kunert, O.; Nogueiras Lima, C.; Bauer, R., *In vitro* antileishmanial activity of sterols from *Trametes versicolor* (Bres. Rivarden). *Molecules* **2016**, *21* (8), 1045.
73. Schnekenburger, M.; Mathieu, V.; Lefranc, F.; Jang, J. Y.; Masi, M.; Kijjoo, A.; Evidente, A.; Kim, H.-J.; Kiss, R.; Dicato, M., The fungal metabolite eurochevalierine, a sesquiterpene alkaloid, displays anti-cancer properties through selective sirtuin 1/2 inhibition. *Molecules* **2018**, *23* (2), 333.
74. Isaka, M.; Prathumpai, W.; Wongsap, P.; Tanticharoen, M., Hirsutellone F, a dimer of antitubercular alkaloids from the seed fungus *Trichoderma* species BCC 7579. *Organic Letters* **2006**, *8* (13), 2815-2817.
75. Kongsaree, P.; Prabpai, S.; Sriubolmas, N.; Vongvein, C.; Wiyakrutta, S., Antimalarial dihydroisocoumarins produced by *Geotrichum* sp., an endophytic fungus of *Crassocephalum c repidioides*. *Journal of Natural Products* **2003**, *66* (5), 709-711.
76. Duarte, M.; Seixas, A.; de Carvalho, M. P.; Tasca, T.; Macedo, A. J., Amaurocine: anti-*Trichomonas vaginalis* protein produced by the basidiomycete *Amauroderma camerarium*. *Experimental Parasitology* **2016**, *161*, 6-11.
77. Nilanonta, C.; Isaka, M.; Kittakoo, P.; Palittapongarnpim, P.; Kamchonwongpaisan, S.; Pittayakhajonwut, D.; Tanticharoen, M.; Thebtaranonth, Y., Antimycobacterial and antiplasmodial cyclodepsipeptides from the insect pathogenic fungus *Paecilomyces tenuipes* BCC 1614. *Planta Medica* **2000**, *66* (08), 756-758.
78. Thongtan, J.; Saenboonrueng, J.; Rachtawee, P.; Isaka, M., An antimalarial tetrapeptide from the entomopathogenic fungus *Hirsutella* sp. BCC 1528. *Journal of Natural Products* **2006**, *69* (4), 713-714.
79. Mishra, K.; Ganju, L.; Sairam, M.; Banerjee, P.; Sawhney, R., A review of high throughput technology for the screening of natural products. *Biomedicine and Pharmacotherapy* **2008**, *62* (2), 94-98.
80. Geris, R.; Simpson, T. J., Meroterpenoids produced by fungi. *Natural Product Report* **2009**, *26* (8), 1063-1094.
81. McGleenon, B.; Dynan, K.; Passmore, A., Acetylcholinesterase inhibitors in Alzheimer's disease. *British Journal of Clinical Pharmacology* **1999**, *48* (4), 471.
82. Martinez, A.; Castro, A., Novel cholinesterase inhibitors as future effective drugs for the treatment of Alzheimer's disease. *Expert Opinion on Investigational Drugs* **2006**, *15* (1), 1-12.
83. Korczyn, A. D.; Giladi, N., Acetylcholinesterase Inhibitors in the Treatment of Dementia in Parkinson's Disease. In *Mental and Behavioral Dysfunction in Movement Disorders*, Springer: **2003**; 295-301.
84. Mehndiratta, M. M.; Pandey, S.; Kuntzer, T., Acetylcholinesterase inhibitor treatment for myasthenia gravis. *Cochrane Database of Systematic Reviews* **2014**, (10).

85. Almasieh, M.; MacIntyre, J. N.; Pouliot, M.; Casanova, C.; Vaucher, E.; Kelly, M. E.; Di Polo, A., Acetylcholinesterase inhibition promotes retinal vasoprotection and increases ocular blood flow in experimental glaucoma. *Investigative Ophthalmology and Visual Science* **2013**, *54* (5), 3171-3183.
86. Futso, L. K. Y. C. P., Territrems, Tremorgenic Mycotoxins of *Aspergillus terreus*. *Applied and Environmental Microbiology* **1979**, *37* (3), 355-357.
87. Kuohuang ling, H.-H. L., Chuen-Mao Yang, Chuen-Mao Yang . Isolation, chemical structure, acute toxicity, and some physicochemical properties of territrems C from *Aspergillus terreus*. *Applied and Environmental Microbiology* **1984**, *47* (1), 98-100.
88. Shoei-Sheng Lee, F.-C. P., Chi-Ming Chiou, Kuohuang Ling., NMR assignments of territrems A, B and C and the structure of MB2, the major metabolite of territrems B by rat liver microsomal fraction. . *Journal of Natural Products* **1992**, *55* (2), 251-255.
89. Kuo Huang Ling, C. M. C., Yun Long Tseng, Biotransformation of territrems by S9 fraction from rat liver. *Drug Metabolism and Disposition* **1991**, *19* (3), 587-695.
90. Peng, F.-C., Structure and Anti-Acetylcholinesterase Activity of 4 α -(Hydroxymethyl)-4 α -demethylterritrem B. *Journal of Natural Products* **1997**, *60* (8), 842-843.
91. P.F. Dowd, F. C. P., J. W. Chen, K.H. Ling., Toxicity and anticholinesterase activity of the fungal metabolites territrems to the corn earworm, *Helicoverpa zea*. *Entomologia Experimentalis et Applicata* **1992**, *65*, 57-64.
92. Satoshi Omura, F. K., et, al., Arisugacin, a novel and selective inhibitor of acetylcholinesterase from *penicillium* sp. FO-4259. *The Journal of Antibiotics* **1995**, *48* (7), 745-746.
93. Ling, K. H.; Peng, F. C.; Chen, B. J., Symposium; isolation, physicochemical properties and toxicities of territrems A'and B'. *Journal of Food Science and Technology* **1986**, *17* (2), 153-160.
94. Peng, F.-C., Acetylcholinesterase inhibition by territrems B derivatives. *Journal of Natural Products* **1995**, *58* (6), 857-862.
95. Nong, X. H.; Wang, Y. F.; Zhang, X. Y.; Zhou, M. P.; Xu, X. Y.; Qi, S. H., Territrems and butyrolactone derivatives from a marine-derived fungus *Aspergillus terreus*. *Marine Drugs* **2014**, *12* (12), 6113-6124.
96. Omura, F. K. K. O. K. S. Y. I. S., Arisugacins A and B, Novel and Selective Acetylcholinesterase Inhibitors from *Penicillium* sp. FO-4259. *The Journal of Antibiotics* **1996**, *49* (8), 742-747.
97. Miyoshi Kuno, K. S., Kazuhiko Ootoguro,; Toshiaki Sunazuka, S. O., Arisugacins A and B, Novel and Selective Acetylcholinesterase Inhibitors from *Penicillium* sp. FO-4259 II. structure elucidation. *The Journal of Antibiotics* **1996**, *49* (8), 748-751.
98. Kazuhiko Ootoguro, Kazuhiko Ootoguro, Miyoshi Kuno, K. S., Arisugacins C and D, Novel acetylcholinesterase inhibitors and their related novel metabolites produced by *Penicillium* sp. FO-4259-II. *The Journal of Antibiotics* **2000**, *53* (1), 50-57.
99. Masaki Handa, T. S., Kenichiro Nagai, Ryouko Kimura, Kazuhiko Ootoguro, Yoshihiro Harigaya, Satoshi Omura, Determination of absolute stereochemistries of arisugacin F and territrems B, novel acetylcholinesterase inhibitors. *The Journal of Antibiotics* **2001**, *54* (4), 386-391.
100. Sunazuka, T.; Handa, M.; Nagai, K.; Shirahata, T.; Harigaya, Y.; Ootoguro, K.; Kuwajima, I.; Omura, S., Absolute stereochemistries and total synthesis of (+)-arisugacins A and B, potent,

- orally bioactive and selective inhibitors of acetylcholinesterase. *Tetrahedron* **2004**, *60* (36), 7845-7859.
101. Xinhua Sun, X. K., Huquan Gao, Tianjiao Zhu, Guangwei Wu, Qianqun Gu, Dehai Li, Two new meroterpenoids produced by the endophytic fungus *Penicillium* sp. SXH-65. *Archives of Pharmacal Research* **2014**, *37*, 978-982.
102. Li, X. D.; Miao, F. P.; Liang, X. R.; Ji, N. Y., Meroterpenes from an algicolous strain of *Penicillium echinulatum*. *Magnetic Resonance Chemistry* **2014**, *52* (5), 247-250.
103. Ick-dong, C. K.-M. K. W.-G. L. C.-K. Y., Terreulactones A, B, C, and D- novel acetylcholinesterase inhibitors produced by *Aspergillus terreus*. *The Journal of Antibiotics* **2003**, *56* (4), 344-350.
104. Kim Won-Gon, C. K.-M., Lee Chong-Kil, Yoo Ick-Dong, Terreulactones A, B, C, and D- novel acetylcholinesterase inhibitors produced by *Aspergillus terreus* I. taxonomy, fermentation, isolation and biological activities. *The Journal of Antibiotics* **2003**, *56* (4), 344-350.
105. Yoo, I. D.; Cho, K. M.; Lee, C. K.; Kim, W. G., Isoterreulactone A, a novel meroterpenoid with anti-acetylcholinesterase activity produced by *Aspergillus terreus*. *Bioorganic Medecinal Chemistry Letter* **2005**, *15* (2), 353-356.
106. Li, J. W.-H.; Vederas, J. C., Drug discovery and natural products: end of an era or an endless frontier? *Science* **2009**, *325* (5937), 161-165.
107. Newman, D. J., Natural products as leads to potential drugs: an old process or the new hope for drug discovery? *Journal of Medicinal Chemistry* **2008**, *51* (9), 2589-2599.
108. Saklani, A.; Kutty, S. K., Plant-derived compounds in clinical trials. *Drug Discovery Today* **2008**, *13* (3-4), 161-171.
109. Kennedy, J.; Marchesi, J. R.; Dobson, A. D., Marine metagenomics: strategies for the discovery of novel enzymes with biotechnological applications from marine environments. *Microbial Cell Factories* **2008**, *7* (1), 27.
110. Xu, J., Fungal DNA barcoding. *Genome* **2016**, *59* (11), 913-932.
111. Casselman, A., Strange but true: The largest organism on Earth is a fungus. *Scientific American* **2007**, *4*.
112. Raja, H. A.; Miller, A. N.; Pearce, C. J.; Oberlies, N. H., Fungal identification using molecular tools: a primer for the natural products research community. *Journal of Natural Products* **2017**, *80* (3), 756-770.
113. Grube, M.; Gaya, E.; Kauserud, H.; Smith, A. M.; Avery, S. V.; Fernstad, S. J.; Muggia, L.; Martin, M. D.; Eivindsen, T.; Koljalg, U., The next generation fungal diversity researcher. *Fungal Biology Reviews* **2017**, *31* (3), 124-130.
114. Drews, G., The developmental biology of fungi—a new concept introduced by Anton de Bary. **2001**.
115. Petersen, R. H.; Knudsen, H., the mycological legacy of Elias Magnus Fries. *IMA Fungus* **2015**, *6* (1), 99-114.
116. Romero, A. I.; Minter, D., Fluorescence microscopy: an aid to the elucidation of ascomycete structures. *Transactions of the British Mycological Society* **1988**, *90* (3), 457.
117. Kurtzman, C.; Fell, J. W.; Boekhout, T., The yeasts: a taxonomic study. Elsevier: 2011.
118. De Hoog, G.; Guarro, J.; Gene, J.; Figueras, M., Atlas of clinical fungi, centraalbureau voor schimmelcultures. *Utrecht, The Netherlands* **2000**, 276-282.
119. Seifert, K. A.; Wingfield, B. D.; Wingfield, M. J., A critique of DNA sequence analysis in the taxonomy of filamentous Ascomycetes and ascomycetous anamorphs. *Canadian Journal of Botany* **1995**, *73* (S1), 760-767.

120. Innis, M. A.; Gelfand, D. H.; Sninsky, J. J.; White, T. J., *PCR protocols: a guide to methods and applications*. Academic press: **2012**.
121. Rossman, A. Y.; Palm-Hernández, M. E., Systematics of plant pathogenic fungi: why it matters. *Plant Disease* **2008**, *92* (10), 1376-1386.
122. Bridge, P. D.; Roberts, P. J.; Spooner, B. M.; Panchal, G., On the unreliability of published DNA sequences. *New Phytologist* **2003**, *160* (1), 43-48.
123. Vilgalys, R., Taxonomic misidentification in public DNA databases. *New Phytologist* **2003**, *160* (1), 4-5.
124. Zamora, J. C.; Svensson, M.; Kirschner, R., Considerations and consequences of allowing DNA sequence data as types of fungal taxa. *IMA Fungus* **2018**, *9* (1), 167-175.
125. Thines, M.; Crous, P. W.; Aime, M. C.; Aoki, T.; Cai, L.; Hyde, K. D.; Miller, A. N.; Zhang, N.; Stadler, M., Ten reasons why a sequence-based nomenclature is not useful for fungi anytime soon. *IMA Fungus* **2018**, *9* (1), 177-183.
126. Nilsson, R. H.; Ryberg, M.; Kristiansson, E.; Abarenkov, K.; Larsson, K.-H.; Kõljalg, U., Taxonomic reliability of DNA sequences in public sequence databases: a fungal perspective. *Plos One* **2006**, *1* (1), 59.
127. Nilsson, R. H.; Kristiansson, E.; Ryberg, M.; Larsson, K.-H., Approaching the taxonomic affiliation of unidentified sequences in public databases – an example from the mycorrhizal fungi. *BMC Bioinformatics* **2005**, *6* (1), 178.
128. Fitzsimmons, M., The problem of uncertainty in strategic planning. *Survival* **2006**, *48* (4), 131-146.
129. Seifert, K. A., Progress towards DNA barcoding of fungi. *Molecular Ecology resources* **2009**, *9*, 83-89.
130. Nilsson, R. H.; Kristiansson, E.; Ryberg, M.; Hallenberg, N.; Larsson, K.-H., Intraspecific ITS variability in the kingdom fungi as expressed in the international sequence databases and its implications for molecular species identification. *Evolutionary Bioinformatics* **2008**, *4*, EBO. S653.
131. SHAREOK Citizen Science Soil Collection Program.
<https://shareok.org/handle/11244/28096>.
132. Ayer, W. A.; Jimenez, L. D., Phomalone, an antifungal metabolite of *Phoma etheridgei*. *Canadian Journal of Chemistry* **1994**, *72* (11), 2326-2332.
133. Li, D. R.; Murugan, A.; Falck, J., Enantioselective, organocatalytic oxy-Michael addition to γ/δ -hydroxy- α , β -enones: boronate-amine complexes as chiral hydroxide synthons. *Journal of the American Chemical Society* **2008**, *130* (1), 46-48.
134. Sappapan, R.; Sommit, D.; Ngamrojanavanich, N.; Pengpreecha, S.; Wiyakrutta, S.; Sriubolmas, N.; Pudhom, K., 11-Hydroxymonocerin from the plant endophytic fungus *Exserohilum rostratum*. *Journal of Natural Products* **2008**, *71* (9), 1657-1659.
135. Zhang, W.; Krohn, K.; Draeger, S.; Schulz, B., Bioactive isocoumarins isolated from the endophytic fungus *Microdochium bolleyi*. *Journal of Natural Products* **2008**, *71* (6), 1078-1081.
136. Li, R.; Chen, S.; Niu, S.; Guo, L.; Yin, J.; Che, Y., Exserolides A–F, new isocoumarin derivatives from the plant endophytic fungus *Exserohilum* sp. *Fitoterapia* **2014**, *96*, 88-94.
137. Krohn, K.; Bahramsari, R.; Flörke, U.; Ludewig, K.; Kliche-Spory, C.; Michel, A.; Aust, H.-J.; Draeger, S.; Schulz, B.; Antus, S., Dihydroisocoumarins from fungi: isolation, structure elucidation, circular dichroism and biological activity. *Phytochemistry* **1997**, *45* (2), 313-320.

138. Seco, J. M.; Quiñoá, E.; Riguera, R., A practical guide for the assignment of the absolute configuration of alcohols, amines and carboxylic acids by NMR. *Tetrahedron: Asymmetry* **2001**, *12* (21), 2915-2925.
139. Su, B.-N.; Park, E. J.; Mbwambo, Z. H.; Santarsiero, B. D.; Mesecar, A. D.; Fong, H. H.; Pezzuto, J. M.; Kinghorn, A. D., New chemical constituents of *Euphorbia quinquecostata* and absolute configuration assignment by a convenient Mosher ester procedure carried out in NMR tubes. *Journal of Natural Products* **2002**, *65* (9), 1278-1282.
140. Cai, S.; King, J. B.; Du, L.; Powell, D. R.; Cichewicz, R. H., Bioactive sulfur-containing sulochrin dimers and other metabolites from an *Alternaria* sp. isolate from a Hawaiian soil sample. *Journal of Natural Products* **2014**, *77* (10), 2280-2287.
141. Sutton, M.; Sternberg, M.; Koumans, E. H.; McQuillan, G.; Berman, S.; Markowitz, L., The prevalence of *Trichomonas vaginalis* infection among reproductive-age women in the United States, 2001-2004. *Clinical Infectious Diseases* **2007**, *45* (10), 1319-1326.
142. Kissinger, P., *Trichomonas vaginalis*: a review of epidemiologic, clinical and treatment issues. *BMC Infectious Diseases* **2015**, *15*, 307.
143. Gabriel, G.; Robertson, E.; Thin, R. N., Single dose treatment of trichomoniasis. *Journal of International Medical Research* **1982**, *10* (2), 129-130.
144. Aubert, J. M.; Sesta, H. J., Treatment of vaginal trichomoniasis. Single, 2-gram dose of metronidazole as compared with a seven-day course. *Journal of Reproductive Medicine* **1982**, *27* (12), 743-745.
145. Howe, K.; Kissinger, P. J., Single-dose compared with multidose metronidazole for the treatment of trichomoniasis in women: a meta-analysis. *Sexually Transmitted Diseases* **2017**, *44* (1), 29-34.
146. Bendesky, A.; Menéndez, D.; Ostrosky-Wegman, P., Is metronidazole carcinogenic? *Mutation Research* **2002**, *511* (2), 133-144.
147. Dobiás, L.; Černá, M.; Rössner, P.; Šrám, R., Genotoxicity and carcinogenicity of metronidazole. *Mutation Research* **1994**, *317* (3), 177-194.
148. Prevention, C. f. D. C. a. 2015 Sexually transmitted diseases treatment guidelines. <https://www.cdc.gov/std/tg2015/trichomoniasis.htm>.
149. Kirkcaldy, R. D.; Augostini, P.; Asbel, L. E.; Bernstein, K. T.; Kerani, R. P.; Mettenbrink, C. J.; Pathela, P.; Schwebke, J. R.; Secor, W. E.; Workowski, K. A.; Davis, D.; Braxton, J.; Weinstock, H. S., *Trichomonas vaginalis* antimicrobial drug resistance in 6 US cities, STD Surveillance Network, 2009-2010. *Emerging Infectious Diseases* **2012**, *18* (6), 939-943.
150. Schwebke, J. R.; Barrientes, F. J., Prevalence of *Trichomonas vaginalis* isolates with resistance to metronidazole and tinidazole. *Antimicrob Agents Chemother* **2006**, *50* (12), 4209-4210.
151. Scopel, M.; dos Santos, O.; Frasson, A.; Abraham, W.; Tasca, T.; Henriques, A.; Macedo, A., Anti-*Trichomonas vaginalis* activity of marine-associated fungi from the South Brazilian Coast. *Experimental Parasitology* **2013**, *133* (2), 211-216.
152. Duarte, M.; Seixas, A.; de Carvalho, M.; Tasca, T.; Macedo, A., Amaurocine: Anti-*Trichomonas vaginalis* protein produced by the basidiomycete *Amauroderma camerarium*. *Experimental Parasitology* **2016**, *161*, 6-11.
153. Desrivot, J.; Waikedre, J.; Cabalion, P.; Herrenknecht, C.; Bories, C.; Hocquemiller, R.; Fournet, A., Antiparasitic activity of some New Caledonian medicinal plants. *Journal of Ethnopharmacology* **2007**, *112*, 7-12.

154. Calzada, F.; Yepez-Mulia, L.; Tapia-Contreras, A., Effect of Mexican medicinal plant used to treat trichomoniasis on *Trichomonas vaginalis* trophozoites. *Journal of Ethnopharmacology* **2007**, *113*, 248-251.
155. Lara-Díaz, V.; Gaytán-Ramos, A.; Dávalos-Balderas, A.; Santos-Guzmán, J.; Mata-Cárdenas, B.; Vargas-Villarreal, J.; Barbosa-Quintana, A.; Sanson, M.; López-Reyes, A.; Moreno-Cuevas, J., Microbiological and toxicological effects of Perla black bean (*Phaseolus vulgaris* L.) extracts: *in vitro* and *in vivo* studies. *Basic Clinical Pharmacology Toxicology* **2009**, *104*, 81-86.
156. Moon, T.; Wilkinson, J.; Cavanagh, H., Antiparasitic activity of two *Lavandula* essential oils against *Giardia duodenalis*, *Trichomonas vaginalis*, and *Hexamita inflata*. *Parasitology Research* **2006**, *99*, 722-728.
157. Kaneda, Y.; Tanaka, T.; Saw, T., Effects of berberine, a plant alkaloid, on the growth of anaerobic protozoa in axenic culture. *Tokai Journal of Experimental and Clinical Medicine* **1990**, *15* (6), 417-423.
158. Wu, J.; Zhang, M.; Ding, D.; Tan, T.; Yan, B., Effect of *Cladonia alpestris* on *Trichomonas vaginalis* *in vitro*. *Zhongguo Ji Sheng Chong Xue Yu Ji Sheng Chong Bing Za Zhi* **1995**, *13* (2), 126-129.
159. Wang, H., Antitrichomonal action of emodin in mice. *Journal of Ethnopharmacology* **1993**, *40* (2), 111-116.
160. Bhagwat, P.; Gokhale, B.; Sane, H.; Thirumalachar, M., Assessment of antitrichomonal activity of hamycin. *Indian Journal of Medical Research* **1964**, *52*, 36-37.
161. He, W.; VanPuyvelde, L.; Maes, L.; Bosselaers, J.; DeKimpe, N., Antitrichomonas *in vitro* activity of *Cussonia holstii*. *England Journal of Natural Product Resarch* **2003**, *17* (2), 127-133.
162. Loyola, L.; Bórquez, J.; Morales, G.; Araya, J.; González, J.; Neira, I.; Sagua, H.; San-Martín, A., Diterpenoids from *Azorella yareta* and their trichomonocidal activities. *Phytochemistry* **2001**, *56* (2), 177-180.
163. Newman, D. J.; Cragg, G. M., Natural Products as Sources of New Drugs from 1981 to 2014. *Journal of Natural Products* **2016**, *79* (3), 629-661.
164. Kayser, O.; Kiderlen, A.; Croft, S., Natural products as antiparasitic drugs. *Parasitology Research* **2003**, *90*, S55-S62.
165. Meingassner, J.; Thurner, J., Strain of *Trichomonas vaginalis* resistant to metronidazole and other 5-nitroimidazoles. *Antimicrobiol Agents Chemother.* **1979**, *15* (2), 254-257.
166. Campos Aldrete, M.; Salgado-Zamora, H.; Luna, J.; Meléndez, E.; Meráz-Ríos, M., A high-throughput colorimetric and fluorometric microassay for the evaluation of nitroimidazole derivatives anti-trichomonas activity. *Toxicology in Vitro* **2005**, *19* (8), 1045-1050.
167. Duarte, M.; Giordani, R.; De Carli, G.; Zuanazzi, J.; Macedo, A.; Tasca, T., A quantitative resazurin assay to determinate the viability of *Trichomonas vaginalis* and the cytotoxicity of organic solvents and surfactant agents. *Experimental Parasitology* **2009**, *123*, 195-198.
168. Chen, J. L.; Steele, T. W. J.; Stuckey, D. C., Modeling and application of a rapid fluorescence-based assay for biotoxicity in anaerobic digestion. *Environmental Science and Technology* **2015**, *49* (22), 13463-13471.
169. Forestier, C.; Späth, G.; Prina, E.; Dasari, S., Simultaneous multi-parametric analysis of *Leishmania* and of its hosting mammal cells: a high content imaging-based method enabling sound drug discovery process. *Microbial Pathogenesis* **2015**, *88*, 103-108.

170. N. J. Philips, J. T. G., A. Fraiman, R. J. Cole, D. G. Lynn, Characterization of the *Fusarium* Toxin Equisetin- The Use of phenylboronates in structure assignment. *Journal of American Chemical Society* **1989**, *111* (21), 8223-8231.
171. Jadulco, R. C.; Koch, M.; Kakule, T. B.; Schmidt, E. W.; Orendt, A.; He, H.; Janso, J. E.; Carter, G. T.; Larson, E. C.; Pond, C.; Matainaho, T. K.; Barrows, L. R., Isolation of pyrrolocins A-C: cis- and trans-decalin tetramic acid antibiotics from an endophytic fungal-derived pathway. *Journal of Natural Products* **2014**, *77* (11), 2537-2544.
172. Minowa, N. K., Y.; Harimaya, K.; Mikawa, T, A degradation study of vermispurin and determination of its absolute configuration. *Heterocycles* **1998**, *48* (8), 1639-1642.
173. Singh, S. B. Z., D. L.; Goetz, M. A.; Dombrowski, A. W.; Polishook, J. D.; Hazuda, D. J., Equisetin and a novel opposite stereochemical homolog phomasetin, two fungal metabolites as inhibitors of HIV-1 integrase. *Tetrahedron Letter* **1998**, *39* (16), 2243-2246.
174. Phillips, N.; Goodwin, J.; Fraiman, A.; Cole, R.; Lynn, D., Characterization of the *Fusarium* toxin equisetin- the use of phenylboronates in structure assignment. *Journal of American Chemical Society* **1989**, *111* (21), 8223-8231.
175. Marfori, E.; Kajiyama, S.; Fukusaki, E.; Kobayashi, A., Trichosetin, a novel tetramic acid antibiotic produced in dual culture of *Trichoderma harzianum* and *Catharanthus roseus* Callus. *Zeitschrift fur Naturforsch C* **2002**, *57* (5-6), 465-470.
176. Neumann, K.; Kehraus, S.; Gütschow, M.; König, G., Cytotoxic and HLE-inhibitory tetramic acid derivatives from marine-derived fungi. *Natural Product Communication* **2009**, *4* (3), 347-354.
177. Singh, S. B.; Zink, D. L.; Goetz, M. A.; W., D. A.; Polishook, J. D.; Hazuda, D. J., Equisetin and a novel opposite stereochemical homolog phomasetin, two fungal metabolites as inhibitors of HIV-1 integrase. *Tetrahedron Letter* **1998**, *39* (16), 2243-2246.
178. Yamada, S.; Hongo, C.; Yoshioka, R.; Chibata, I., Method for the racemization of optically active amino acids. *Journal of Organic Chemistry* **1983**, *48* (6), 843-846.
179. Kiyonaga Fujii, Y. I., Hisao Oka, Makoto Suzuki, ken-ichi Harada., A Nonempirical method using LC/MS for determination of the absolute configuration of constituent amino acids in a peptide- combination of Marfey's method with Mass Spectrometry and Its practical application. *Analytical chemistry* **1997**, *69* (24), 5146-5151.
180. Fujii, K.; Ikai, Y.; Oka, H.; Suzuki, M.; Harada, K., A nonempirical method using LC/MS for determination of the absolute configuration of constituent amino acids in a peptide-combination of Marfey's method with mass spectrometry and Its practical application. *Analytical Chemistry* **1997**, *69* (24), 5146-5151.
181. Ratnaweera, P. B.; de Silva, E. D.; Williams, D. E.; Andersen, R. J., Antimicrobial activities of endophytic fungi obtained from the arid zone invasive plant *Opuntia dillenii* and the isolation of equisetin, from endophytic *Fusarium* sp. *BMC Complementary and Alternative Medicine* **2015**, *15* (1), 220.
182. Putri, S. P.; Kinoshita, H.; Ihara, F.; Igarashi, Y.; Nihira, T., Ophiosetin, a new tetramic acid derivative from the mycopathogenic fungus *Elaphocordyceps ophioglossoides*. *The Journal of Antibiotics* **2010**, *63* (4), 195.
183. Davids, B.; Gillin, F., Methods for *Giardia* culture, cryopreservation, encystation, and excystation *in vitro*. In *Giardia A Model Organism*, SpringerWienNewYork: **2011**; 381-394.
184. Paget, T.; Lloyd, D., *Trichomonas vaginalis* requires traces of oxygen and high concentrations of carbon dioxide for optimal growth. *Molecular and Biochemical Parasitology* **1990**, *41* (1), 65-72.

185. Du, L.; Risinger, A.; King, J.; Powell, D.; Cichewicz, R., A potent HDAC inhibitor, 1-alaninechlamydocin, from a *Tolypocladium* sp. induces G2/M cell cycle arrest and apoptosis in MIA PaCa-2 cells. *Journal of Natural Products* **2014**, *77* (7), 1753-1757.
186. Hansen, M.; Nielsen, S.; Berg, K., Re-examination and further development of a precise and rapid dye method for measuring cell growth/cell kill. *Journal of Immunological. Methods* **1989**, *119* (2), 203-210.
187. Colovic, M. B.; Krstic, D. Z.; Lazarevic-Pasti, T. D.; Bondzic, A. M.; Vasic, V. M., Acetylcholinesterase inhibitors: pharmacology and toxicology. *Current Neuropharmacology* **2013**, *11* (3), 315-335.
188. Houghton, P. J.; Ren, Y.; Howes, M. J., Acetylcholinesterase inhibitors from plants and fungi. *Natural Product Reports* **2006**, *23* (2), 181-199.
189. Lazarevic-Pasti, T.; Leskovac, A.; Momic, T.; Petrovic, S.; Vasic, V., Modulators of acetylcholinesterase activity: from Alzheimer's disease to anti-cancer drugs. *Current Medicinal Chemistry* **2017**, *24* (30), 3283-3309.
190. Pinho, B. R.; Ferreres, F.; Valentao, P.; Andrade, P. B., Nature as a source of metabolites with cholinesterase-inhibitory activity: an approach to Alzheimer's disease treatment. *The Journal of Pharmacy and Pharmacology* **2013**, *65* (12), 1681-700.
191. Ahmed, F.; Ghalib, R. M.; Sasikala, P.; Ahmed, K. K., Cholinesterase inhibitors from botanicals. *Pharmacognosy Reviews* **2013**, *7* (14), 121-130.
192. Loizzo, M. R.; Tundis, R.; Menichini, F.; Menichini, F., Natural products and their derivatives as cholinesterase inhibitors in the treatment of neurodegenerative disorders: an update. *Current Medicinal Chemistry* **2008**, *15* (12), 1209-1228.
193. Viegas, C., Jr.; Bolzani Vda, S.; Barreiro, E. J.; Fraga, C. A., New anti-Alzheimer drugs from biodiversity: the role of the natural acetylcholinesterase inhibitors. *Mini Reviews in Medicinal Chemistry* **2005**, *5* (10), 915-926.
194. Farrokhnia, M.; Nabipour, I., Marine natural products as acetylcholinesterase inhibitor: comparative quantum mechanics and molecular docking study. *Current Computer-Aided Drug Design* **2014**, *10* (1), 83-95.
195. Rennekamp, A. J.; Peterson, R. T., 15 years of zebrafish chemical screening. *Current Opinion in Chemical Biology* **2015**, *24*, 58-70.
196. MacRae, C. A.; Peterson, R. T., Zebrafish as tools for drug discovery. *Nature Reviews Drug Discovery* **2015**, *14* (10), 721-731.
197. Sandoval, I. T.; Manos, E. J.; Van Wagoner, R. M.; Delacruz, R. G.; Edes, K.; Winge, D. R.; Ireland, C. M.; Jones, D. A., Juxtaposition of chemical and mutation-induced developmental defects in zebrafish reveal a copper-chelating activity for kalihinol F. *Chemistry and Biology* **2013**, *20* (6), 753-763.
198. Asnani, A.; Peterson, R. T., The zebrafish as a tool to identify novel therapies for human cardiovascular disease. *Disease Models and Mechanisms* **2014**, *7* (7), 763-767.
199. Baraban, S. C.; Dinday, M. T.; Hortopan, G. A., Drug screening in Scn1a zebrafish mutant identifies clemizole as a potential Dravet syndrome treatment. *Nature Communications* **2013**, *4*, 2410.
200. Santoriello, C.; Zon, L. I., Hooked! Modeling human disease in zebrafish. *The Journal of Clinical Investigation* **2012**, *122* (7), 2337-2343.
201. Kokel, D.; Bryan, J.; Laggner, C.; White, R.; Cheung, C. Y. J.; Mateus, R.; Healey, D.; Kim, S.; Werdich, A. A.; Haggarty, S. J., Rapid behavior-based identification of neuroactive small molecules in the zebrafish. *Nature Chemical Biology* **2010**, *6* (3), 231.

202. Rihel, J.; Prober, D. A.; Arvanites, A.; Lam, K.; Zimmerman, S.; Jang, S.; Haggarty, S. J.; Kokel, D.; Rubin, L. L.; Peterson, R. T., Zebrafish behavioral profiling links drugs to biological targets and rest/wake regulation. *Science* **2010**, *327* (5963), 348-351.
203. Porazzi, P.; Calebiro, D.; Benato, F.; Tiso, N.; Persani, L., Thyroid gland development and function in the zebrafish model. *Molecular and Cellular Endocrinology* **2009**, *312* (1-2), 14-23.
204. Paffett-Lugassy, N.; Hsia, N.; Fraenkel, P. G.; Paw, B.; Leshinsky, I.; Barut, B.; Bahary, N.; Caro, J.; Handin, R.; Zon, L. I., Functional conservation of erythropoietin signaling in zebrafish. *Blood* **2007**, *110* (7), 2718-2726.
205. McKeown, K. A.; Downes, G. B.; Hutson, L. D., Modular laboratory exercises to analyze the development of zebrafish motor behavior. *Zebrafish* **2009**, *6* (2), 179-185.
206. Behra, M.; Cousin, X.; Bertrand, C.; Vonesch, J.-L.; Biellmann, D.; Chatonnet, A.; Strähle, U., Acetylcholinesterase is required for neuronal and muscular development in the zebrafish embryo. *Nature Neuroscience* **2002**, *5* (2), 111.
207. Kazuhiko Otoguro, K. S., Yuuichi Yamaguchi, Noriko Aral, Toshiaki Sunazuka, Rokuro Masuma, Yuzuru Jwai, Satoshi Omura., Arisugacins C and D, novel acetylcholinesterase inhibitors and their related novel metabolites produced by *Penicilium* sp. FO-4259-11. *The Journal of Antibiotics* **2000**, *53* (1), 50-57.
208. Otoguro, K.; Kuno, F.; Ōmura, S., Arisugacins, selective acetylcholinesterase inhibitors of microbial origin. *Pharmacology and Therapeutics* **1997**, *76* (1-3), 45-54.
209. Triggle, D. J.; Mitchell, J. M.; Filler, R., The pharmacology of physostigmine. *CNS Drug Reviews* **1998**, *4* (2), 87-136.
210. Koelle, G. B.; Davis, R.; Diliberto Jr, E. J.; Koelle, W. A., Selective, near-total, irreversible inactivation of peripheral pseudocholin-esterase and acetylcholinesterase in cats in vivo. *Biochemical Pharmacology* **1974**, *23* (2), 175-188.
211. Mehta, M.; Adem, A.; Sabbagh, M., New acetylcholinesterase inhibitors for Alzheimer's disease. *International Journal of Alzheimer's Disease* **2012**, *2012*.
212. Shao, Y.; Molnar, L. F.; Jung, Y.; Kussmann, J.; Ochsenfeld, C., Advances in methods and algorithms in a modern quantum chemistry program package. *Physical Chemistry Chemical Physics* **2006**, *8* (27), 3172-3191.
213. Frisch, M. J.; Trucks, G.; Schlegel, H. B.; Scuseria, G.; Robb, M., Gaussian 09, revision A. 1. *Gaussian Inc. Wallingford CT* **2009**, *27*, 34.
214. Bruhn, T.; Schaumlöffel, A.; Hemberger, Y.; Bringmann, G., SpecDis: Quantifying the comparison of calculated and experimental electronic circular dichroism spectra. *Chirality* **2013**, *25* (4), 243-249.
215. Akimenko, M.-A.; Johnson, S. L.; Westerfield, M.; Ekker, M., Differential induction of four msx homeobox genes during fin development and regeneration in zebrafish. *Development* **1995**, *121* (2), 347-357.
216. Thisse, C.; Thisse, B., High-resolution in situ hybridization to whole-mount zebrafish embryos. *Nature Protocols* **2008**, *3* (1), 59.

Appendix A: Supporting Data for Chapter 3

Appendix Table of Contents

Figure A1. ^1H NMR spectrum of compound 3.1 (CDCl_3 , 400 MHz).....	119
Figure A2. ^{13}C NMR spectrum of compound 3.1 (CDCl_3 , 100 MHz)	119
Figure A3. COSY spectrum of compound 3.1 (CDCl_3 , 400 MHz)	120
Figure A4. HSQC spectrum of compound 3.1 (CDCl_3 , 400 MHz)	120
Figure A5. HMBC spectrum of compound 3.1 (CDCl_3 , 400 MHz)	121
Figure A6. ^1H NMR spectrum of compound 3.3 ($\text{MeOH-}d_4$, 400 MHz)	121
Figure A7. ^{13}C NMR spectrum of compound 3.3 ($\text{MeOH-}d_4$, 100 MHz).....	122
Figure A8. COSY spectrum of compound 3.3 ($\text{MeOH-}d_4$, 400 MHz)	122
Figure A9. HSQC spectrum of compound 3.3 ($\text{MeOH-}d_4$, 400 MHz)	123
Figure A10. HMBC spectrum of compound 3.3 ($\text{MeOH-}d_4$, 400 MHz).....	123
Figure A11. HRESIMS spectrum of compound 3.	124
Figure A12. ^1H NMR spectrum of compound 3.4 ($\text{MeOH-}d_4$, 400 MHz)	124
Figure A13. ^{13}C NMR spectrum of compound 3.4 ($\text{MeOH-}d_4$, 100 MHz)	125
Figure A14. COSY spectrum of compound 3.4 ($\text{MeOH-}d_4$, 400 MHz)	125
Figure A15. HSQC spectrum of compound 3.4 ($\text{MeOH-}d_4$, 400 MHz)	126
Figure A16. HMBC spectrum of compound 3.4 ($\text{MeOH-}d_4$, 400 MHz).....	126
Figure A17. HRESIMS spectrum of compound 3.4	127
Figure A18. ^1H NMR spectrum of compound 3.5 ($\text{MeOH-}d_4$, 400 MHz)	127
Figure A19. ^{13}C NMR spectrum of compound 3.5 ($\text{MeOH-}d_4$, 100 MHz)	128
Figure A20. COSY spectrum of compound 3.5 ($\text{MeOH-}d_4$, 400 MHz)	128
Figure A21. HSQC spectrum of compound 3.5 ($\text{MeOH-}d_4$, 400 MHz)	129
Figure A22. HMBC spectrum of compound 3.5 ($\text{MeOH-}d_4$, 400 MHz).....	129
Figure A23. HRESIMS spectrum of compound 3.5	130

Figure A24. ^1H NMR spectrum of compound 3.6 (MeOH- d_4 , 400 MHz).....	130
Figure A25. ^{13}C NMR spectrum of compound 3.6 (MeOH- d_4 , 100 MHz)	131
Figure A26. COSY spectrum of compound 3.6 (MeOH- d_4 , 400 MHz)	131
Figure A27. HSQC spectrum of compound 3.6 (MeOH- d_4 , 400 MHz)	132
Figure A28. HMBC spectrum of compound 3.6 (MeOH- d_4 , 400 MHz)	132
Figure A29. HRESIMS spectrum of compound 3.6	133
Figure A30. ^1H NMR spectrum of compound 3.7 (MeOH- d_4 , 400 MHz)	133
Figure A31. ^{13}C NMR spectrum of compound 3.7 (MeOH- d_4 , 100 MHz)	134
Figure A32. COSY spectrum of compound 3.7 (MeOH- d_4 , 400 MHz)	134
Figure A33. HSQC spectrum of compound 3.7 (MeOH- d_4 , 400 MHz)	135
Figure A34. HMBC spectrum of compound 3.7 (MeOH- d_4 , 400 MHz)	135
Figure A35. HRESIMS spectrum of compound 3	136
Figure A36. ^1H NMR spectrum of compound 3.8 (MeOH- d_4 , 400 MHz)	136
Figure A37. ^{13}C NMR spectrum of compound 3.8 (MeOH- d_4 , 100 MHz)	137
Figure A38. COSY spectrum of compound 3.8 (MeOH- d_4 , 400 MHz)	137
Figure A39. HSQC spectrum of compound 3.8 (MeOH- d_4 , 400 MHz)	138
Figure A40. HMBC spectrum of compound 3.8 (MeOH- d_4 , 400 MHz).....	138
Figure A41. ROESY spectrum of compound 3.8 (MeOH- d_4 , 400 MHz).....	139
Figure A42. HRESIMS spectrum of compound 3.8	139
Figure A43. ^1H NMR spectrum of compound 3.9 (MeOH- d_4 , 400 MHz)	140
Figure A44. ^{13}C NMR spectrum of compound 3.9 (MeOH- d_4 , 100 MHz)	140
Figure A45. COSY spectrum of compound 3.9 (MeOH- d_4 , 400 MHz)	141
Figure A46. HSQC spectrum of compound 3.9 (MeOH- d_4 , 400 MHz)	141
Figure A47. HMBC spectrum of compound 3.9 (MeOH- d_4 , 400 MHz).....	142
Figure A48. ROESY spectrum of compound 3.9 (MeOH- d_4 , 400 MHz).....	142

Figure A49. HRESIMS spectrum of compound 3.9	143
Figure A50. ^1H NMR spectrum of compound 3.10 (MeOH- d_4 , 400 MHz)	143
Figure A51. ^{13}C NMR spectrum of compound 3.10 (MeOH- d_4 , 100 MHz)	144
Figure A52. COSY spectrum of compound 3.10 (MeOH- d_4 , 400 MHz)	144
Figure A53. HSQC spectrum of compound 3.10 (MeOH- d_4 , 400 MHz)	145
Figure A54. HMBC spectrum of compound 3.10 (MeOH- d_4 , 400 MHz)	145
Figure A55. ROESY spectrum of compound 3.10 (MeOH- d_4 , 400 MHz).....	146
Figure A56. HRESIMS spectrum of compound 3.10	146
Figure A57. ^1H NMR spectrum of compound 3.11 (MeOH- d_4 , 400 MHz)	147
Figure A58. ^{13}C NMR spectrum of compound 3.11 (MeOH- d_4 , 100 MHz)	147
Figure A59. COSY spectrum of compound 3.11 (MeOH- d_4 , 400 MHz)	148
Figure A60. HSQC spectrum of compound 3.11 (MeOH- d_4 , 400 MHz)	148
Figure A61. HMBC spectrum of compound 3.11 (MeOH- d_4 , 400 MHz).....	149
Figure A62. ROESY spectrum of compound 3.11 (MeOH- d_4 , 400 MHz	149
Figure A63. HRESIMS spectrum of compound 3.11	150
Figure A64. ^1H NMR spectrum of compound 3.12 (MeOH- d_4 , 400 MHz)	150
Figure A65. ^{13}C NMR spectrum of compound 3.12 (MeOH- d_4 , 100 MHz)	151
Figure A66. COSY spectrum of compound 3.12 (MeOH- d_4 , 400 MHz)	151
Figure A67. HSQC spectrum of compound 3.12 (MeOH- d_4 , 400 MHz)	152
Figure A68. HMBC spectrum of compound 3.12 (MeOH- d_4 , 400 MHz).....	152
Figure A69. ROESY spectrum of compound 3.12 (MeOH- d_4 , 400 MHz).....	153
Figure A70. HRESIMS spectrum of compound 3.12	153
Figure A71. ^1H NMR spectrum of compound 3.13 (MeOH- d_4 , 400 MHz)	154
Figure A72. ^{13}C NMR spectrum of compound 3.13 (MeOH- d_4 , 100 MHz)	154
Figure A73. COSY spectrum of compound 3.13 (MeOH- d_4 , 400 MHz)	155

Figure A74. HSQC spectrum of compound 3.13 (MeOH- <i>d</i> ₄ , 400 MHz)	155
Figure A75. HMBC spectrum of compound 3.13 (MeOH- <i>d</i> ₄ , 400 MHz).....	156
Figure A76. ROESY spectrum of compound 3.13 (MeOH- <i>d</i> ₄ , 400 MHz).....	156
Figure A77. HRESIMS spectrum of compound 3.13	157

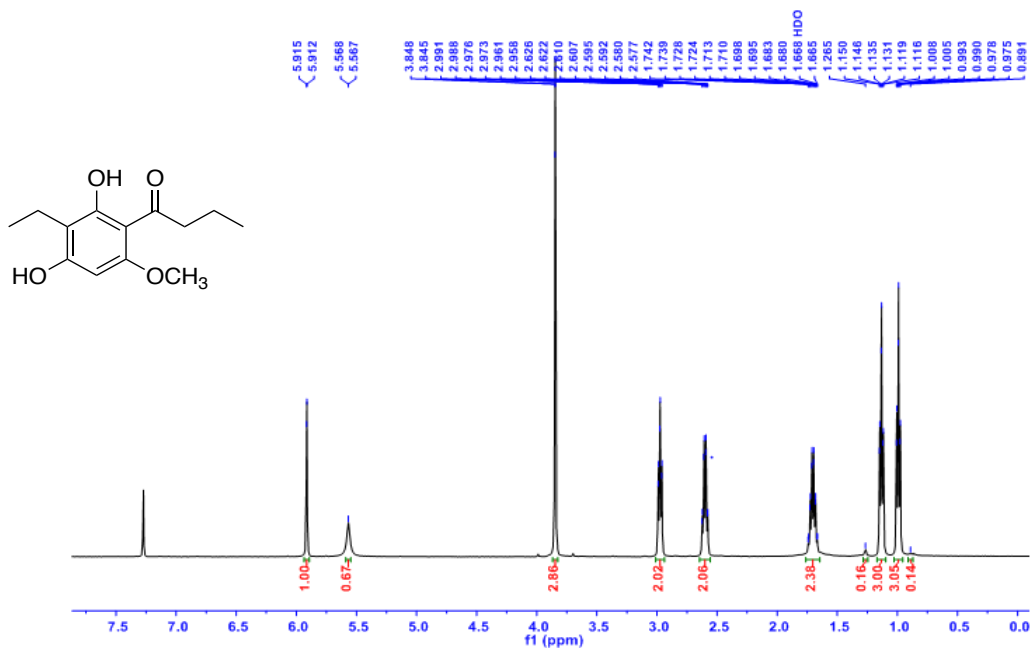


Figure A1. ¹H NMR spectrum of compound **3.1** (CDCl₃, 400 MHz)

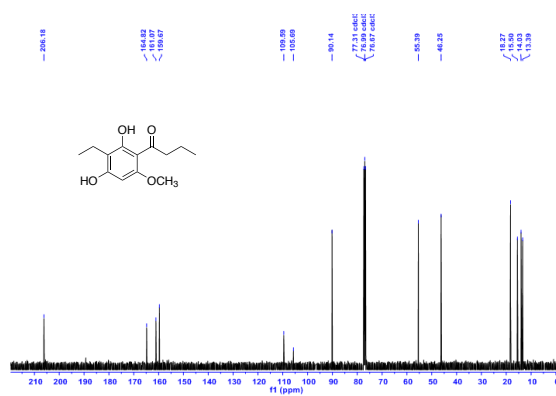


Figure A2. ¹³C NMR spectrum of compound **3.1** (CDCl₃, 100 MHz)

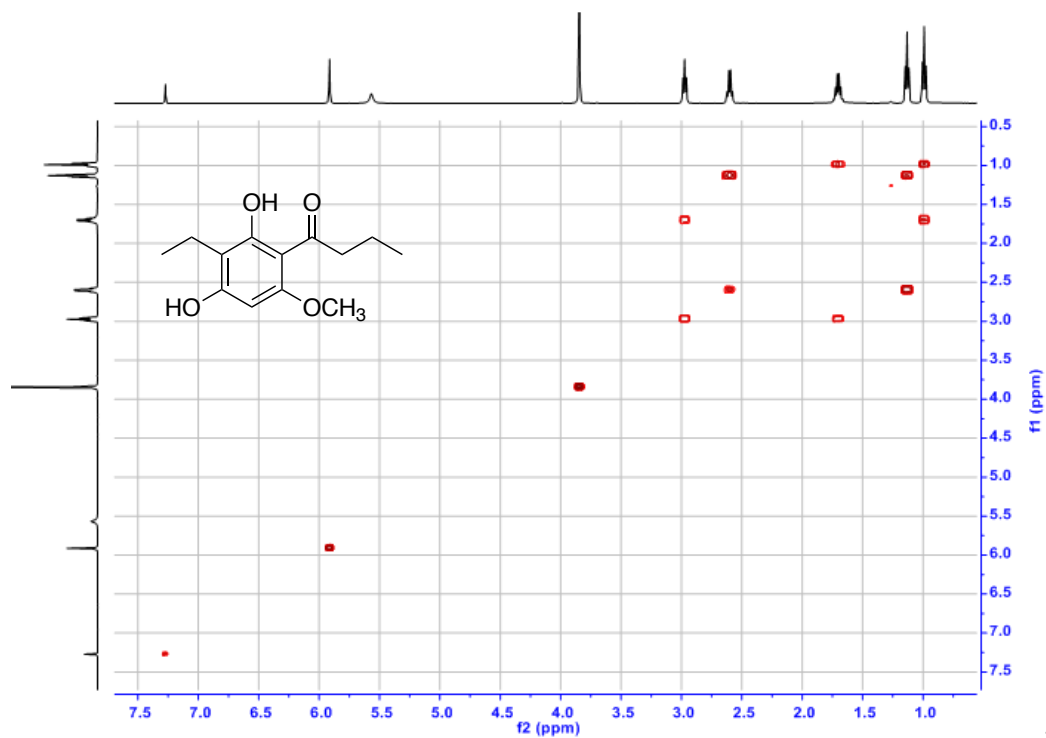


Figure A3. COSY spectrum of compound **3.1** (CDCl₃, 400 MHz)

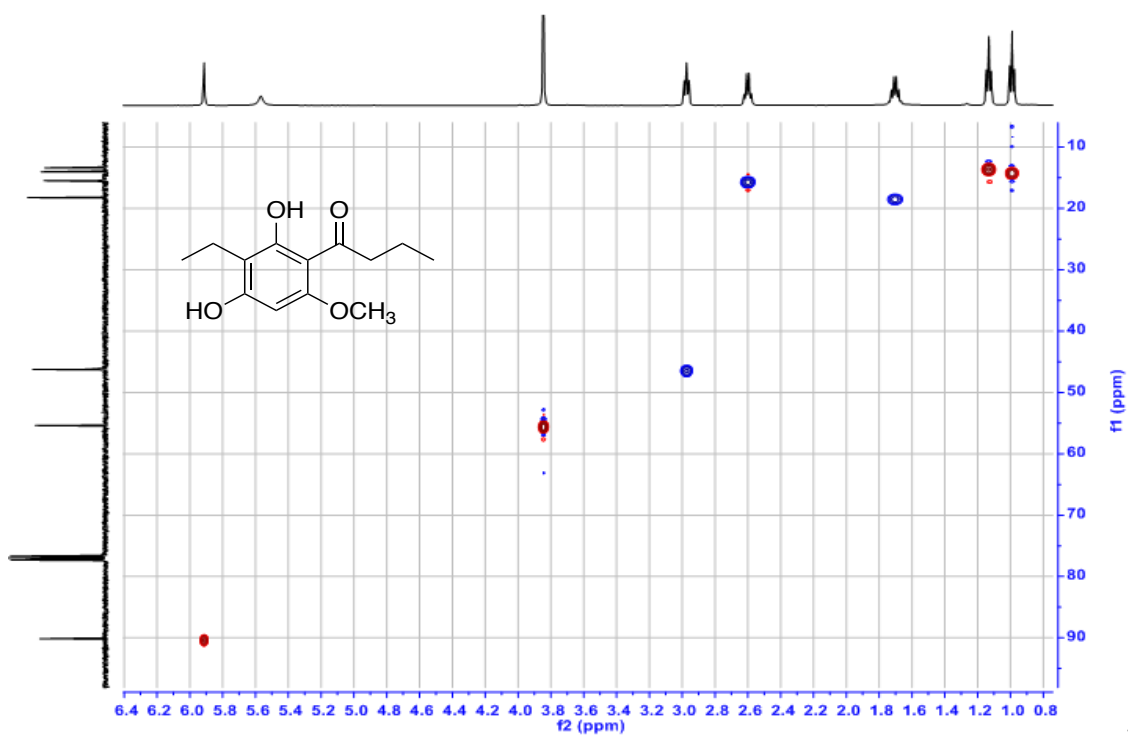


Figure A4. HSQC spectrum of compound **3.1** (CDCl₃, 400 MHz)

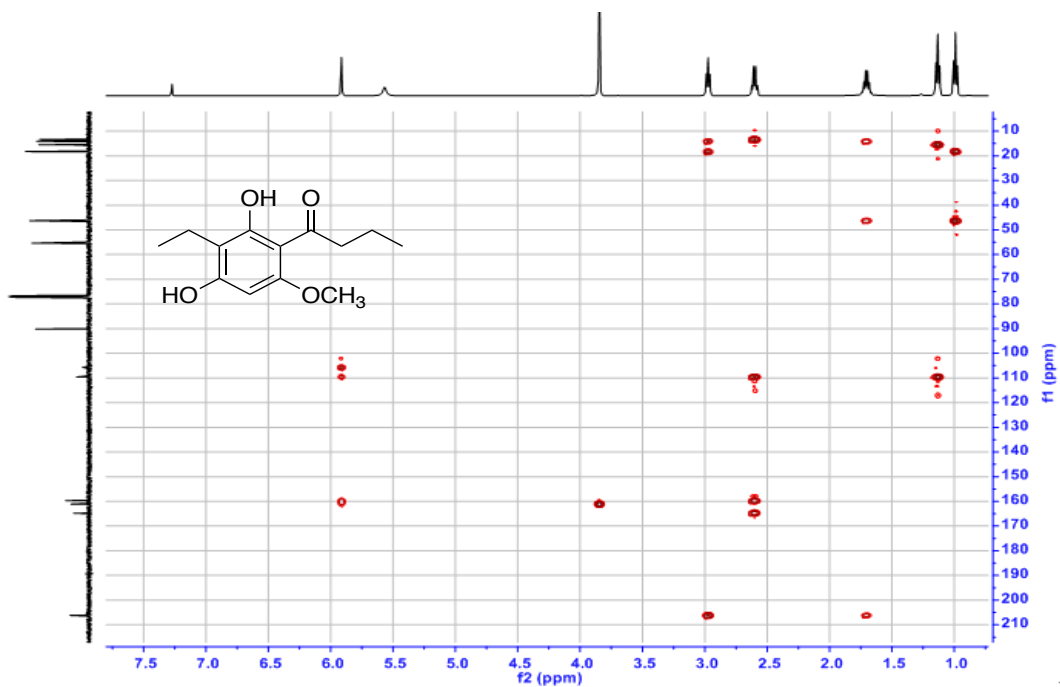


Figure A5. HMBC Spectrum of Compound 3.1 (CDCl₃, 400 MHz)

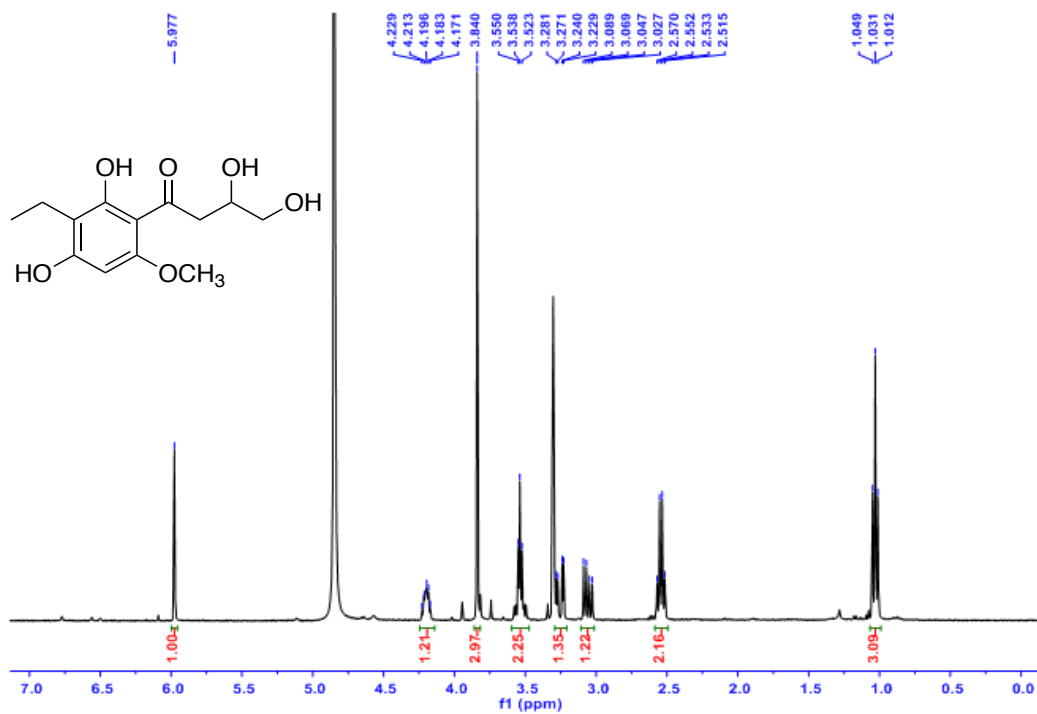


Figure A6. ¹H NMR Spectrum of Compound 3.3 (MeOH-*d*₄, 400 MHz)

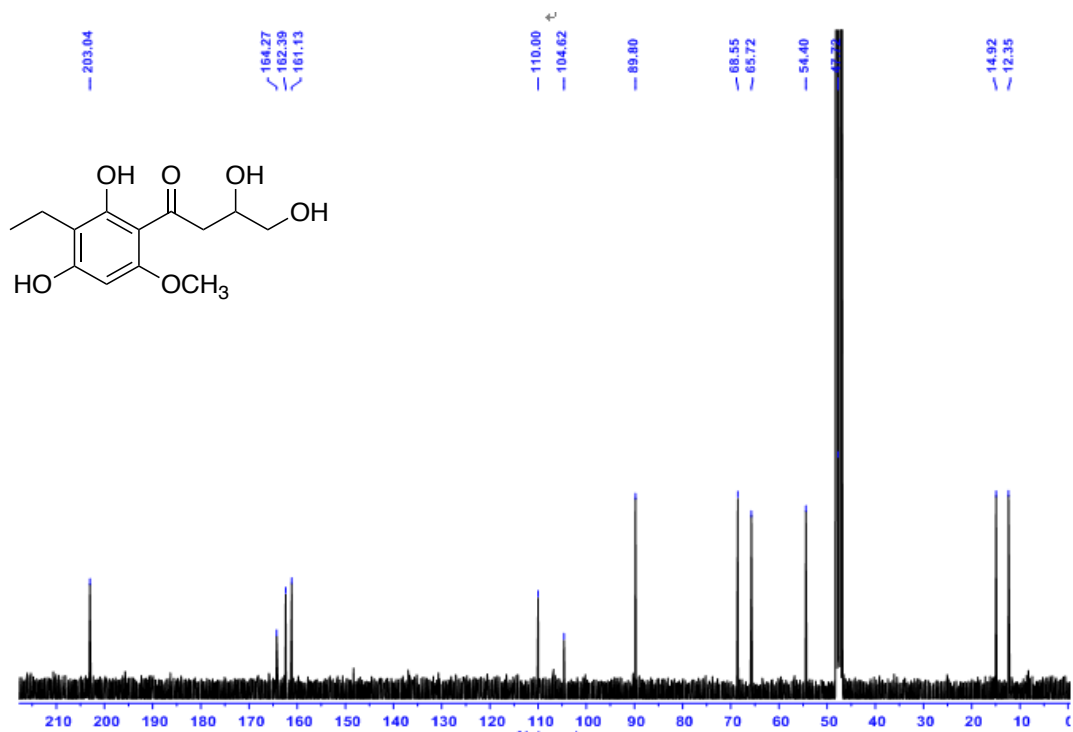


Figure A7. ^{13}C NMR Spectrum of Compound 3.3 (MeOH- d_4 , 100 MHz)

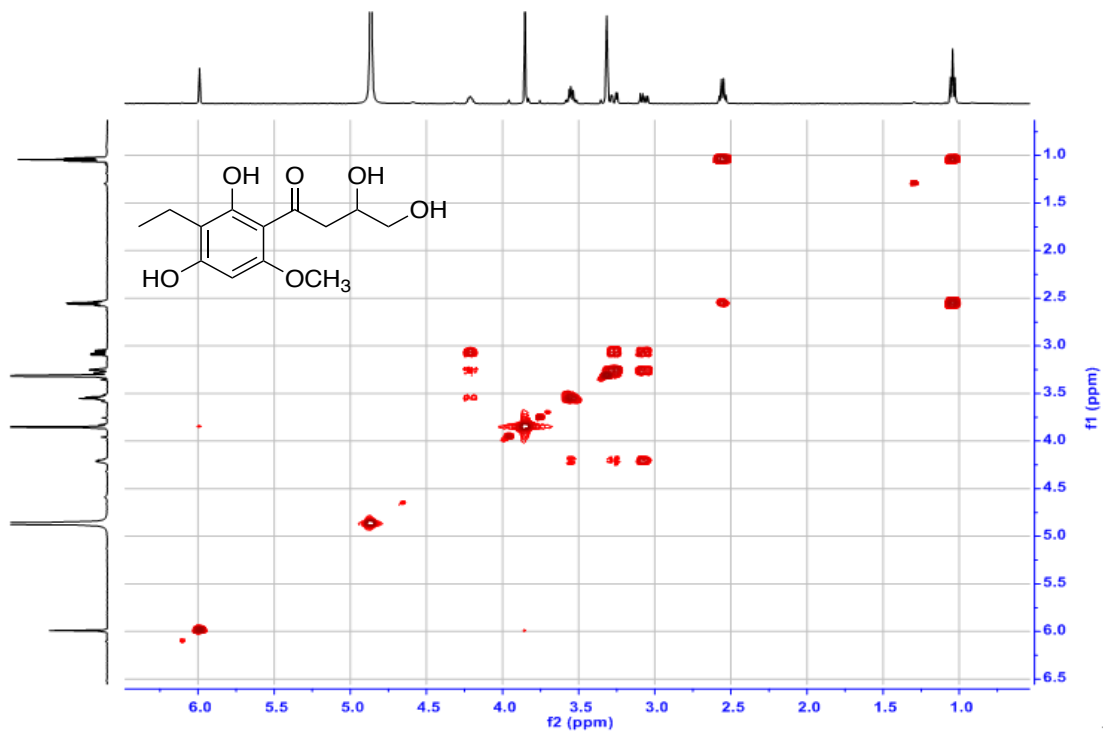


Figure A8. COSY Spectrum of Compound 3.3 (MeOH- d_4 , 400 MHz)

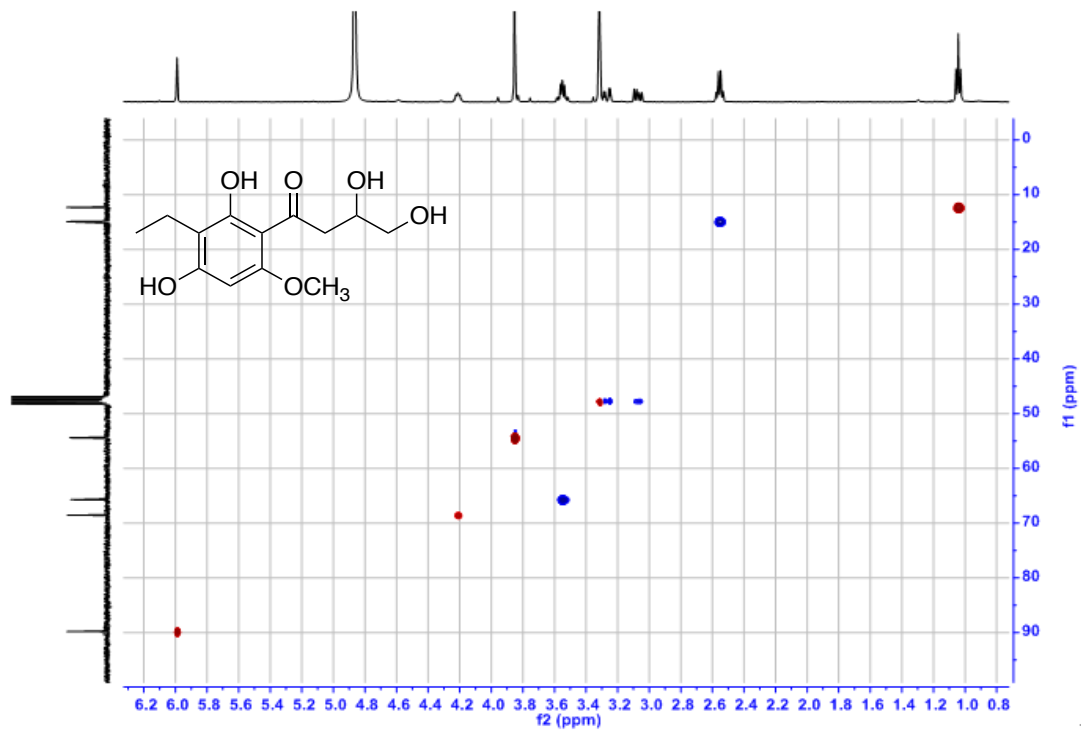


Figure A9. HSQC Spectrum of Compound 3.3 (MeOH- d_4 , 400 MHz)

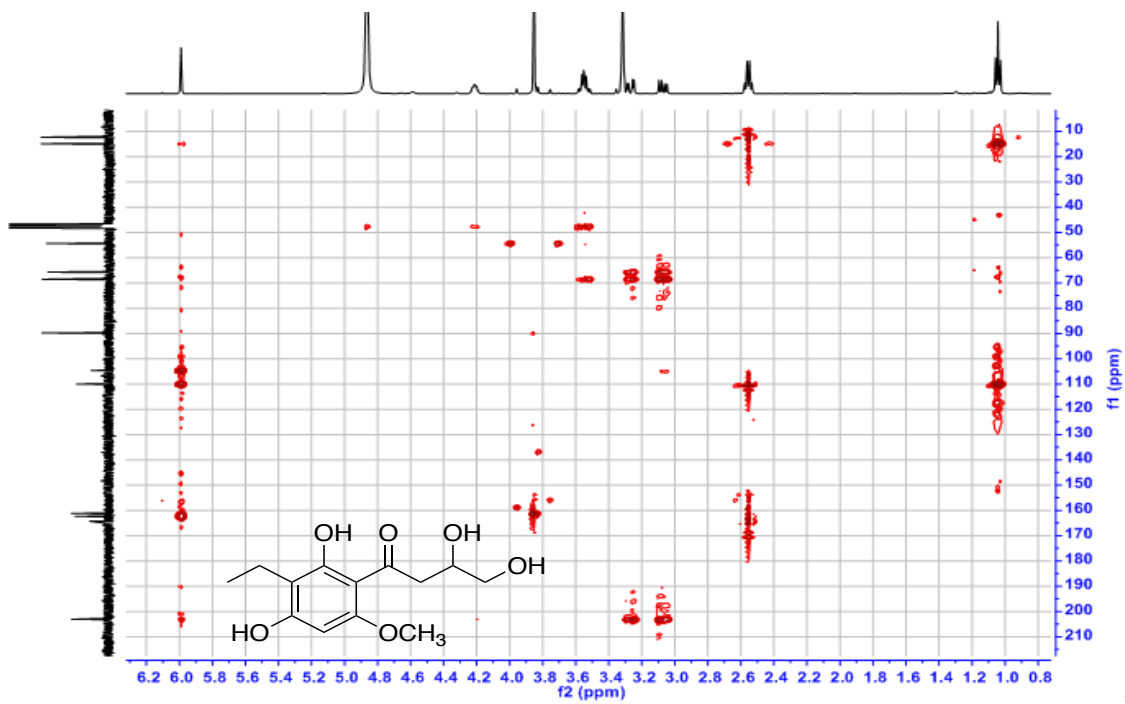


Figure A10. HMBC Spectrum of Compound 3.3 (MeOH- d_4 , 400 MHz)

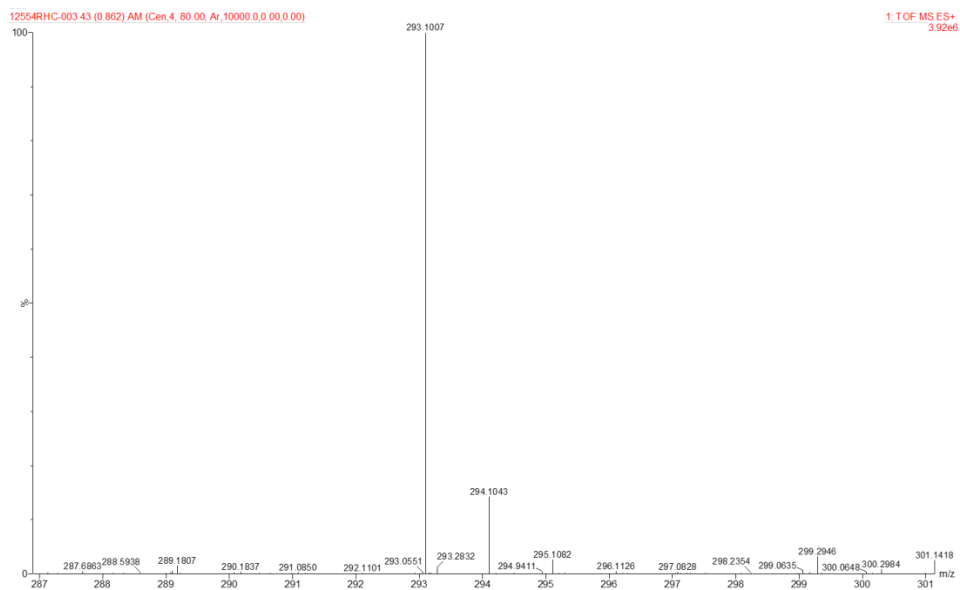


Figure A11. HRESIMS Spectrum of Compound **3.3**

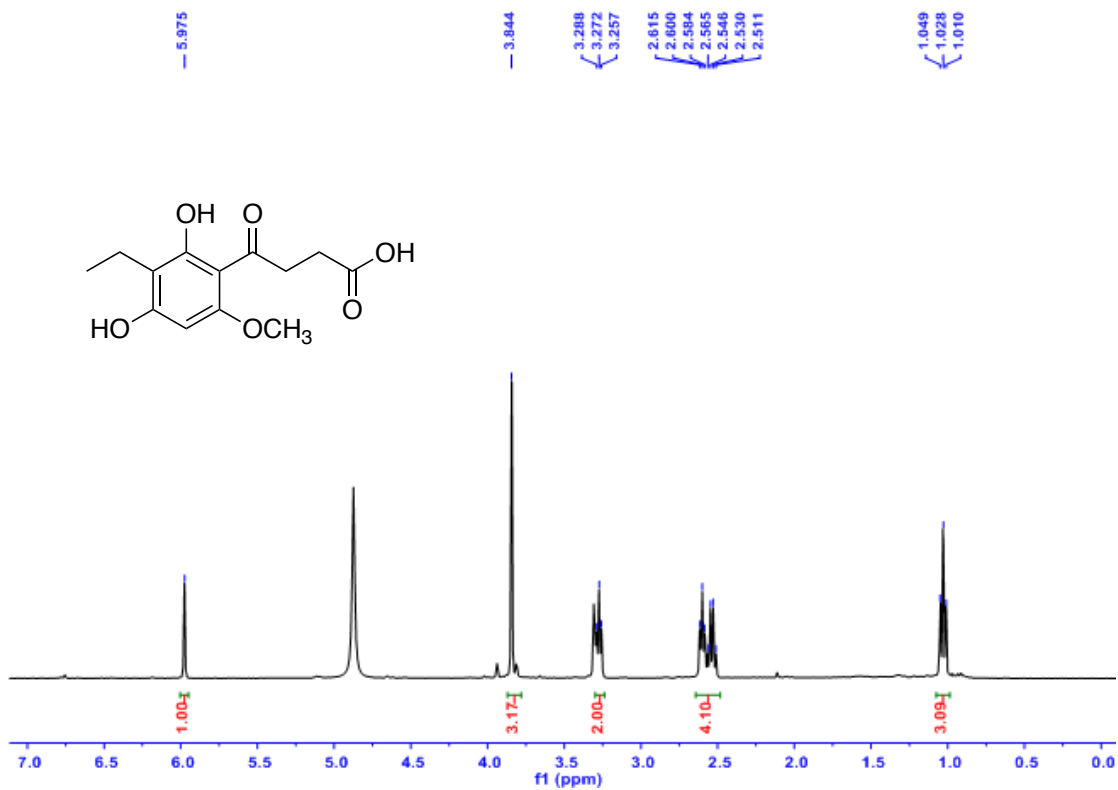


Figure A12. ^1H NMR Spectrum of Compound **3.4** (MeOH- d_4 , 400 MHz)

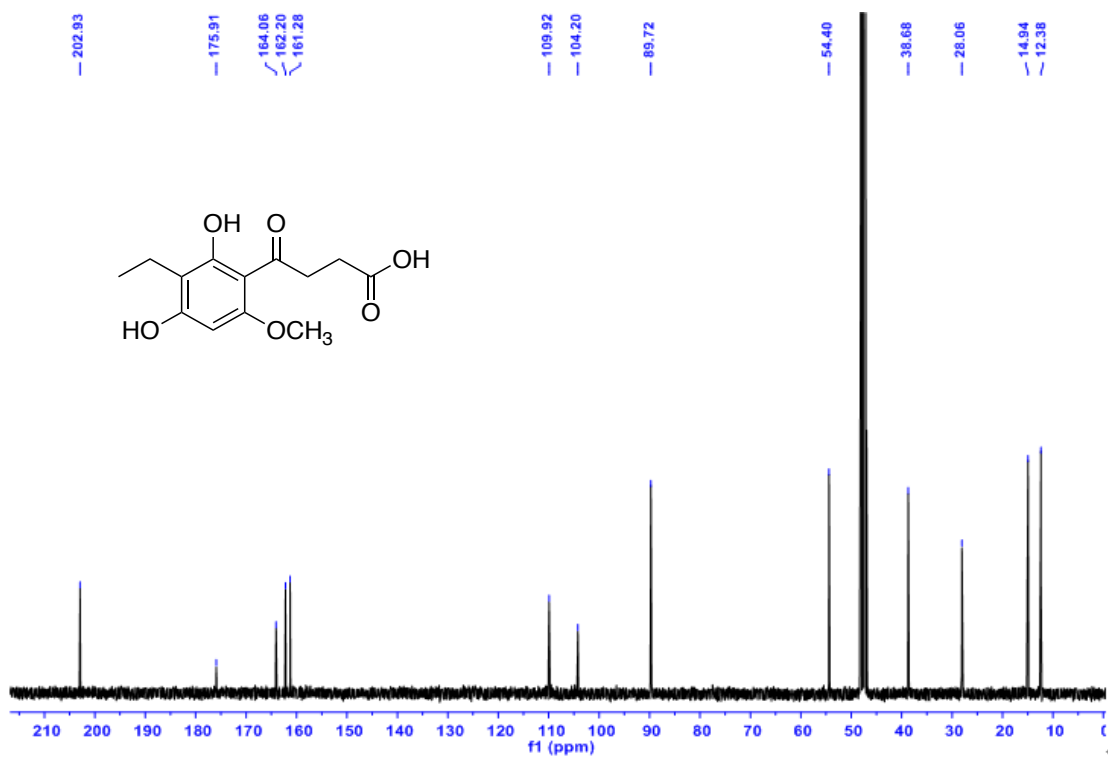


Figure A13. ^{13}C NMR Spectrum of Compound **3.4** (MeOH- d_4 , 100 MHz)

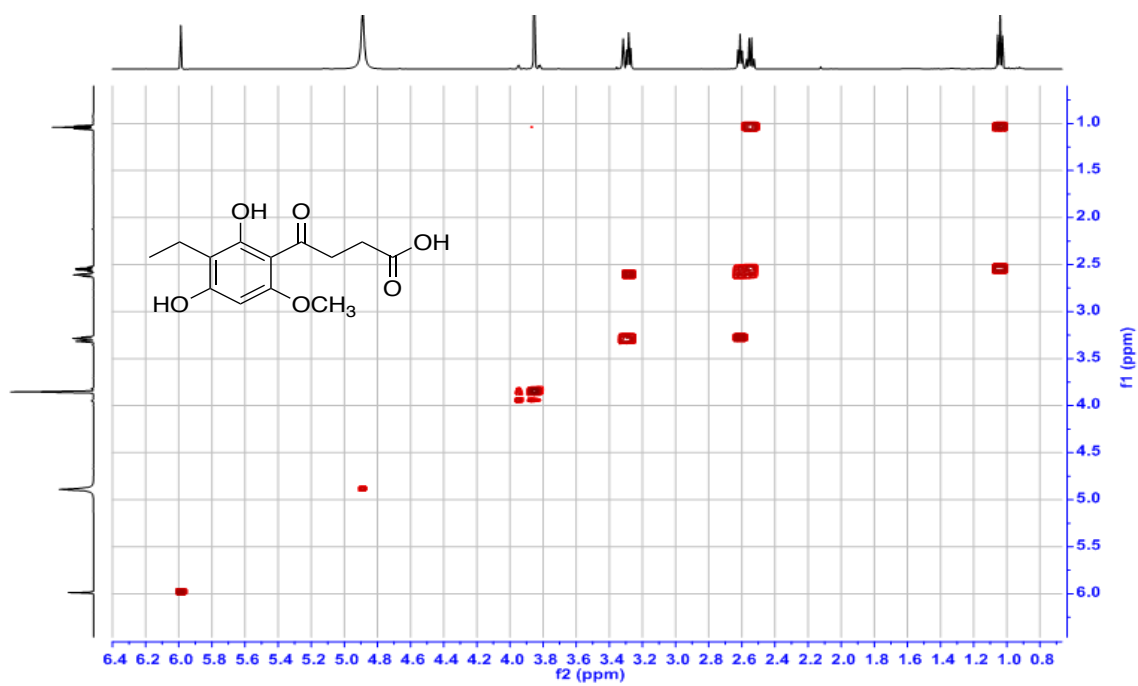


Figure A14. COSY Spectrum of Compound **3.4** (MeOH- d_4 , 400 MHz)

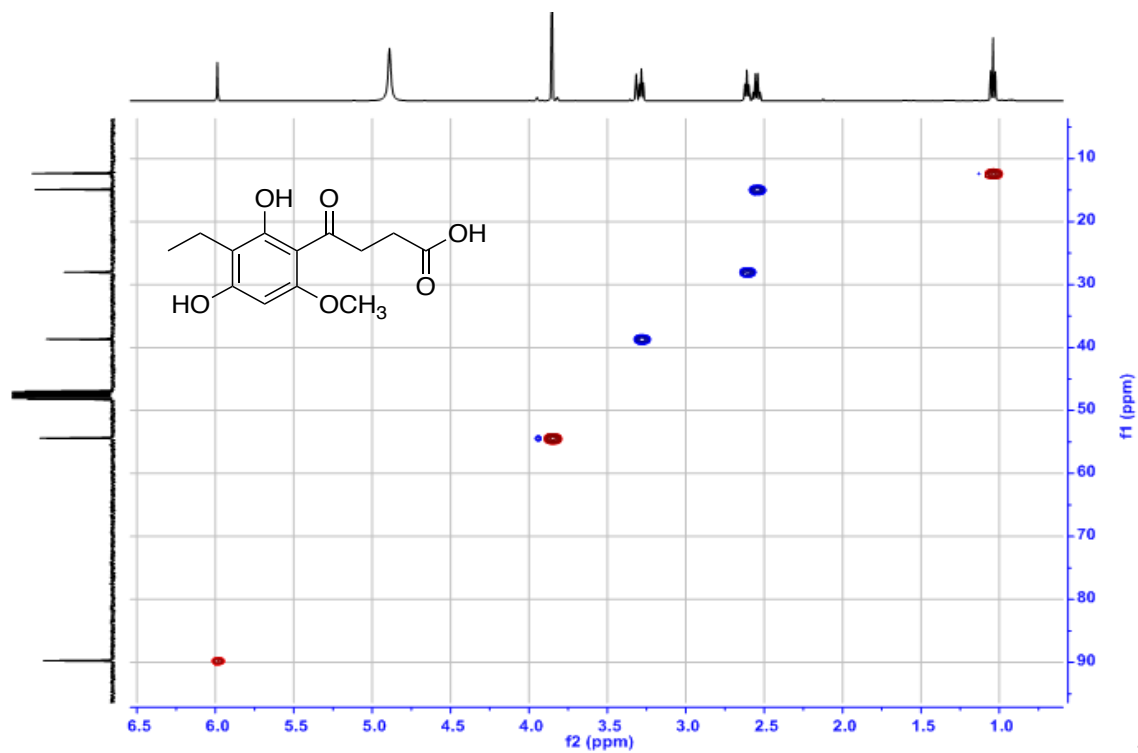


Figure A15. HSQC Spectrum of Compound **3.4** (MeOH- d_4 , 400 MHz)

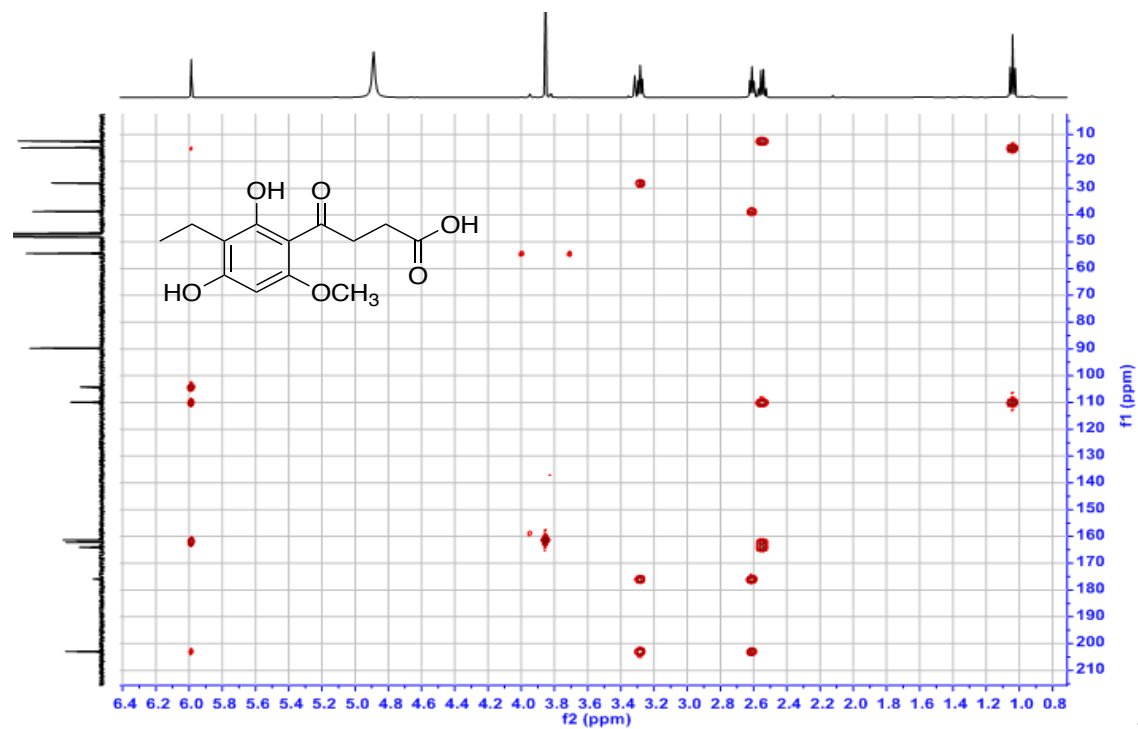


Figure A16. HMBC spectrum of compound **3.4** (MeOH- d_4 , 400 MHz)

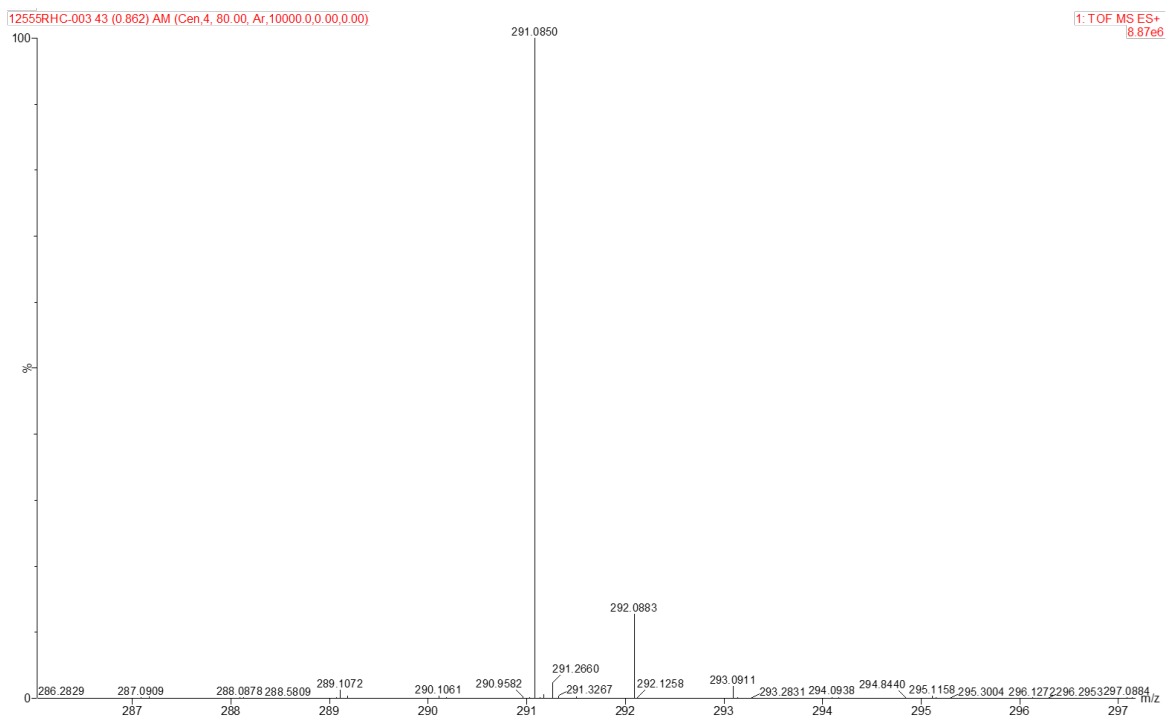


Figure A17. HRESIMS spectrum of compound **3.4**.

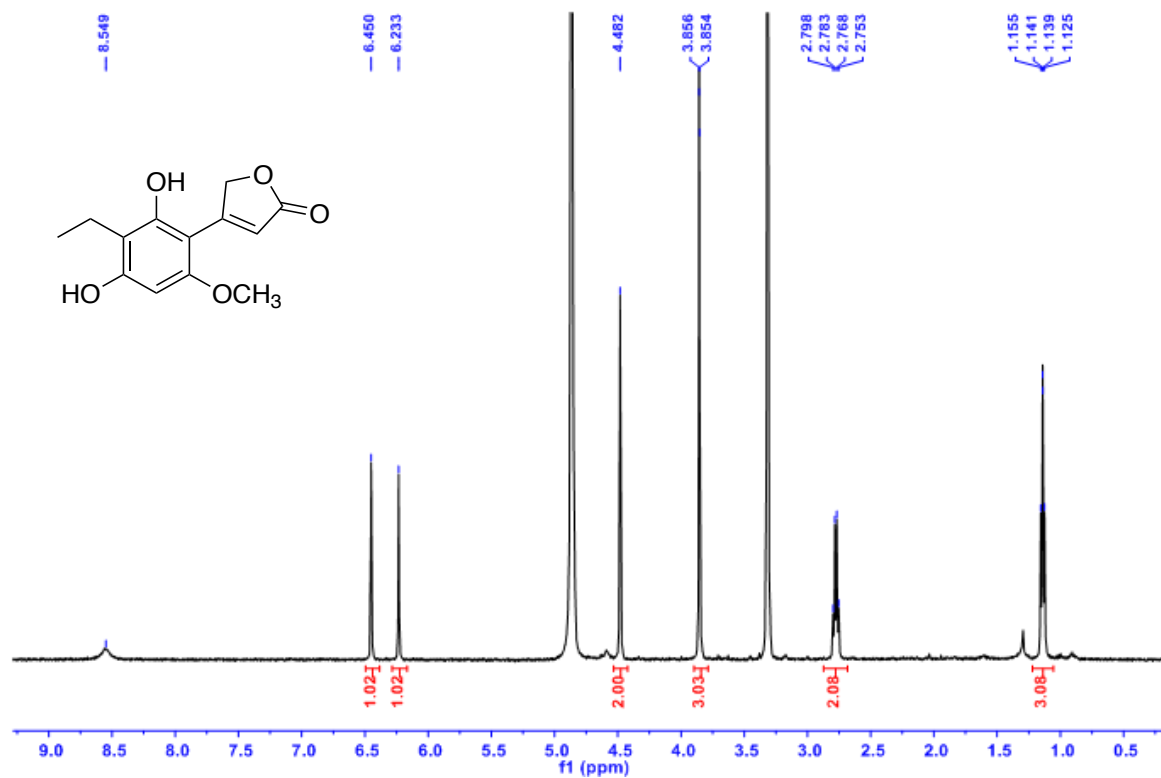


Figure A18. ^1H NMR spectrum of compound **3.5** ($\text{MeOH-}d_4$, 400 MHz)

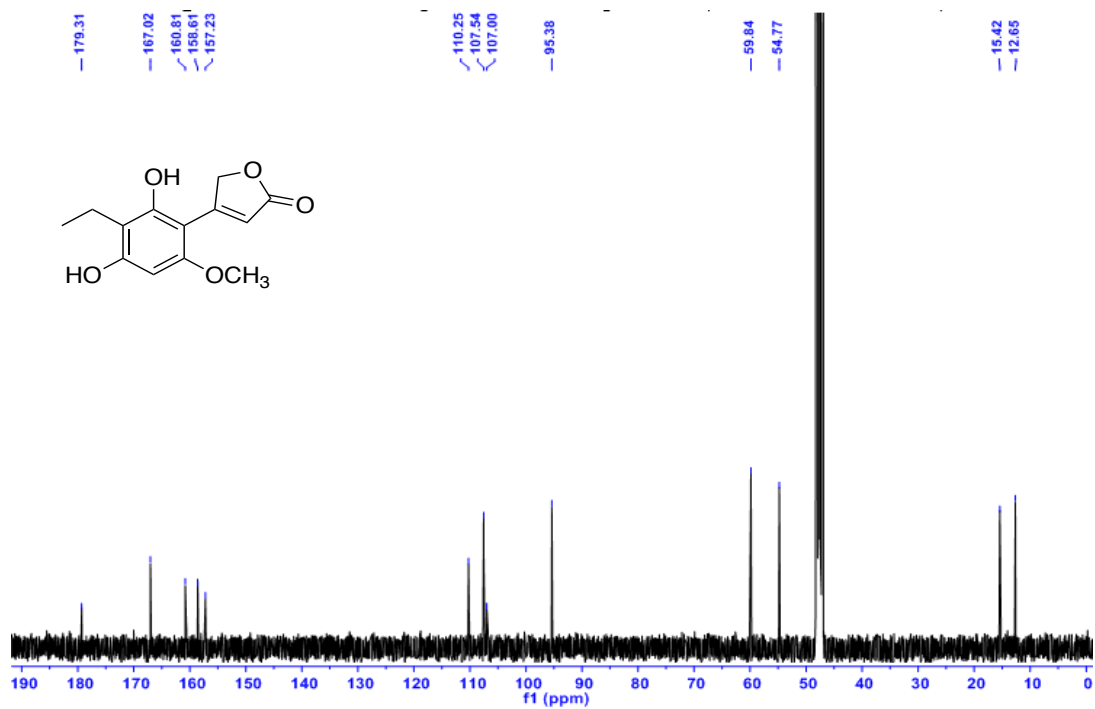


Figure A19. ^{13}C NMR spectrum of compound 3.5 (MeOH- d_4 , 100 MHz)

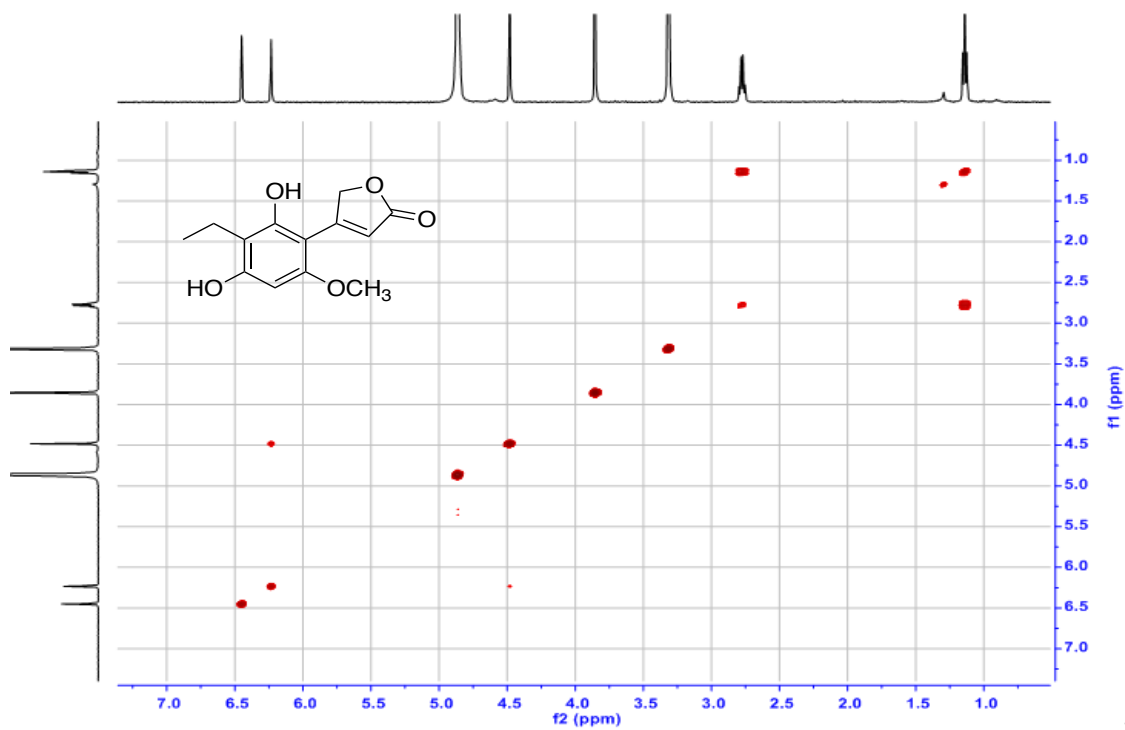


Figure A20. COSY spectrum of compound 3.5 (MeOH- d_4 , 400 MHz)

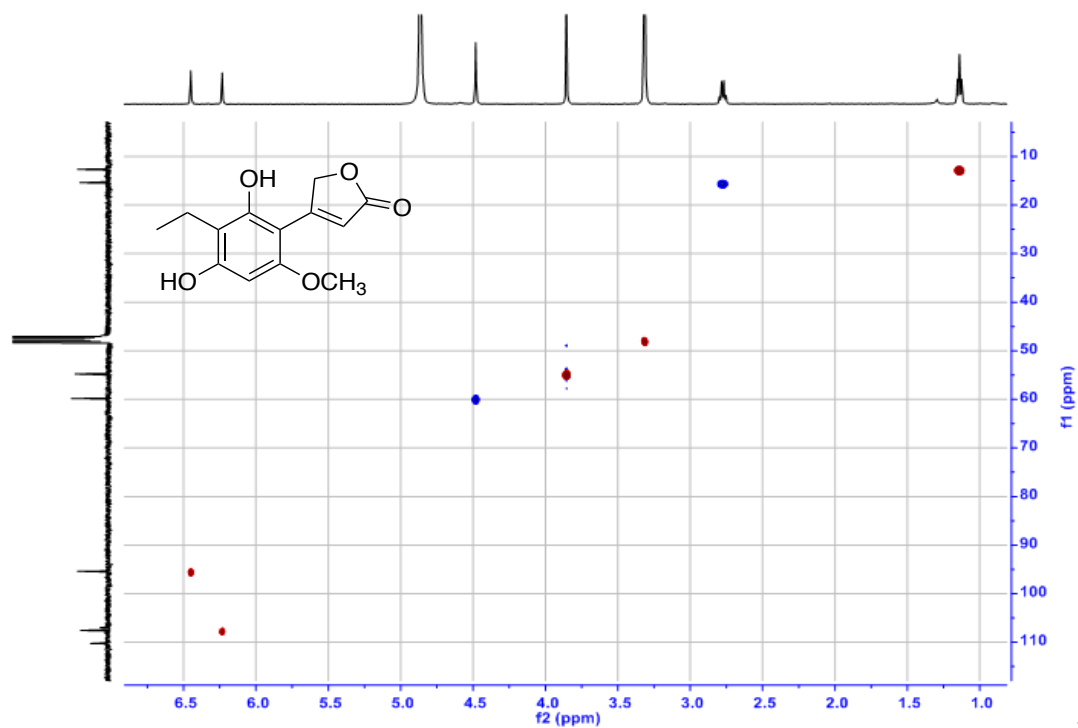


Figure A21. HSQC spectrum of compound **3.5** (MeOH-*d*₄, 400 MHz)

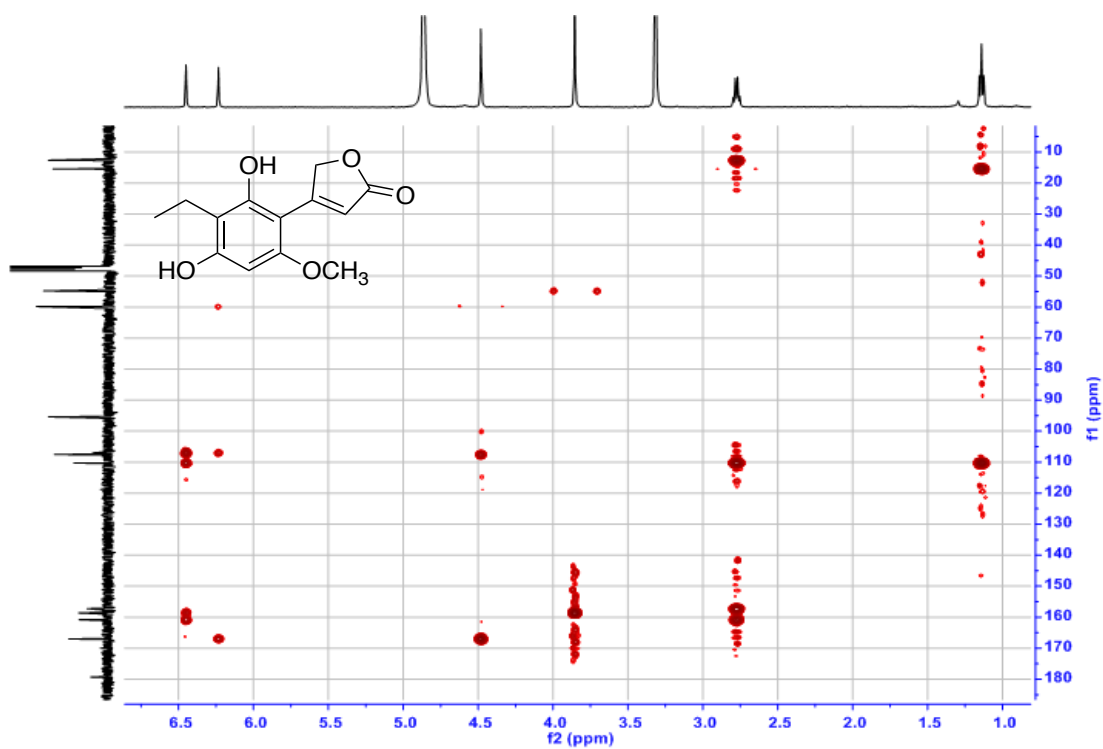


Figure A22. HMBC spectrum of compound **3.5** (MeOH-*d*₄, 400 MHz)

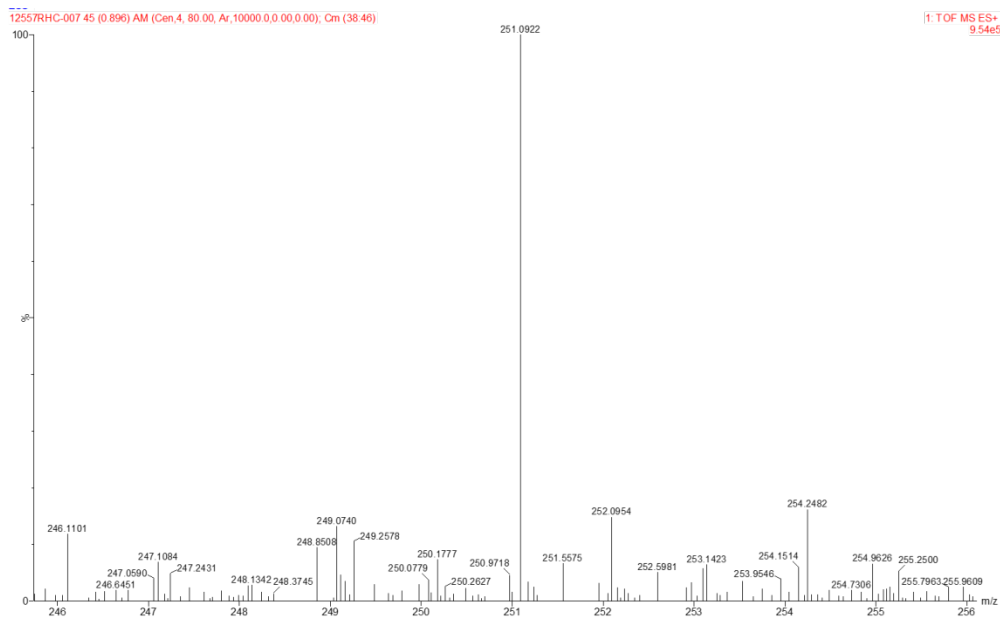


Figure A23. HRESIMS spectrum of compound 3.5

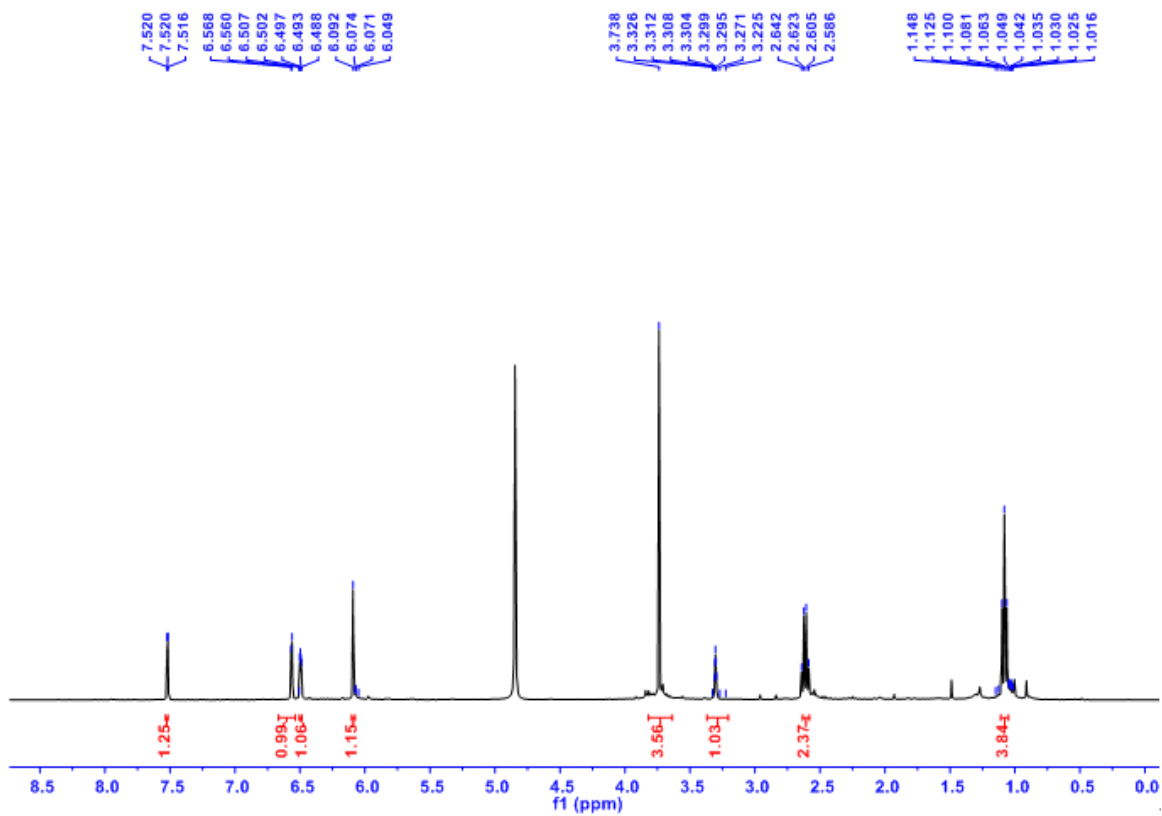


Figure A24. ¹H NMR spectrum of compound 3.6 (MeOH-*d*₄, 400 MHz)

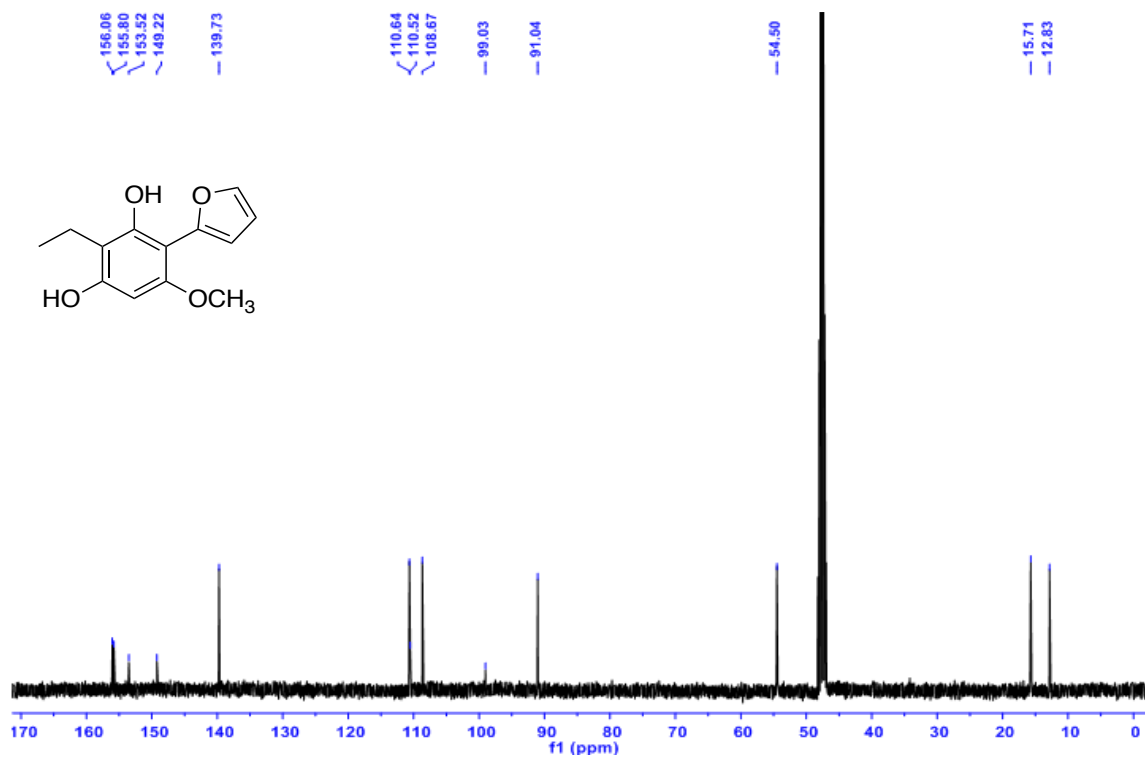


Figure A25. ^{13}C NMR spectrum of compound 3.6 (MeOH- d_4 , 100 MHz)

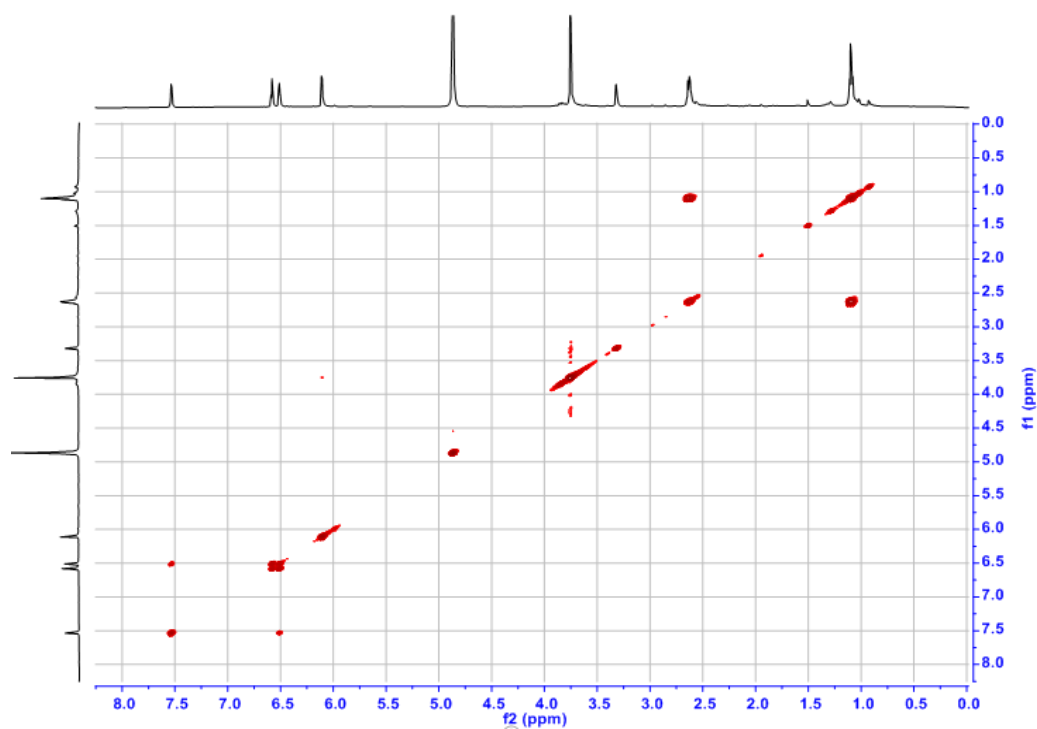


Figure A26. COSY spectrum of compound 3.6 (MeOH- d_4 , 400 MHz)

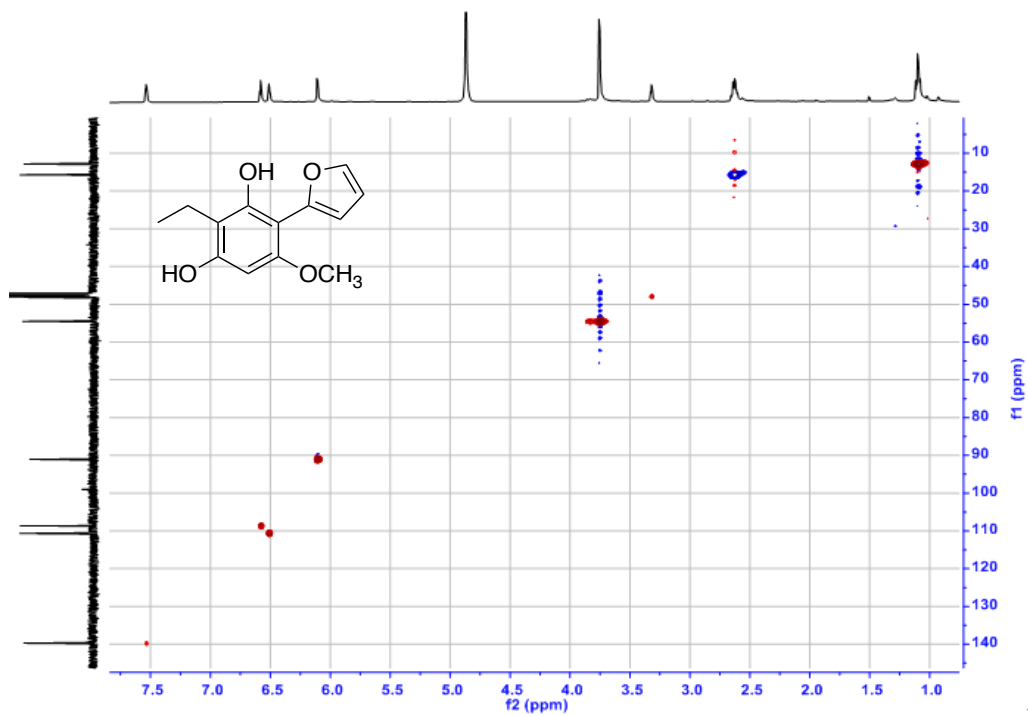


Figure A27. HSQC spectrum of compound **3.6** (MeOH-*d*₄, 400 MHz)

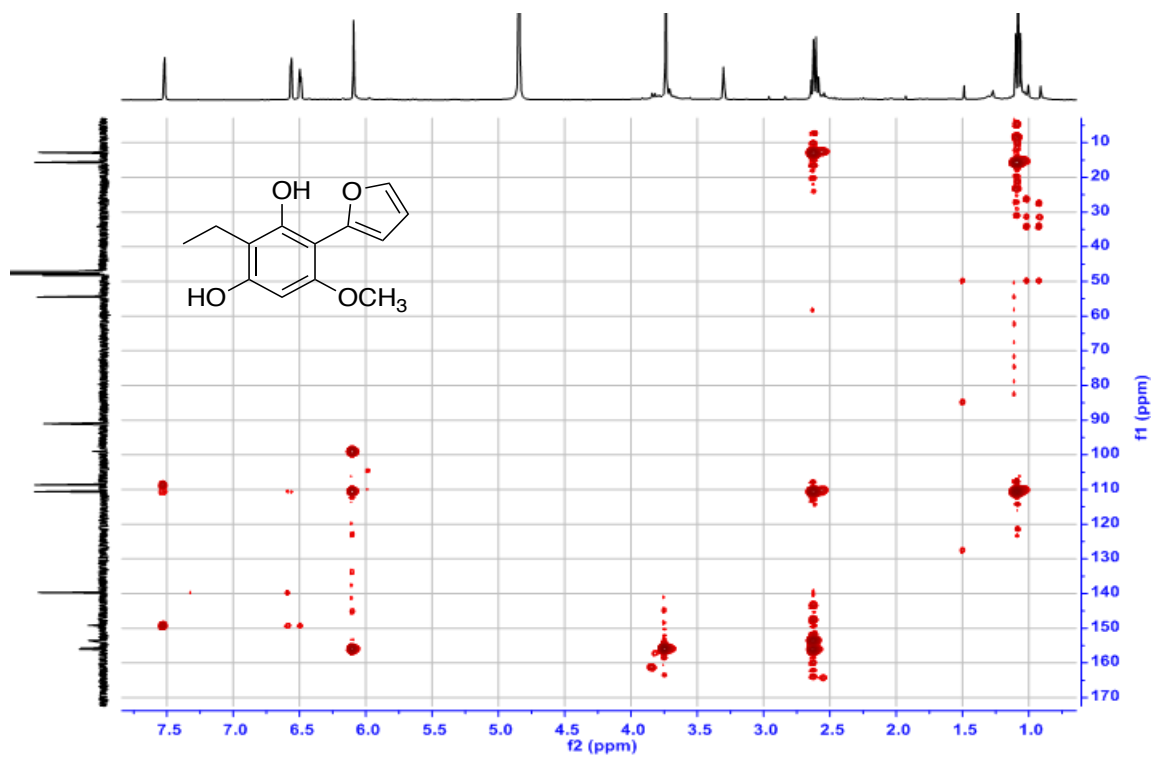


Figure A28. HMBC spectrum of compound **3.6** (MeOH-*d*₄, 400 MHz)

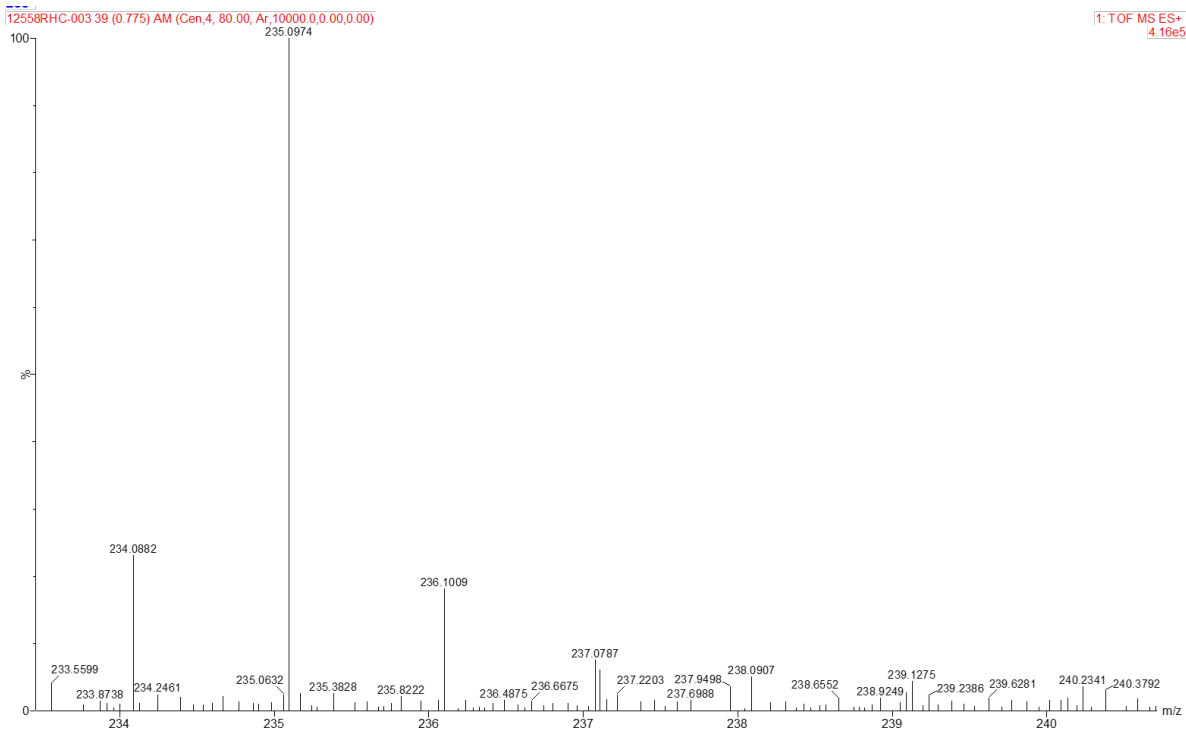


Figure A29. HRESIMS spectrum of compound **3.6**

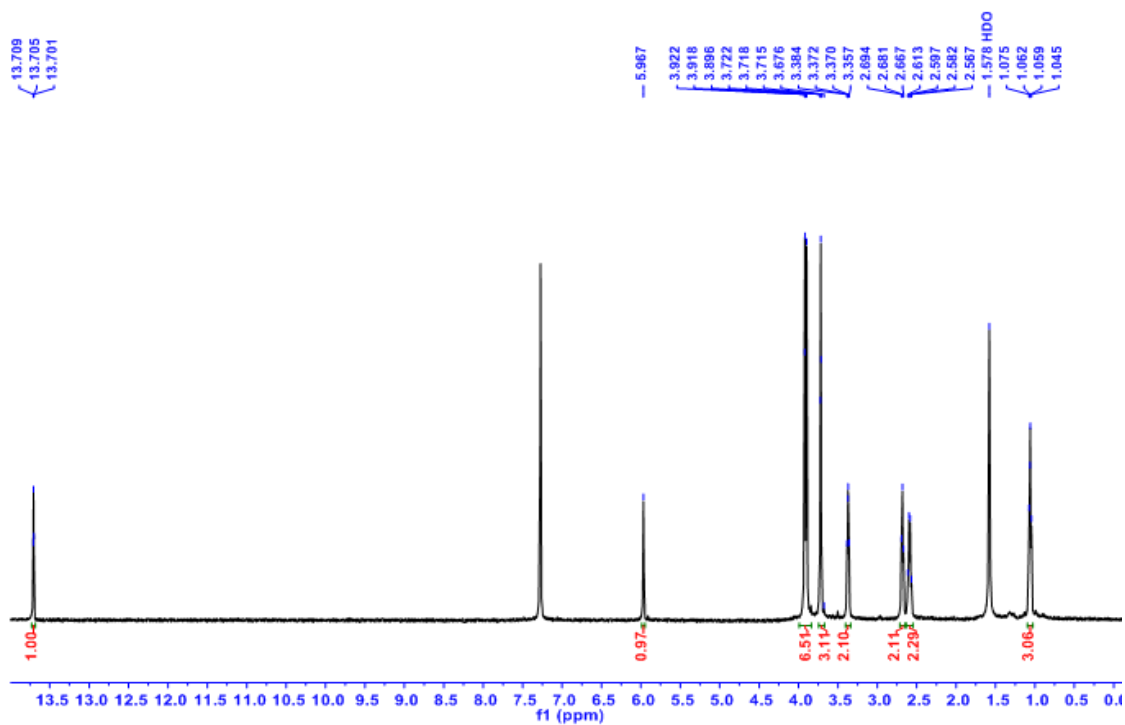


Figure A30. ¹H NMR spectrum of compound **3.7** (MeOH-*d*₄, 400 MHz)

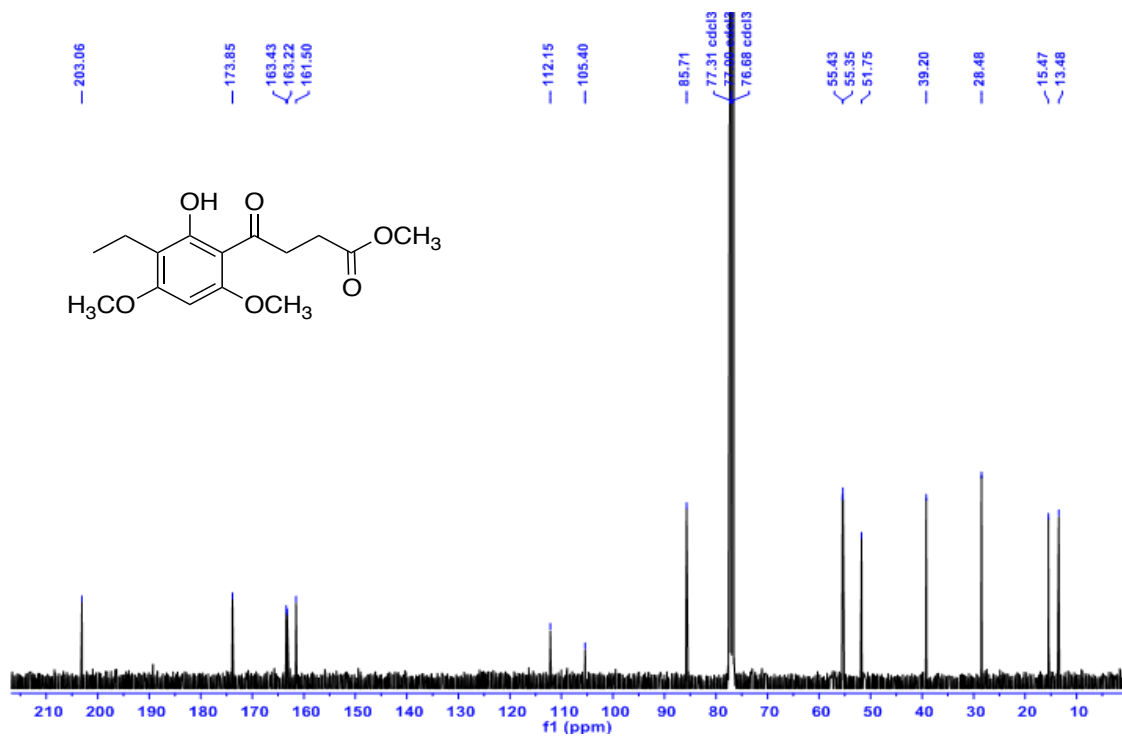


Figure A31. ^{13}C NMR spectrum of compound 3.7 (MeOH- d_4 , 100 MHz)

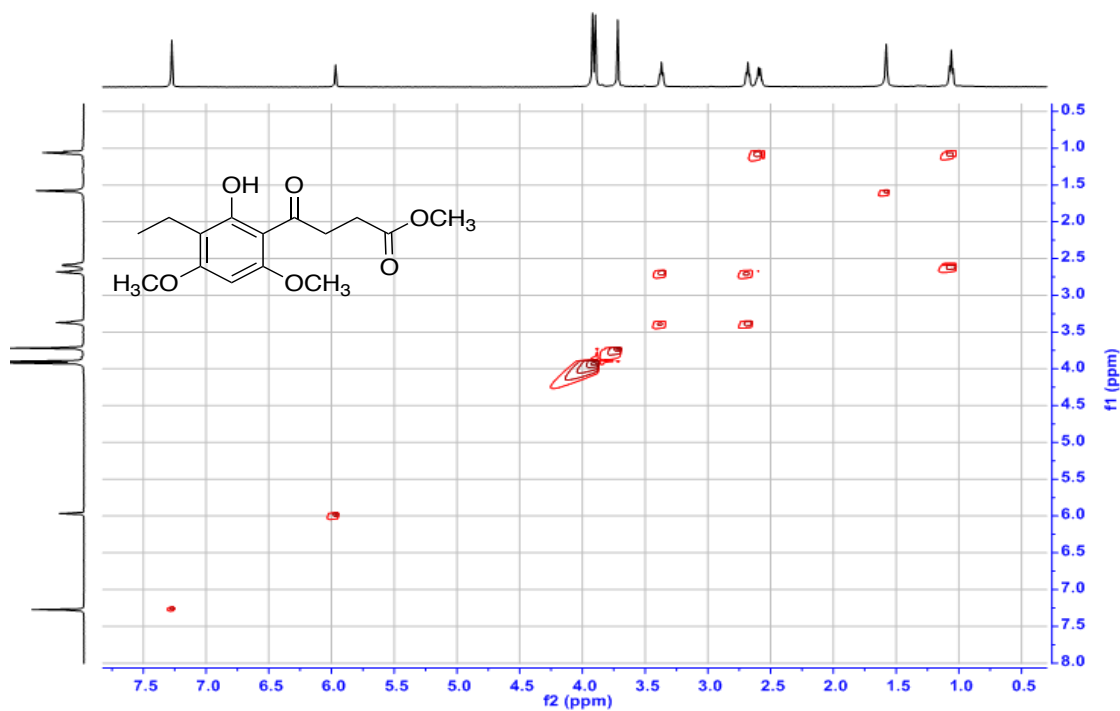


Figure A32. COSY spectrum of compound 3.7 (MeOH- d_4 , 400 MHz)

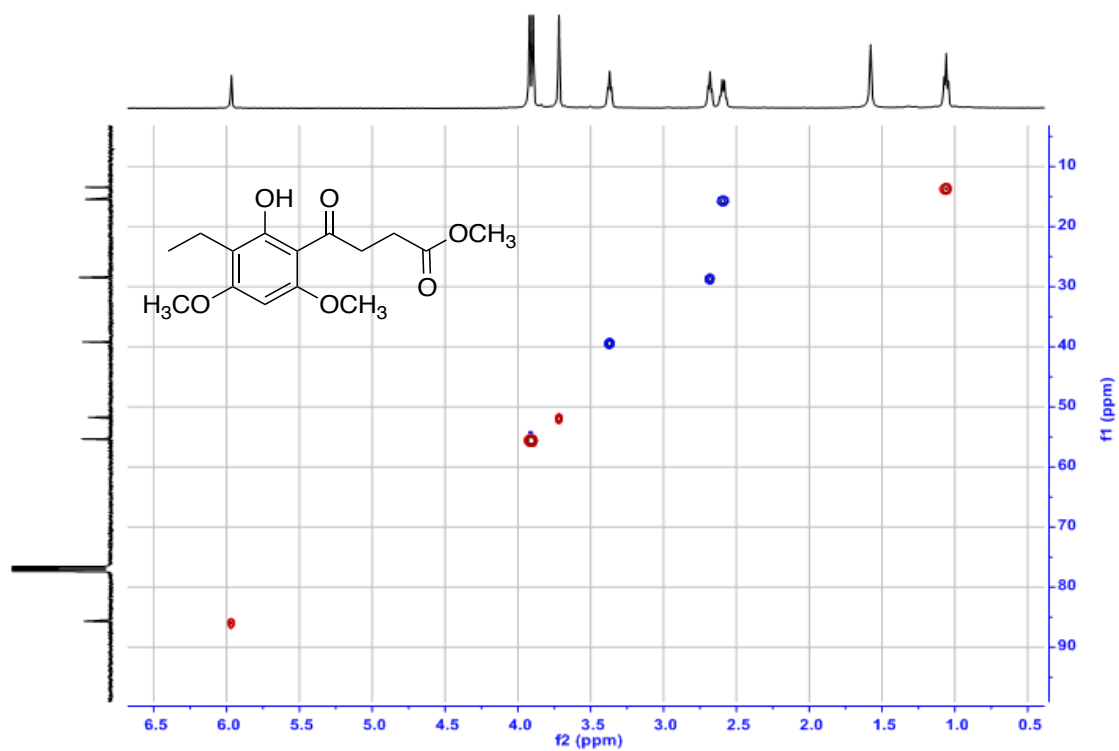


Figure A33. HSQC spectrum of compound **3.7** (MeOH-*d*₄, 400 MHz)

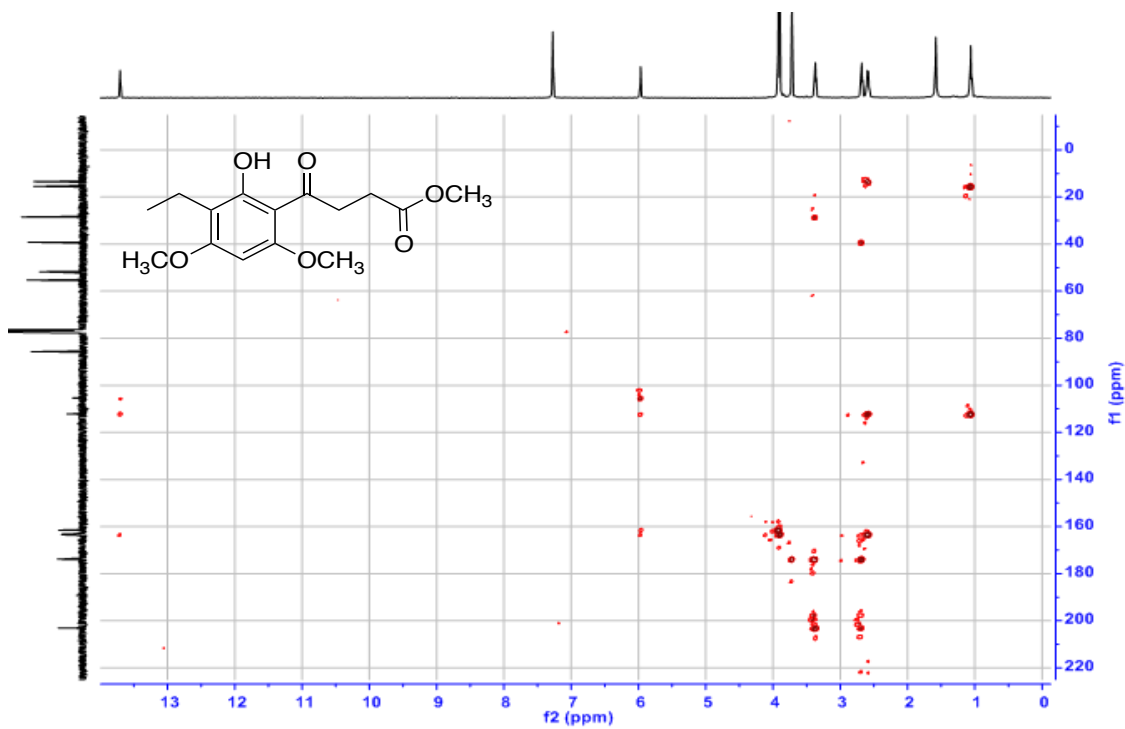


Figure A34. HMBC spectrum of compound **3.7** (MeOH-*d*₄, 400 MHz)

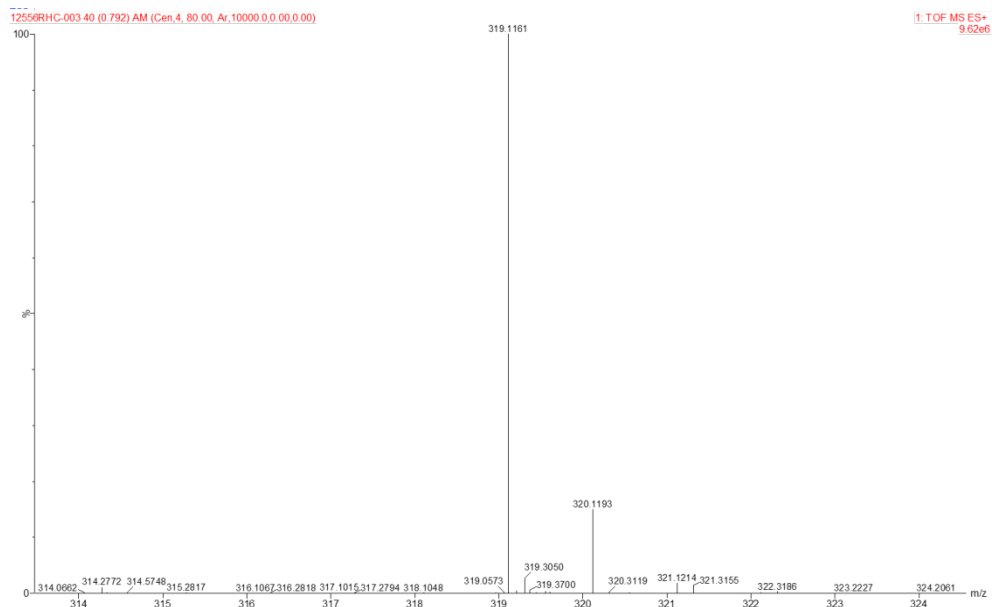


Figure A35. HRESIMS spectrum of compound **3.7**

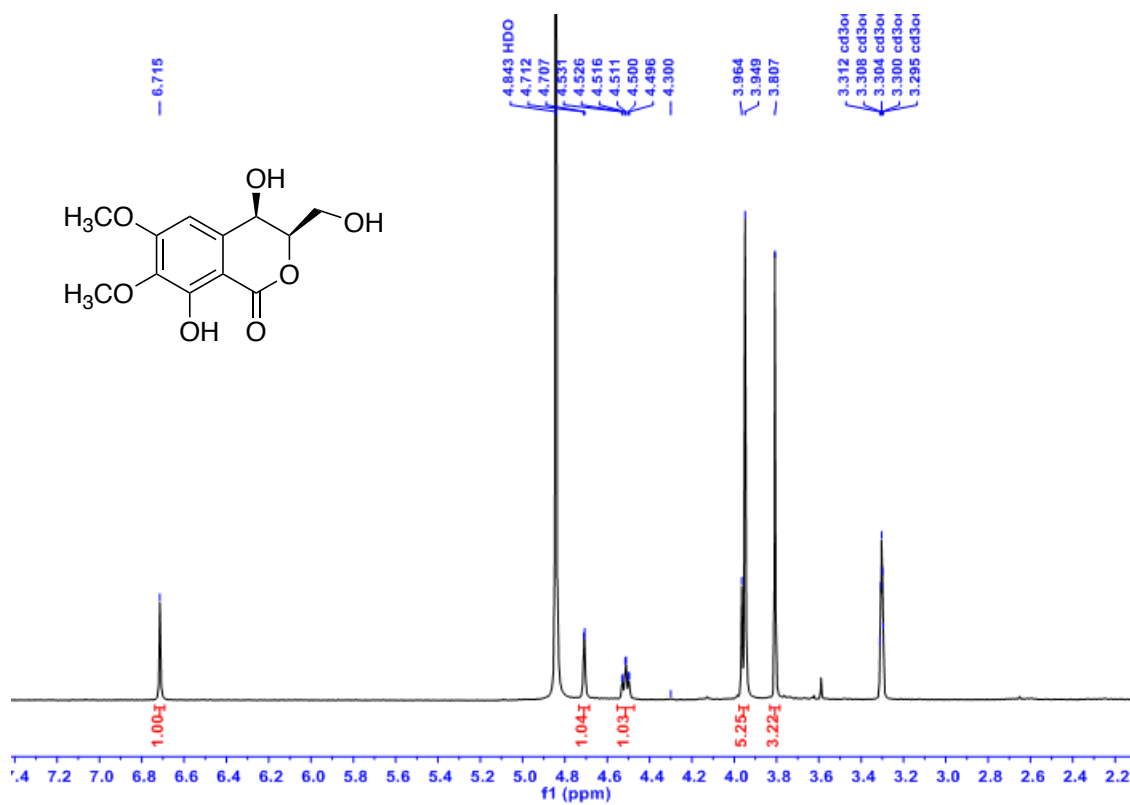


Figure A36. ^1H NMR spectrum of compound **3.8** ($\text{MeOH-}d_4$, 400 MHz)

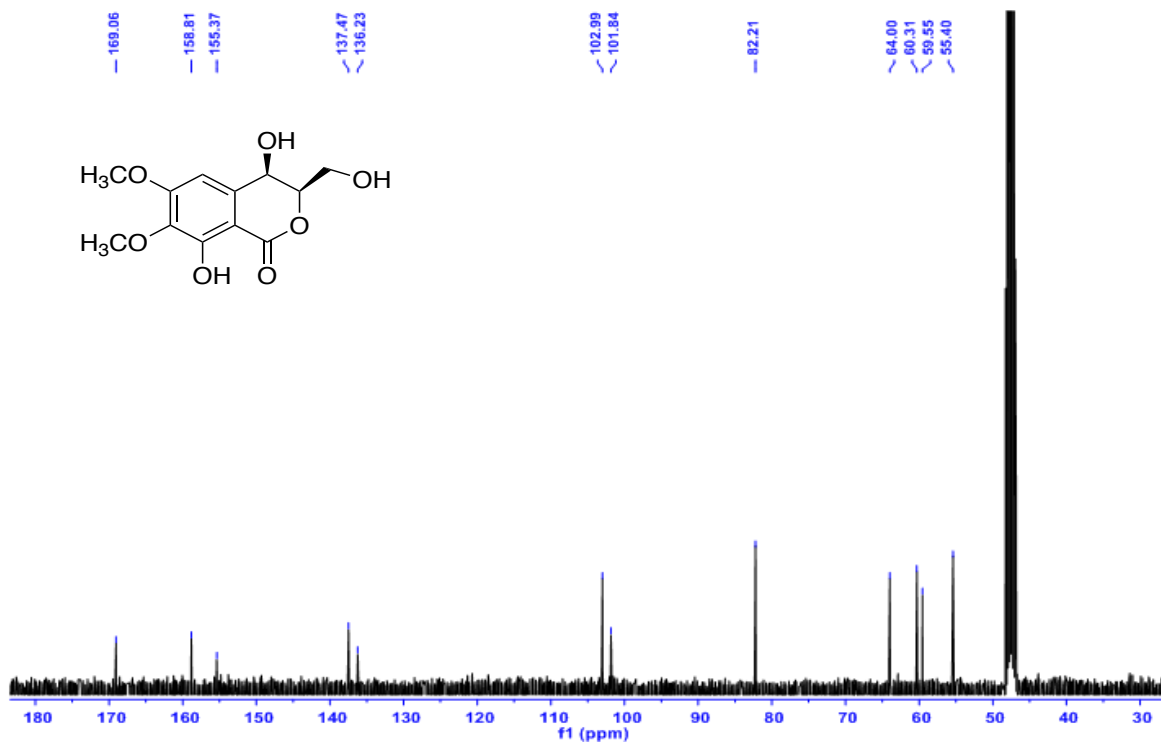


Figure A37. ^{13}C NMR spectrum of compound **3.8** (MeOH- d_4 , 100 MHz)

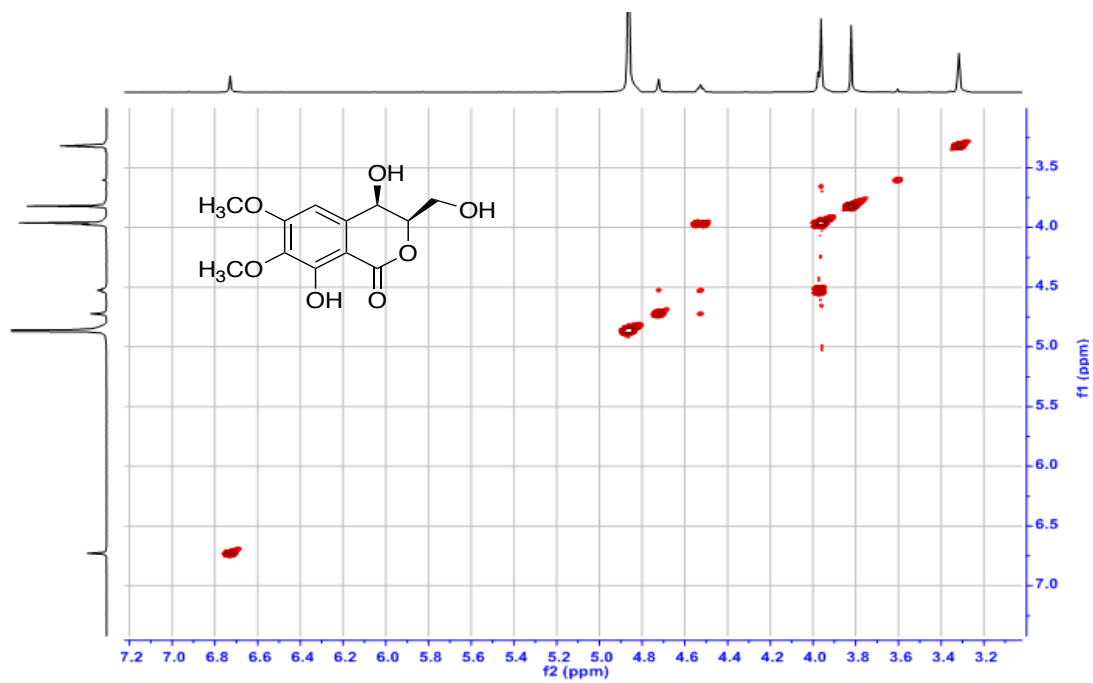


Figure A38. COSY spectrum of compound **3.8** (MeOH- d_4 , 400 MHz)

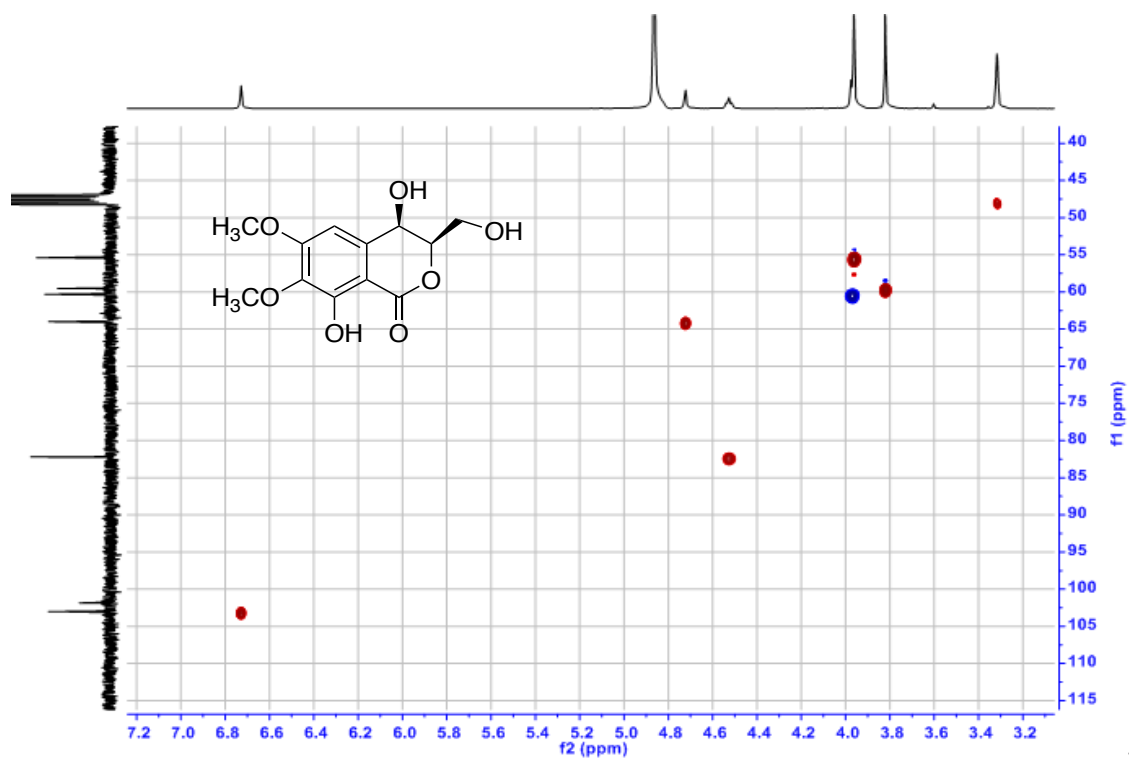


Figure A39. HSQC spectrum of compound **3.8** (MeOH-*d*₄, 400 MHz)

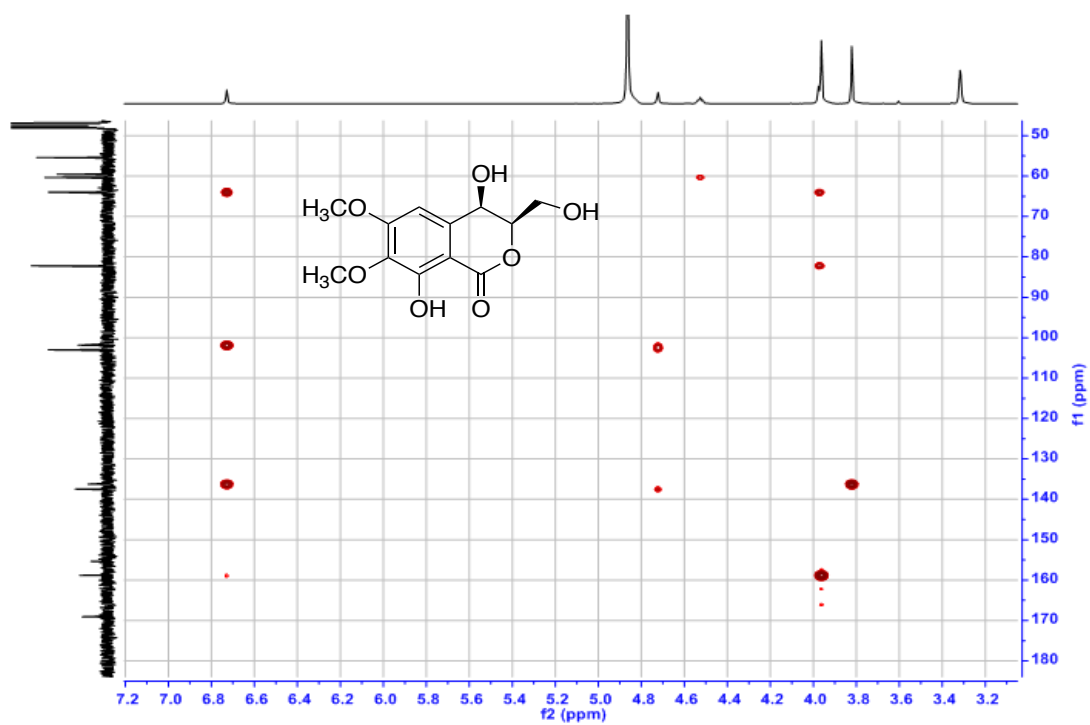


Figure A40. HMBC spectrum of compound **3.8** (MeOH-*d*₄, 400 MHz)

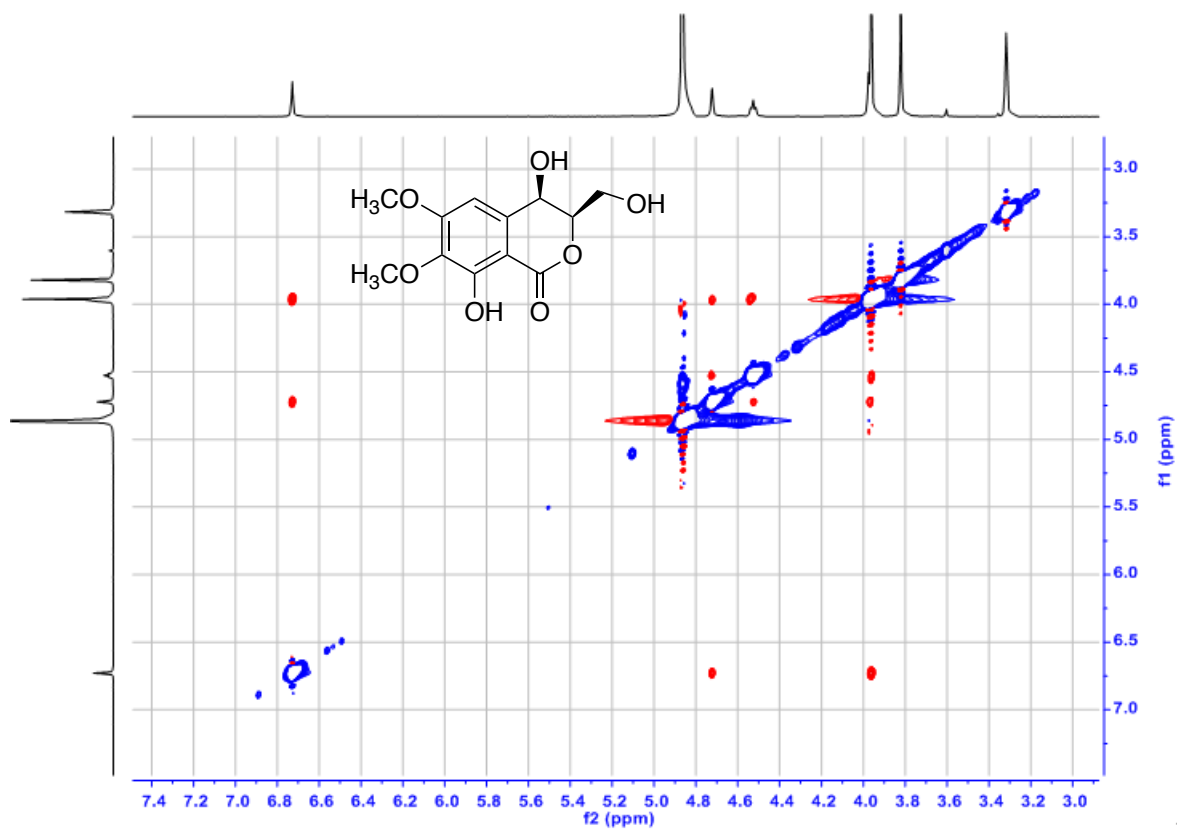


Figure A41. ROESY spectrum of compound **3.8** (MeOH- d_4 , 400 MHz)

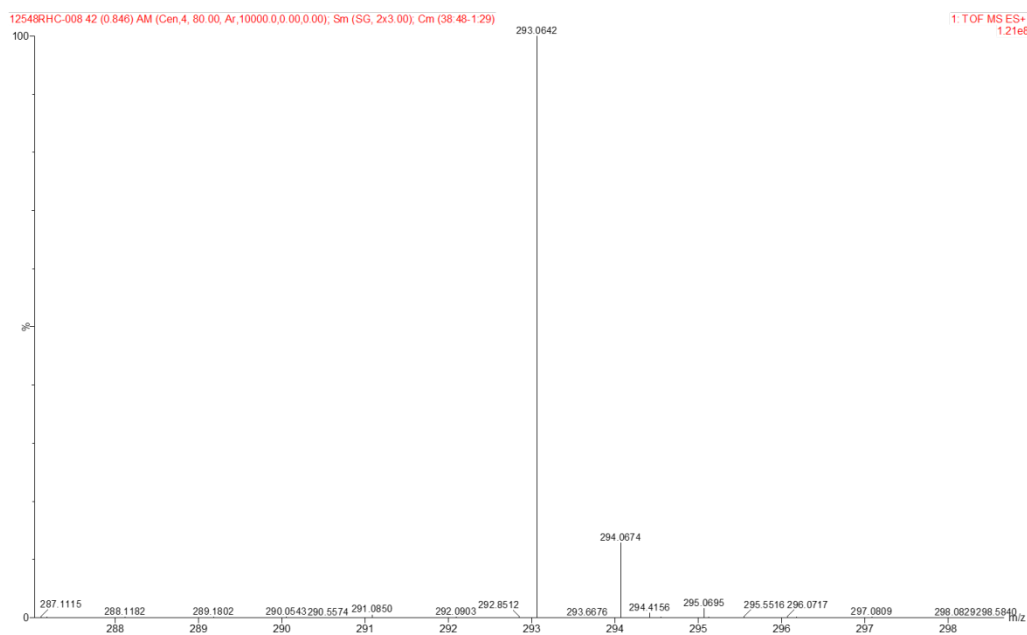


Figure A42. HRESIMS spectrum of compound **3.8**

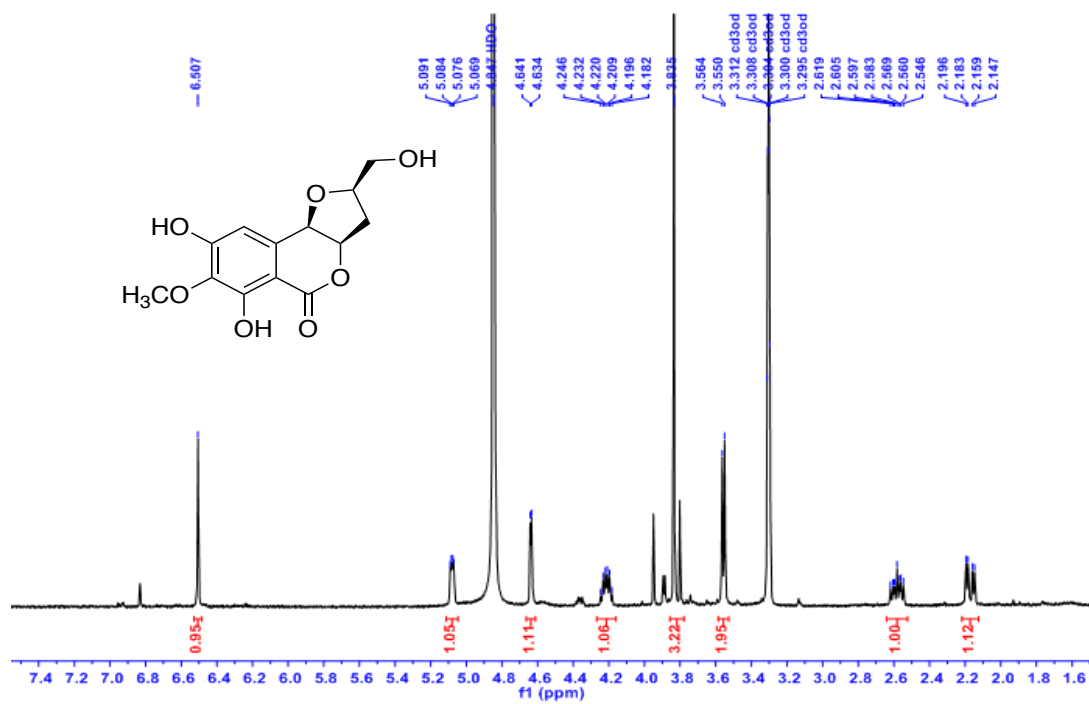


Figure A43. ¹H NMR spectrum of compound 3.9 (MeOH-*d*₄, 400 MHz)

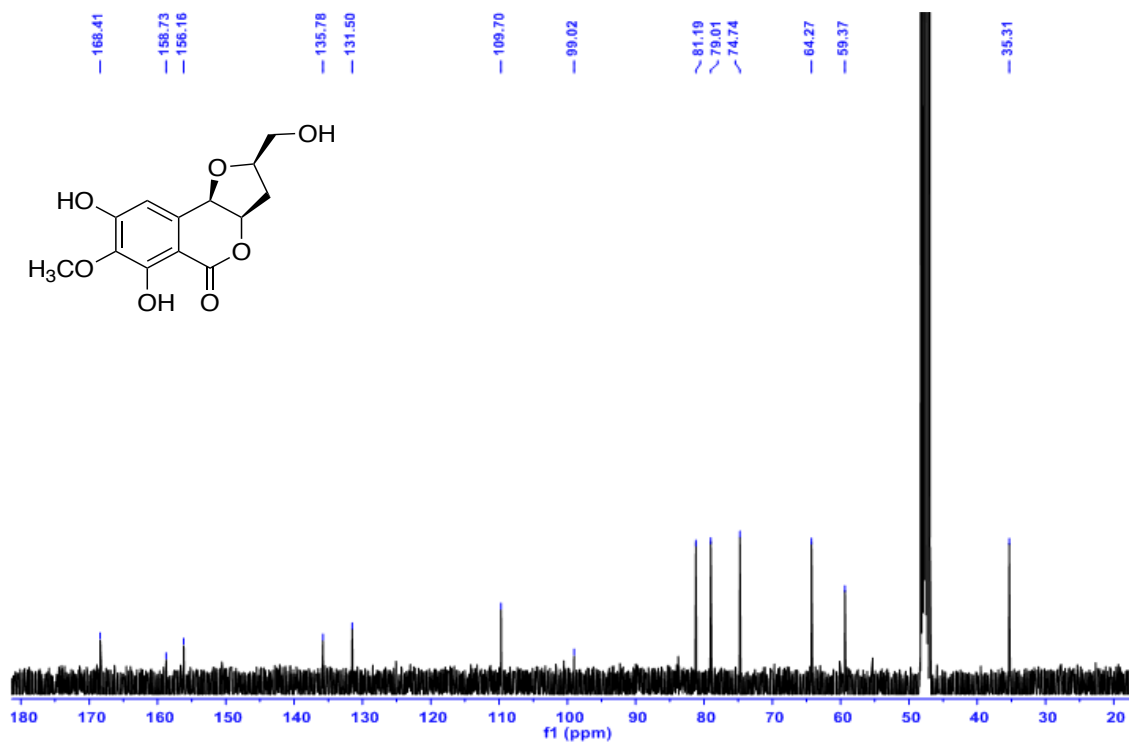


Figure A44. ¹³C NMR spectrum of compound 3.9 (MeOH-*d*₄, 100 MHz)

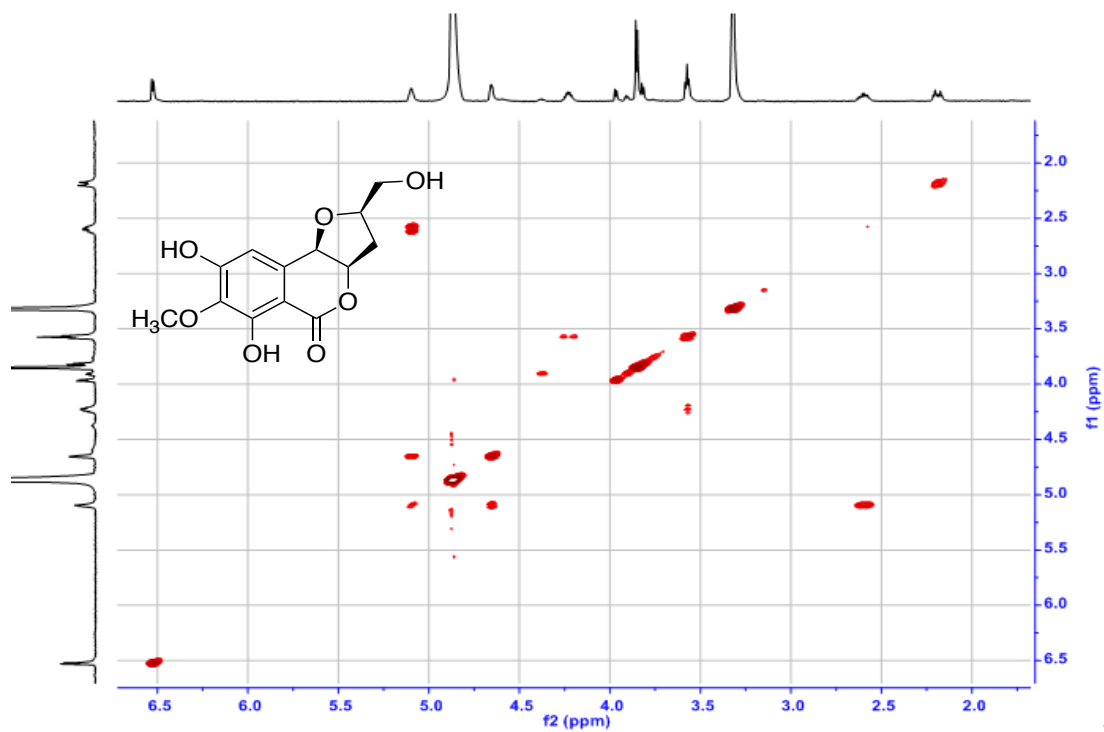


Figure A45. COSY spectrum of compound **3.9** (MeOH-*d*₄, 400 MHz)

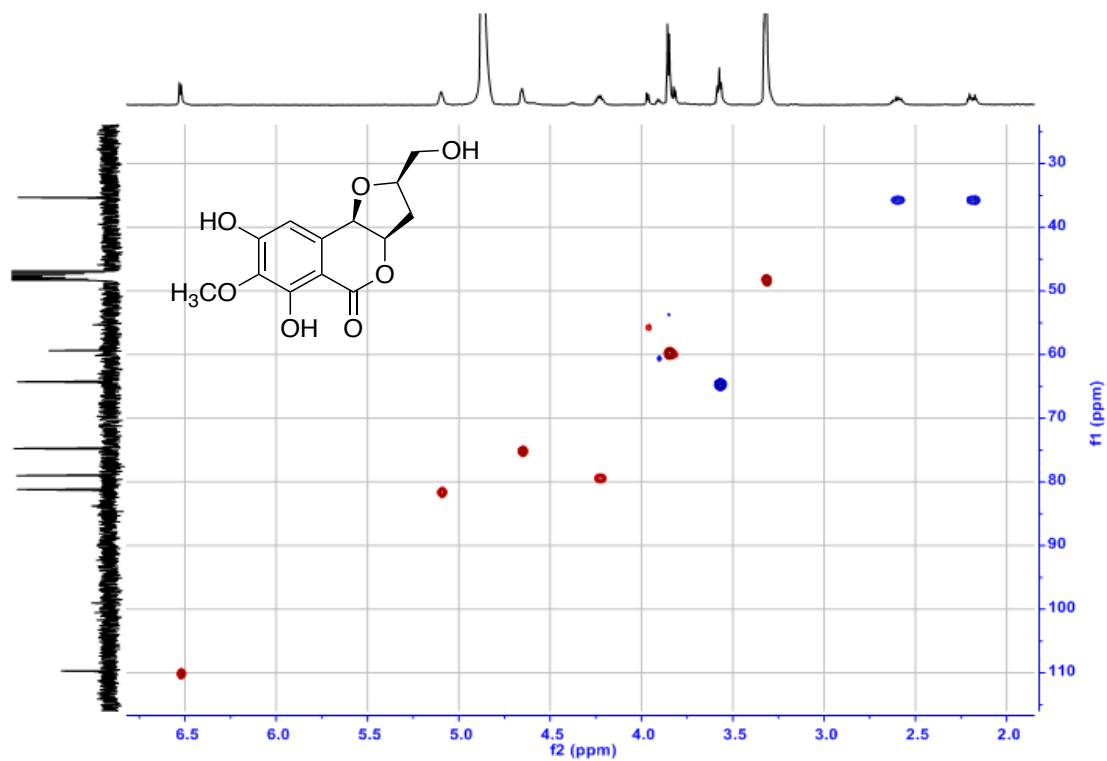


Figure A46. HSQC spectrum of compound **3.9** (MeOH-*d*₄, 400 MHz)

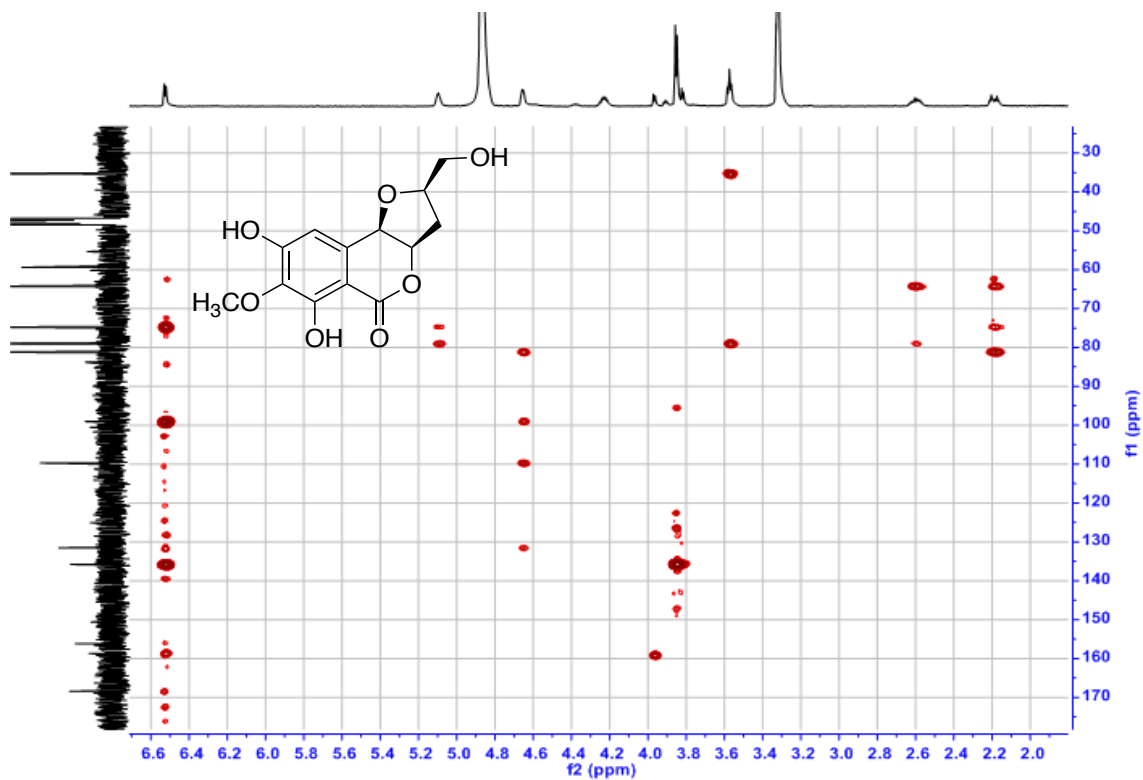


Figure A47. HMBC spectrum of compound 3.9 (MeOH- d_4 , 400 MHz)

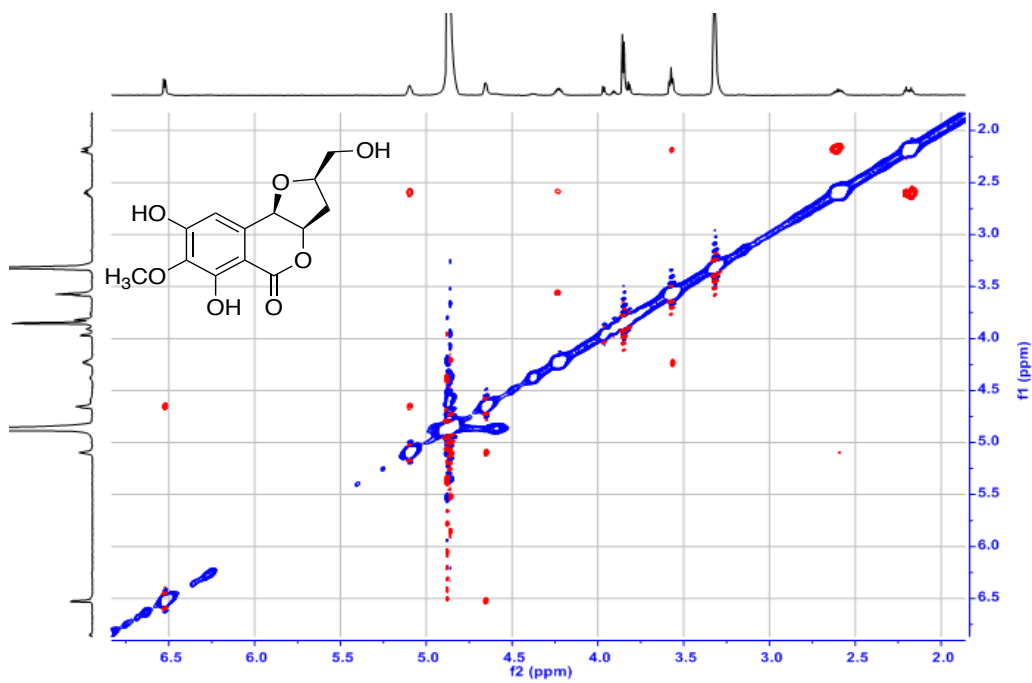


Figure A48. ROESY spectrum of compound 3.9 (MeOH- d_4 , 400 MHz)

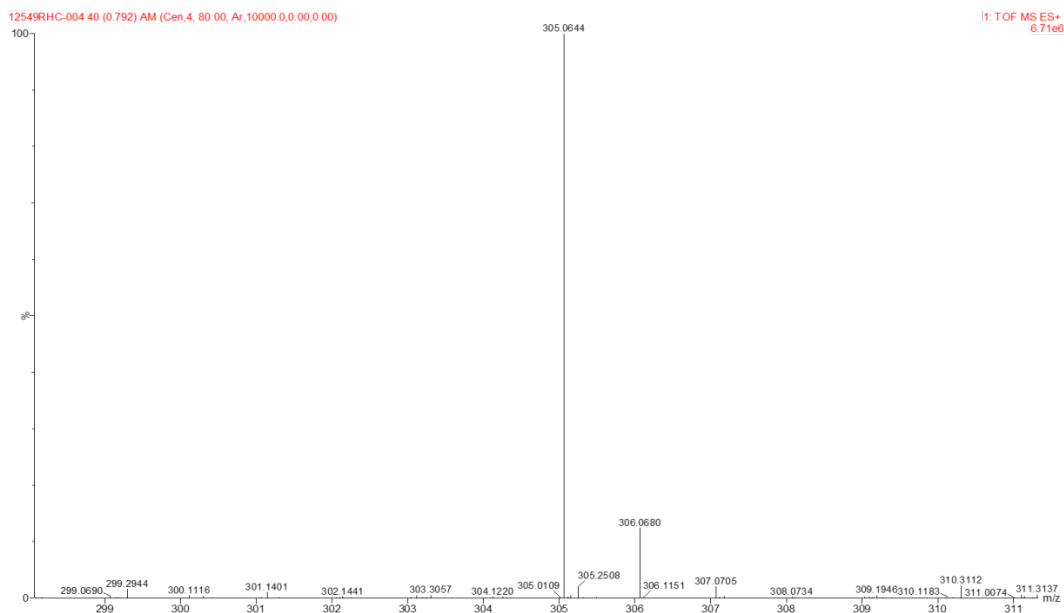


Figure A49. HRESIMS spectrum of compound **3.9**

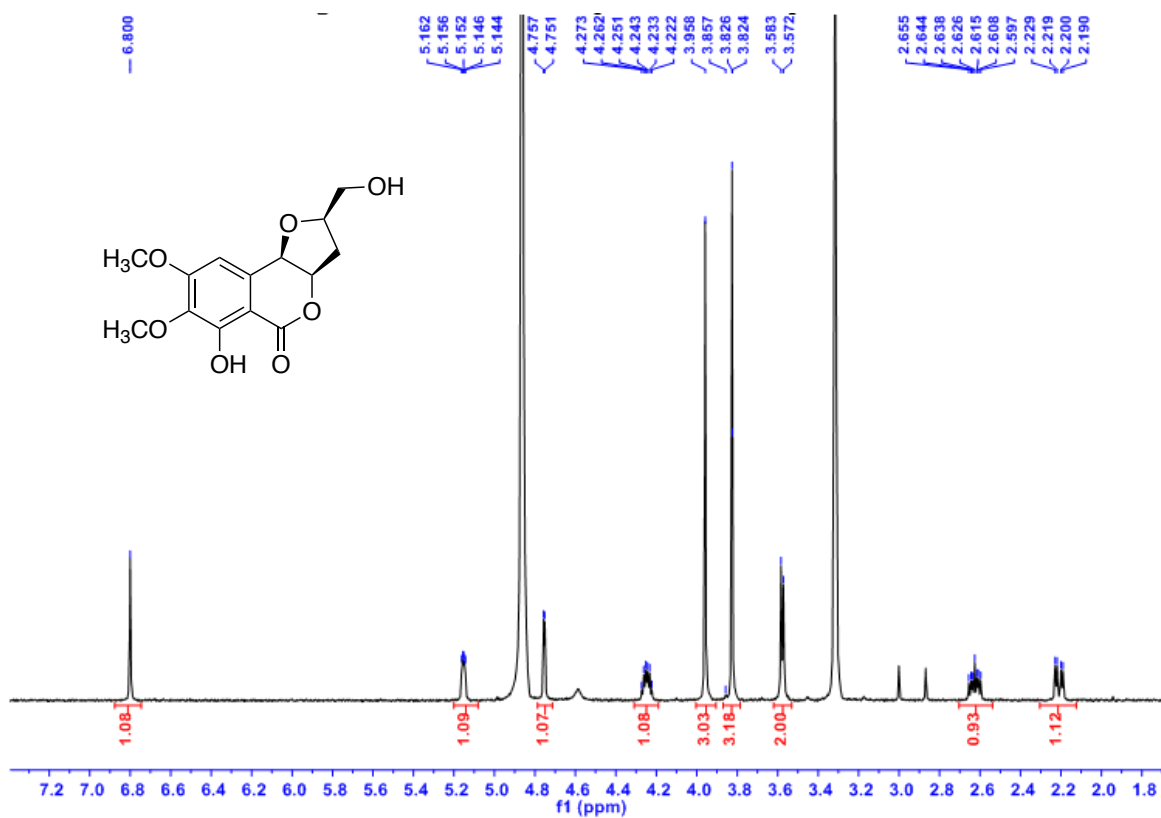


Figure A50. ^1H NMR spectrum of compound **3.10** (MeOH- d_4 , 400 MHz)

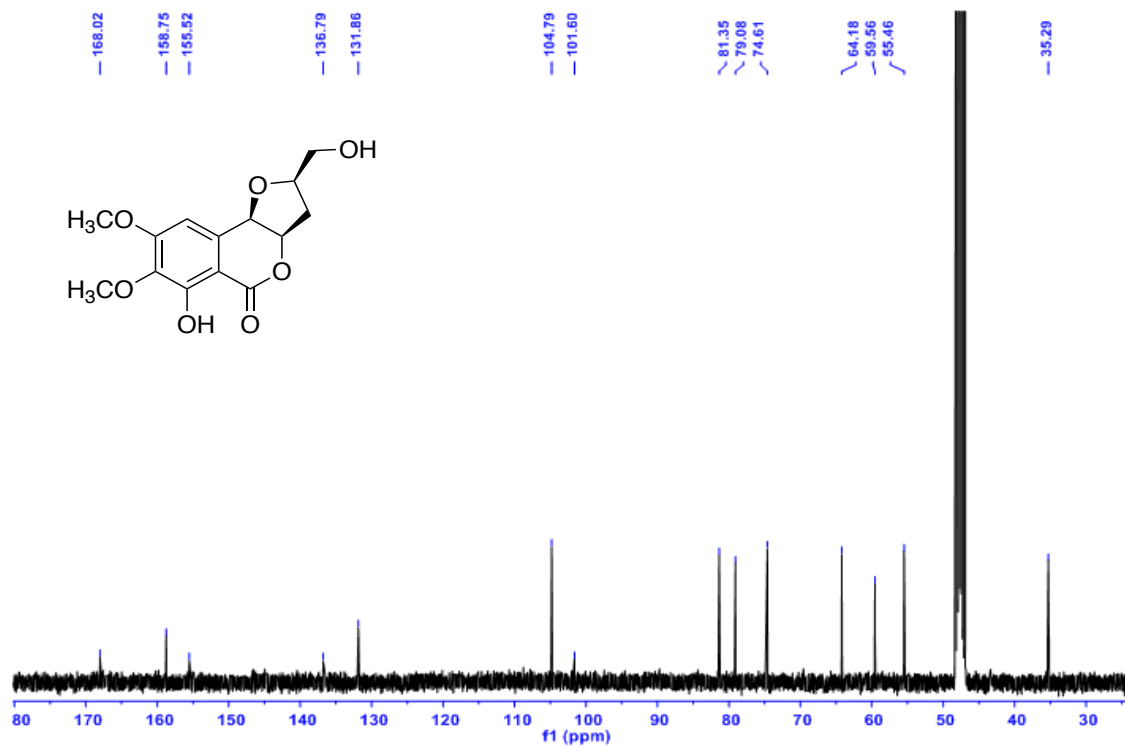


Figure A51. ^{13}C NMR spectrum of compound **3.10** (MeOH- d_4 , 100 MHz)

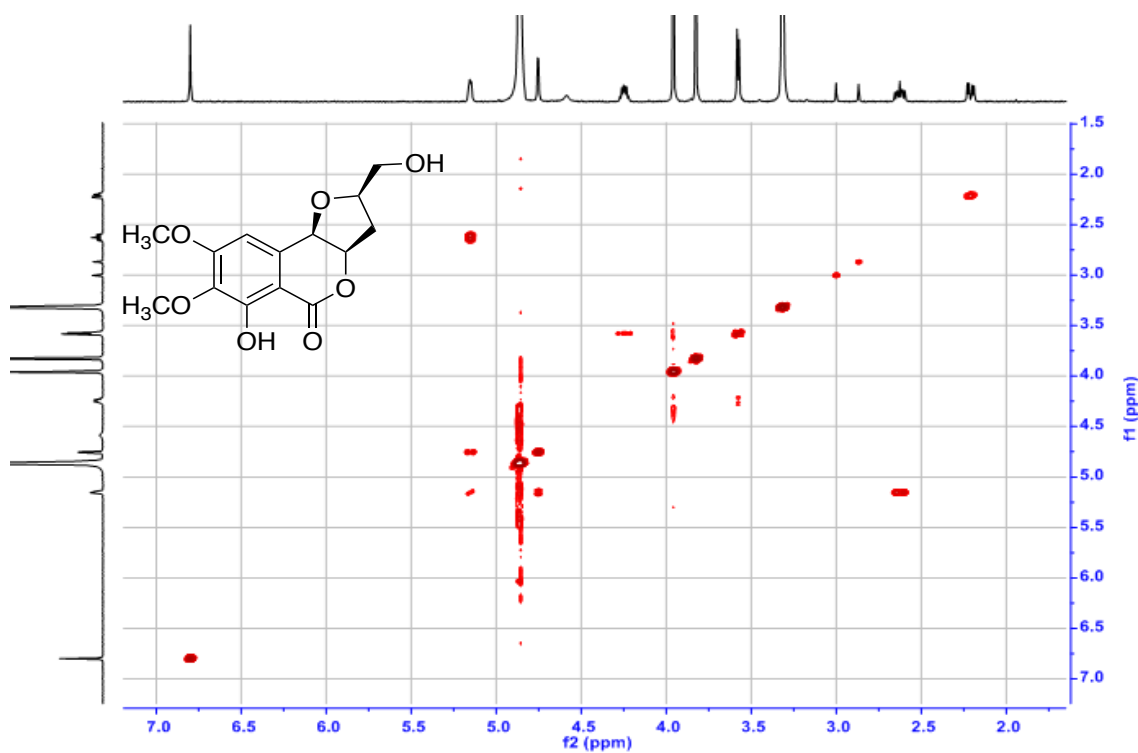


Figure A52. COSY spectrum of compound **3.10** (MeOH- d_4 , 400 MHz)

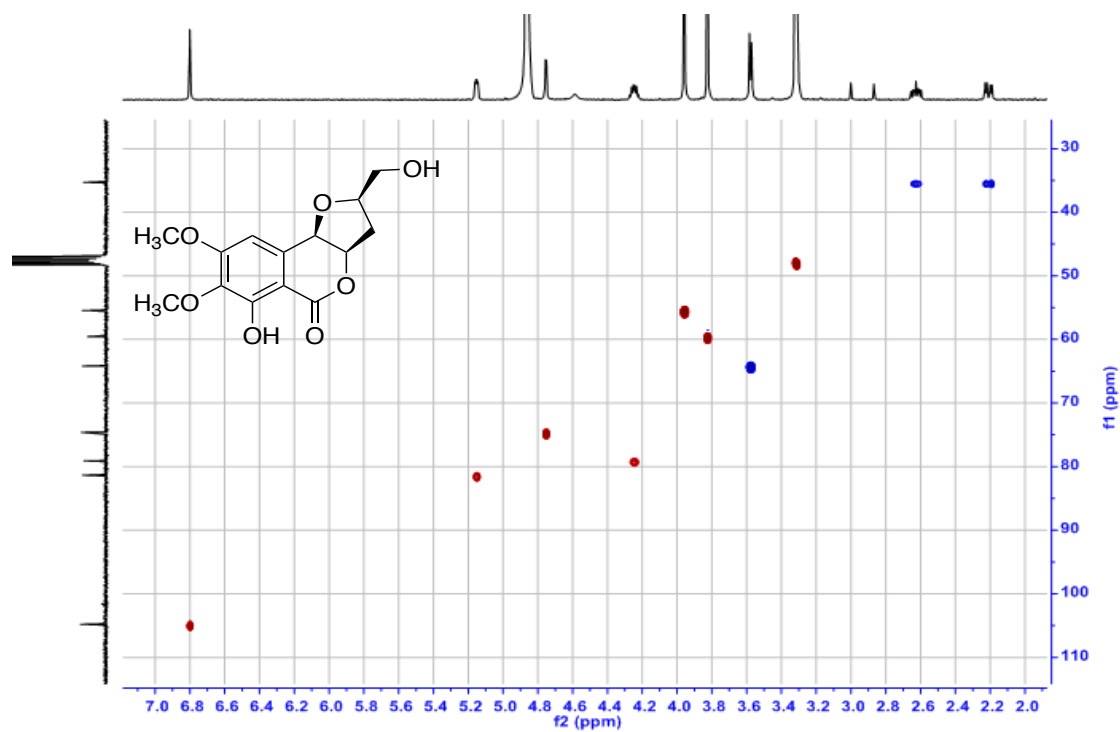


Figure A53. HSQC spectrum of compound **3.10** (MeOH-*d*₄, 400 MHz)

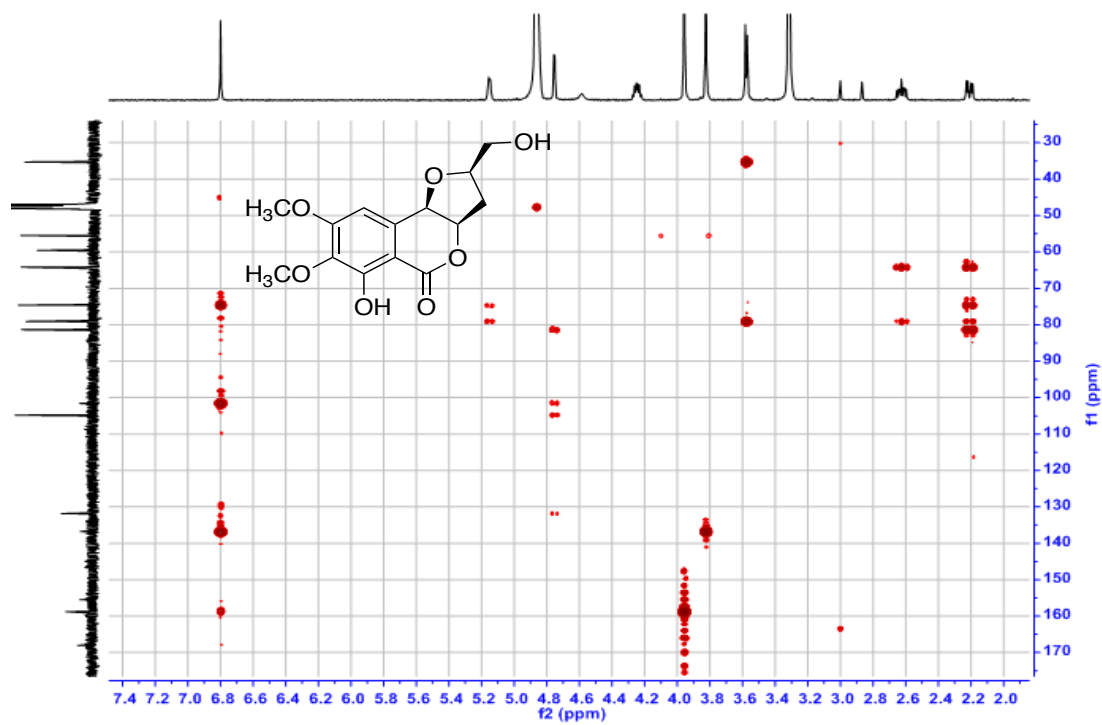


Figure A54. HMBC spectrum of compound **3.10** (MeOH-*d*₄, 400 MHz)

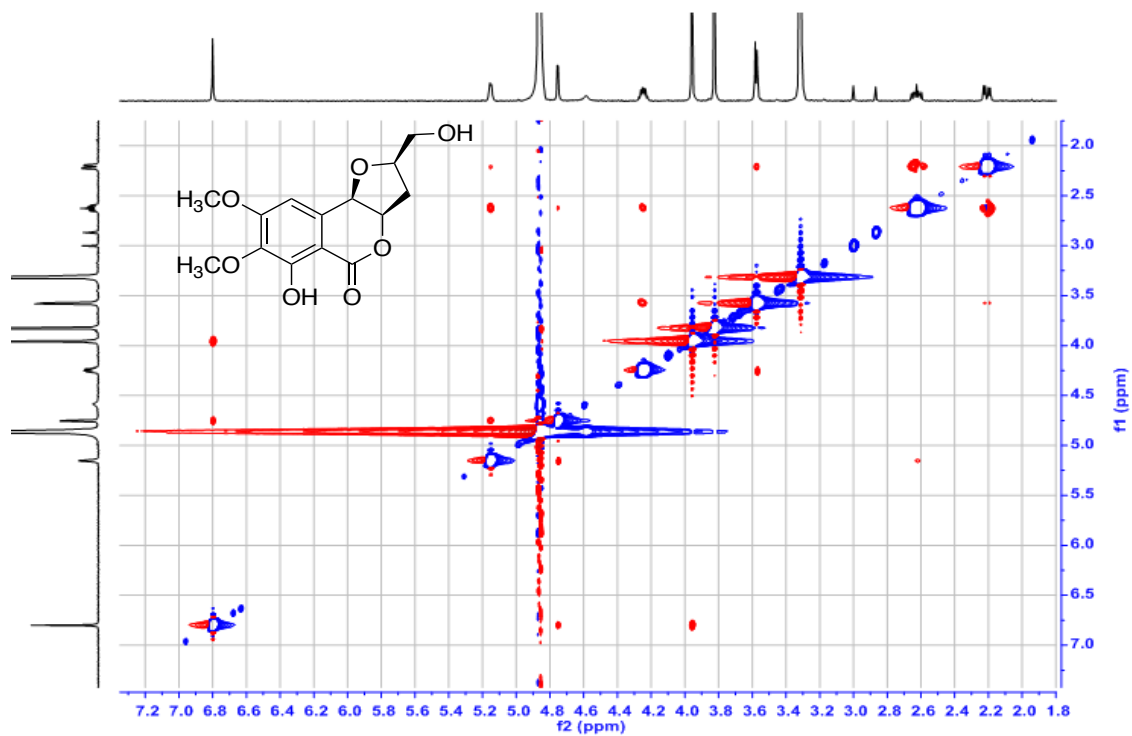


Figure A55. ROESY spectrum of compound **3.10** (MeOH- d_4 , 400 MHz)

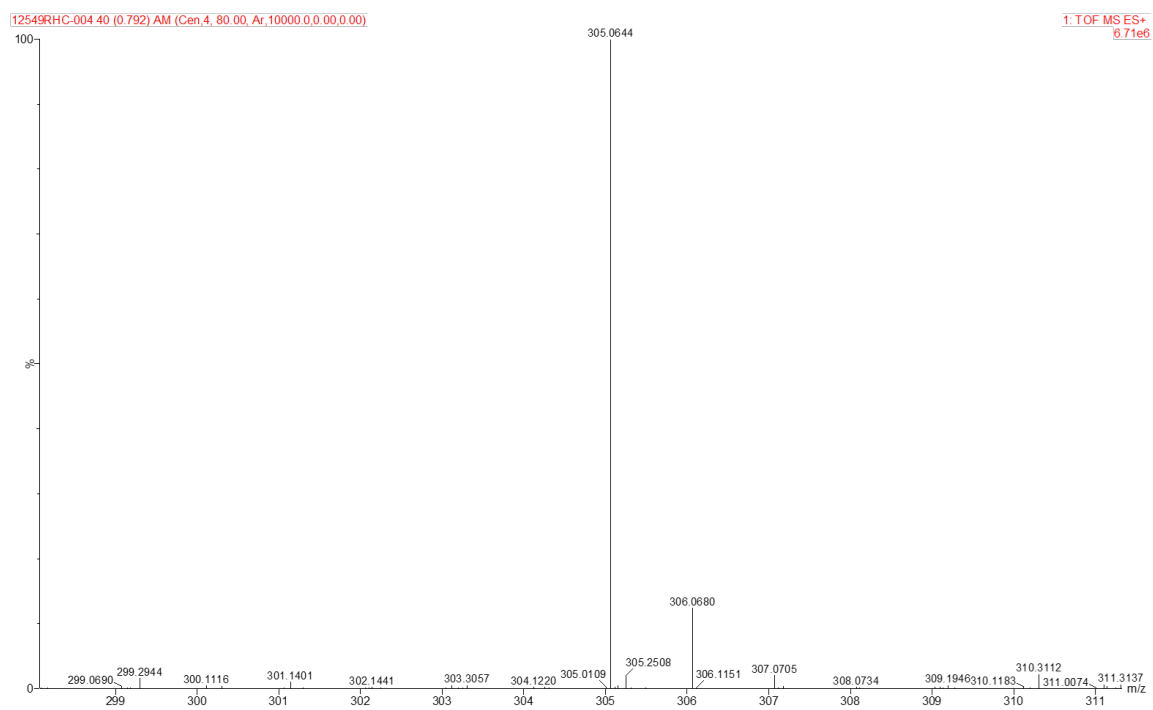


Figure A56. HRMSIMS spectrum of compound **3.10**

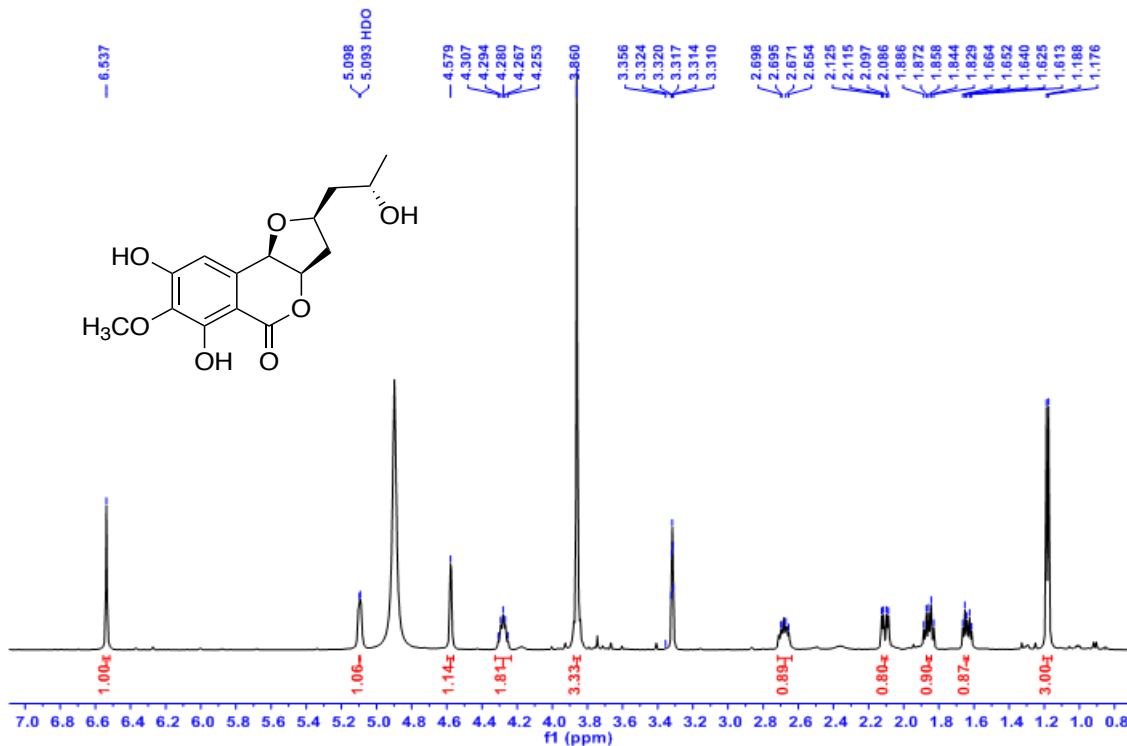


Figure A57. ¹H NMR spectrum of compound **3.11** (MeOH-*d*₄, 400 MHz)

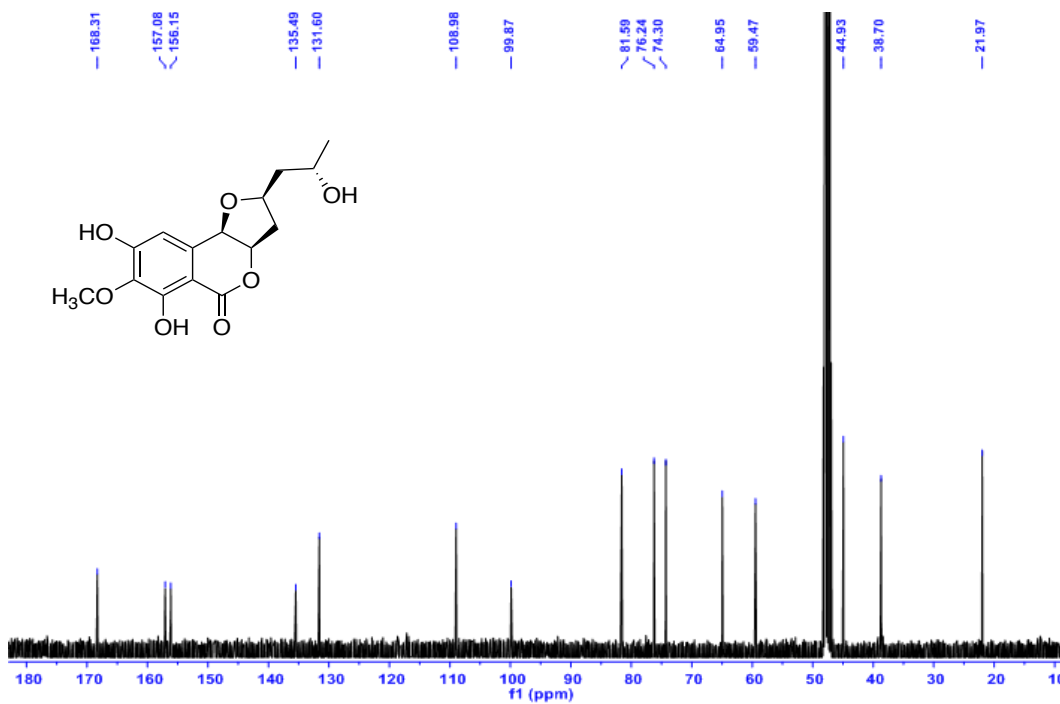


Figure A58. ¹³C NMR spectrum of compound **3.11** (MeOH-*d*₄, 100 MHz)

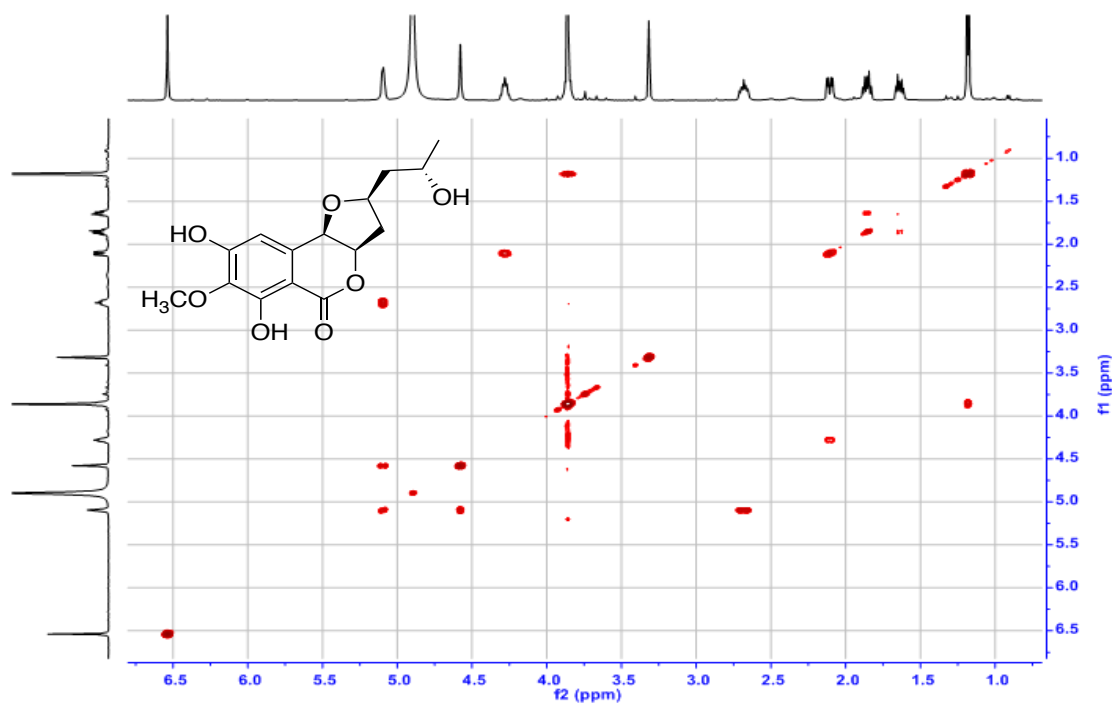


Figure A59. COSY spectrum of compound **3.11** (MeOH- d_4 , 400 MHz)

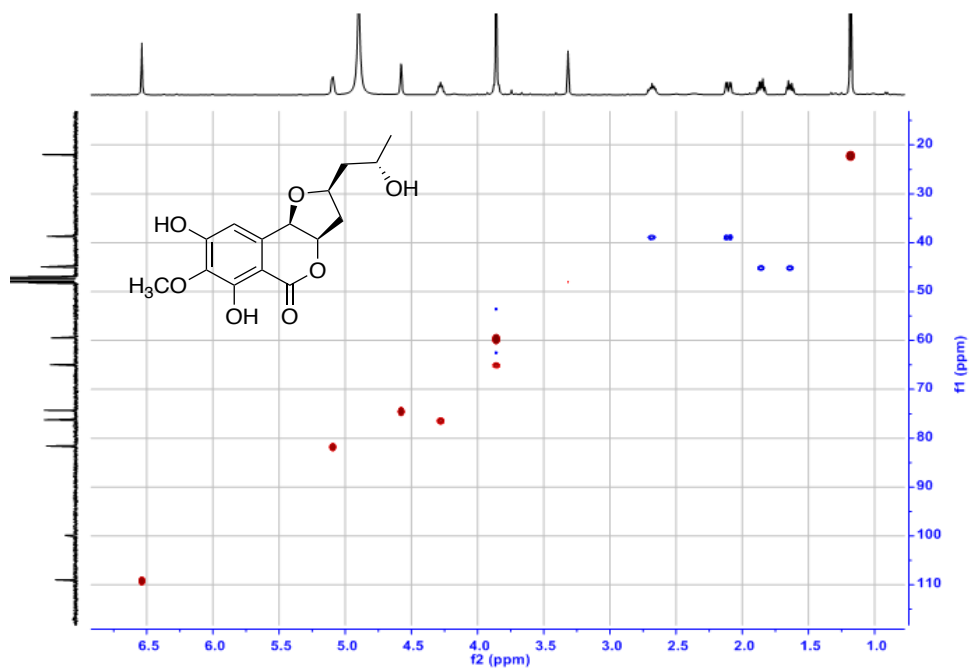


Figure A60. HSQC spectrum of compound **3.11** (MeOH- d_4 , 400 MHz)

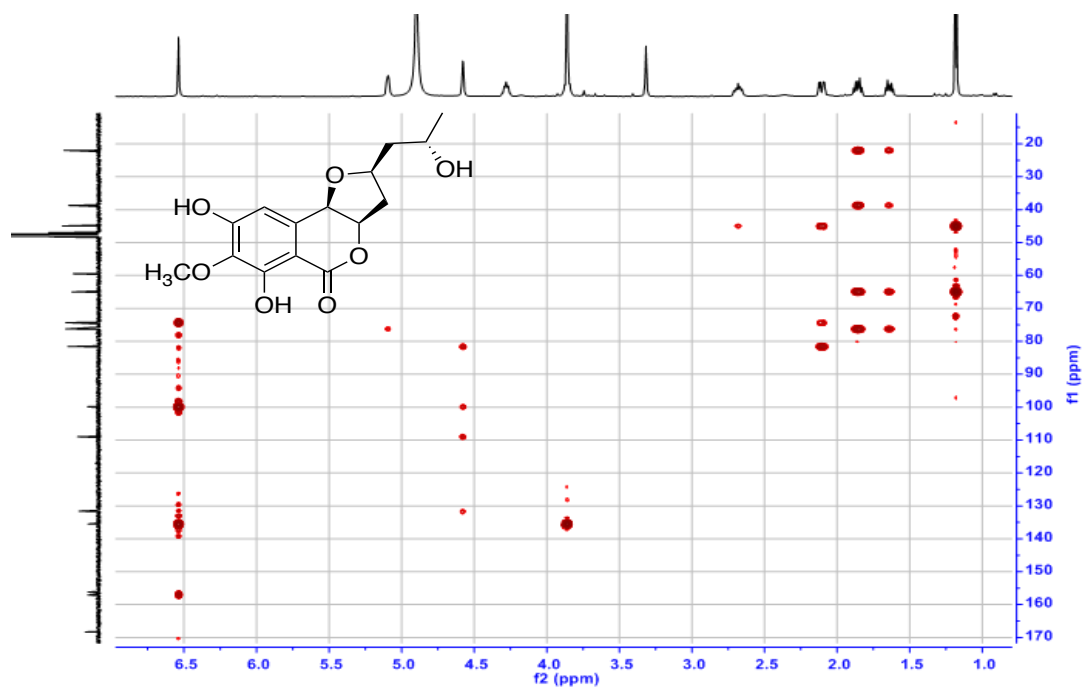


Figure A61. HMBC spectrum of compound **3.11** ($\text{MeOH-}d_4$, 400 MHz)

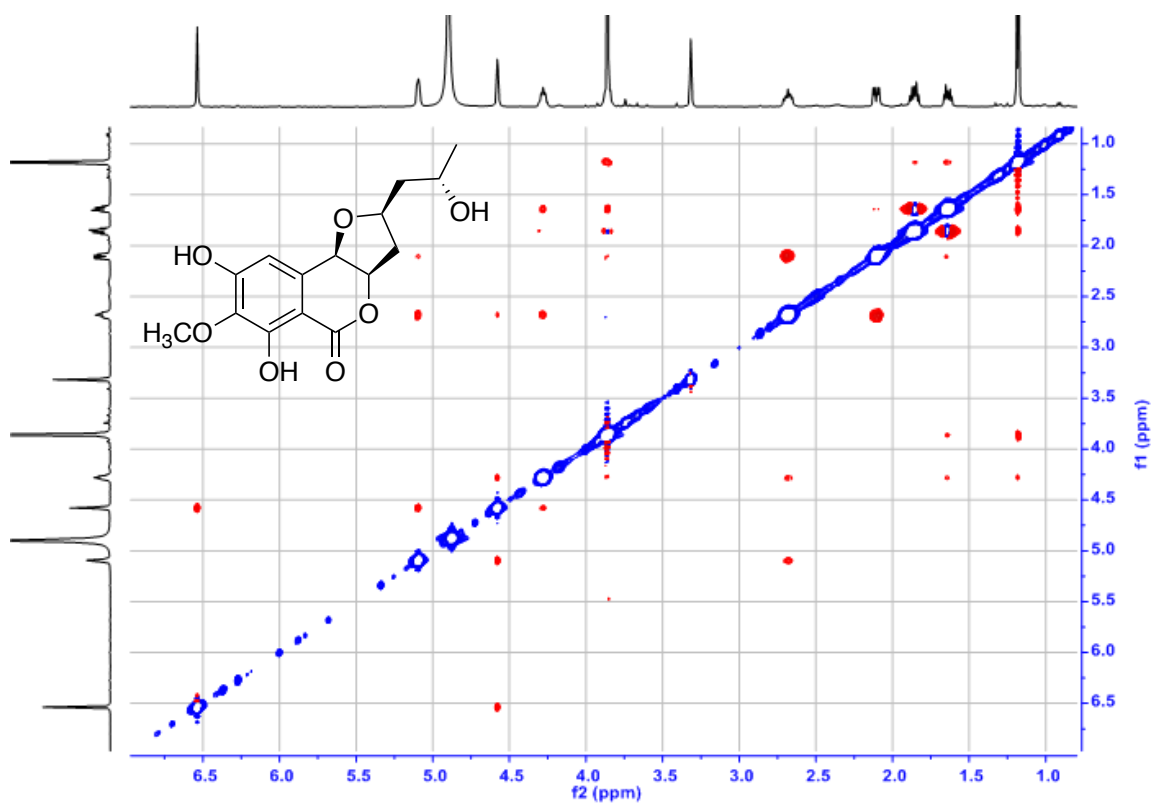


Figure A62. ROESY spectrum of compound **3.11** ($\text{MeOH-}d_4$, 400 MHz)

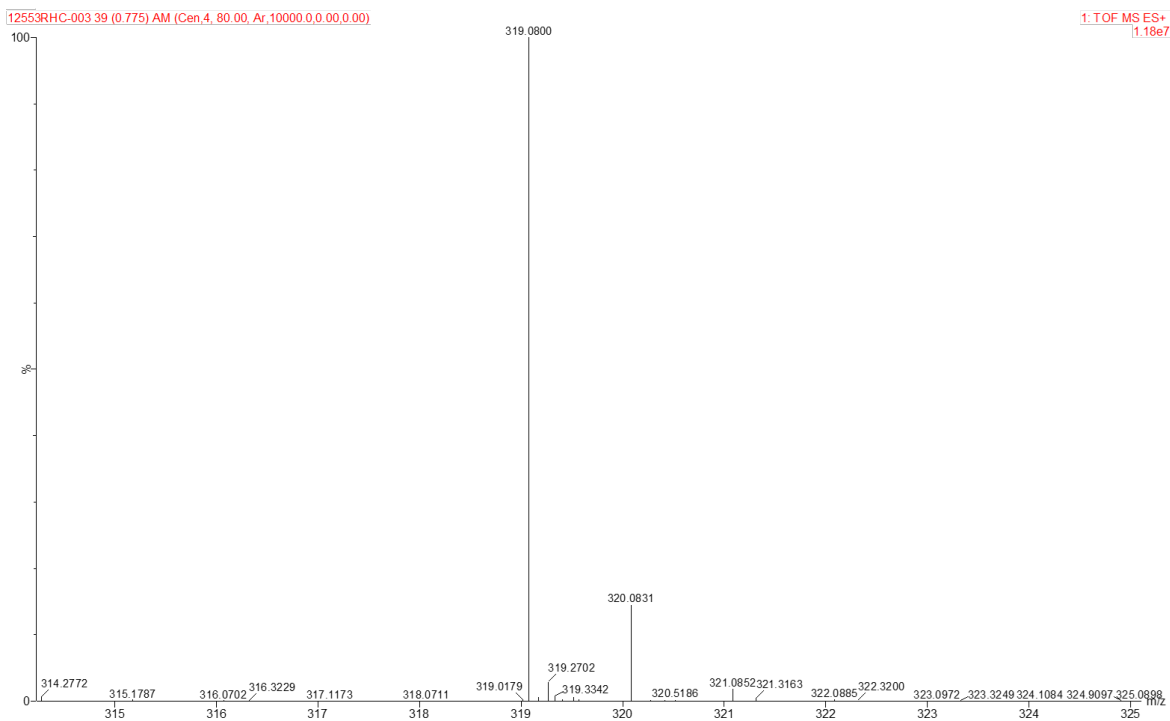


Figure A63. HRESIMS spectrum of compound 3.11

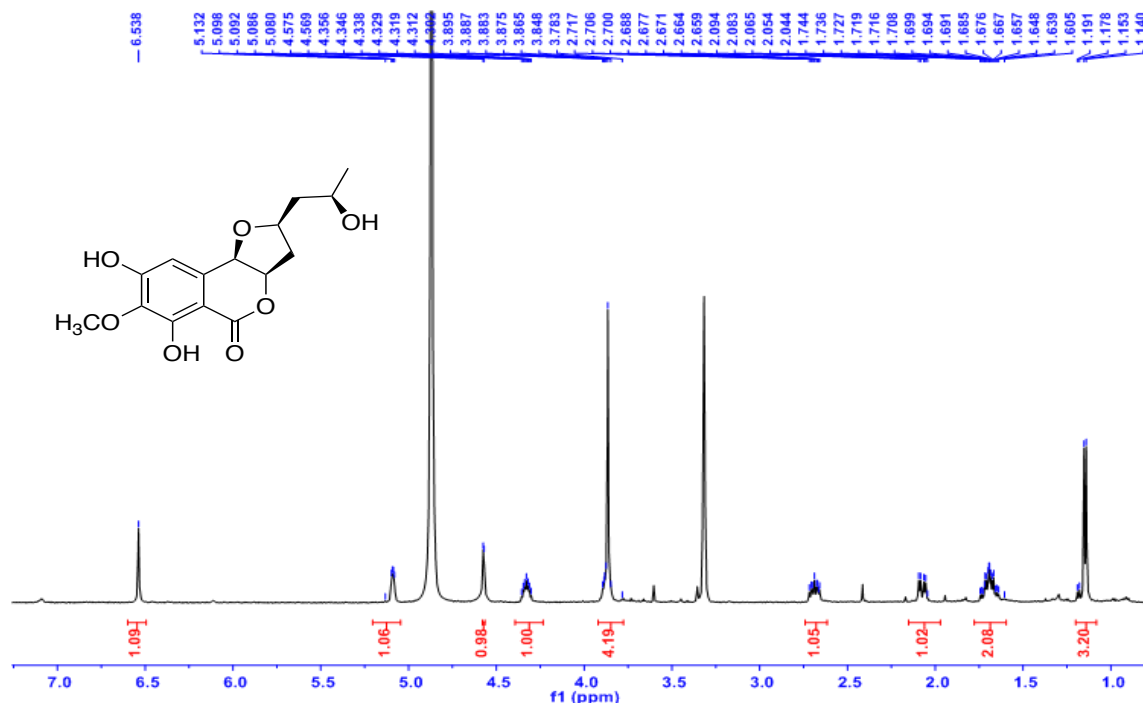


Figure A64. ^1H NMR spectrum of compound 3.12 (MeOH- d_4 , 400 MHz)

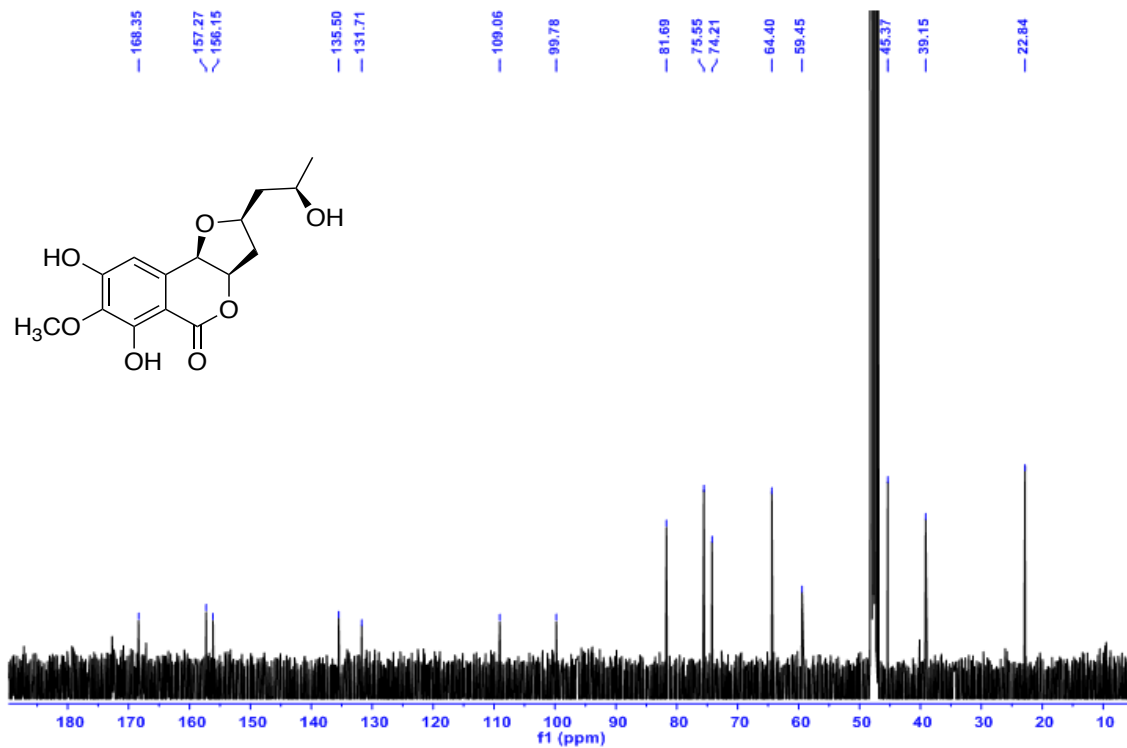


Figure A65. ^{13}C NMR spectrum of compound **3.12** (MeOH- d_4 , 100 MHz)

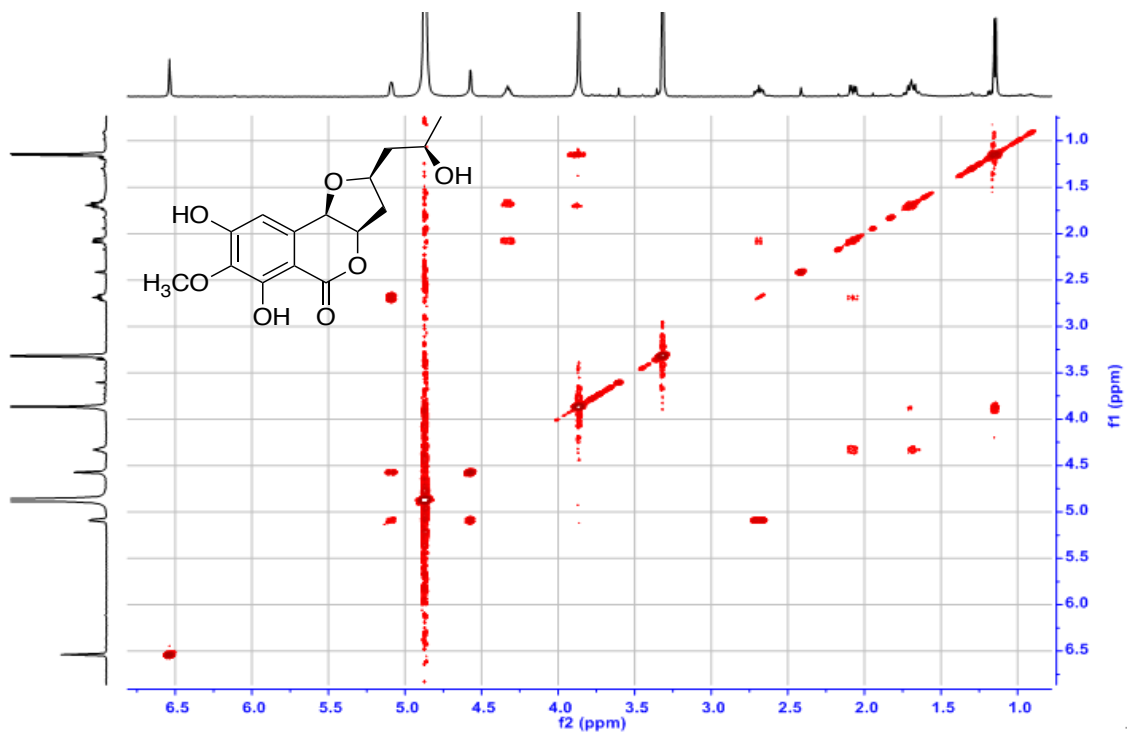


Figure A66. COSY spectrum of compound **3.12** (MeOH- d_4 , 400 MHz)

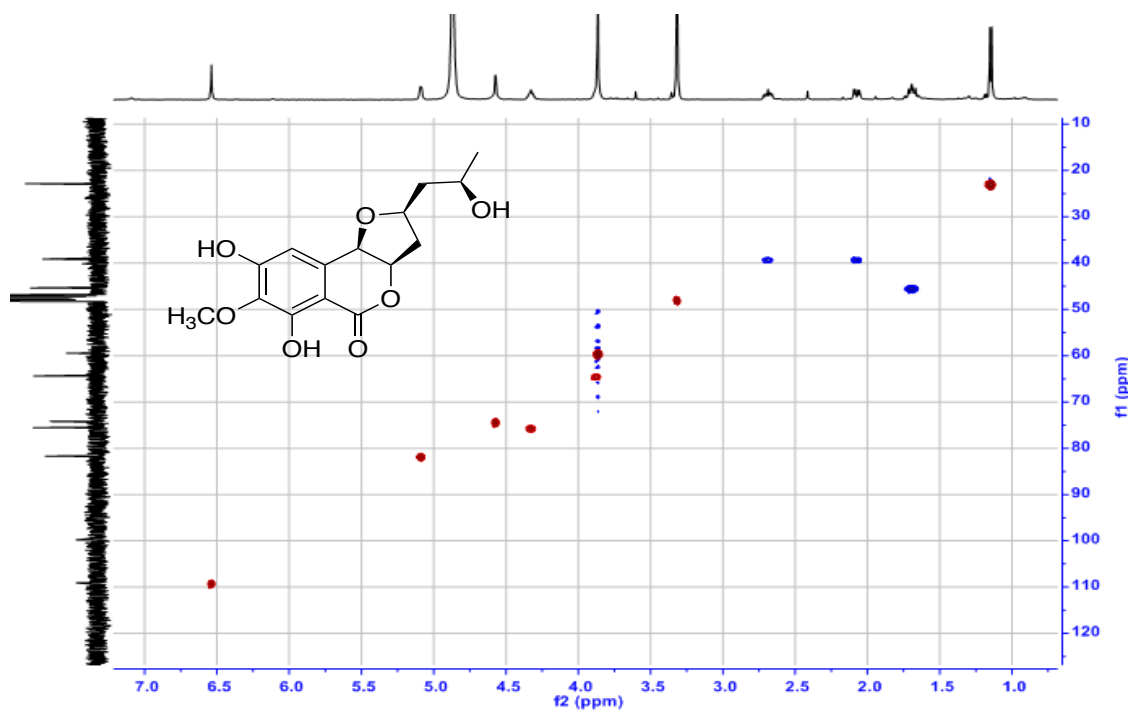


Figure A67. HSQC spectrum of compound **3.12** (MeOH-*d*₄, 400 MHz)

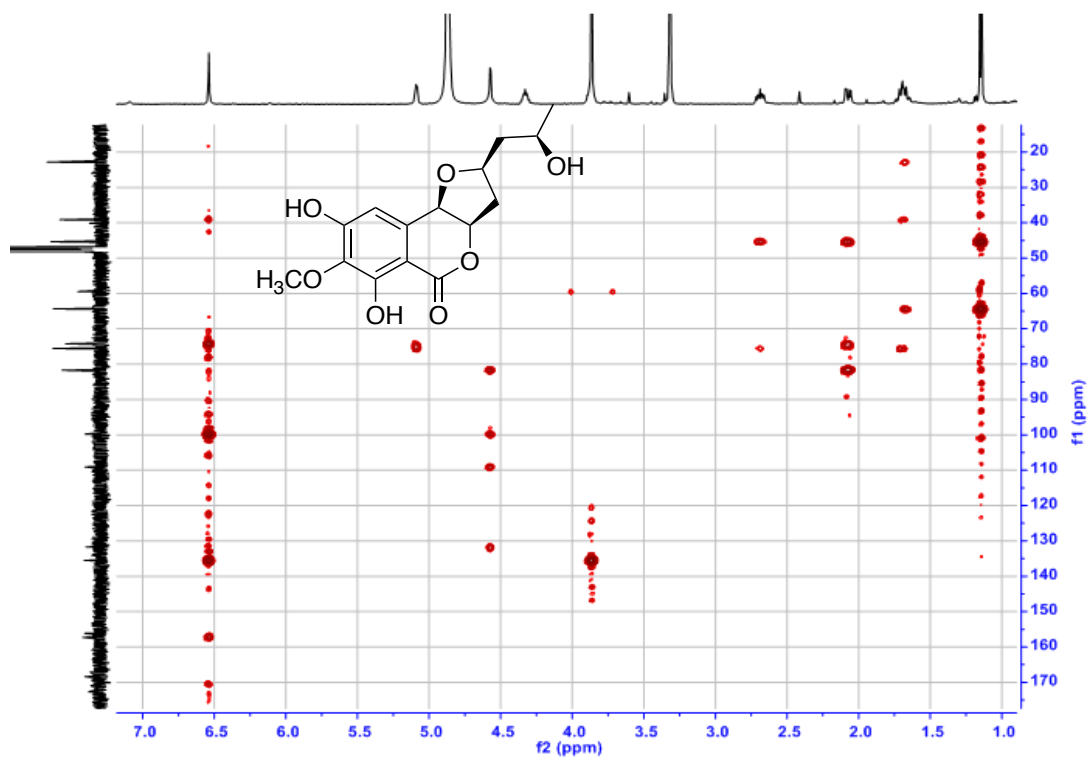


Figure A68. HMBC spectrum of compound **3.12** (MeOH-*d*₄, 400 MHz)

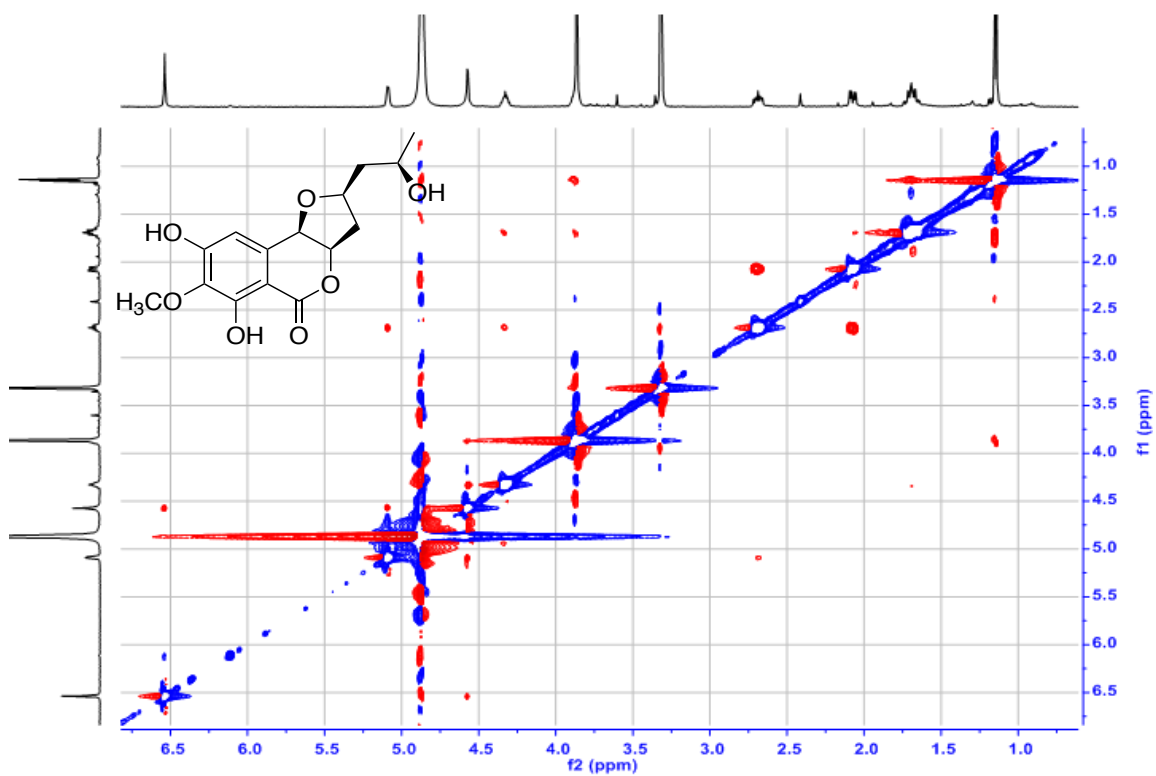


Figure A69.ROESY spectrum of compound **3.12** (MeOH- d_4 , 400 MHz)

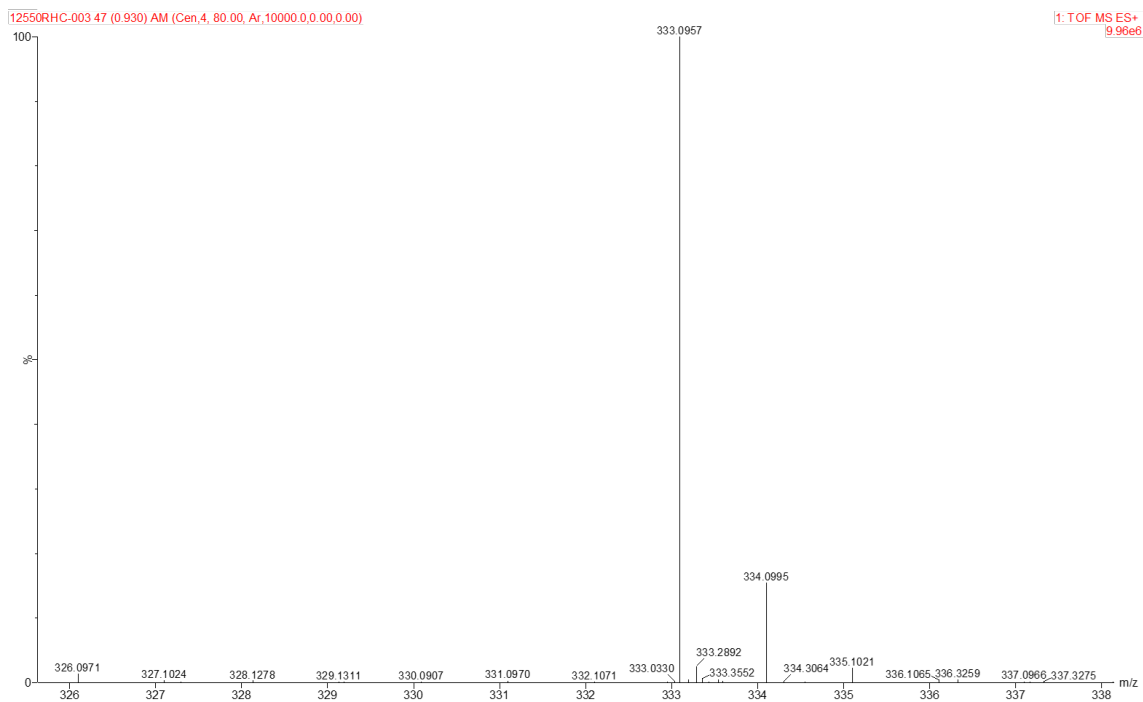


Figure A70. HRESIMS spectrum of compound **3.12**

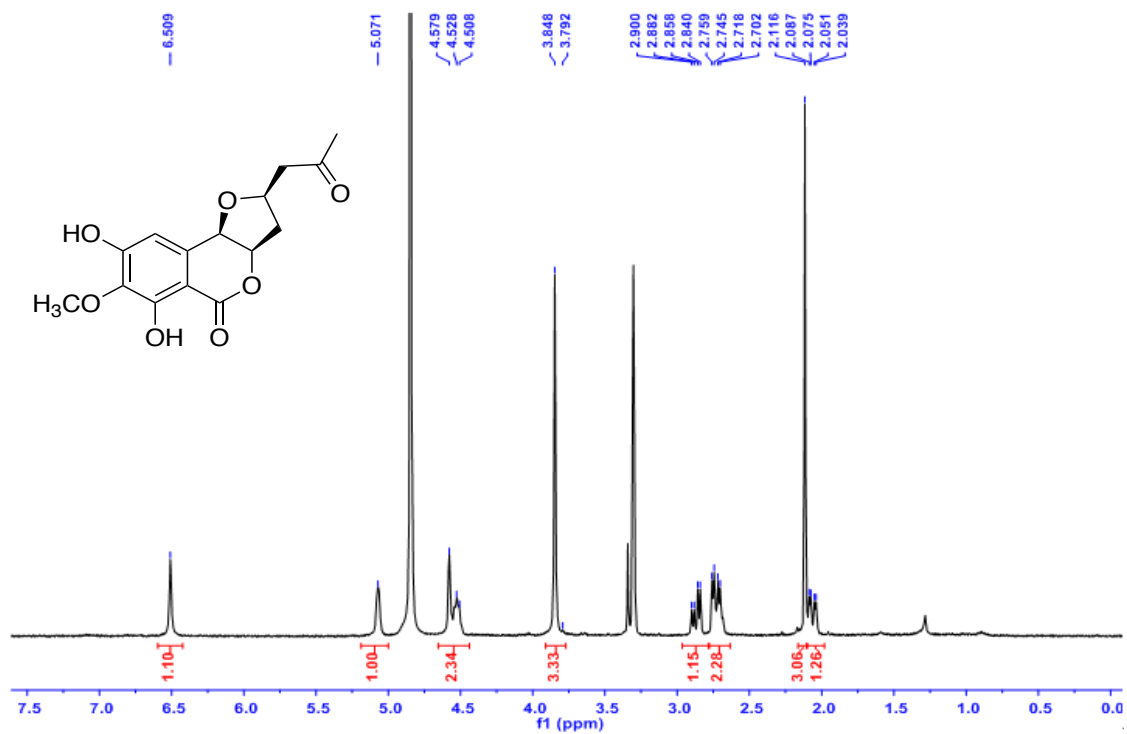


Figure A71. ^1H NMR spectrum of compound **3.13** (MeOH- d_4 , 400 MHz)

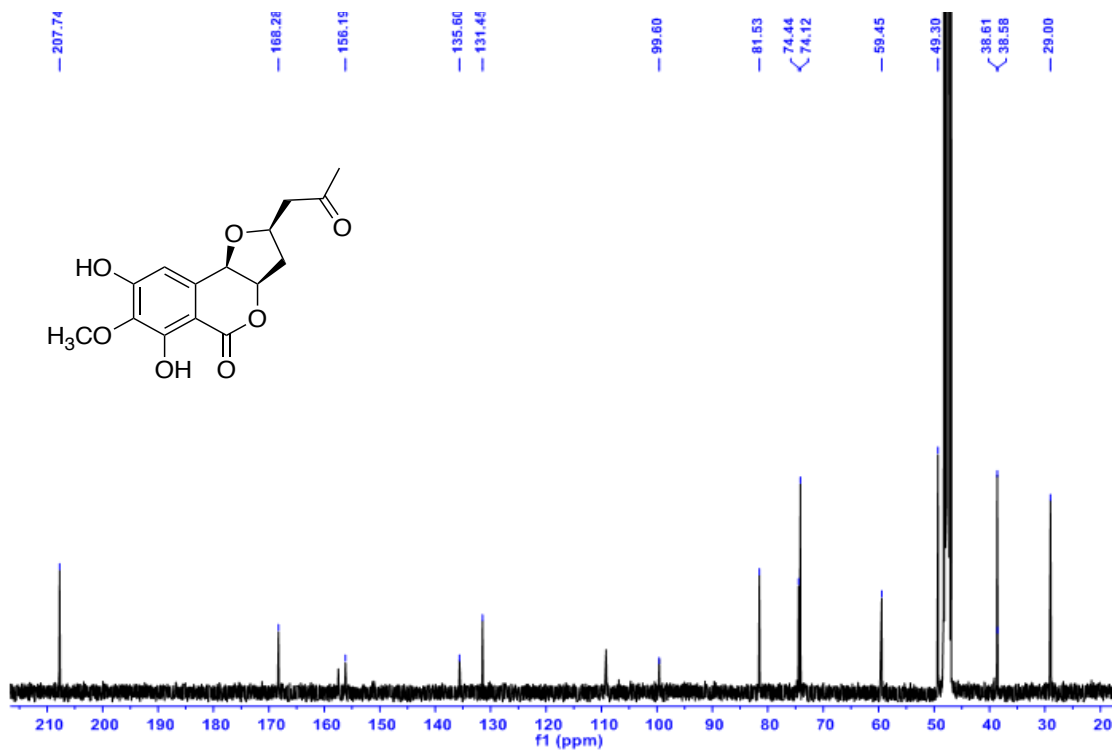


Figure A72. ^{13}C NMR spectrum of compound **3.13** (MeOH- d_4 , 100 MHz)

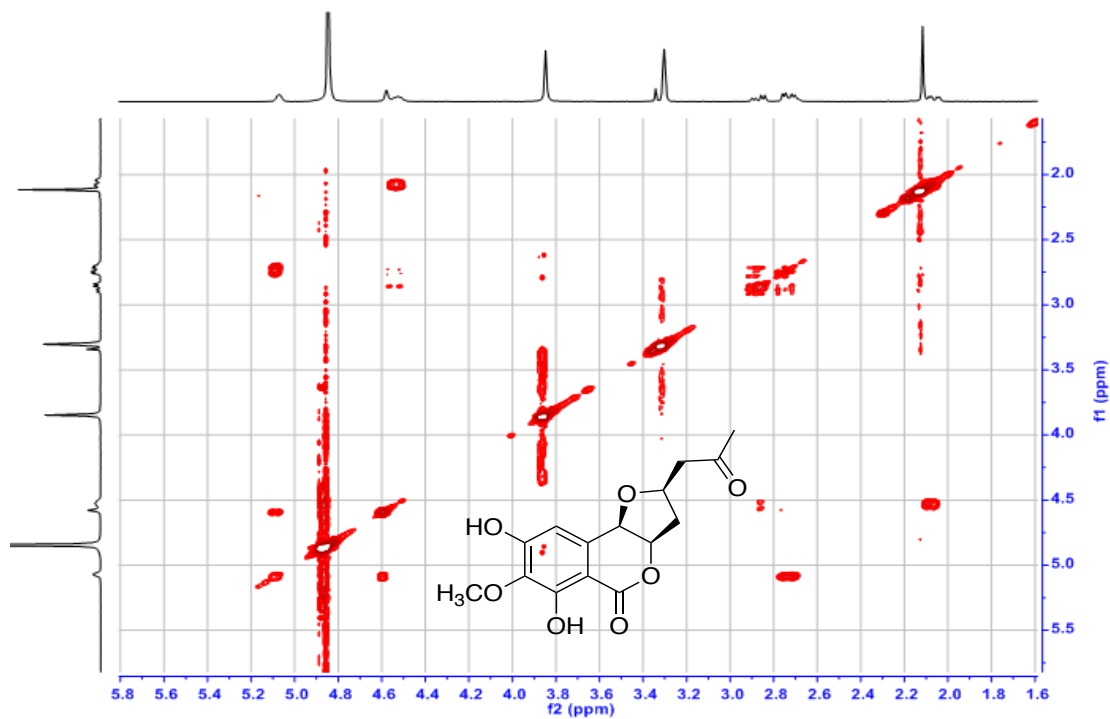


Figure A73. COSY spectrum of compound 3.13 (MeOH- d_4 , 400 MHz)

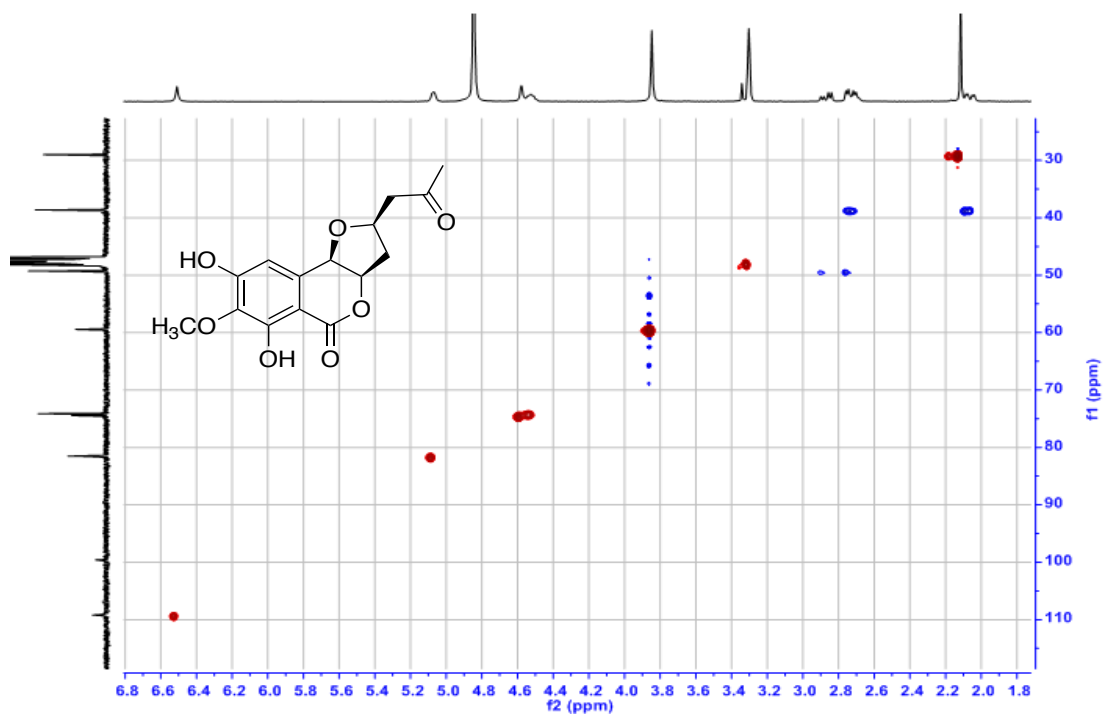


Figure A74. HSQC spectrum of compound 3.13 (MeOH- d_4 , 400 MHz)

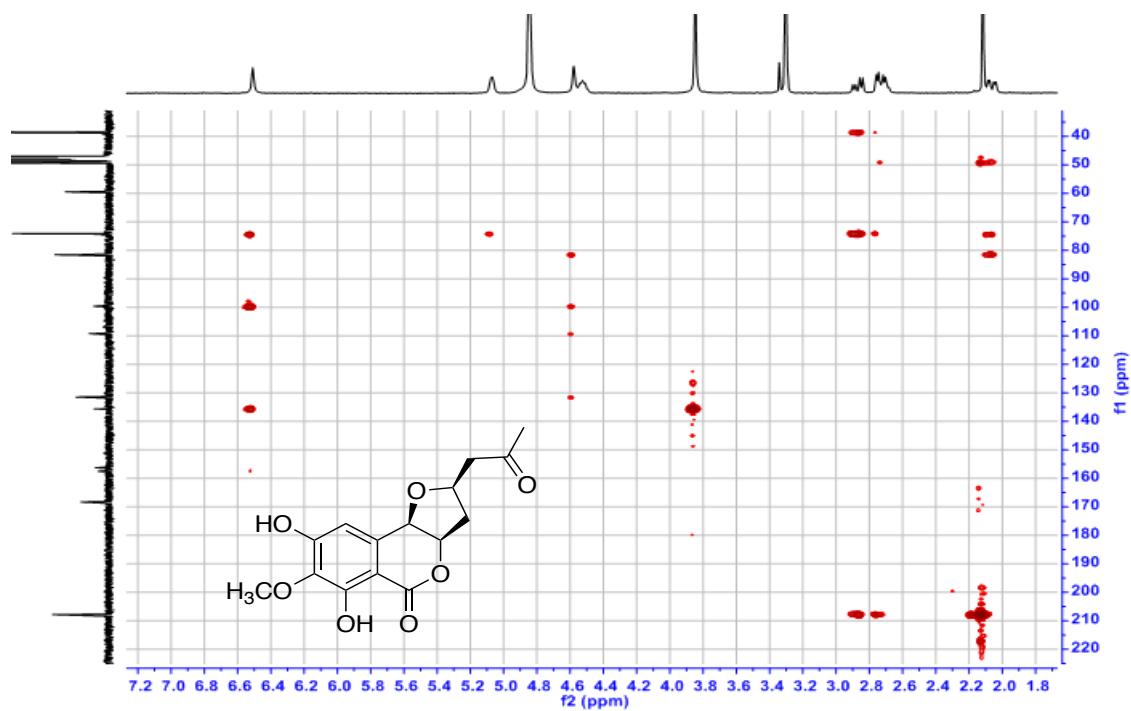


Figure A75. HMBC spectrum of compound **3.13** ($\text{MeOH-}d_4$, 400 MHz)

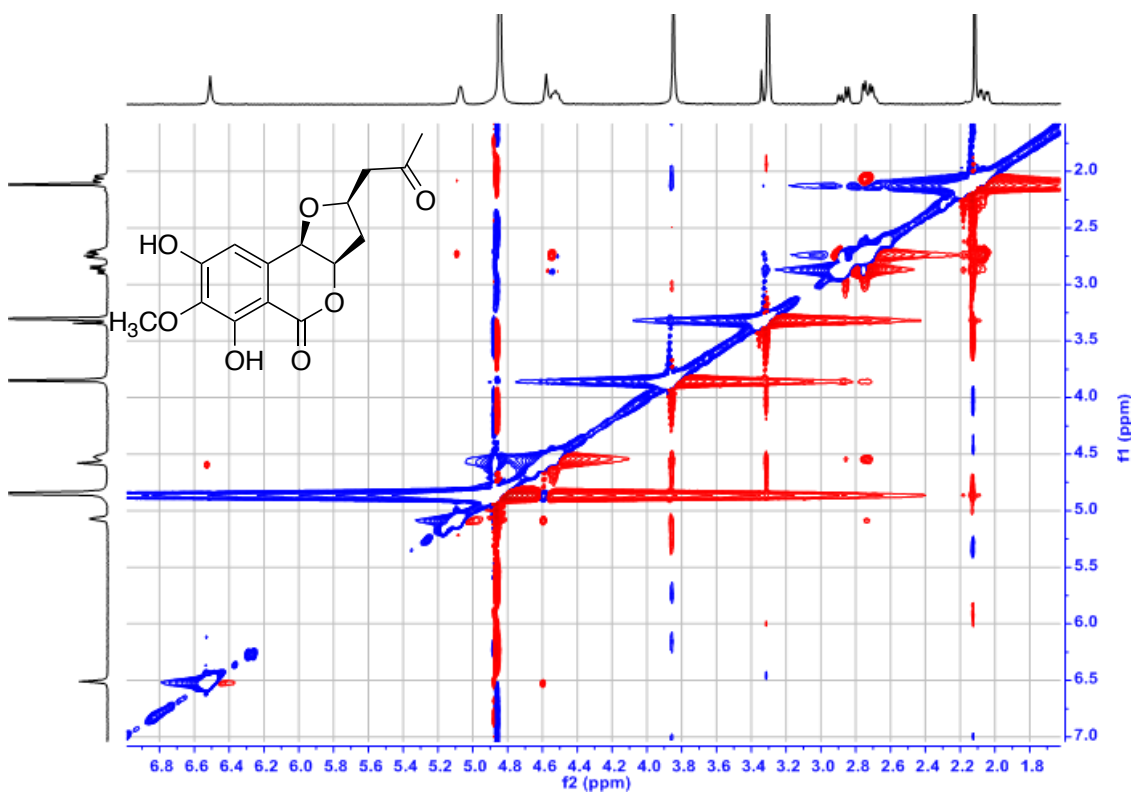


Figure A76. ROESY spectrum of compound **3.13** ($\text{MeOH-}d_4$, 400 MHz)

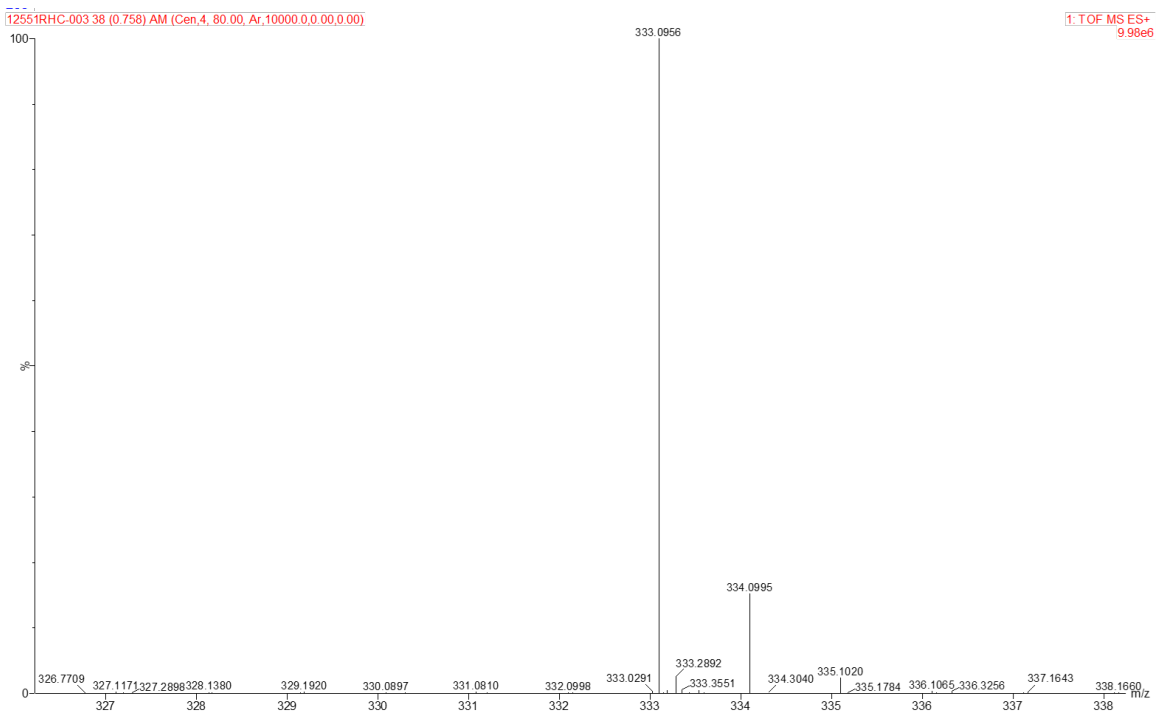


Figure A77. HRESIMS spectrum of compound **3.13**

Appendix B: Supporting Data for Chapter 4

Appendix Table of Contents

Figure B.1. LC-MS analysis (selected ion at m/z 356.15 under ESI ⁻ mode) for FDAA derivatives of beauversetin-derived hydrolysate (A), and D- (B) and L-Ser (C)	160
Figure B.2. LC-MS analysis (selected ion at m/z 370.20 under ESI negative mode) for FDAA derivatives of equisetin-derived hydrolysate(A), L-(B) and L, D-N-methyl serine (C)	161
Figure B.3. LC-MS analysis (selected ion at m/z 370.05 under ESI ⁻ mode) for FDAA derivatives of <i>epi</i> -pyrrolocin A-derived hydrolysate (A), and L- <i>N</i> -met-ser (B) and L, D- <i>N</i> -met-ser mixture (C)	162
Figure B.4. ¹ H NMR Spectrum of Compound 4.4 (DMSO- <i>d</i> ₆ , 500MHz)	163
Figure B.5. ¹³ C NMR Spectrum of Compound 4.4 (DMSO- <i>d</i> ₆ , 100MHz)	163
Figure B.6. ¹ H NMR Spectrum of Compound 4.5 (DMSO- <i>d</i> ₆ , 500MHz)	164
Figure B.7. ¹³ C NMR Spectrum of Compound 4.5 (DMSO- <i>d</i> ₆ , 100MHz)	164
Figure B.8. COSY Spectrum of Compound 4.5 (DMSO- <i>d</i> ₆)	165
Figure B.9. HSQC Spectrum of Compound 4.5 (DMSO- <i>d</i> ₆)	165
Figure B.10. HMBC Spectrum of Compound 4.5 (DMSO- <i>d</i> ₆)	166
Figure B.11. ROESY Spectrum of Compound 4.5 (DMSO- <i>d</i> ₆)	166
Figure B.12. ¹ H NMR Spectrum of Compound 4.6 (DMSO- <i>d</i> ₆ , 500MHz)	167
Figure B.13. ¹³ C NMR Spectrum of Compound 4.6 (DMSO- <i>d</i> ₆ , 100MHz)	167
Figure B.14. ¹ H NMR Spectrum of Compound 4.7 (DMSO- <i>d</i> ₆ , 500MHz)	168
Figure B.15. ¹³ C NMR Spectrum of Compound 4.7 (DMSO- <i>d</i> ₆ , 100MHz)	168
Figure B.16. COSY Spectrum of Compound 4.7 (DMSO- <i>d</i> ₆)	169
Figure B.17. HSQC Spectrum of Compound 4.7 (DMSO- <i>d</i> ₆)	169
Figure B.18. HMBC Spectrum of Compound 4.7 (DMSO- <i>d</i> ₆)	170
Figure B.19. ROESY Spectrum of Compound 4.7 (DMSO- <i>d</i> ₆)	170
Figure B.20. CD Spectra of Compounds 4.1-4.3	171

Figure B.21. CD Spectra of Compounds 4.4, 4.6	171
Figure B.22. CD Spectra of Compounds 4.7-4.8	171

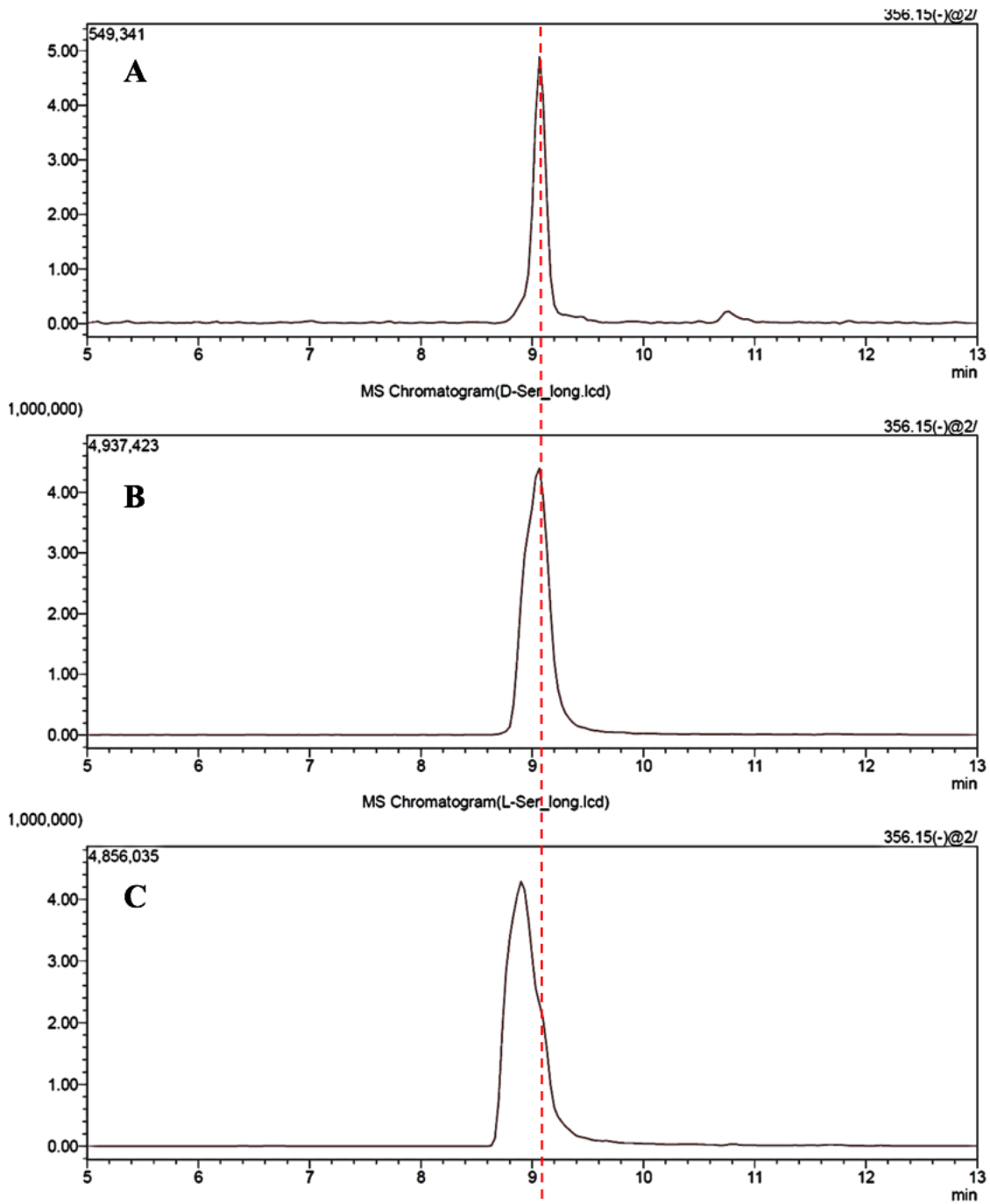


Figure B.1. LC-MS analysis (selected ion at m/z 356.15 under ESI^- mode) for FDAA derivatives of beauversetin-derived hydrolysate (A), and D- (B) and L-Ser (C).

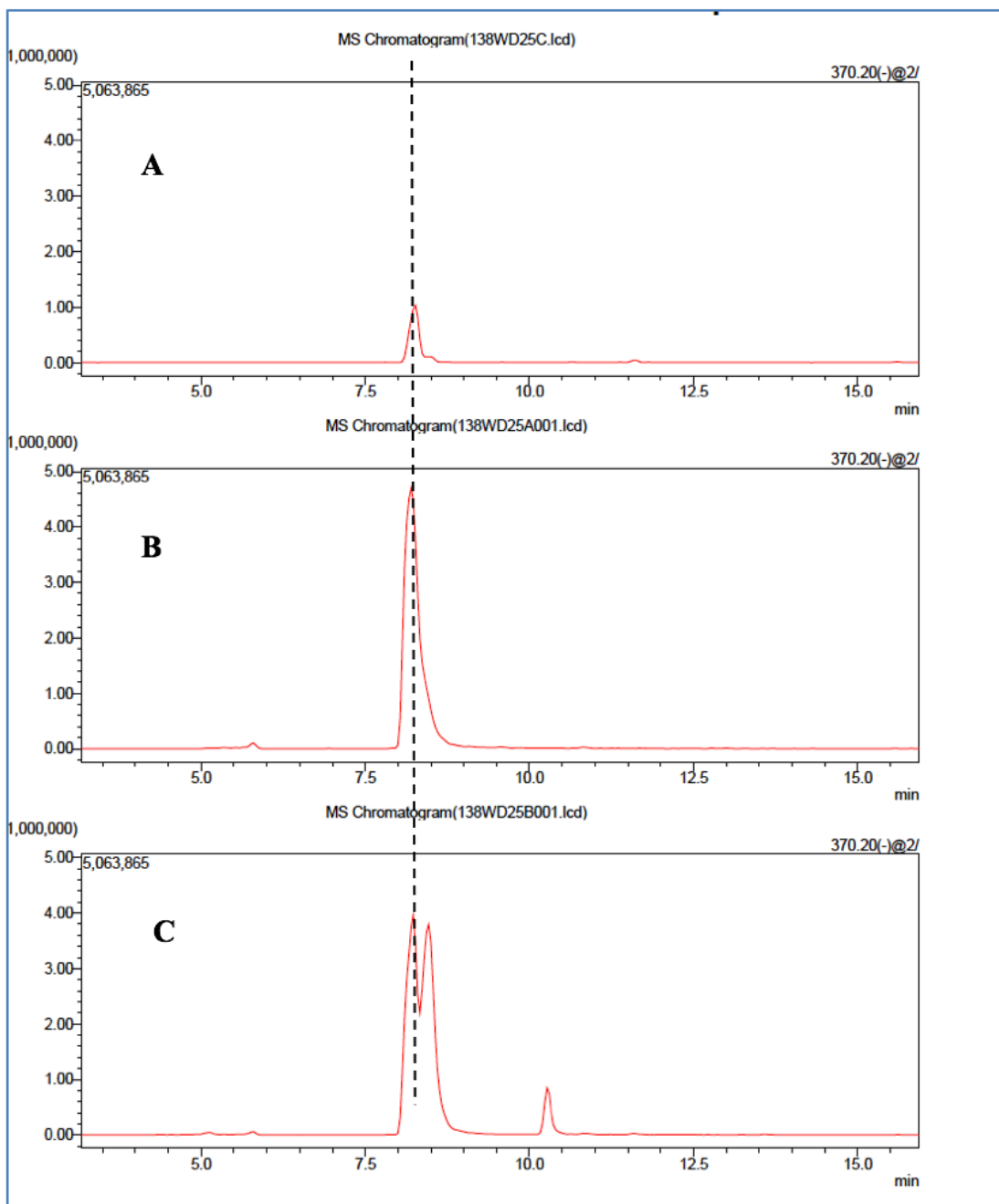


Figure B.2. LC-MS analysis (selected ion at m/z 370.20 under ESI negative mode) for FDAA derivatives of equisetin-derived hydrolysate(A), and L-(B) and L, D-N-methyl serine (C).

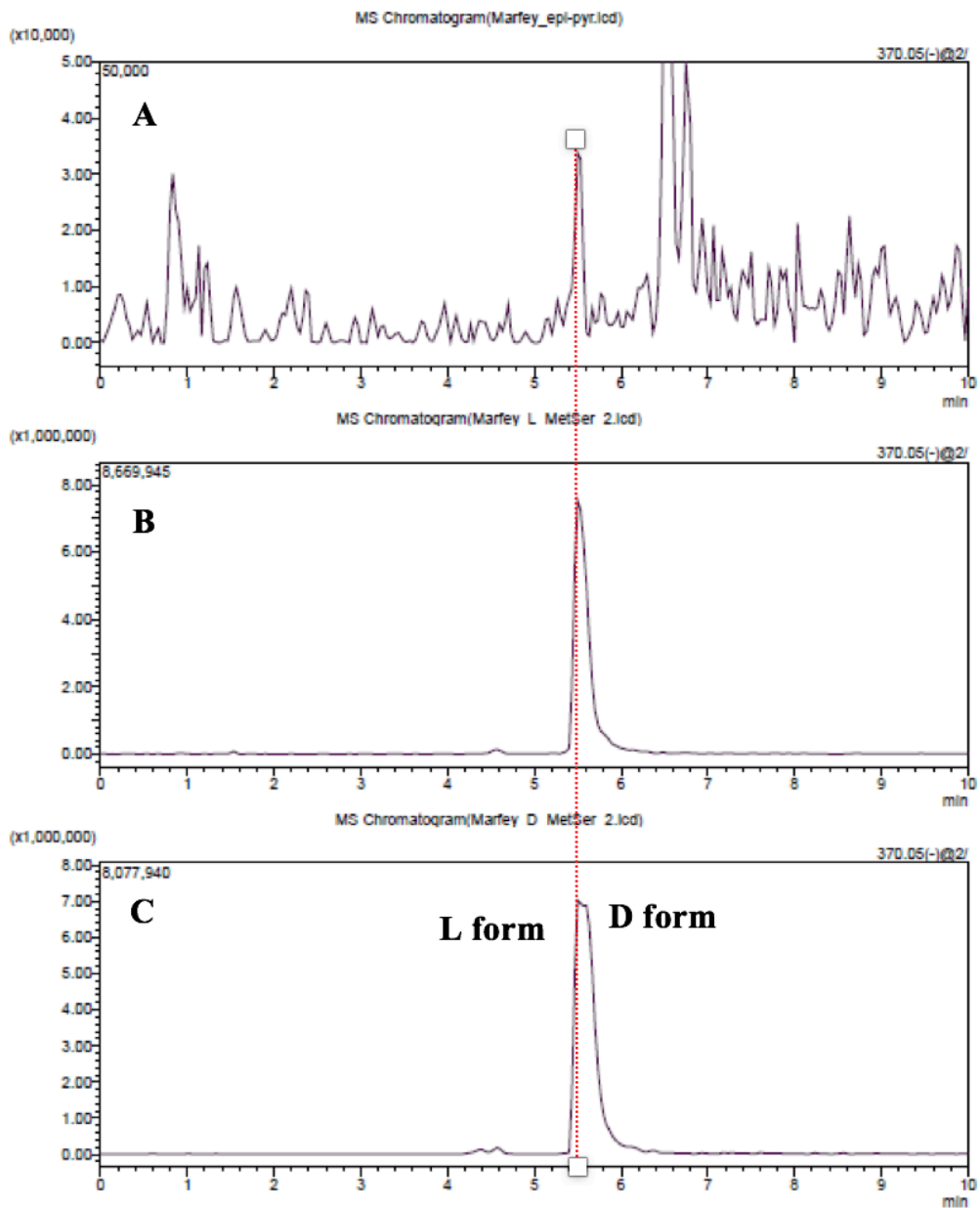


Figure B.3. LC-MS analysis (selected ion at m/z 370.05 under ESI^- mode) for FDAA derivatives of *epi*-pyrrolocin A-derived hydrolysate (A), and L-*N*-met-ser (B) and L, D-*N*-met-ser mixture (C).

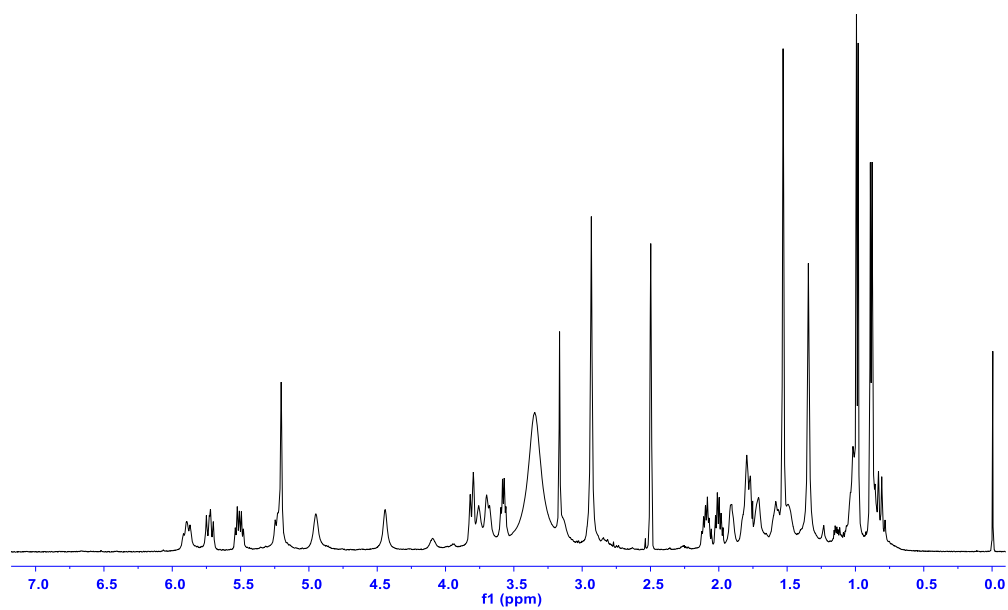


Figure B.4. ^1H NMR Spectrum of Compound 4.4 (DMSO- d_6 , 500MHz)

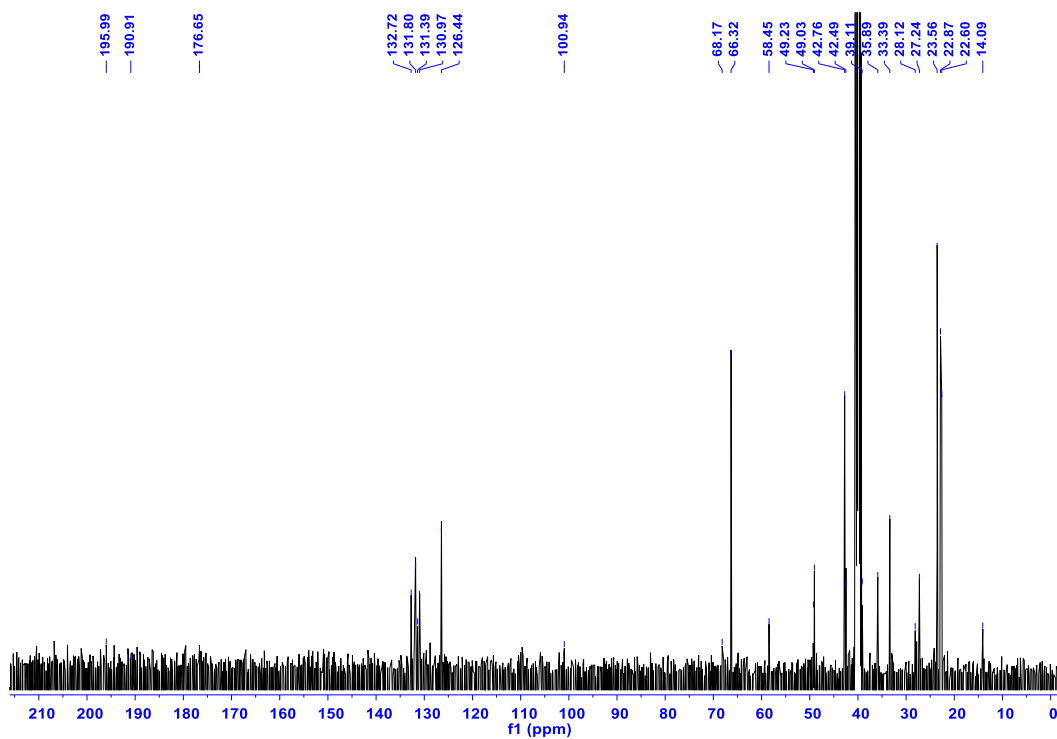


Figure B.5. ^{13}C NMR Spectrum of Compound 4.4 (DMSO- d_6 , 100MHz)

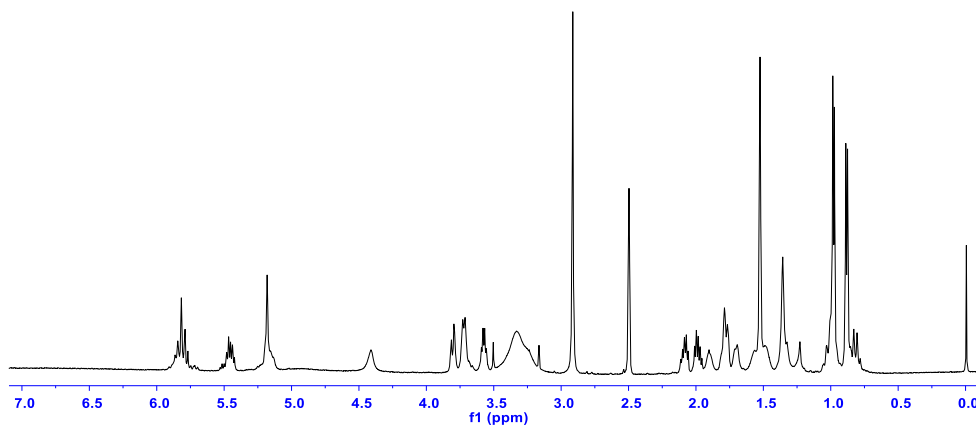


Figure B.6. ^1H NMR Spectrum of Compound **4.5** ($\text{DMSO-}d_6$, 500MHz)

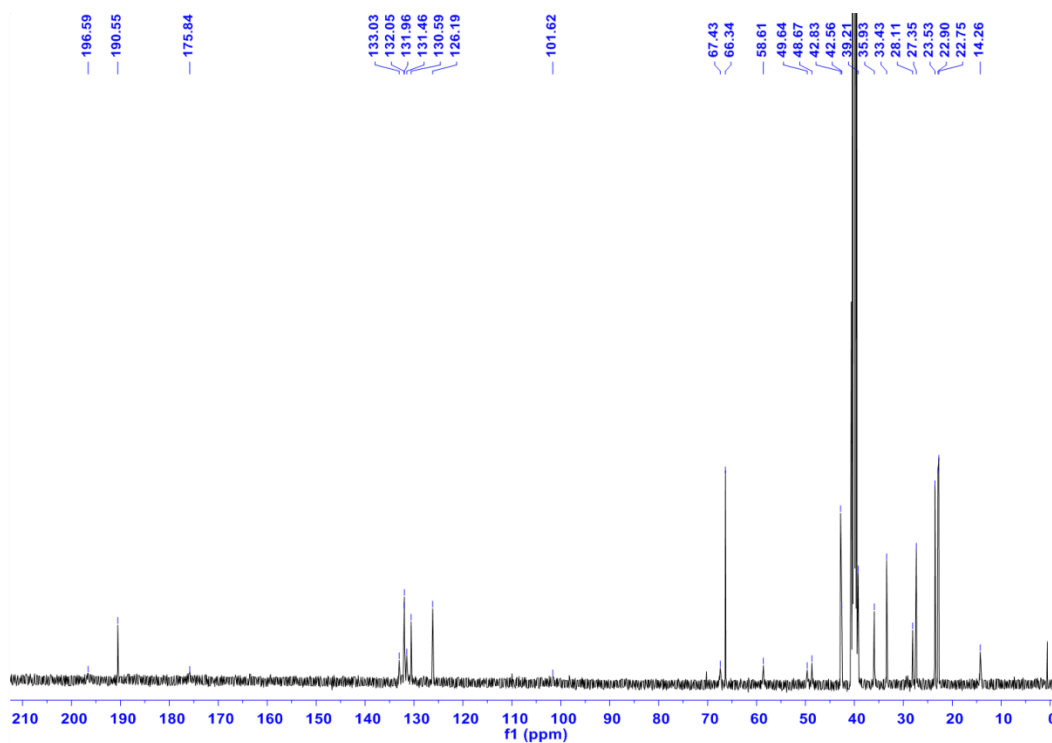


Figure B.7. ^{13}C NMR Spectrum of Compound **4.5** ($\text{DMSO-}d_6$, 100MHz)

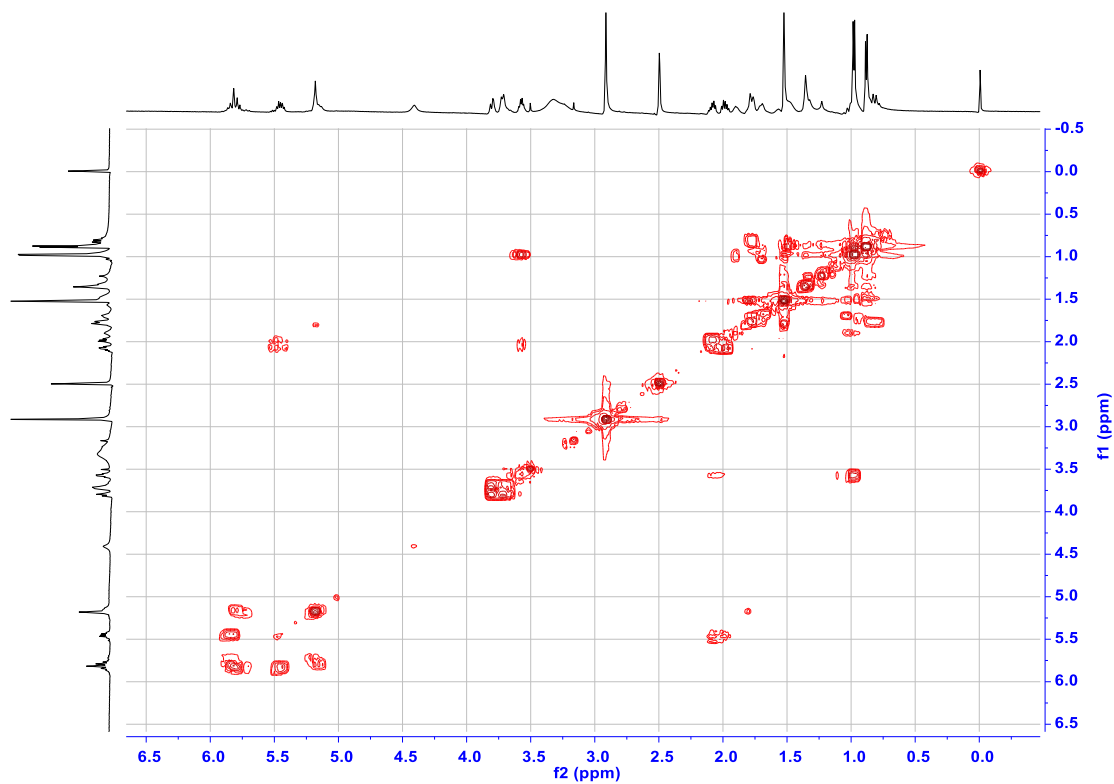


Figure B.8. COSY Spectrum of Compound 4.5 (DMSO-*d*₆)

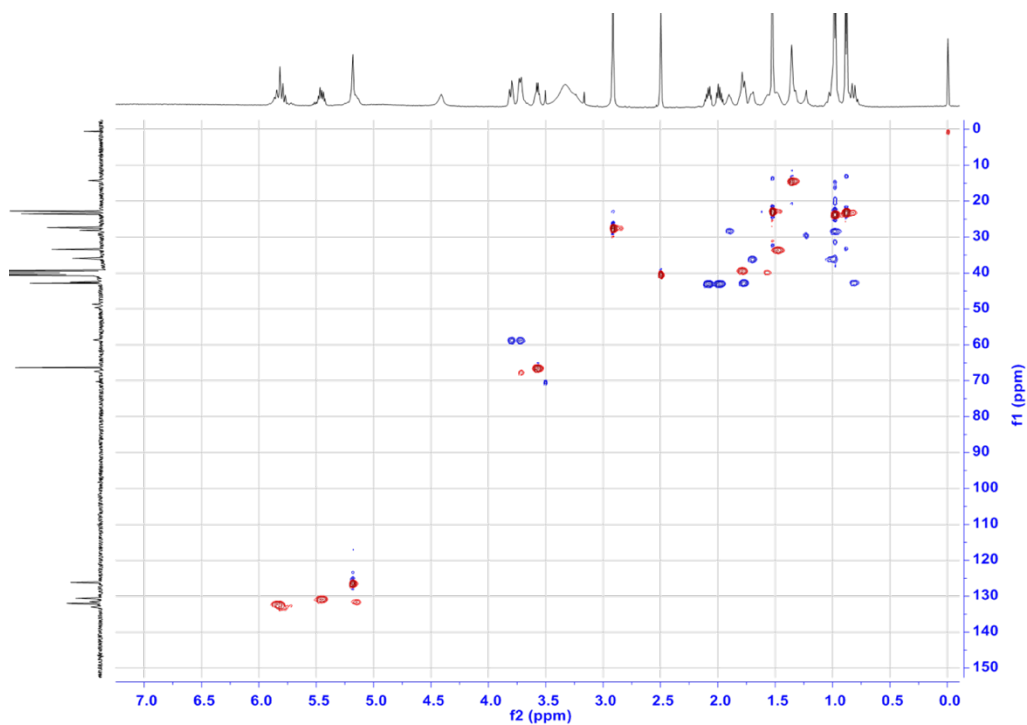


Figure B.9. HSQC Spectrum of Compound 4.5 (DMSO-*d*₆)

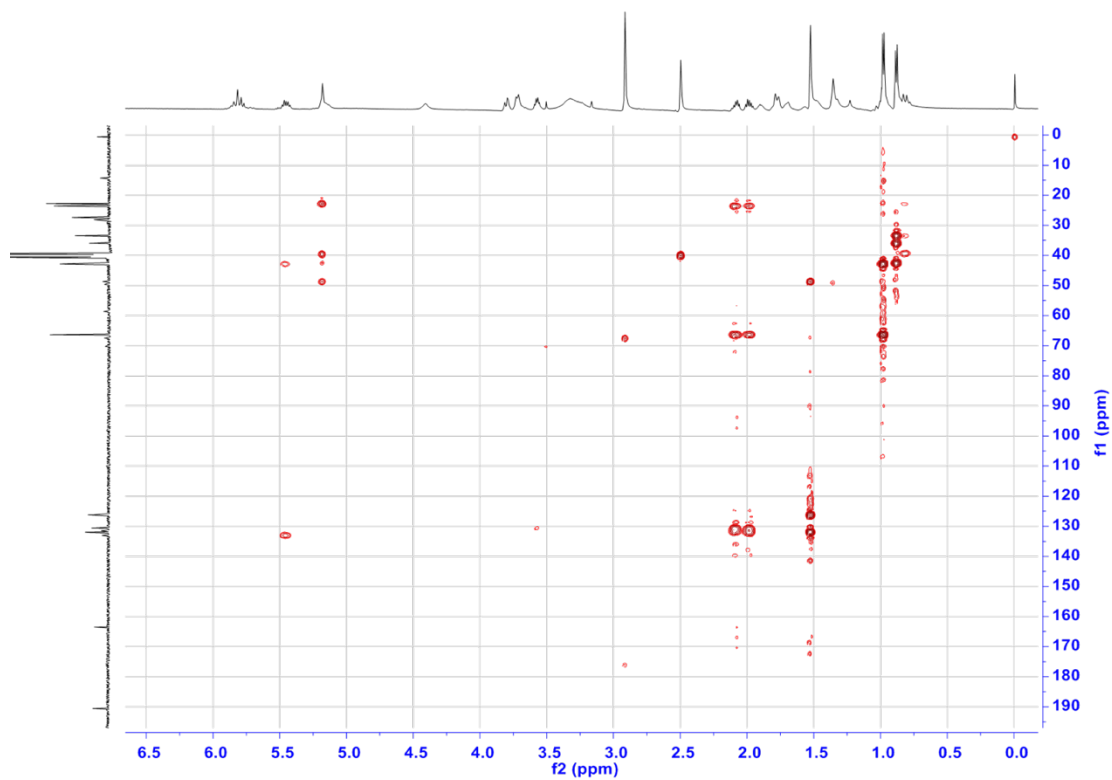


Figure B.10. HMBC Spectrum of Compound 4.5 (DMSO- d_6)

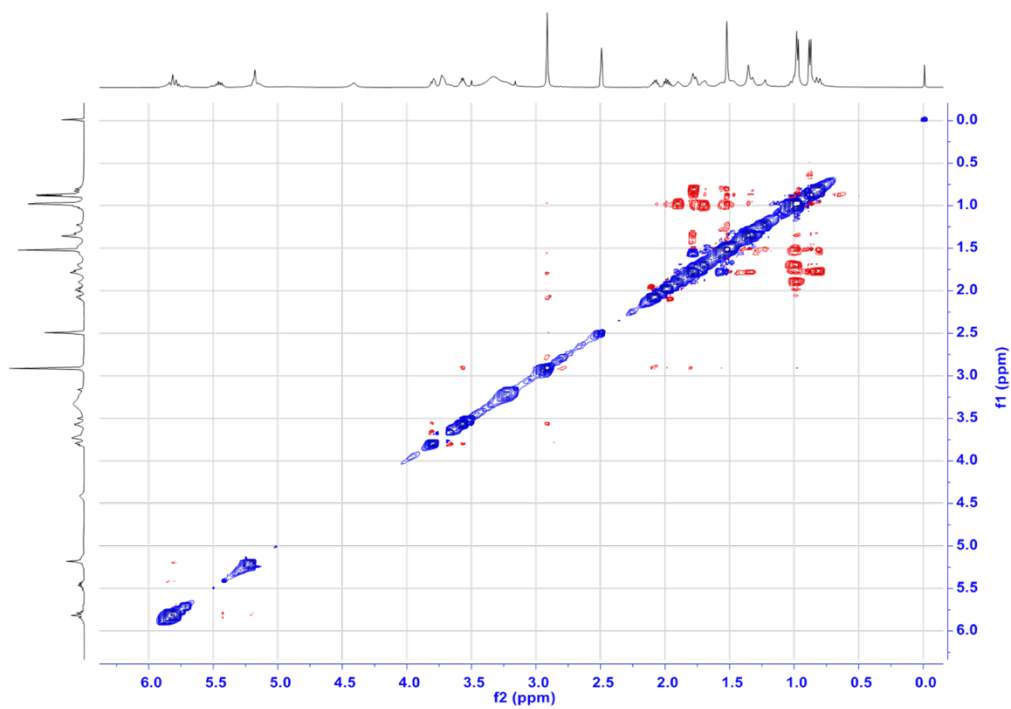


Figure B.11. ROESY Spectrum of Compound 4.5 (DMSO- d_6)

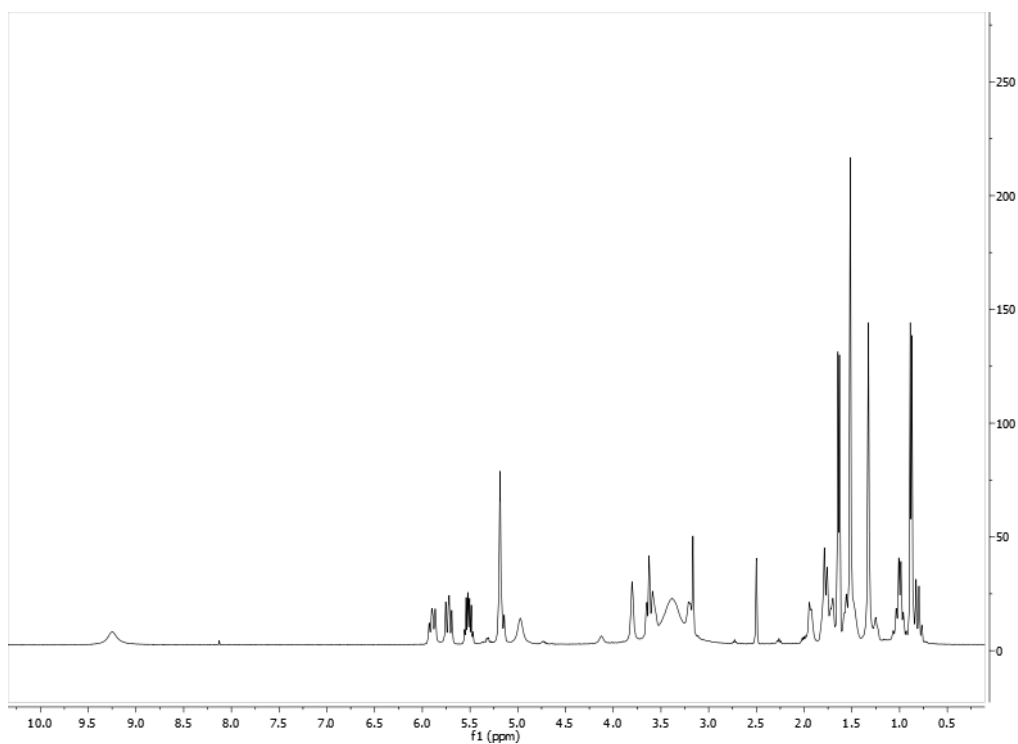


Figure B.12. ^1H NMR Spectrum of Compound **4.6** ($\text{DMSO-}d_6$, 500MHz)

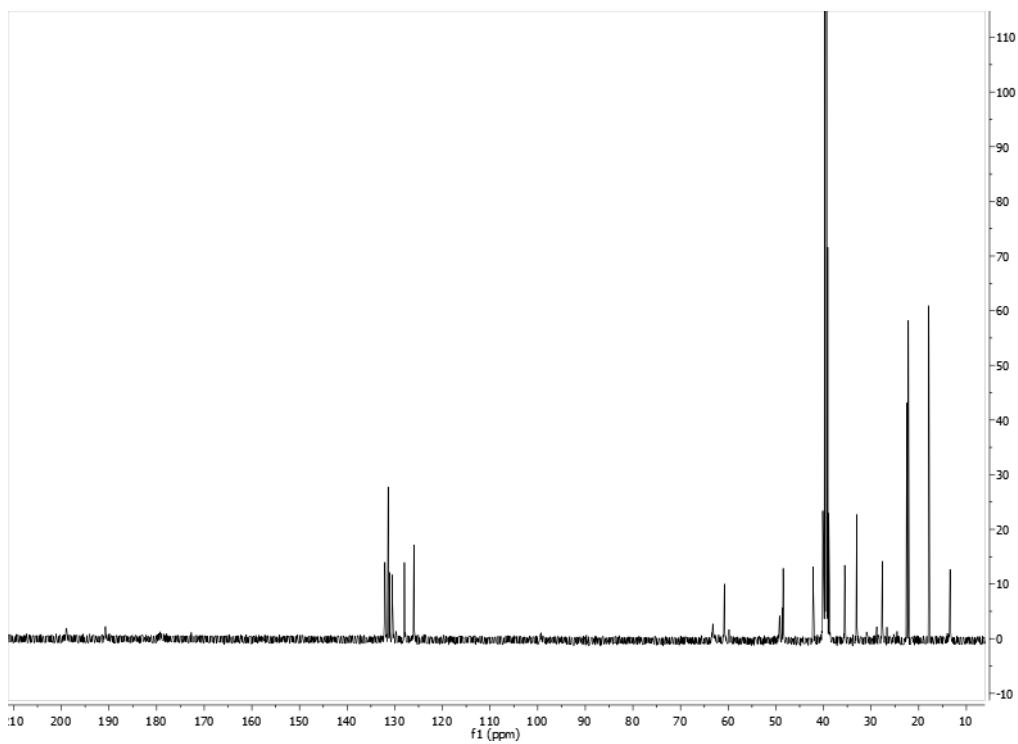


Figure B.13. ^{13}C NMR Spectrum of Compound **4.6** ($\text{DMSO-}d_6$, 100MHz)

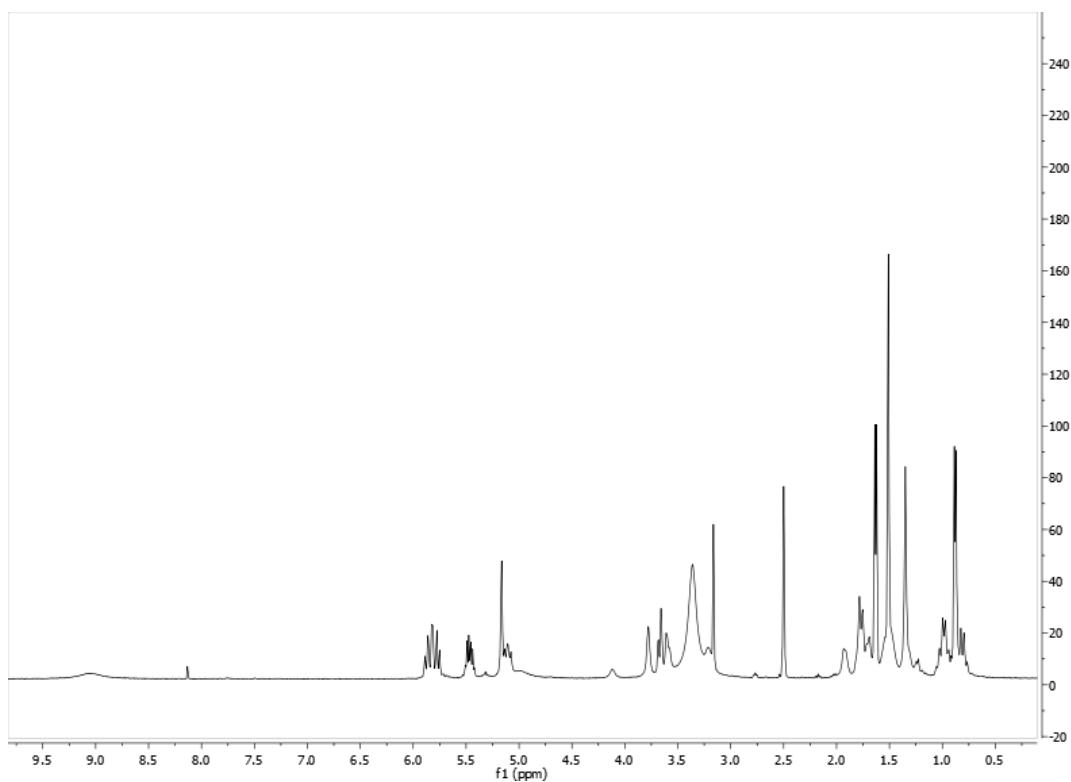


Figure B.14. ^1H NMR Spectrum of Compound 4.7 (DMSO- d_6 , 500MHz)

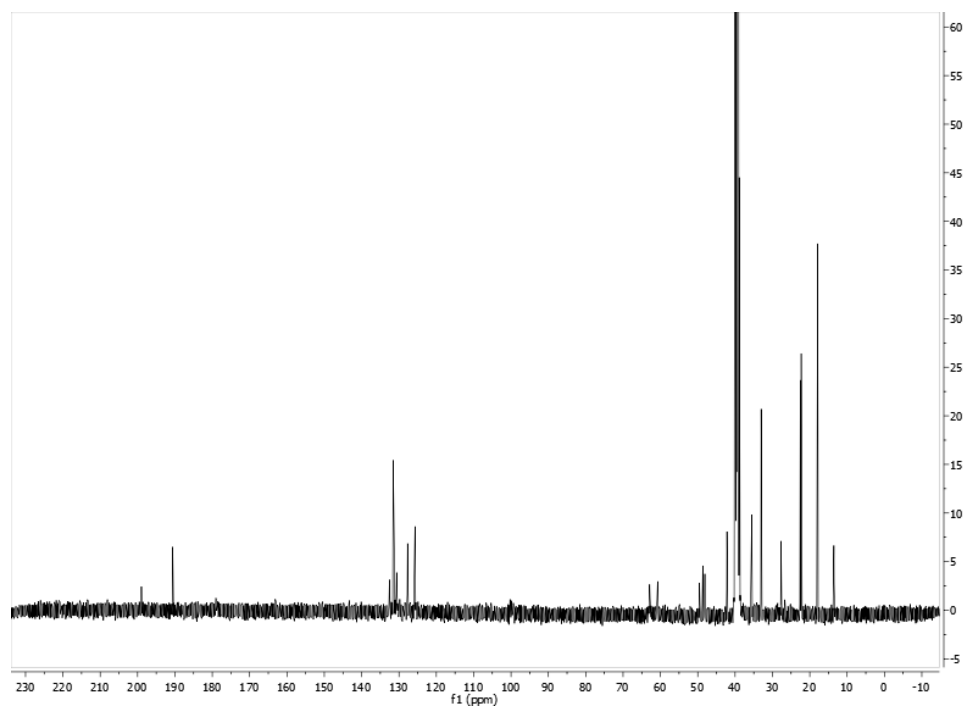


Figure B.15. ^{13}C NMR Spectrum of Compound 4.7 (DMSO- d_6 , 100MHz)

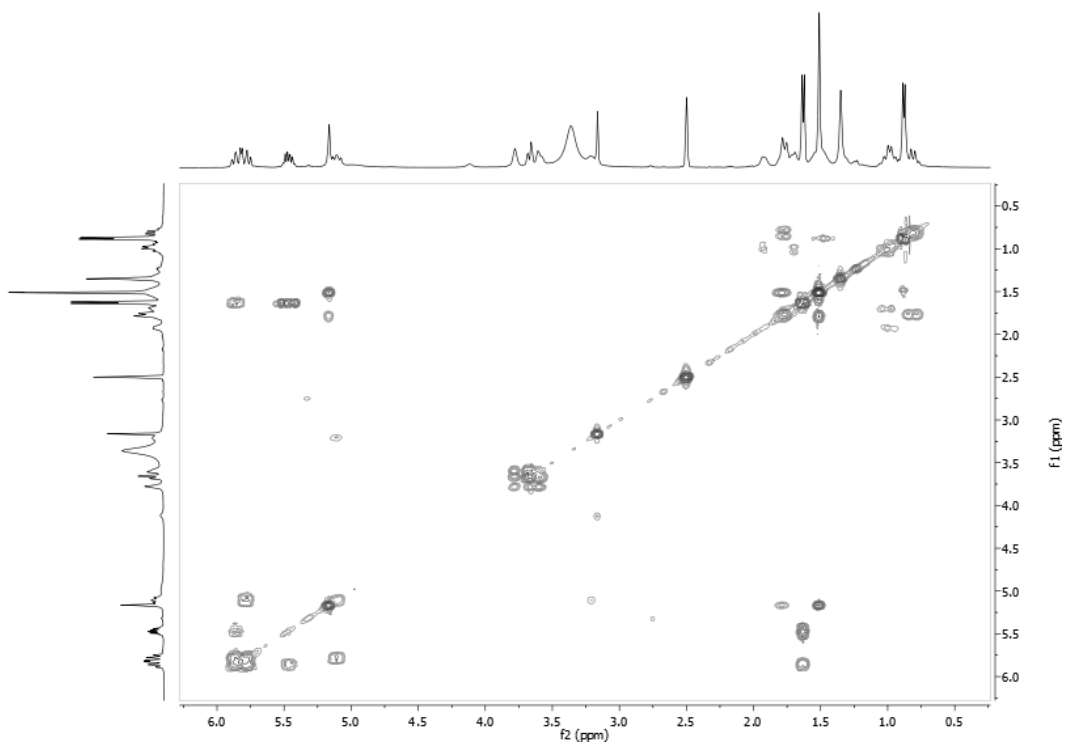


Figure B.16. COSY Spectrum of Compound **4.7** (DMSO- d_6)

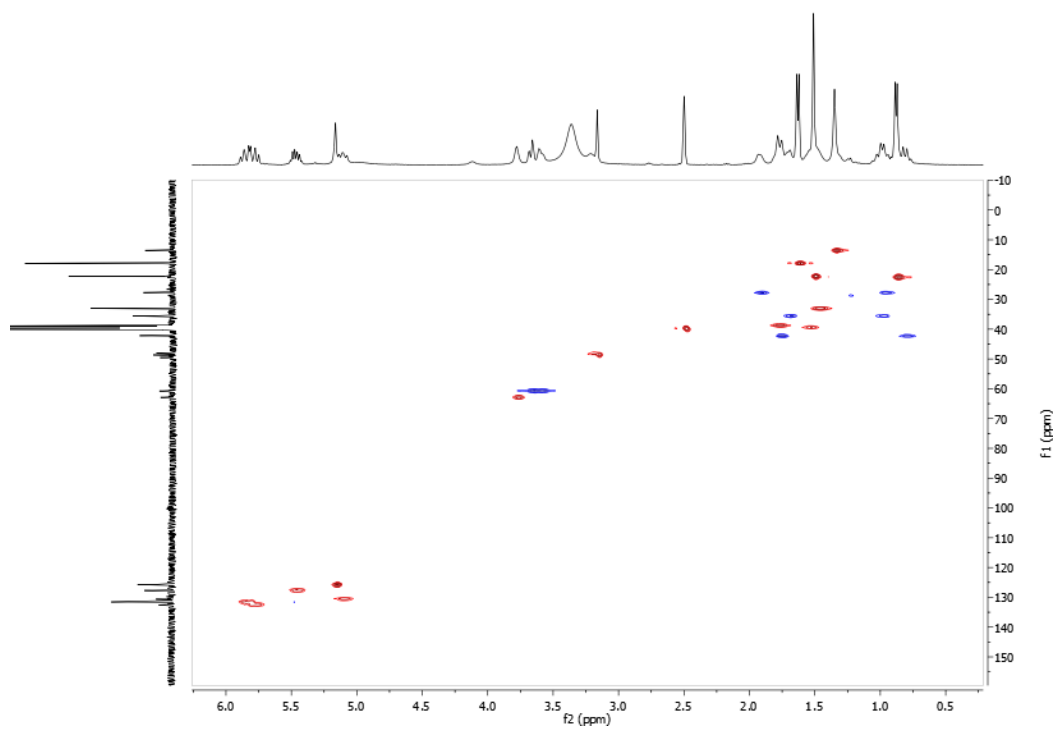


Figure B.17. HSQC Spectrum of Compound **4.7** (DMSO- d_6)

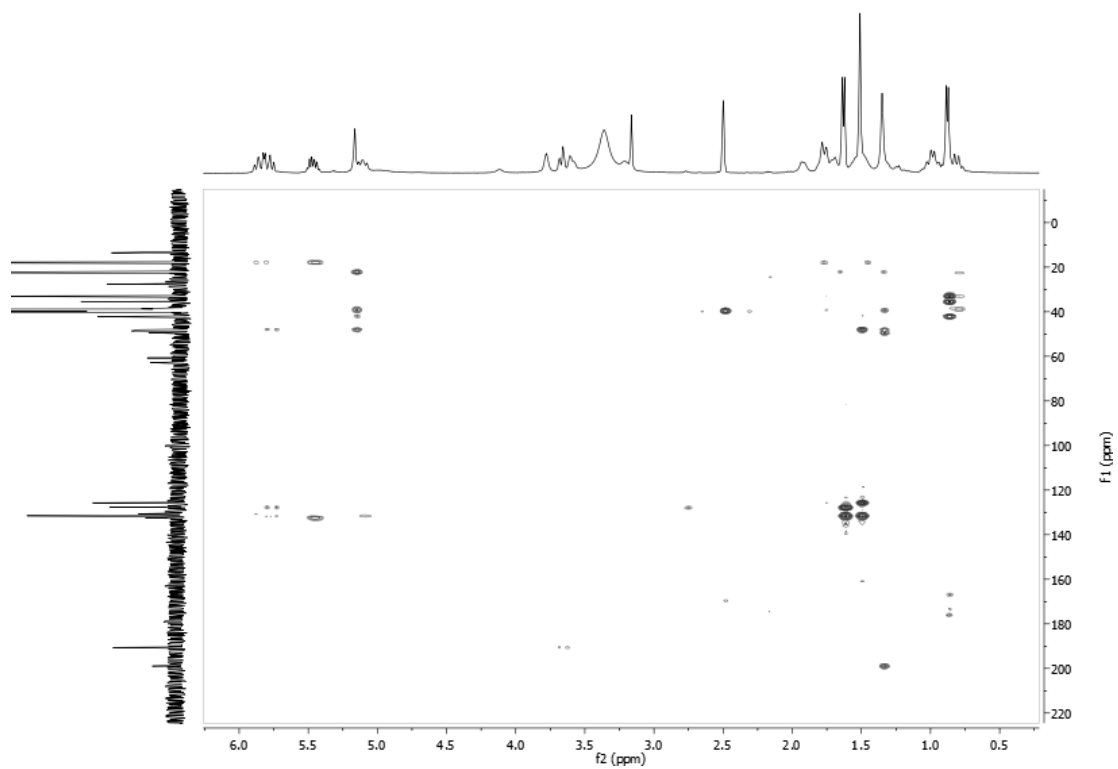


Figure B.18. HMBC Spectrum of Compound **4.7** (DMSO- d_6)

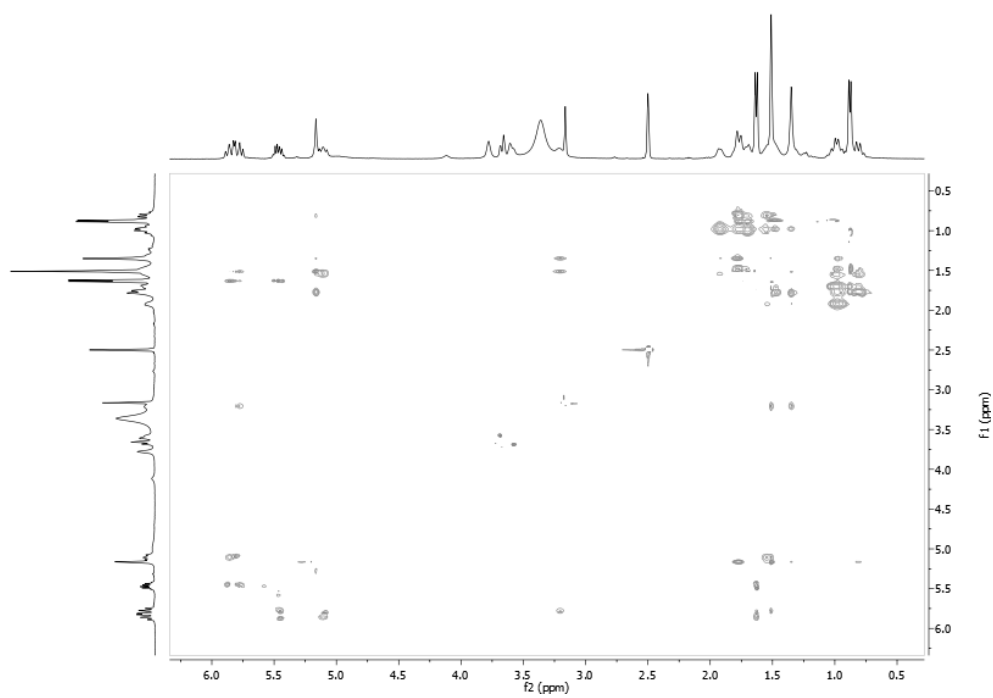


Figure B.19. ROESY Spectrum of Compound **4.7** (DMSO- d_6)

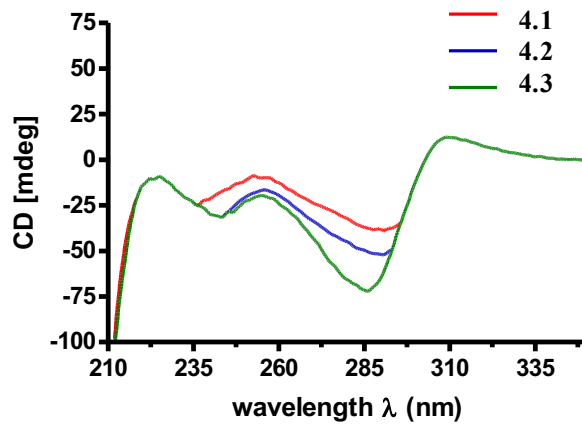


Figure B.20. CD Spectra of Compounds 4.1-4.3.

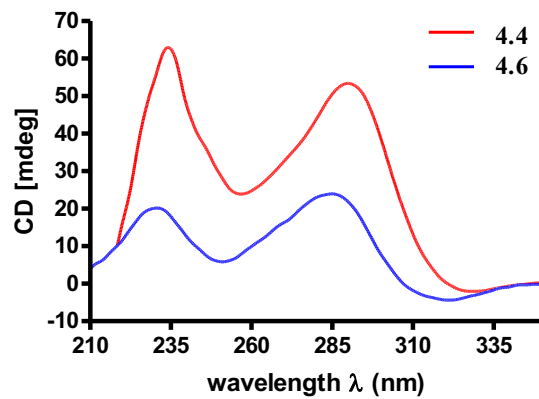


Figure B.21. CD Spectra of Compounds 4.4, 4.6.

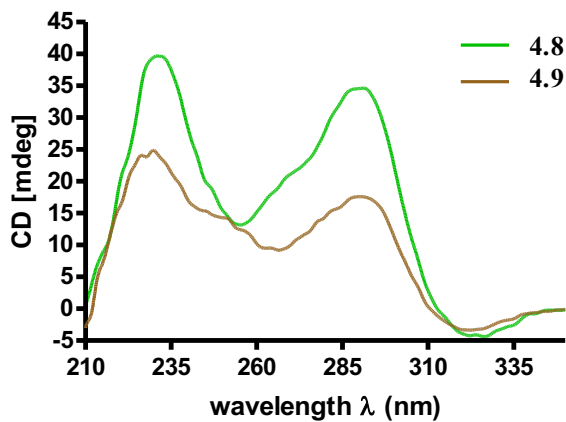


Figure B.22. CD Spectra of Compounds 4.7-4.8.

Appendix C: Supporting Data for Chapter 5

Appendix Table of Contents

Table C1. Identification codes and associated information for the fungal isolate.....	175
Table C2. Dose curve analysis of toxic crude fungal extracts.....	176
Table C3. ROESY correlations of compounds 5.4	177
Table C4. ROESY correlations of compounds 5.5	177
Table C5. ROESY correlations of compounds 5.8	178
Table C6. ROESY correlations of compounds 5.12	178
Table C7. ROESY correlations of compounds 5.13	179
Figure C1. Zebrafish phenotype screen reveals fungal extracts that impaired motility. Frame-by-frame images representing response of zebrafish embryos to external stimulus (represented by black line).....	179
Figure C2. ¹ H-NMR spectrum of compound 5.4 in Acetone- <i>d</i> ₆ (500 MHz).....	180
Figure C3. ¹³ C-NMR spectrum of compound 5.4 in Acetone- <i>d</i> ₆ (100 MHz).....	180
Figure C4. ¹ H- ¹ H COSY spectrum of compound 5.4 in Acetone- <i>d</i> ₆ (500 MHz).....	181
Figure C5. HSQC spectrum of compound 5.4 in Acetone- <i>d</i> ₆ (500 MHz).....	181
Figure C6. HMBC spectrum of compound 5.4 in Acetone- <i>d</i> ₆ (500 MHz).....	182
Figure C7. ROESY spectrum of compound 5.4 in Acetone- <i>d</i> ₆ (500 MHz).....	182
Figure C8. HRESIMS of compound 5.4	183
Figure C9. ¹ H-NMR spectrum of compound 5.5 in CDCl ₃ (500 MHz).....	184
Figure C10. ¹³ C-NMR spectrum of compound 5.5 in CDCl ₃ (100 MHz).....	184
Figure C11. ¹ H- ¹ H COSY spectrum of compound 5.5 in CDCl ₃ (500 MHz).....	185
Figure C12. HSQC spectrum of compound 5.5 in CDCl ₃ (500 MHz).....	185
Figure C13. HMBC spectrum of compound 5.5 in CDCl ₃ (500 MHz).....	186
Figure C14. ¹ H-NMR spectrum of compound 5.5 in DMSO- <i>d</i> ₆ (600 MHz).....	186

Figure C15. ^1H - ^1H COSY spectrum of compound 5.5 in DMSO- d_6 (600 MHz)	187
Figure C16. HSQC spectrum of compound 5.5 in DMSO- d_6 (600 MHz).....	187
Figure C17. HMBC spectrum of compound 5.5 in DMSO- d_6 (600 MHz).....	188
Figure C18. ROESY spectrum of compound 5.5 in DMSO- d_6 (500 MHz)	188
Figure C19. HRESIMS of compound 5.5	189
Figure C20. ^1H -NMR spectrum of compound 5.8 in DMSO- d_6 (500 MHz).....	190
Figure C21. ^{13}C -NMR spectrum of compound 5.8 in DMSO- d_6 (100 MHz).....	190
Figure C22. ^1H - ^1H spectrum of compound 5.8 in DMSO- d_6 (500 MHz)	191
Figure C23. HSQC spectrum of compound 5.8 in DMSO- d_6 (500 MHz).....	191
Figure C24. HMBC spectrum of compound 5.8 in DMSO- d_6 (500 MHz)	192
Figure C25. ROESY spectrum of compound 5.8 in DMSO- d_6 (500 MHz)	192
Figure C26. HRESIMS of compound 5.8	193
Figure C27. ^1H -NMR spectrum of compound 5.12 in DMSO- d_6 (500 MHz).....	194
Figure C28. ^{13}C -NMR spectrum of compound 5.12 in DMSO- d_6 (100 MHz)	194
Figure C29. ^1H - ^1H spectrum of compound 5.12 in DMSO- d_6 (500 MHz)	195
Figure C30. HSQC spectrum of compound 5.12 in DMSO- d_6 (500 MHz)	195
Figure C31. HMBC spectrum of compound 5.12 in DMSO- d_6 (500 MHz).....	196
Figure C32. ROESY spectrum of compound 5.12 in DMSO- d_6 (500 MHz)	196
Figure C33. HRESIMS of compound 5.12	197
Figure C34. ^1H -NMR spectrum of compound 5.13 in DMSO- d_6 (500 MHz).....	198
Figure C35. ^{13}C -NMR spectrum of compound 5.13 in DMSO- d_6 (100 MHz).....	198
Figure C36. ^1H - ^1H spectrum of compound 5.13 in DMSO- d_6 (500 MHz)	199
Figure S37. HSQC spectrum of compound 5.13 in DMSO- d_6 (500 MHz).....	199
Figure C38. HMBC spectrum of compound 5.13 in DMSO- d_6 (500 MHz)	200

Figure C39. ROESY spectrum of compound 5.13 in DMSO- <i>d</i> ₆ (500 MHz)	200
Figure C40. HRESIMS of compound 5.13	201
Figure C41. ¹ H-NMR spectrum of compound 5.14 in Acetone- <i>d</i> ₆ (500 MHz).....	201
Figure C42. ¹³ C-NMR spectrum of compound 5.14 in Acetone- <i>d</i> ₆ (100 MHz).....	202
Figure C43. ¹ H- ¹ H spectrum of compound 5.14 in Acetone- <i>d</i> ₆ (500 MHz).....	203
Figure C44. HSQC spectrum of compound 5.14 in Acetone- <i>d</i> ₆ (500 MHz).....	203
Figure C45. HMBC spectrum of compound 5.14 in Acetone- <i>d</i> ₆ (500 MHz)	204
Figure C46. ROESY spectrum of compound 5.14 in Acetone- <i>d</i> ₆ (500 MHz).....	204
Figure C47. HRESIMS of compound 5.14	205

Table C1. Identification codes and associated information for the fungal isolate

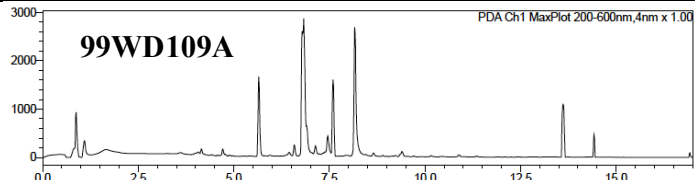
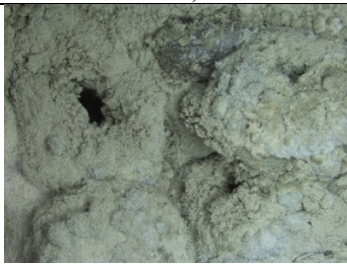
Fungus name used in this report:	<i>Penicillium sp.</i>
Full ID code for the sample from which the fungal isolate was obtained:	10263, soil
SHAREOK link for citizen-science-derived sample (if available):	https://shareok.org/handle/11244/300790
Internal lab sample ID code:	OK0263
Full fungal isolate ID code:	OK0263 PDA-20
Plate number and well for fungal initial extract:	87-B1
First chemistry notebook code assigned to fungal extract and PDA chromatogram of the crude extract:	 <p>LCMS condition: MeCN-H₂O gradient containing 0.1% HCOOH (10:90-100:0 in 15 min)</p>
Pictures of fungal isolate:	
ITS sequence used to assign taxonomy:	<p>GCGGGTGACAAAGCCCCATACGCTCGAGGACCGGAC GCGGTGCCCGCTGCCTTTCGGGCCCGTCCCCCGGA AATCGGAGGACGGGGCCCAACACACAAGCCGGGCTT GAGGGCAGCAATGACGCTCGGACAGGCATGCCCCCC GGAATACCAGGGGGCGCAATGTGCGTTCAAAGACTC GATGATTCACTGAATTTGCAATTCACATTACGTATCG CATTCGCTGCGTTCCTCATCGATGCCGGAACCAAGA GATCCGTTGTTGAAAGTTTTAAATAATTTATATTTTC ACTCAGACTTCAATCTTCAGACAGAGTTCGAGGGTGT CTTCGGCGGGCGCGGGCCCCGGGGCGTGAGCCCCC GGCGGCCAGTTAAGGCGGGCCCCGCCGAAGCAACAAG GTAAAATAAACACGGGTGCGGAGGTTGGACCCAGAG GGCCCTCACTCGGTAATGATCCTTCCGCAGGTTACC TACGGAAACCTTGTTACGACTTTTACTTCC</p>
GenBank accession number:	MK722362
Notes on the taxonomic affiliation of the fungal isolate:	Multiple <i>Penicillium</i> species all at 98.90% identity, 100% query cover, cannot assign species level identification, BLAST date April 1 2019

Table C2. Dose curve analysis of toxic crude fungal extracts.

Sample ID	Phenotype Observed ^a	Dose, μg/mL ^b
P86-B12	Edema	0.1
P86-C4	Misshapen tail	1
P86-C6	Misshapen tail, necrosis	2
P86-D7	Misshapen tail, necrosis	1
P86-D10	Edema, necrosis, enlarged hindbrain	0.2
P86-E9	Hemorrhage	0.2
P86-F1	Edema, misshapen tail, necrosis, lack of blood circulation	0.1
P87-A3	Edema	1
P87-A5	Misshapen tail	2
P87-A7	Growth arrest, necrosis	1
P87-A8	N	-
P87-A9	Necrosis	0.1
P87-A11	N	-
P87-A12	N	-
P87-B2	N	-
P87-B5	N	-
P87-B8	Misshapen tail and body	1
P87-B10	N	-
P87-B12	N	-
P87-C2	N	-
P87-C8	N	-
P87-C9	Hemorrhage	0.1
P87-C10	N	-
P87-D8	N	-
P87-E8	N	-
P87-F12	N	-
P87-H6	Hemorrhage	2
P87-H8	N	-
GL6-A8	N	-
GL6-B8	N	-
GL6-B12	N	-
GL6-F9	Small embryo	10
GL6-F10	Loss of pigmentation, impaired motility	2
GL7-H8	N	-

^aN- no phenotype observed at all concentrations tested.
^bDose when phenotype was initially observed.

Table C3. ROESY correlations of compounds **5.4**.

Proton	ROESY correlations
H-12 (δ_{H} 2.71)	H-25 (δ_{H} 1.44), H-26 (δ_{H} 1.19)
H-12 (δ_{H} 3.14)	OH-13 (δ_{H} 6.72), H-19 (δ_{H} 4.91)
OH-13 (δ_{H} 6.72)	H-12 (δ_{H} 3.14), H-15 (δ_{H} 2.38), H-19 (δ_{H} 4.91), H-23 (δ_{H} 1.10)
H-15 (δ_{H} 2.38)	OH-13 (δ_{H} 6.72), OH-17 (δ_{H} 6.81)
H-16 (δ_{H} 1.73)	H-23 (δ_{H} 1.10)
H-16 (δ_{H} 1.94)	H-24 (δ_{H} 1.04), H-25 (δ_{H} 1.44), H-26 (δ_{H} 1.19)
OH-17 (δ_{H} 6.81)	H-15 (δ_{H} 2.38), H-19 (δ_{H} 4.91), H-23 (δ_{H} 1.10)
H-19 (δ_{H} 4.91)	H-12 (δ_{H} 3.14), OH-13 (δ_{H} 6.72), OH-17 (δ_{H} 6.81), OH-21 (δ_{H} 5.44)
OH-19 (δ_{H} 3.63)	H-12 (δ_{H} 3.14), H-26 (δ_{H} 1.19)
H-20 (δ_{H} 2.16)	H-24 (δ_{H} 1.04), H-26 (δ_{H} 1.19), OH-19 (δ_{H} 3.63)
H-20 (δ_{H} 2.05)	OH-19 (δ_{H} 3.63)
H-21 (δ_{H} 3.66)	H-23 (δ_{H} 1.10), H-24 (δ_{H} 1.04), H-20 (δ_{H} 2.05, δ_{H} 2.16)
OH-21 (δ_{H} 5.44)	H-23 (δ_{H} 1.10), H-19 (δ_{H} 4.91)

Table C4. ROESY correlations of compounds **5.5**.

Proton	ROESY correlations
H-12 (δ_{H} 2.19)	H-19 (δ_{H} 1.14), OH-13 (δ_{H} 6.66)
H-12 (δ_{H} 2.60)	H-25 (δ_{H} 1.34), H-26 (δ_{H} 1.07)
OH-13 (δ_{H} 6.66)	H-12 (δ_{H} 2.19), H-15 (δ_{H} 2.28), H-19 (δ_{H} 2.11), H-23 (δ_{H} 0.91)
H-15 (δ_{H} 1.57)	H-25 (δ_{H} 1.37)
H-15 (δ_{H} 2.28)	OH-13 (δ_{H} 6.66), OH-17 (δ_{H} 6.08)
H-16 (δ_{H} 1.61)	H-23 (δ_{H} 0.91)
H-16 (δ_{H} 1.89)	H-24 (δ_{H} 0.84), H-25 (δ_{H} 1.34), H-26 (δ_{H} 1.07)
OH-17 (δ_{H} 6.08)	H-15 (δ_{H} 2.28), H-16 (δ_{H} 1.61), H-19 (δ_{H} 2.11), H-23 (δ_{H} 0.91)
H-19 (δ_{H} 1.14)	H-26 (δ_{H} 1.07)
H-19 (δ_{H} 2.11)	H-21 (δ_{H} 3.72), OH-17 (δ_{H} 6.08)
H-21 (δ_{H} 3.72)	H-19 (δ_{H} 2.11), H-23 (δ_{H} 0.91)
OH-21 (δ_{H} 4.19)	H-23 (δ_{H} 0.91)

Table C5. ROESY correlations of compounds **5.8**.

Proton	ROESY correlations
H-12 (δ_{H} 2.65)	H-25 (δ_{H} 1.38), H-26 (δ_{H} 1.10)
H-12 (δ_{H} 2.95)	H-19 (δ_{H} 4.74)
OH-13 (δ_{H} 6.63)	H-19 (δ_{H} 4.74)
H-15 (δ_{H} 1.63)	H-24 (0.96), H-25 (δ_{H} 1.38)
H-15 (δ_{H} 2.23)	OH-17 (δ_{H} 6.46)
H-16 (δ_{H} 1.63)	H-23 (δ_{H} 1.10)
H-16 (δ_{H} 1.96)	H-25 (δ_{H} 1.38), H-26 (δ_{H} 1.10)
OH-17 (δ_{H} 6.46)	H-15 (δ_{H} 2.23), H-19 (δ_{H} 4.74)
H-19 (δ_{H} 4.74)	H-23 (δ_{H} 1.10), H-12 (δ_{H} 2.95), OH-13 (δ_{H} 6.63), OH-17 (δ_{H} 6.46)
OH-19 (δ_{H} 5.05)	H-26 (δ_{H} 1.10)
H-20 (δ_{H} 2.54)	H-23 (δ_{H} 1.10)
H-20 (δ_{H} 2.74)	H-24 (δ_{H} 0.91)

Table C6. ROESY correlations of compounds **5.12**.

Proton	ROESY correlations
H-12 (δ_{H} 2.72)	H-25 (δ_{H} 1.37), H-26 (δ_{H} 1.24)
H-12 (δ_{H} 3.39)	OH-13 (δ_{H} 6.44)
OH-13 (δ_{H} 6.44)	H-12 (δ_{H} 3.39), H-15 (δ_{H} 2.22)
H-15 (δ_{H} 1.60)	H-25 (δ_{H} 1.37)
H-15 (δ_{H} 2.22)	OH-13 (δ_{H} 6.44), OH-17 (δ_{H} 6.73)
H-16 (δ_{H} 1.74)	H-23 (δ_{H} 0.94), H-24 (δ_{H} 1.11), OH-17 (δ_{H} 6.73)
H-16 (δ_{H} 1.92)	H-24 (δ_{H} 1.11), H-25 (δ_{H} 1.37), H-26 (δ_{H} 1.24)
OH-17 (δ_{H} 6.73)	H-15 (δ_{H} 2.22), H-16 (δ_{H} 1.74), H-23 (δ_{H} 0.94)
H-20 (δ_{H} 2.65)	H-21 (δ_{H} 3.94), H-24 (δ_{H} 1.11), H-26 (δ_{H} 1.24)
H-20 (δ_{H} 2.79)	H-23 (δ_{H} 0.94),
H-21 (δ_{H} 3.94)	H-23 (δ_{H} 0.94), H-24 (δ_{H} 1.11), H-26 (δ_{H} 1.24)
OH-21 (δ_{H} 5.10)	H-23 (δ_{H} 0.94)

Table C7. ROESY correlations of compounds **5.13**.

Proton	ROESY correlations
H-12 (δ_H 2.31)	H-25 (δ_H 1.30), H-26 (δ_H 1.10)
H-12 (δ_H 2.67)	H-13 (δ_H 1.78)
H-13 (δ_H 1.78)	H-12 (δ_H 2.67)
H-15 (δ_H 2.11)	H-25 (δ_H 1.30)
H-16 (δ_H 1.62)	H-24 (δ_H 1.02), H-25 (δ_H 1.30), H-26 (δ_H 1.10)
H-16 (δ_H 1.74)	H-23 (δ_H 1.09)
H-17 (δ_H 1.86)	H-23 (δ_H 1.09)

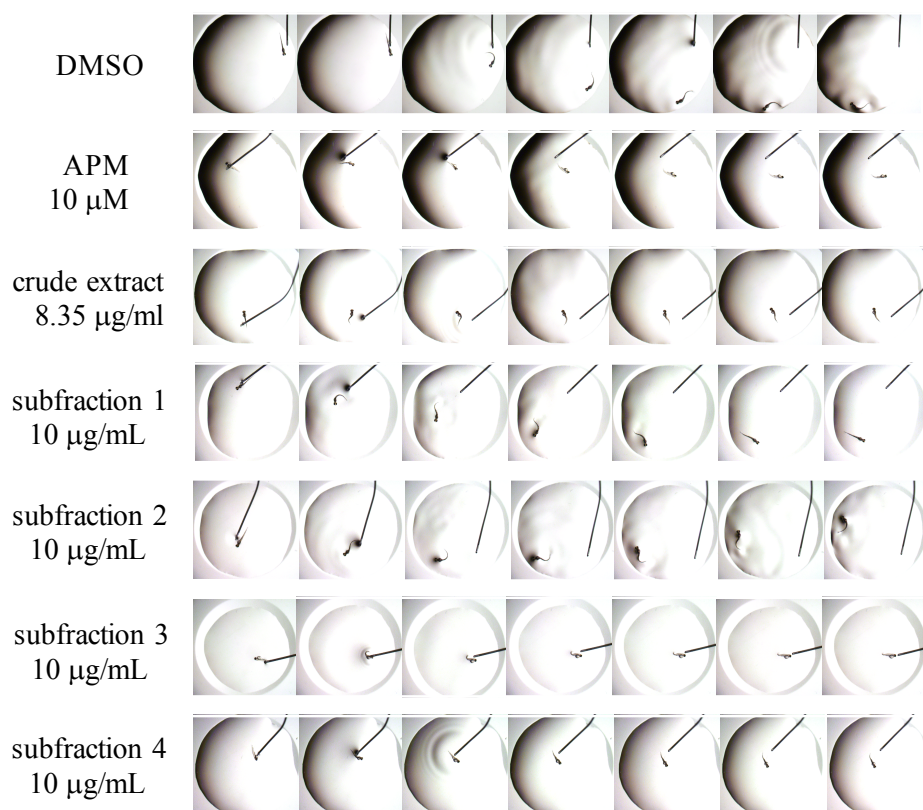


Figure C1. Zebrafish phenotype screen reveals fungal extracts that impaired motility. Frame-by-frame images representing response of zebrafish embryos to external stimulus (represented by black line).

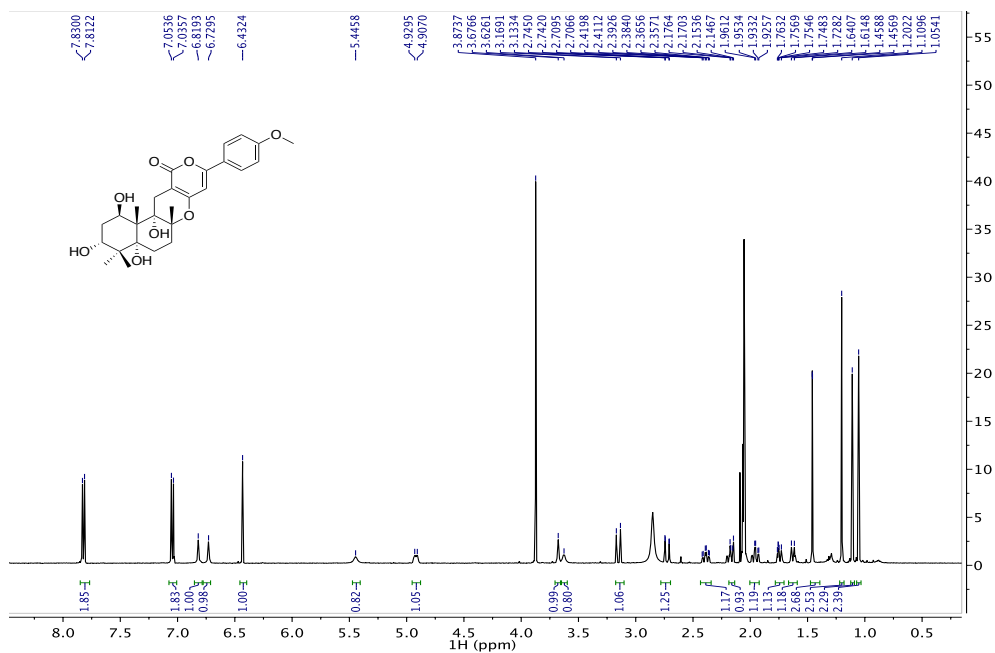


Figure C2. $^1\text{H-NMR}$ spectrum of compound 5.4 in Acetone- d_6 (500 MHz).

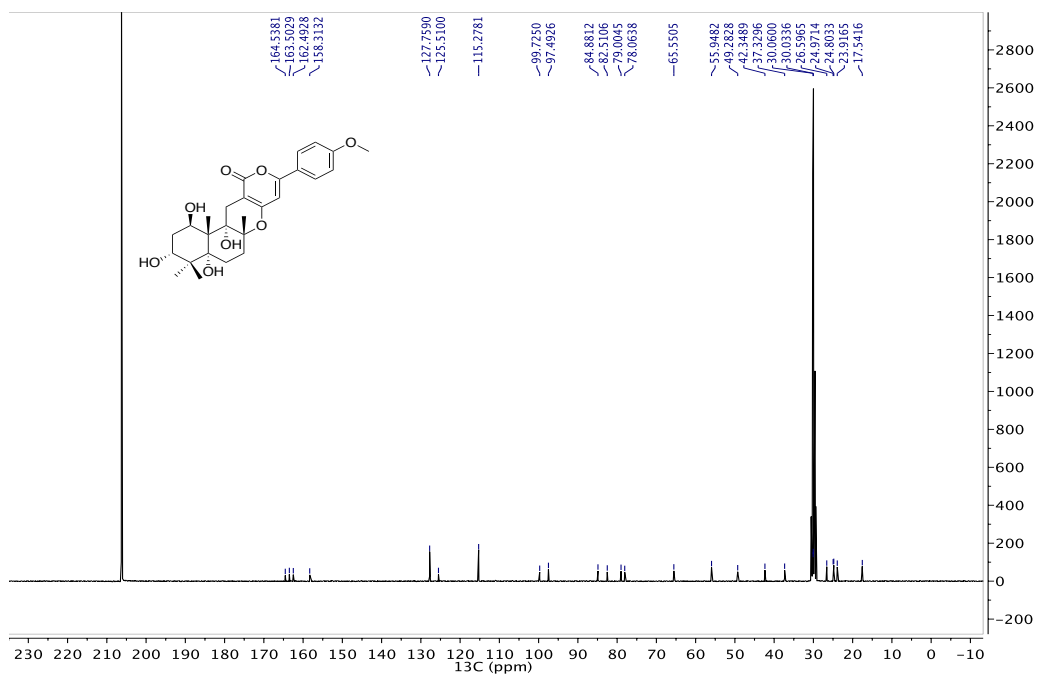


Figure C3. $^{13}\text{C-NMR}$ spectrum of compound 5.4 in Acetone- d_6 (100 MHz).

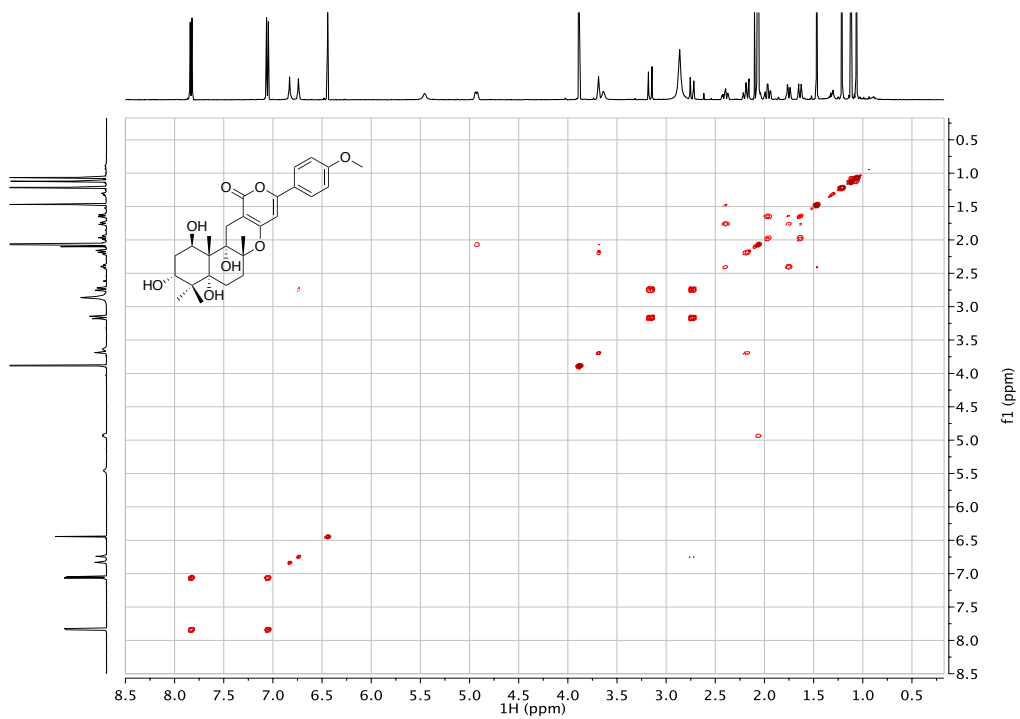


Figure C4. ^1H - ^1H COSY spectrum of compound **5.4** in Acetone- d_6 (500 MHz).

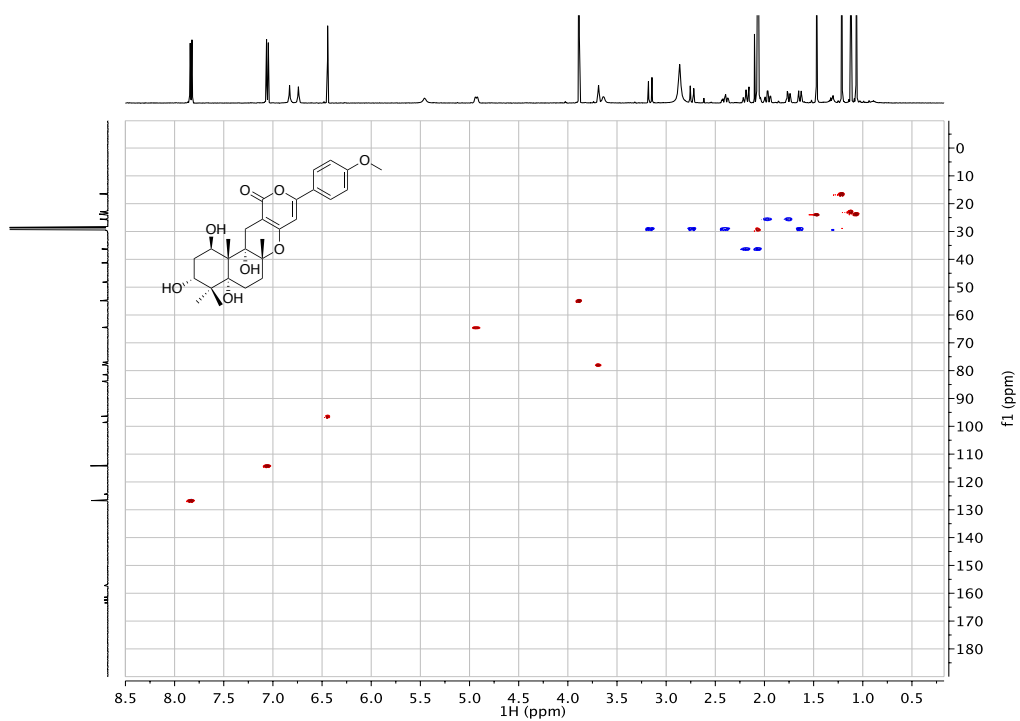


Figure C5. HSQC spectrum of compound **5.4** in Acetone- d_6 (500 MHz).

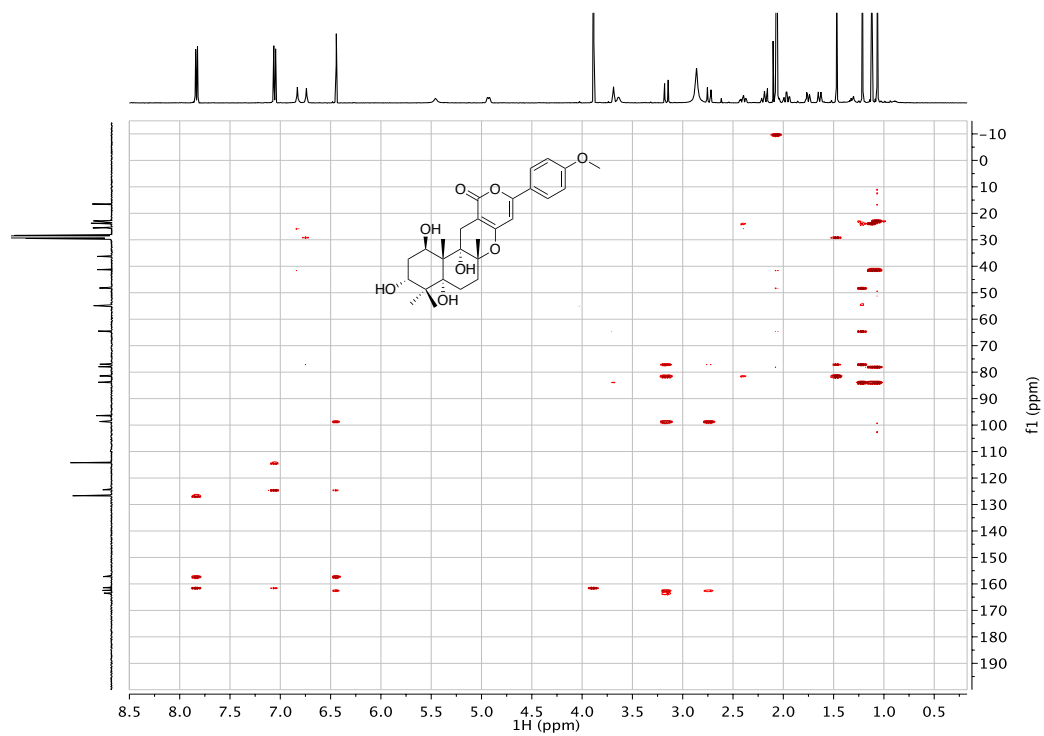


Figure C6. HMBC spectrum of compound **5.4** in Acetone-*d*₆ (500 MHz).

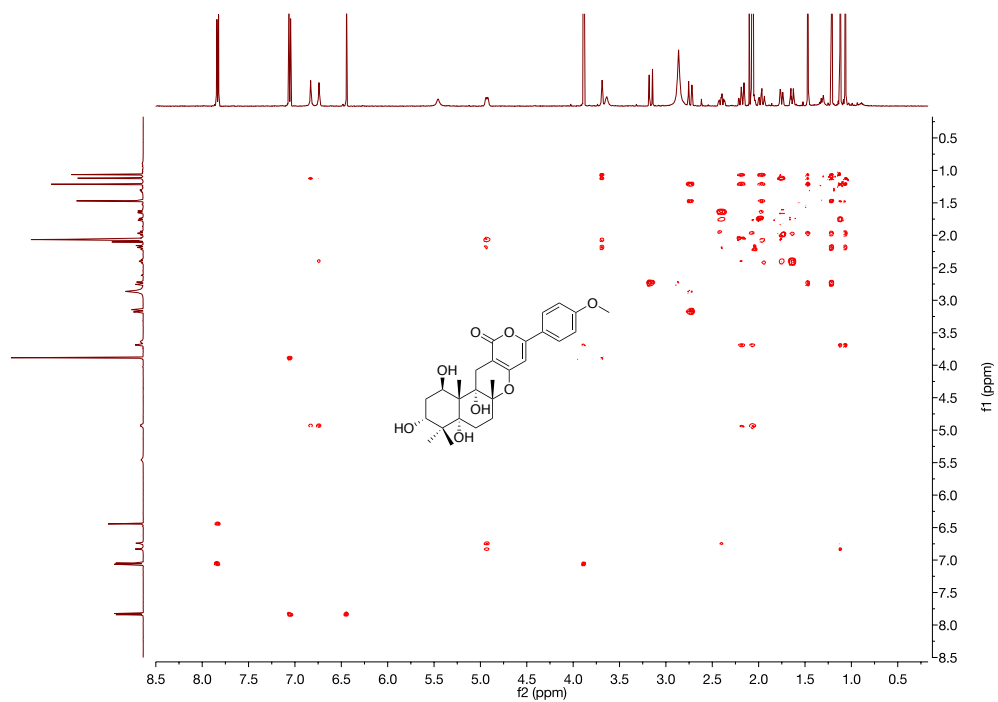


Figure C7. ROESY spectrum of compound **5.4** in Acetone-*d*₆ (500 MHz).

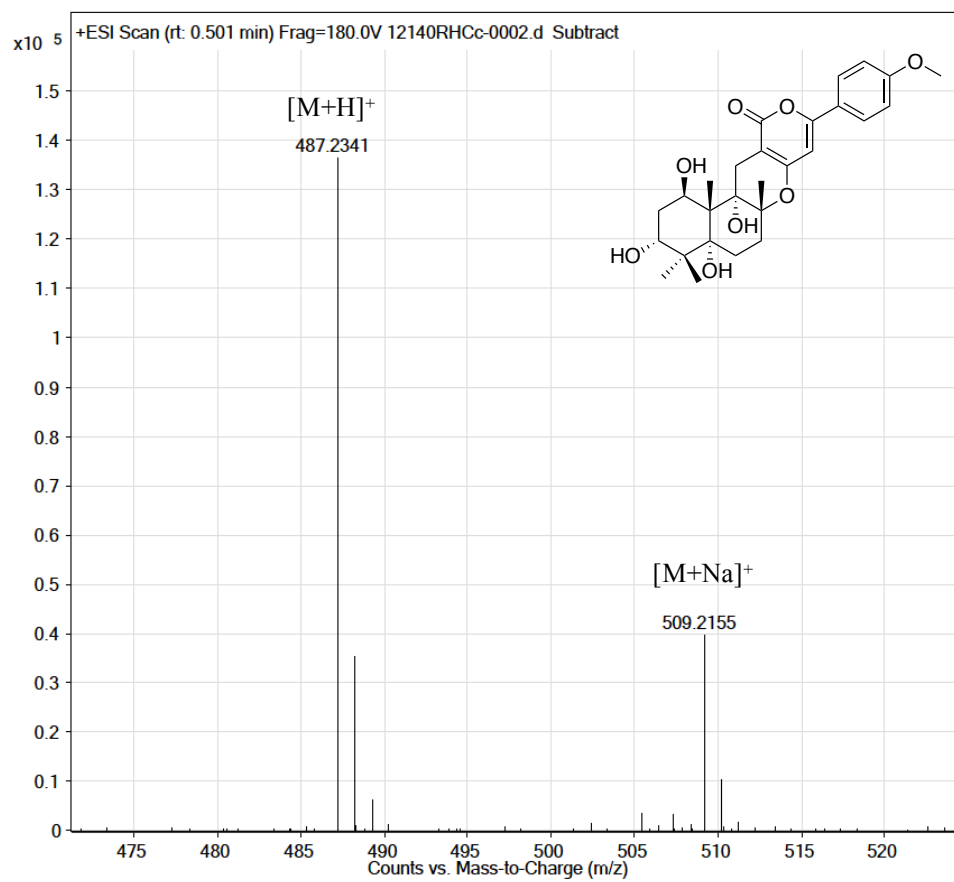


Figure C8. HRESIMS of compound **5.4**.

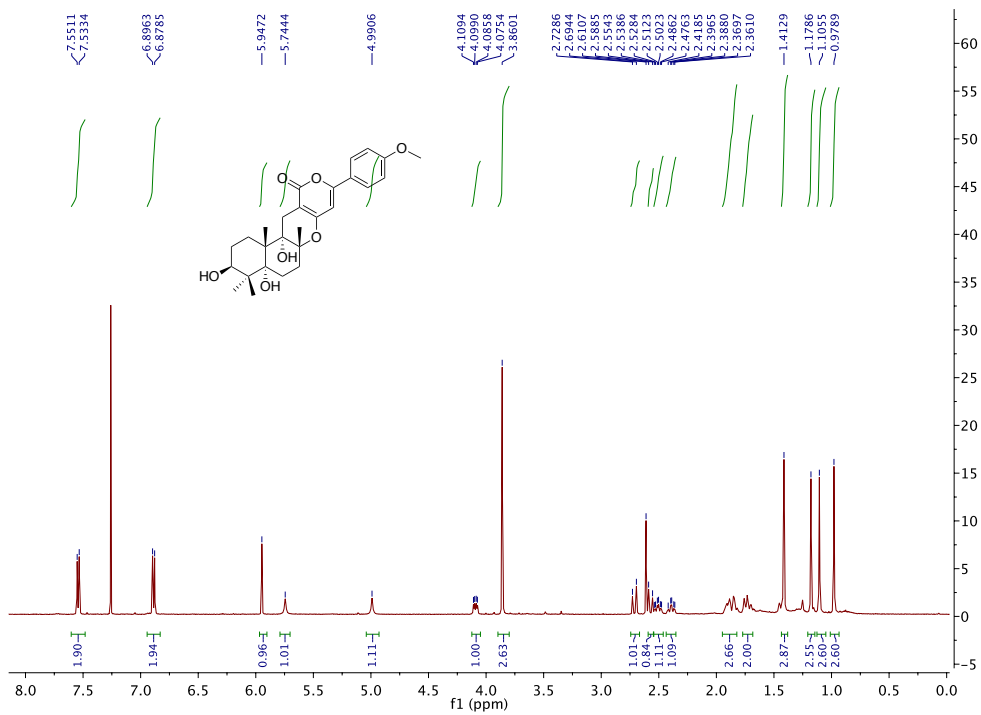


Figure C9. $^1\text{H-NMR}$ spectrum of compound **5.5** in CDCl_3 (500 MHz).

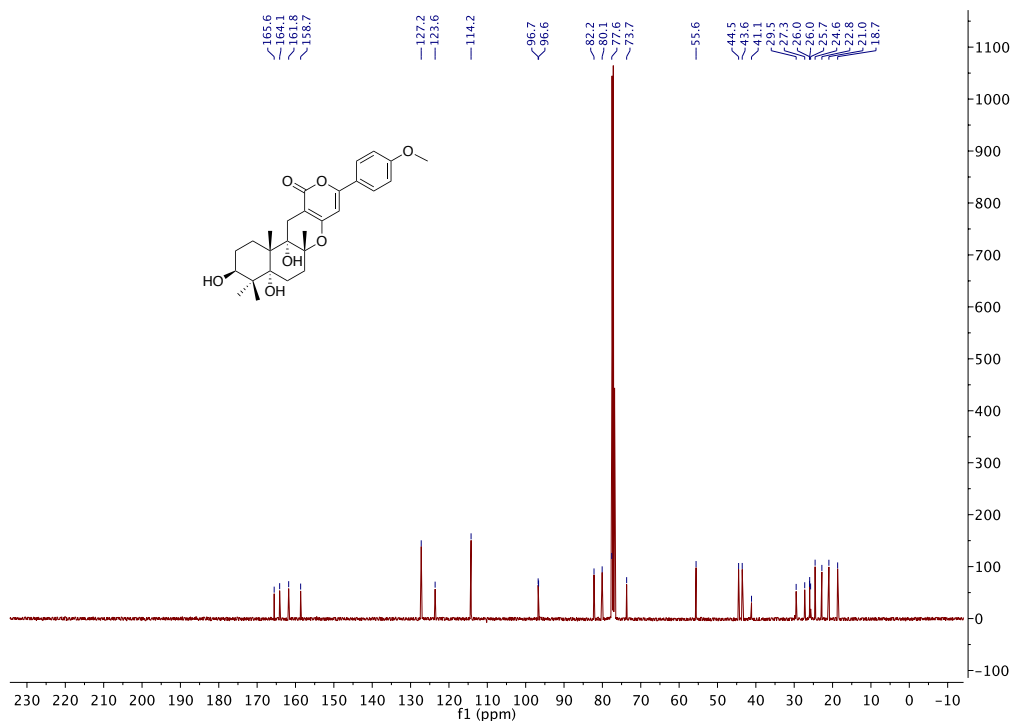


Figure C10. $^{13}\text{C-NMR}$ spectrum of compound **5.5** in CDCl_3 (100 MHz).

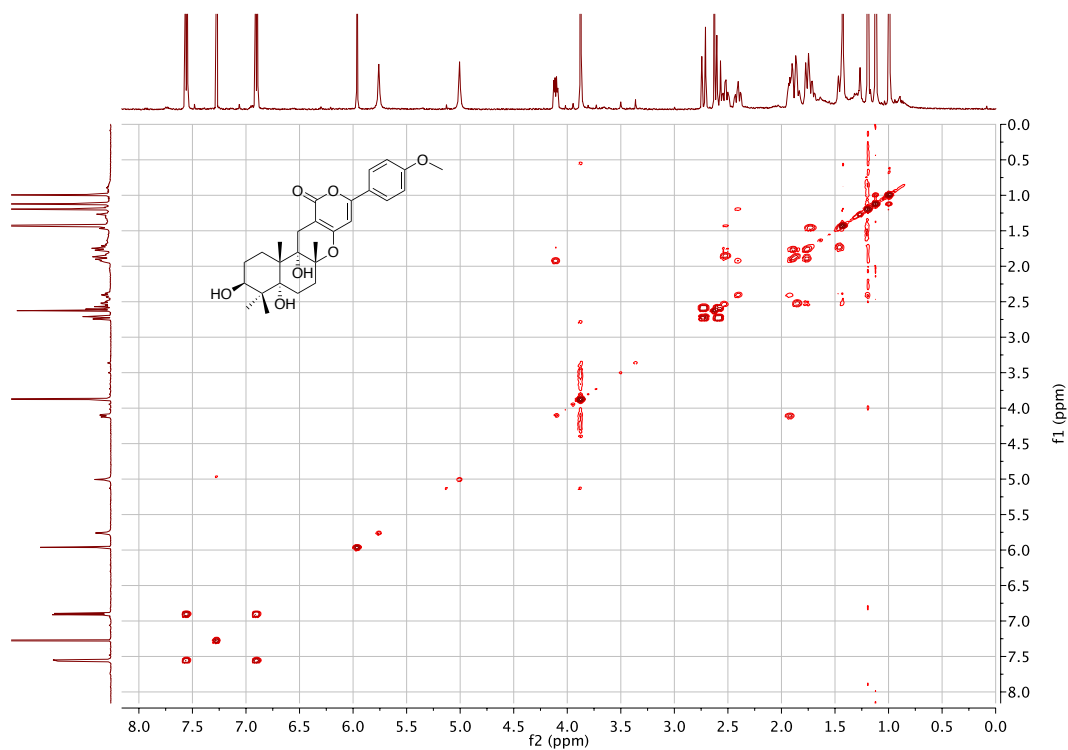


Figure C11. ^1H - ^1H COSY spectrum of compound **5.5** in CDCl_3 (500 MHz).

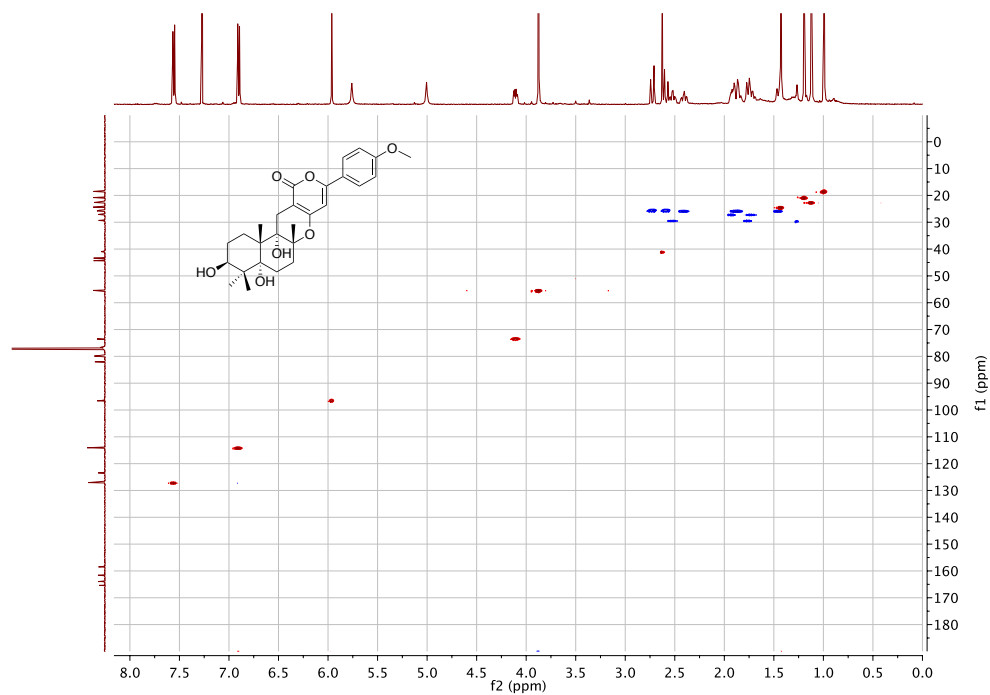


Figure C12. HSQC spectrum of compound **5.5** in CDCl_3 (500 MHz).

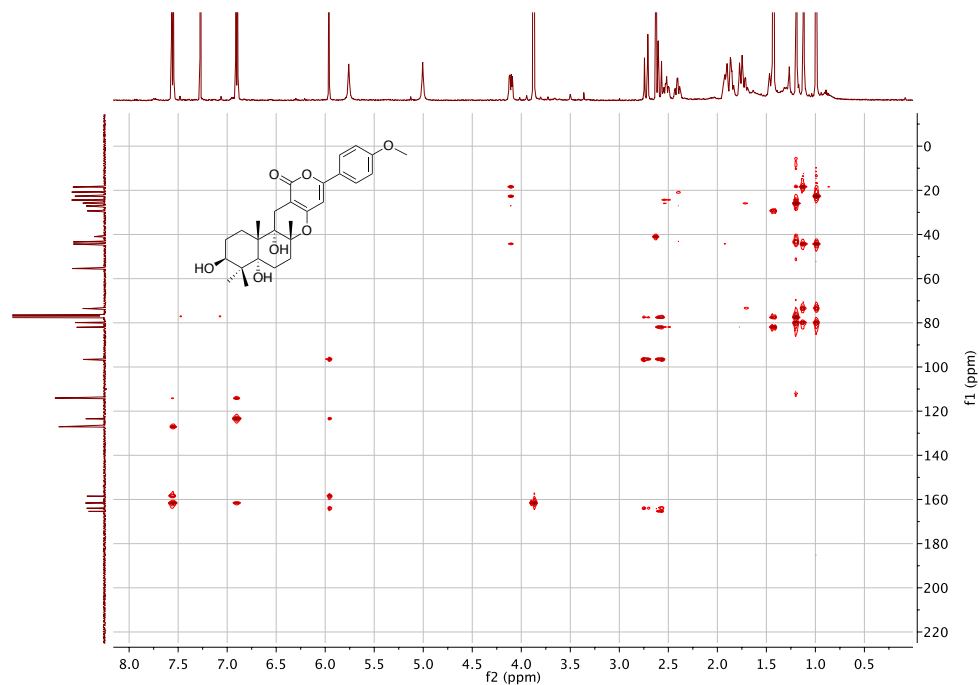


Figure C13. HMBC spectrum of compound 5.5 in CDCl_3 (500 MHz).

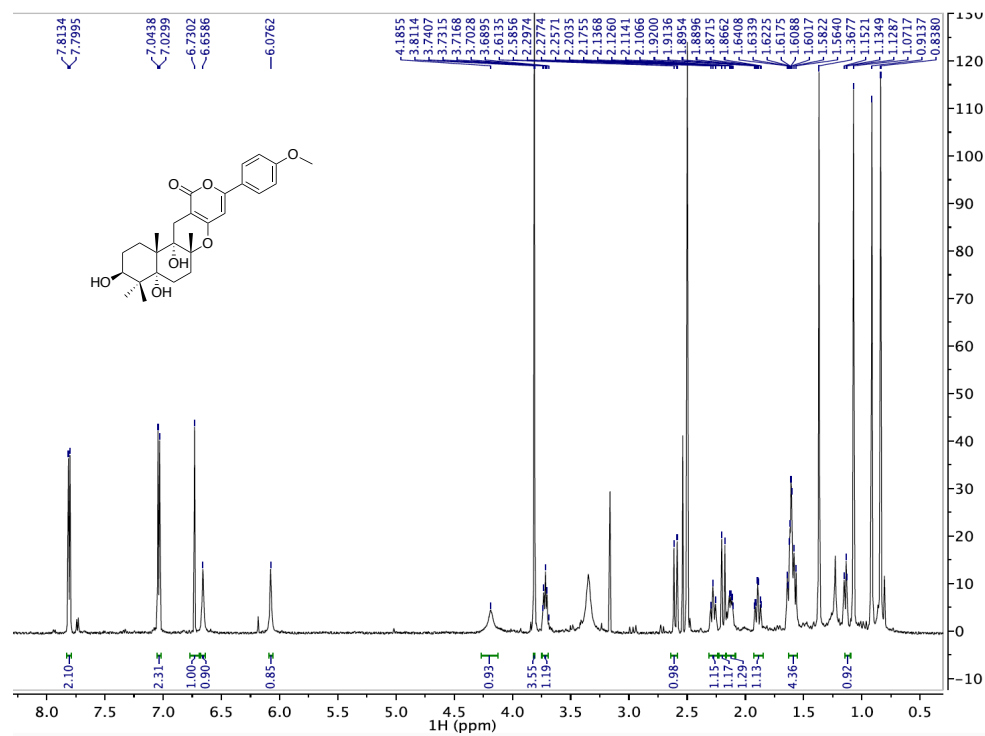


Figure C14. ^1H -NMR spectrum of compound 5.5 in $\text{DMSO}-d_6$ (600 MHz).

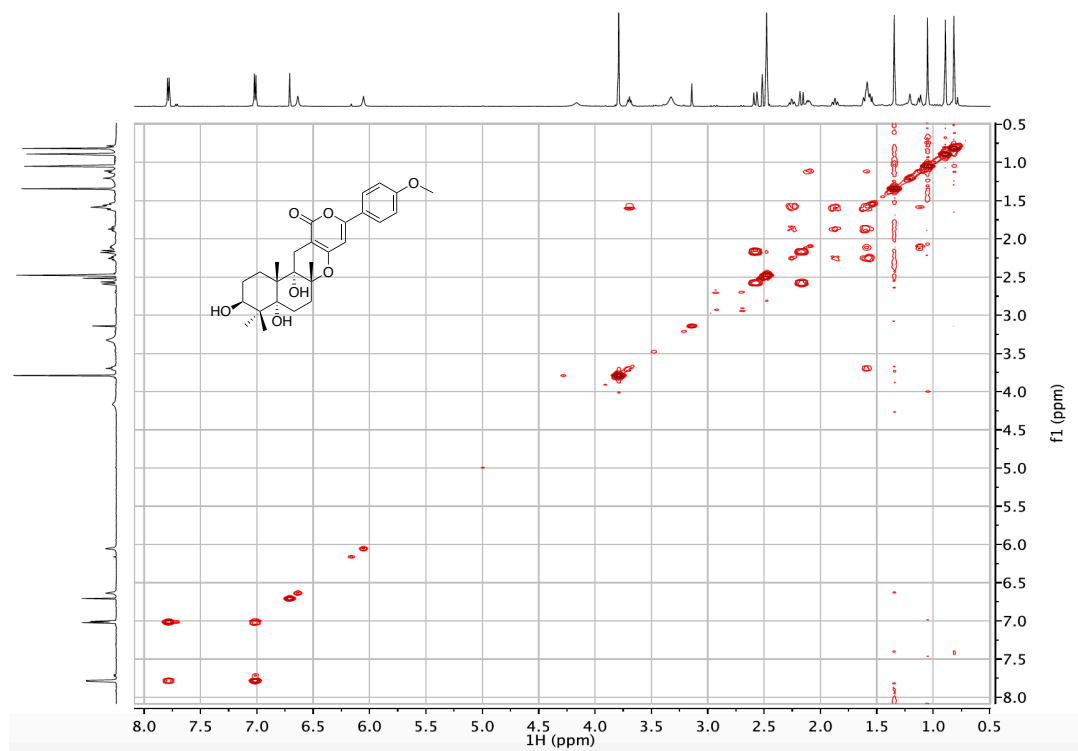


Figure C15. ^1H - ^1H COSY spectrum of compound **5.5** in $\text{DMSO-}d_6$ (600 MHz).

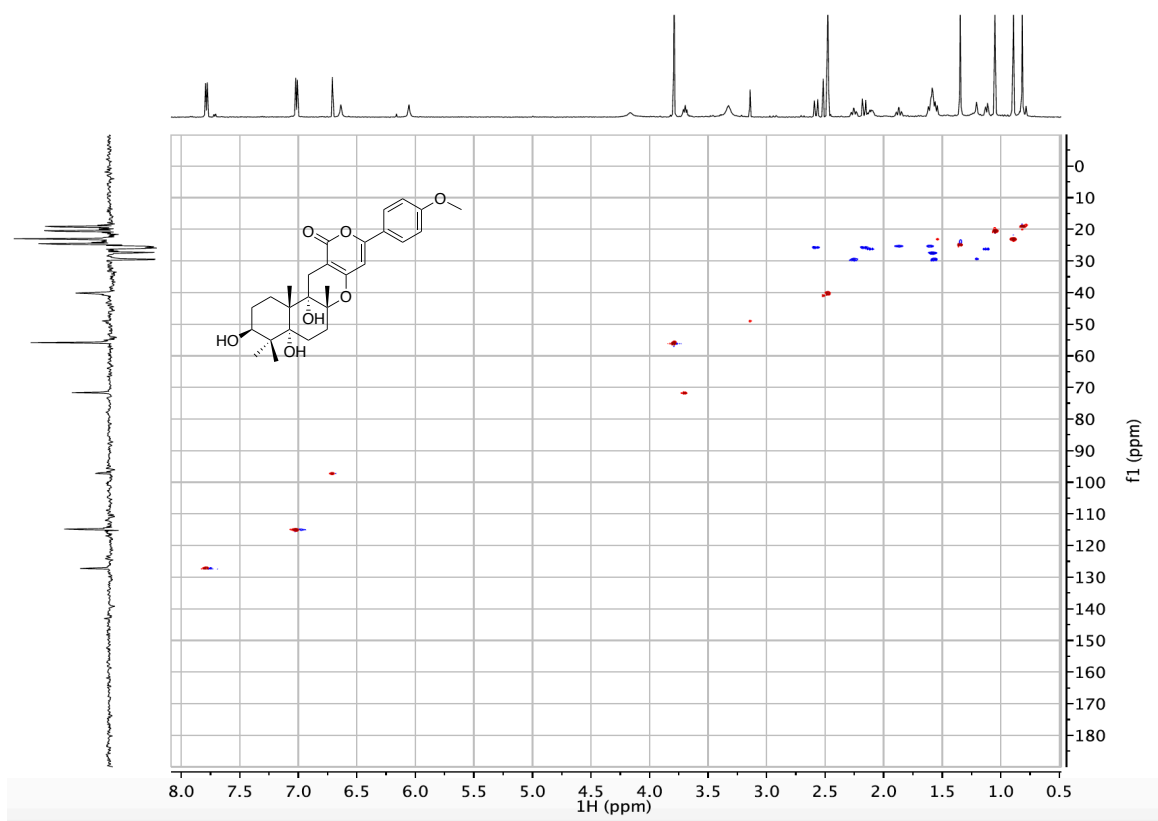


Figure C16. HSQC spectrum of compound **5.5** in $\text{DMSO-}d_6$ (600 MHz).

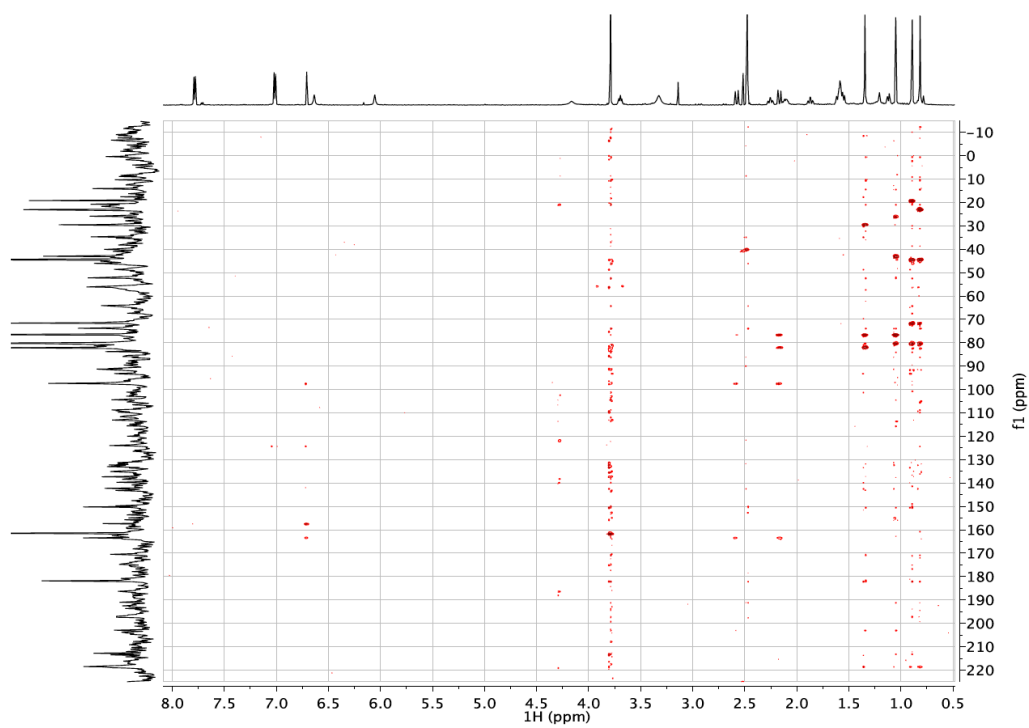


Figure C17. HMBC spectrum of compound **5.5** in DMSO-*d*₆ (600 MHz).

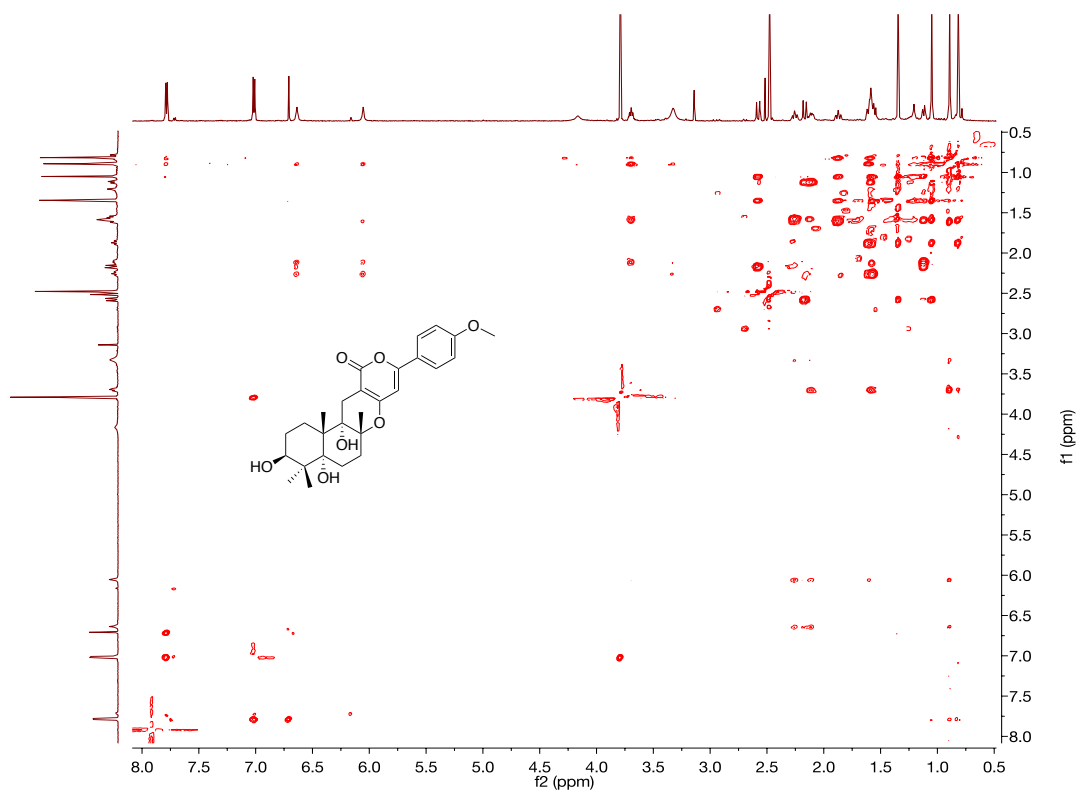


Figure C18. ROESY spectrum of compound **5.5** in DMSO-*d*₆ (500 MHz).

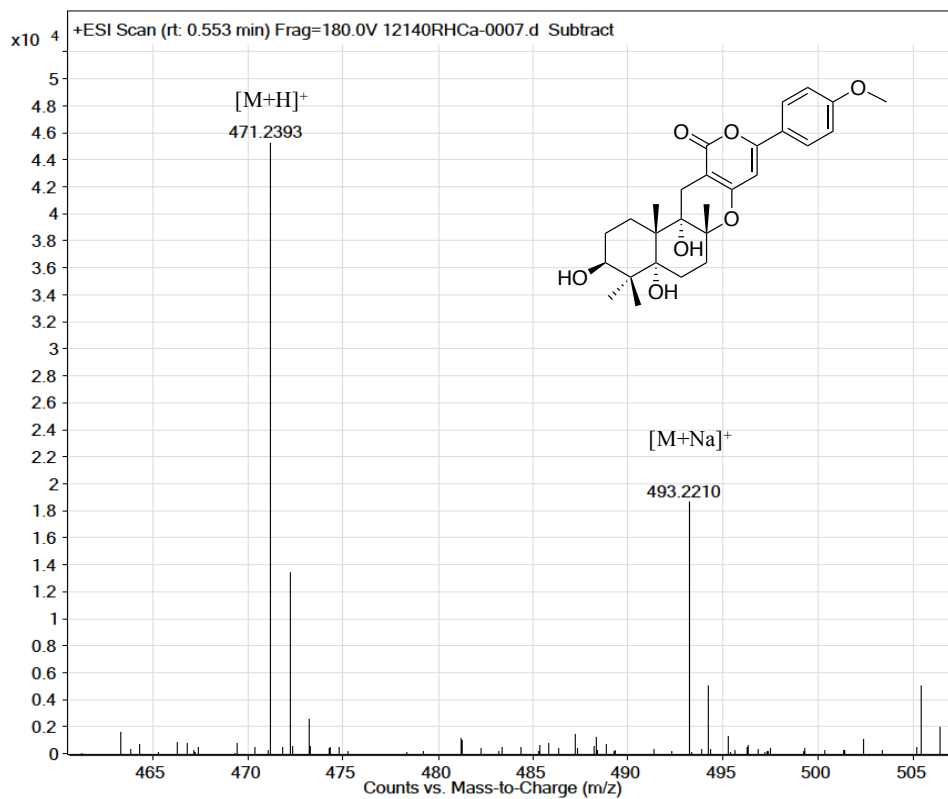


Figure C19. HRESIMS of compound **5.5**.

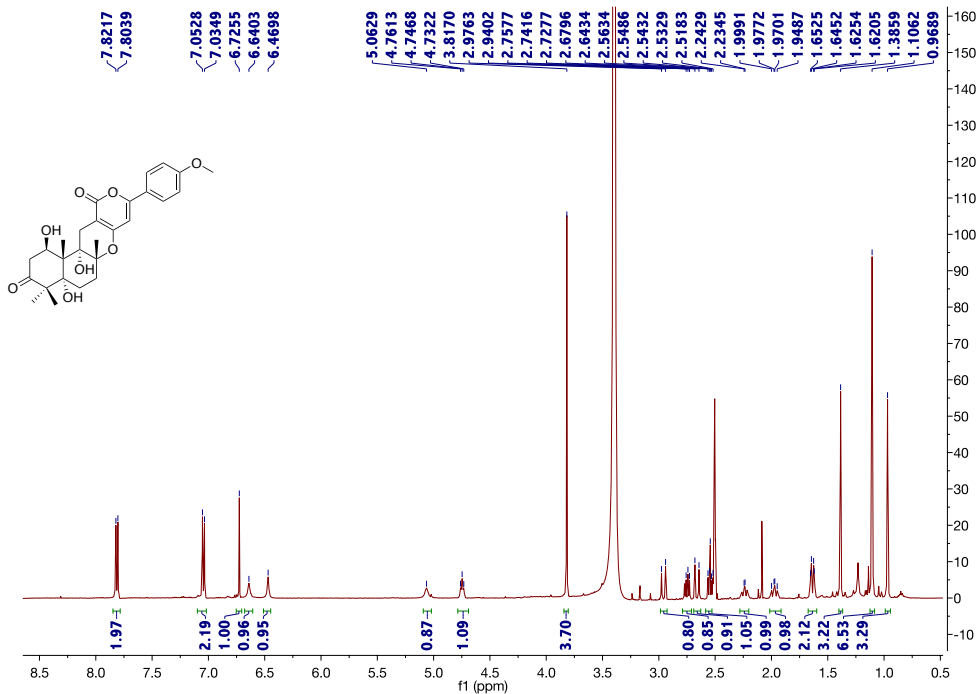


Figure C20. $^1\text{H-NMR}$ spectrum of compound **5.8** in $\text{DMSO-}d_6$ (500 MHz).

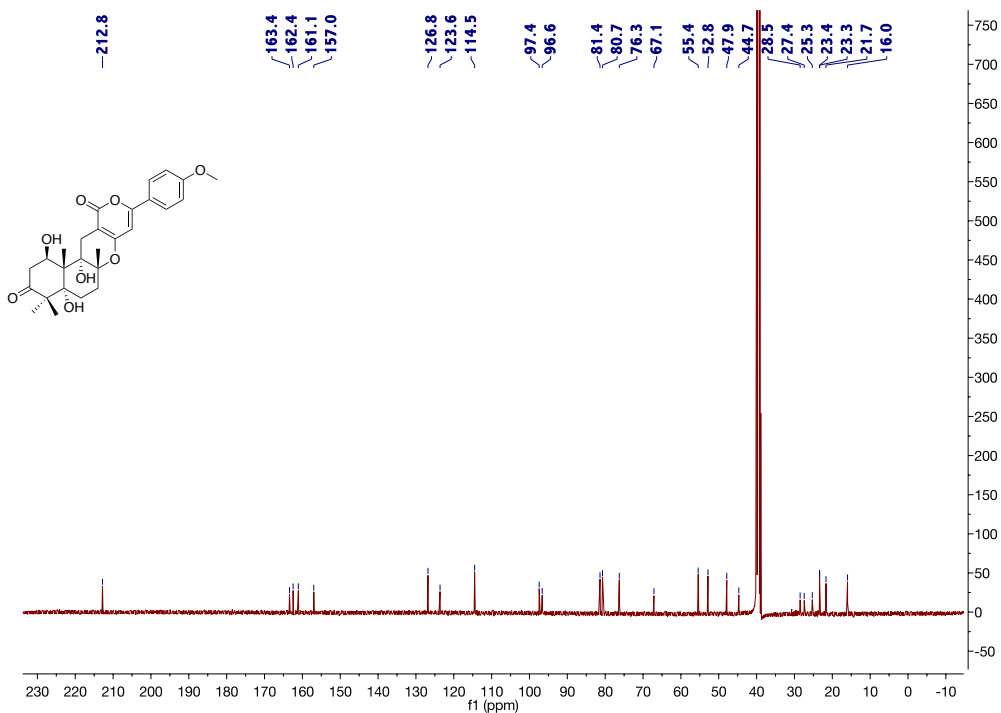


Figure C21. $^{13}\text{C-NMR}$ spectrum of compound **5.8** in $\text{DMSO-}d_6$ (100 MHz).

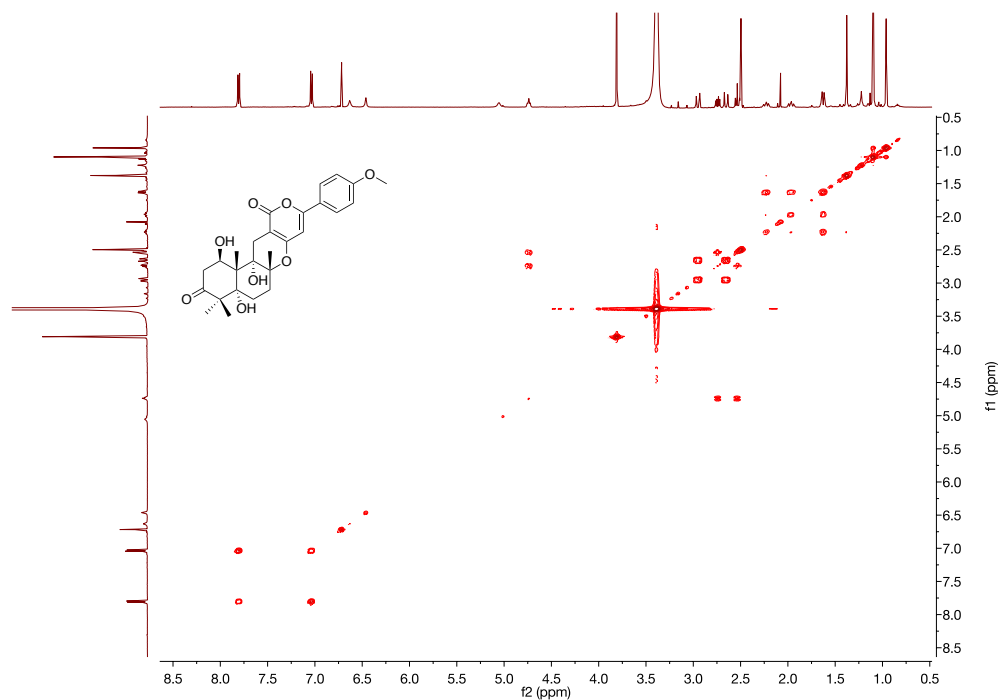


Figure C22. ^1H - ^1H spectrum of compound **5.8** in $\text{DMSO-}d_6$ (500 MHz).

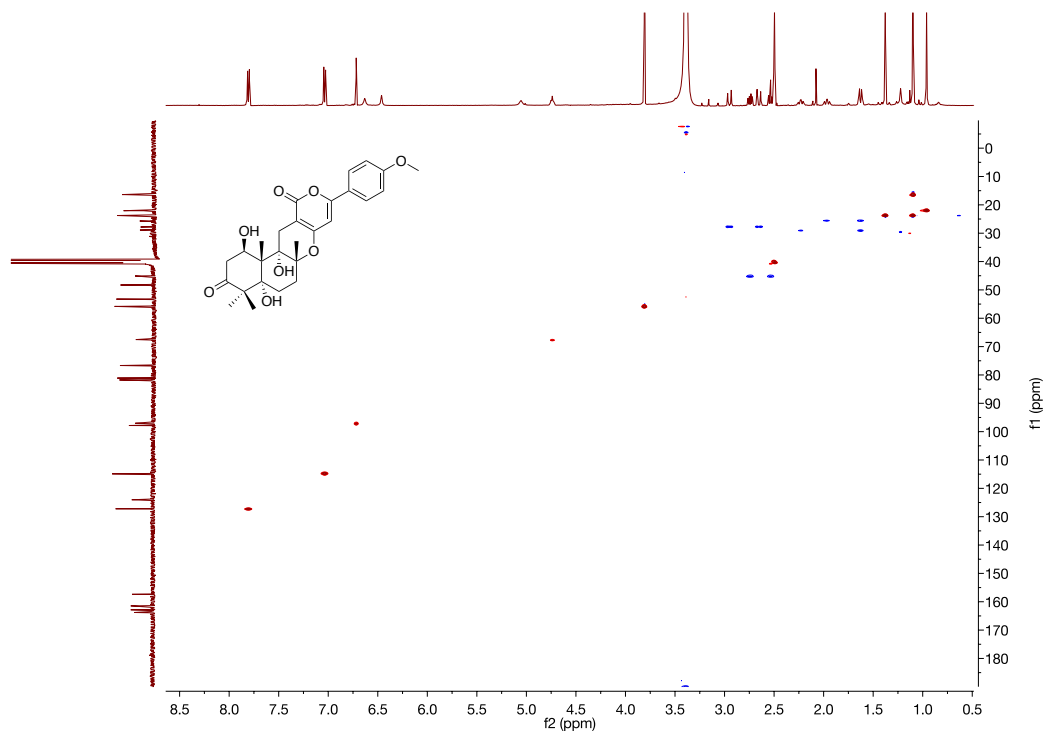


Figure C23. HSQC spectrum of compound **5.8** in $\text{DMSO-}d_6$ (500 MHz).

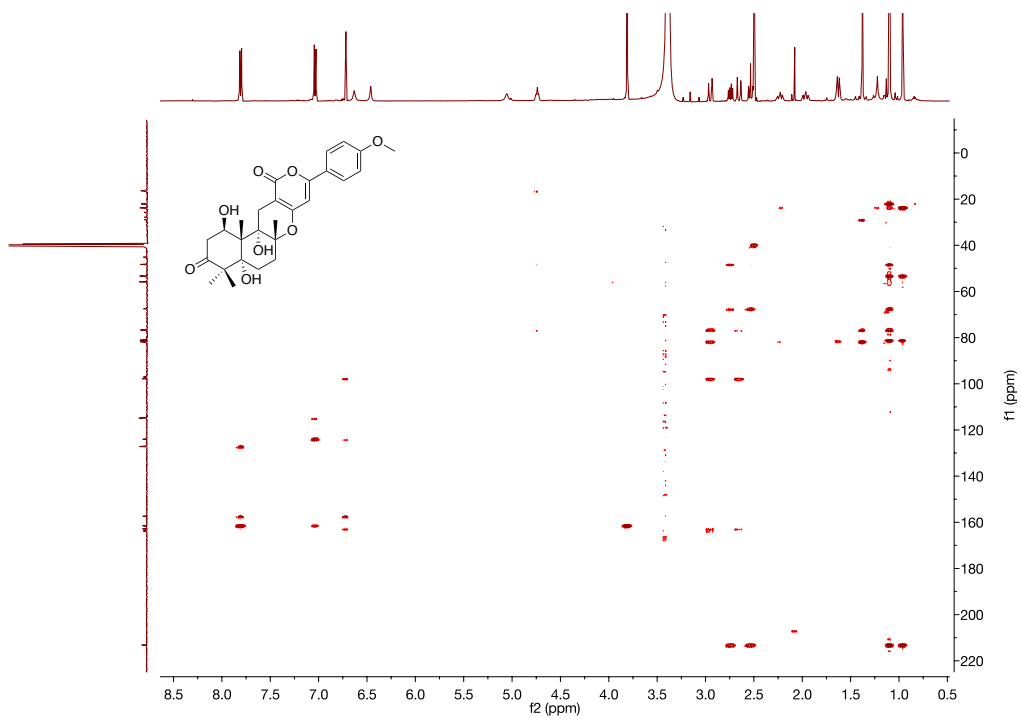


Figure C24. HMBC spectrum of compound **5.8** in DMSO-*d*₆ (500 MHz).

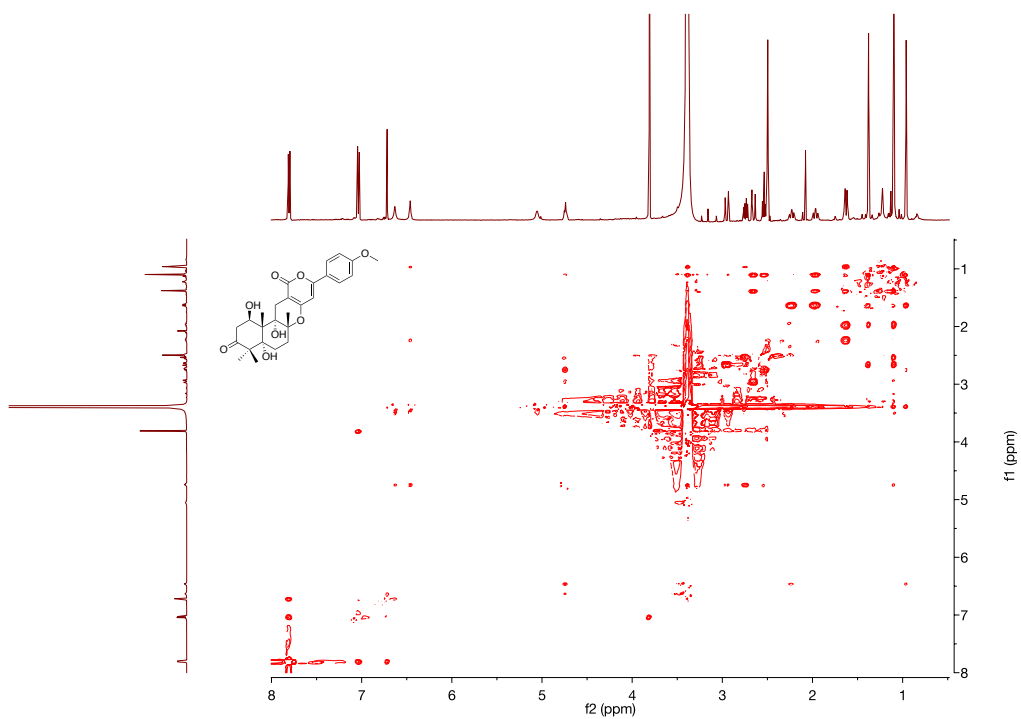


Figure C25. ROESY spectrum of compound **5.8** in DMSO-*d*₆ (500 MHz).

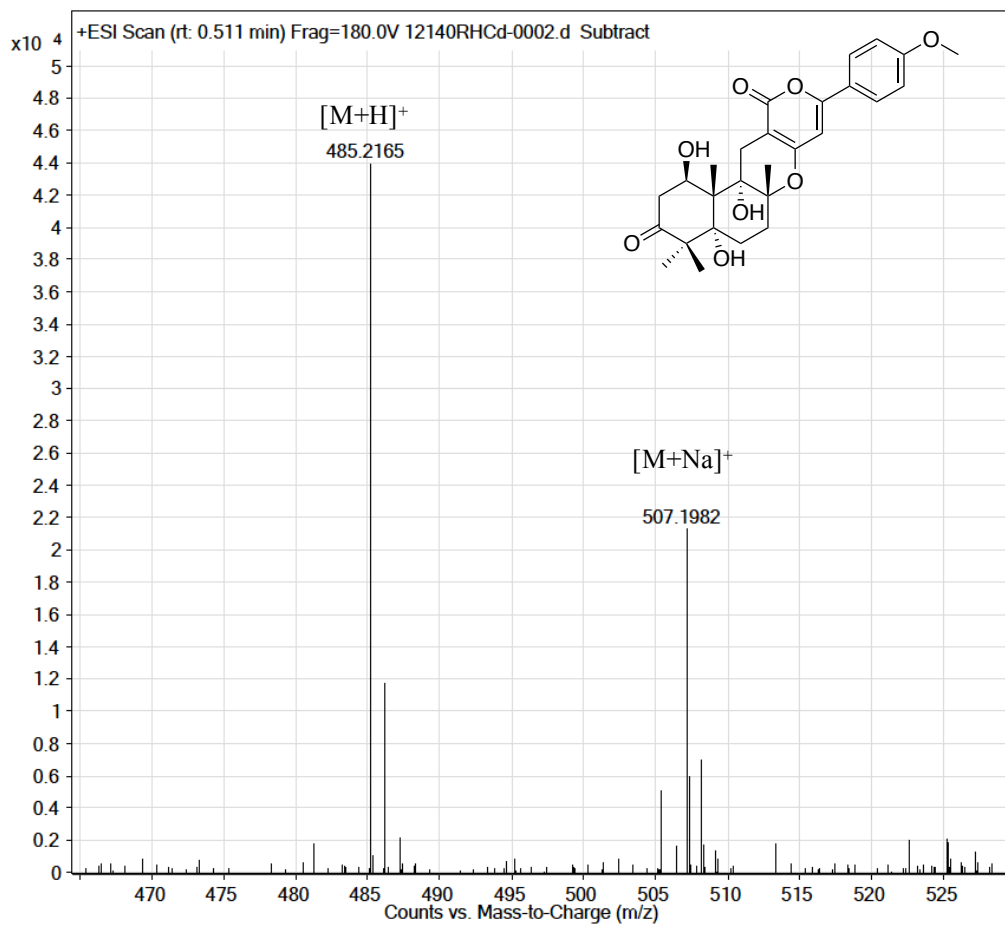


Figure C26. HRESIMS of compound **5.8**.

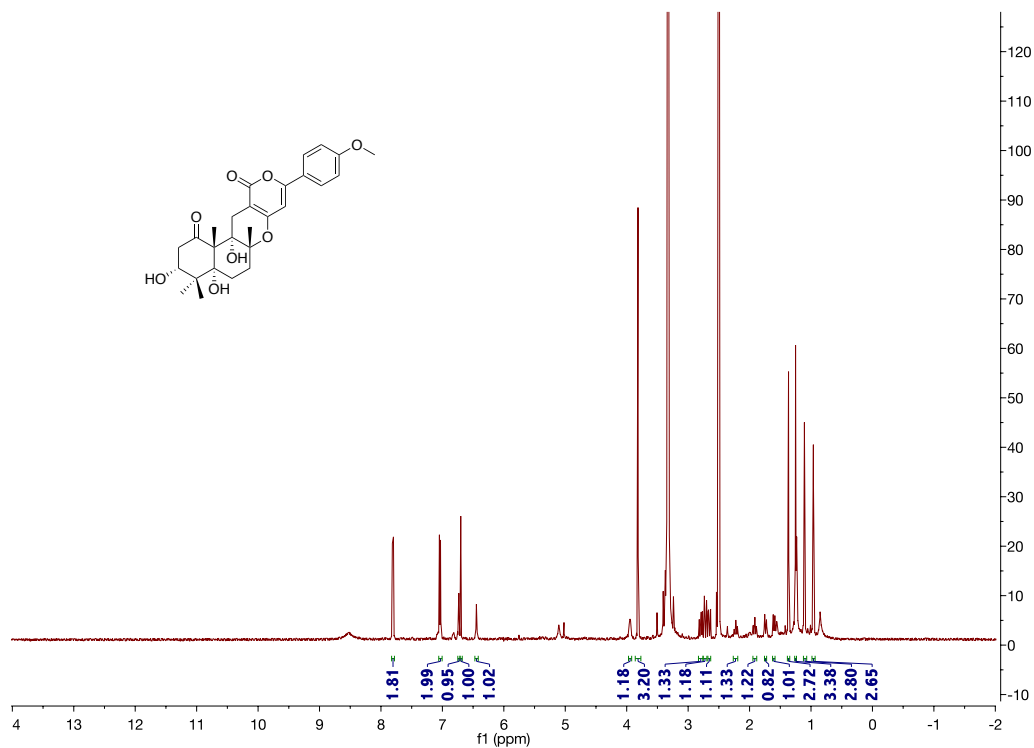


Figure C27. $^1\text{H-NMR}$ spectrum of compound **5.12** in $\text{DMSO-}d_6$ (500 MHz).

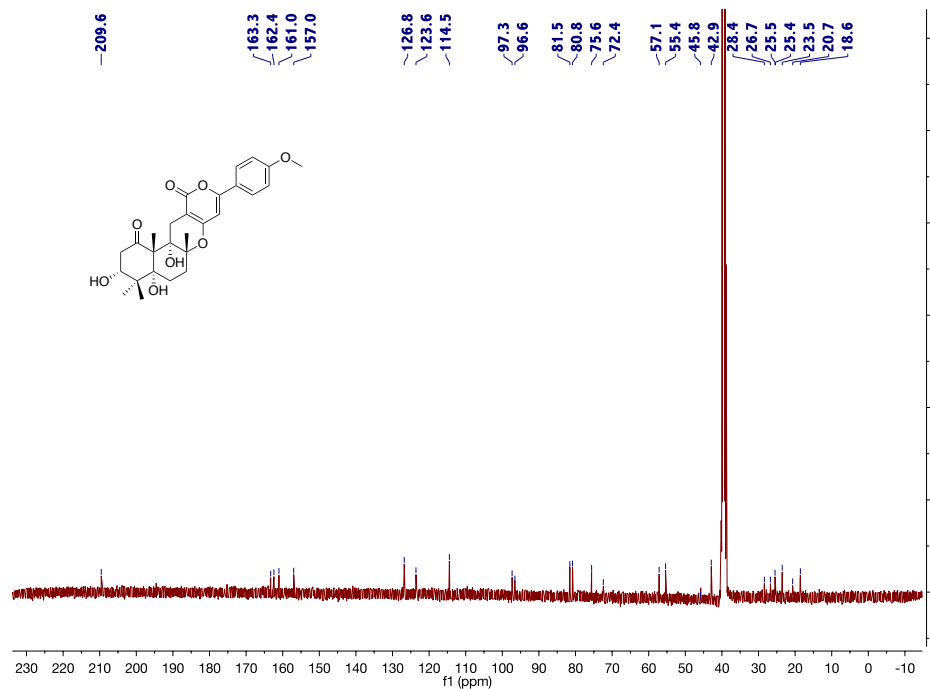


Figure C28. $^{13}\text{C-NMR}$ spectrum of compound **5.12** in $\text{DMSO-}d_6$ (100 MHz).

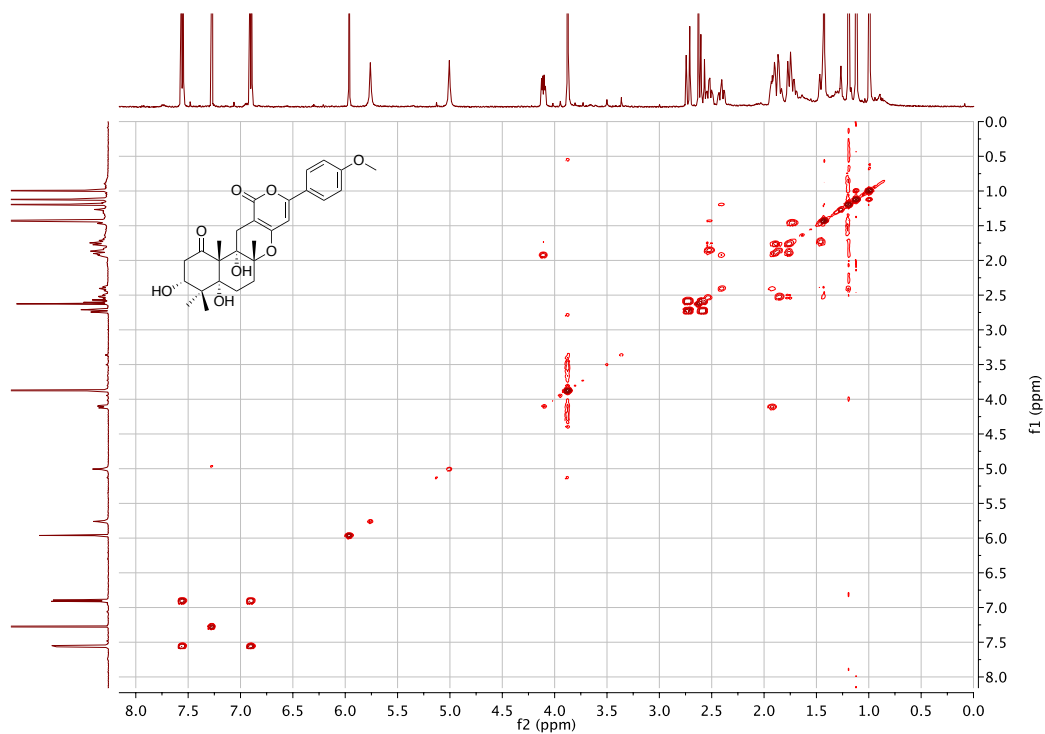


Figure C29. ^1H - ^1H spectrum of compound **5.12** in $\text{DMSO-}d_6$ (500 MHz).

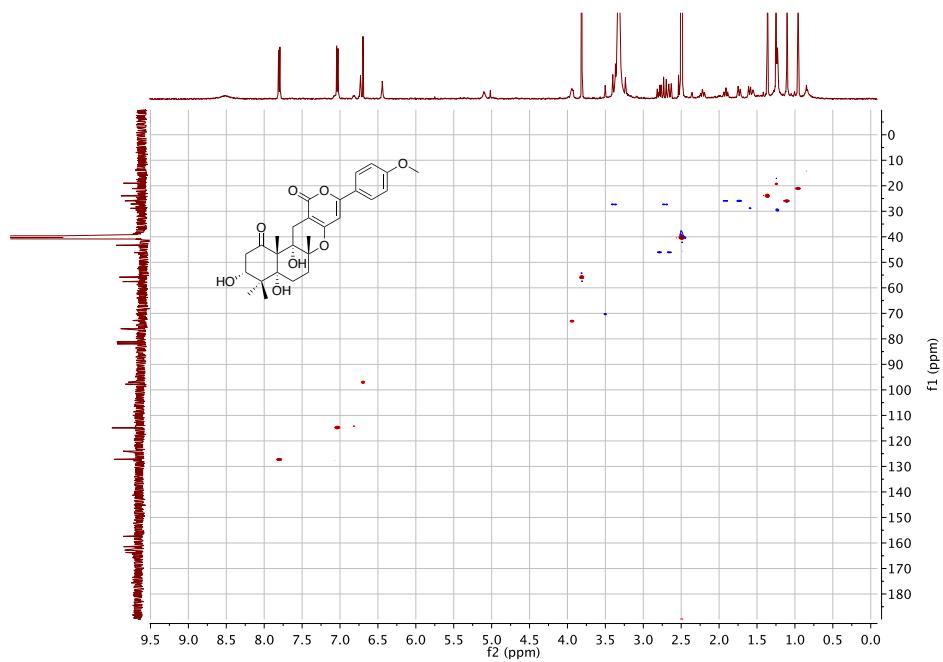


Figure C30. HSQC spectrum of compound **5.12** in $\text{DMSO-}d_6$ (500 MHz).

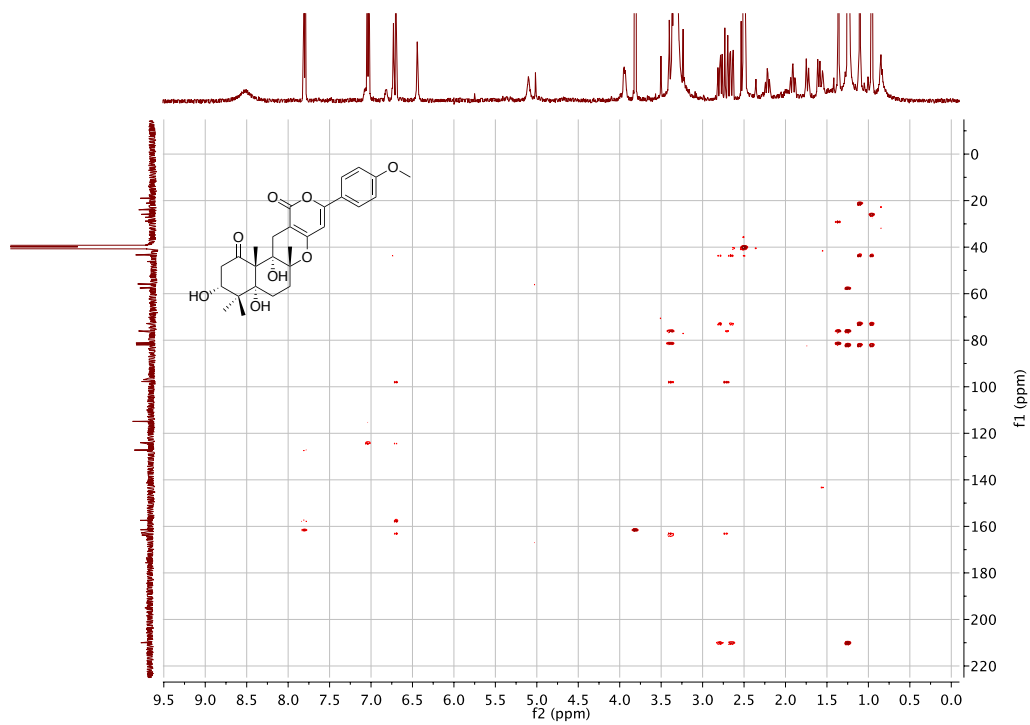


Figure C31. HMBC spectrum of compound **5.12** in DMSO- d_6 (500 MHz).

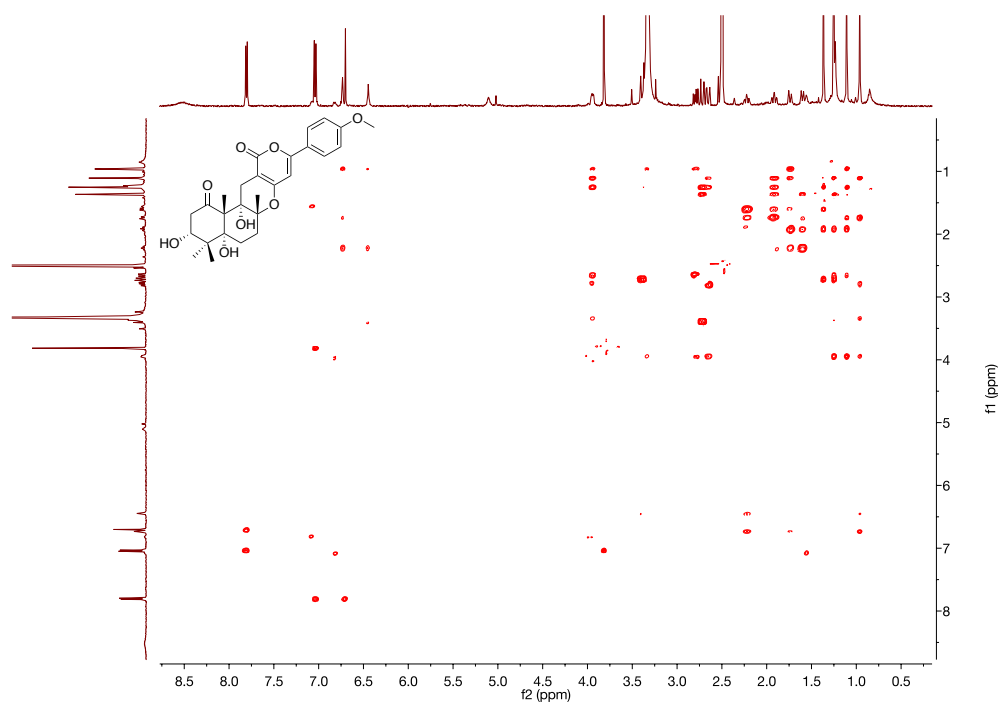


Figure C32. ROESY spectrum of compound **5.12** in DMSO- d_6 (500 MHz).

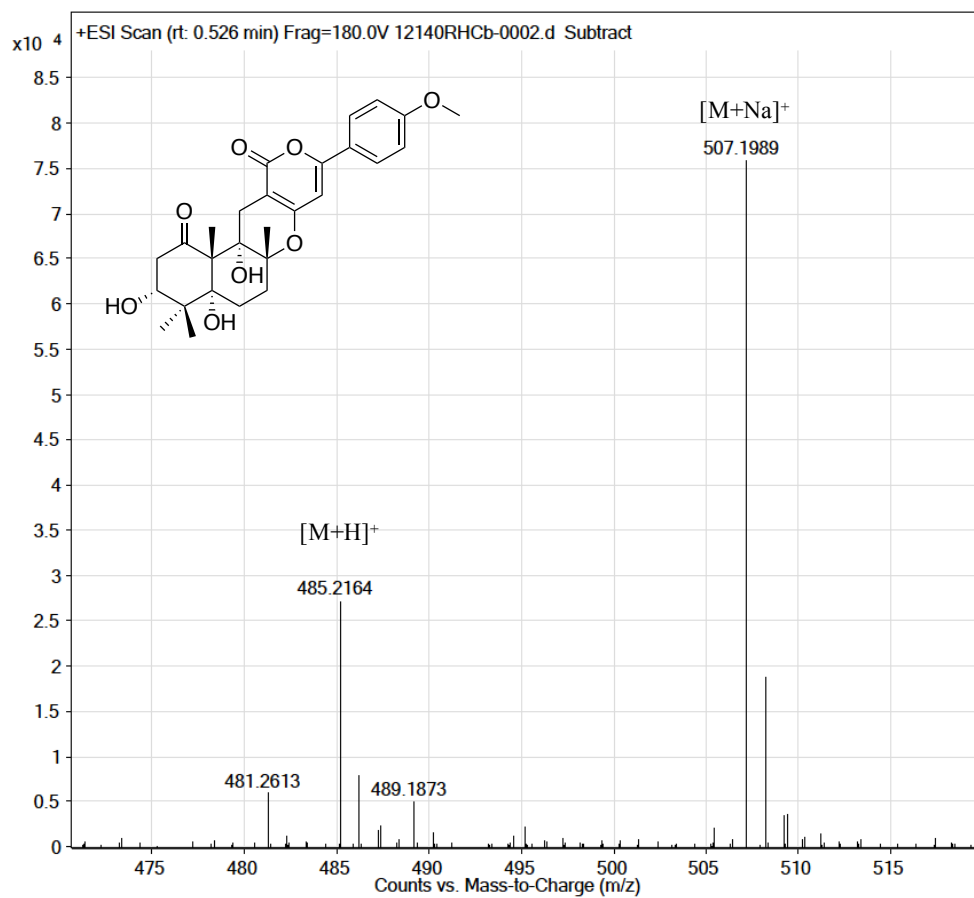


Figure C33. HRESIMS of compound **5.12**.

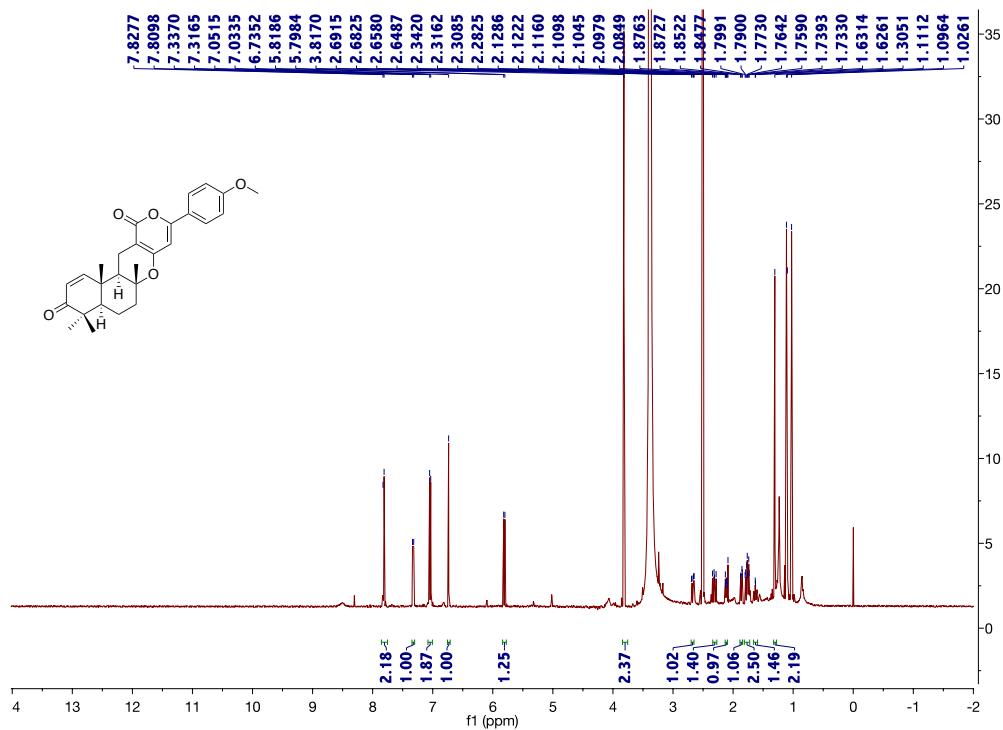


Figure C34. $^1\text{H-NMR}$ spectrum of compound **5.13** in $\text{DMSO-}d_6$ (500 MHz).

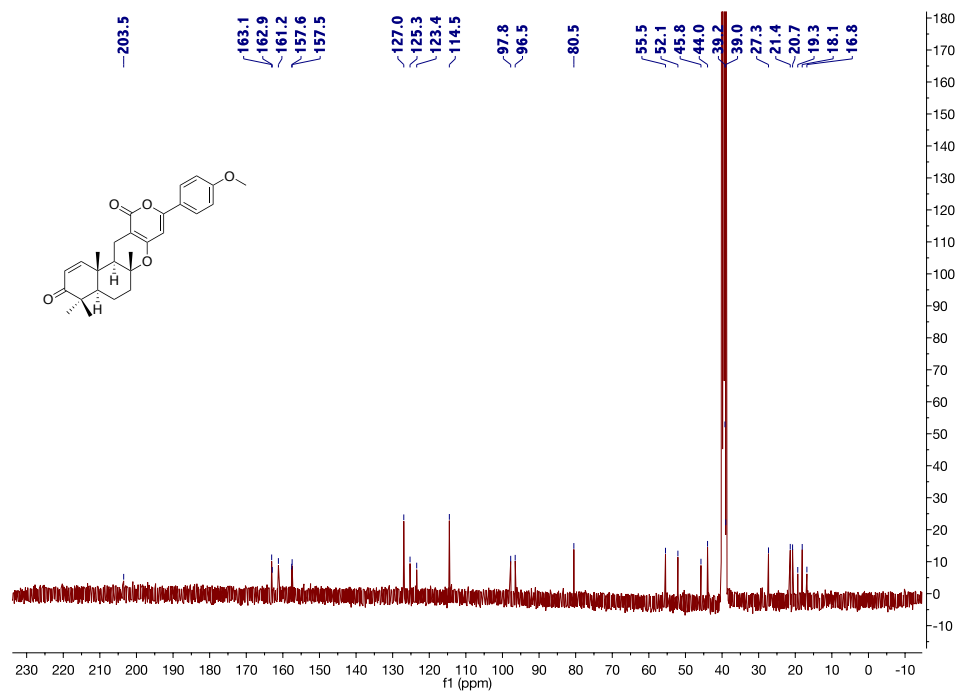


Figure C35. $^{13}\text{C-NMR}$ spectrum of compound **5.13** in $\text{DMSO-}d_6$ (100 MHz).

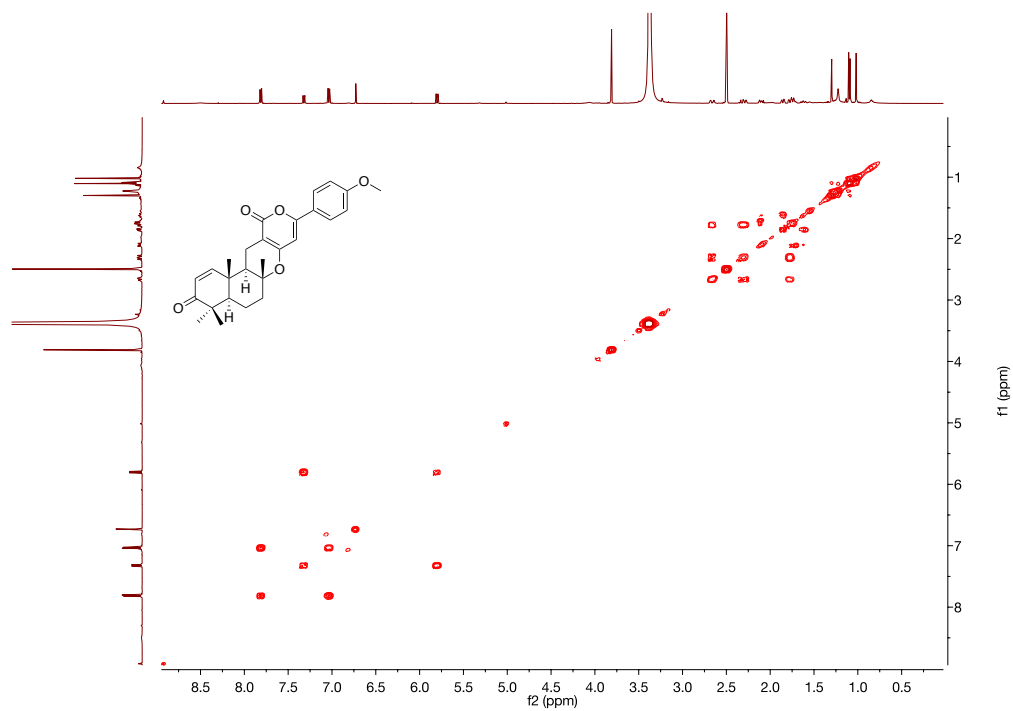


Figure C36. ^1H - ^1H spectrum of compound **5.13** in $\text{DMSO-}d_6$ (500 MHz).

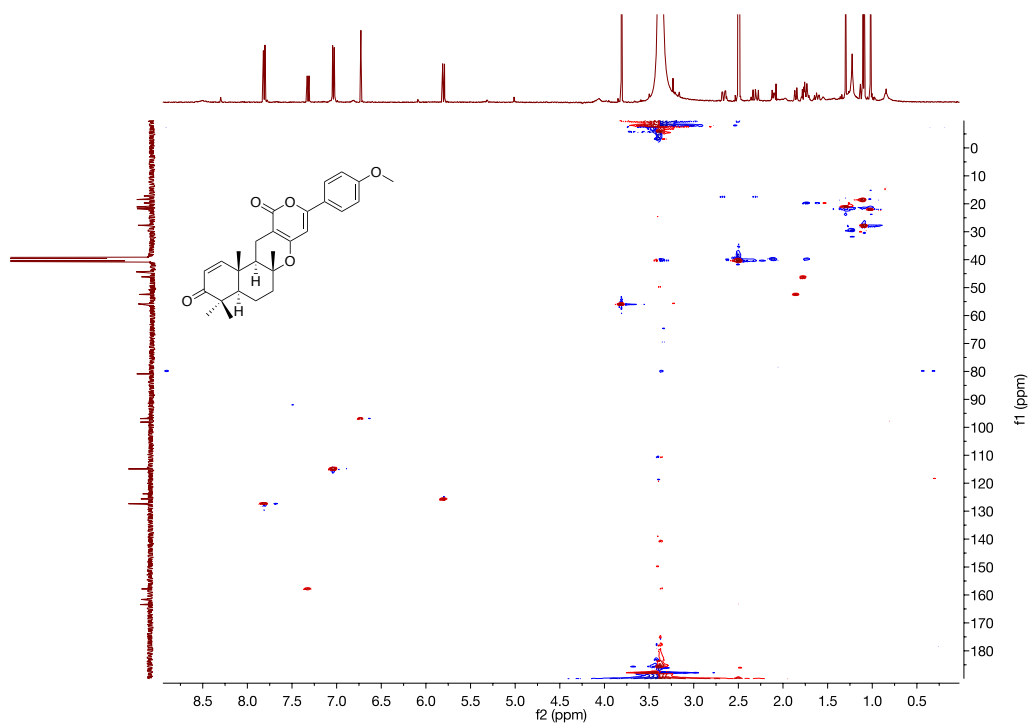


Figure S37. HSQC spectrum of compound **5.13** in $\text{DMSO-}d_6$ (500 MHz).

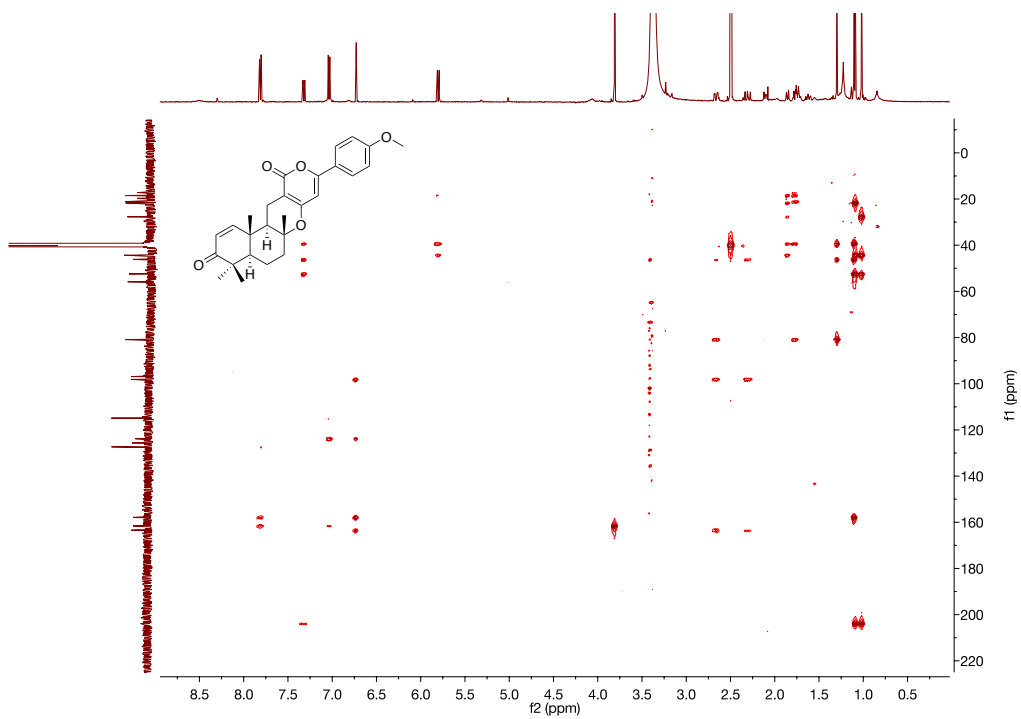


Figure C38. HMBC spectrum of compound **5.13** in DMSO- d_6 (500 MHz).

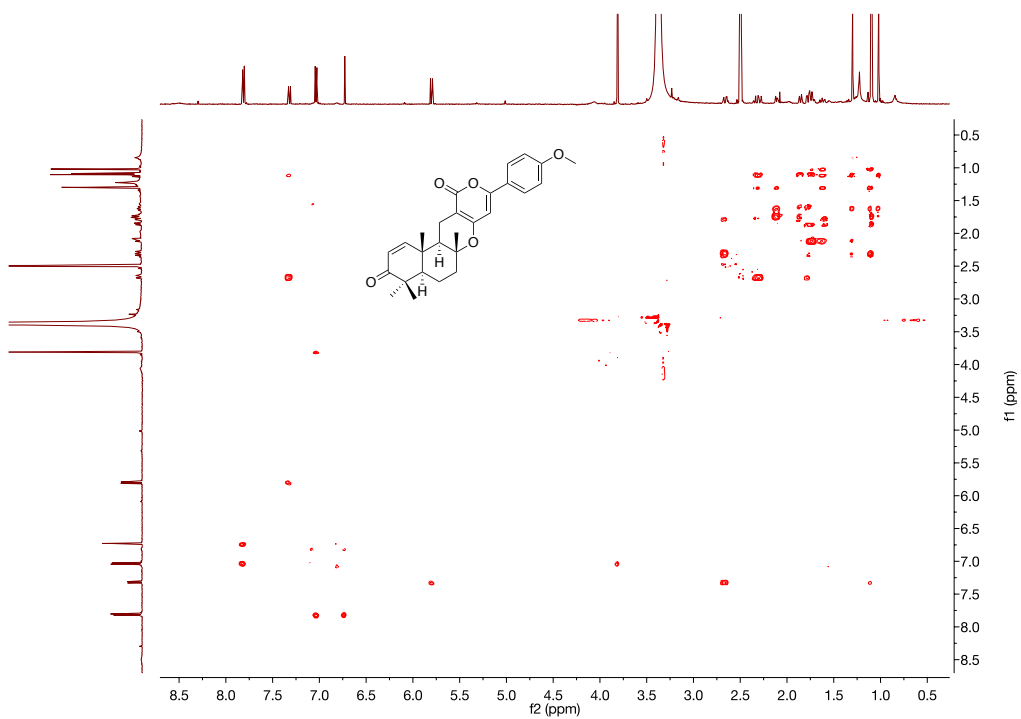


Figure C39. ROESY spectrum of compound **5.13** in DMSO- d_6 (500 MHz).

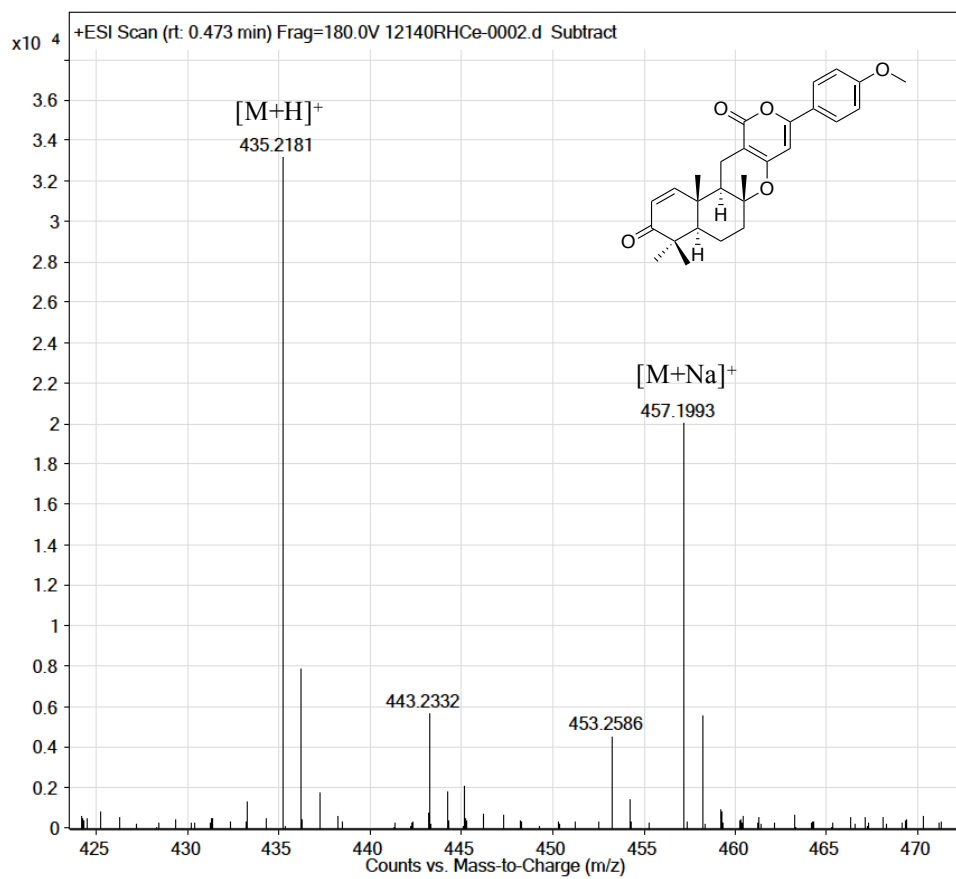


Figure C40. HRESIMS of compound **5.13**.

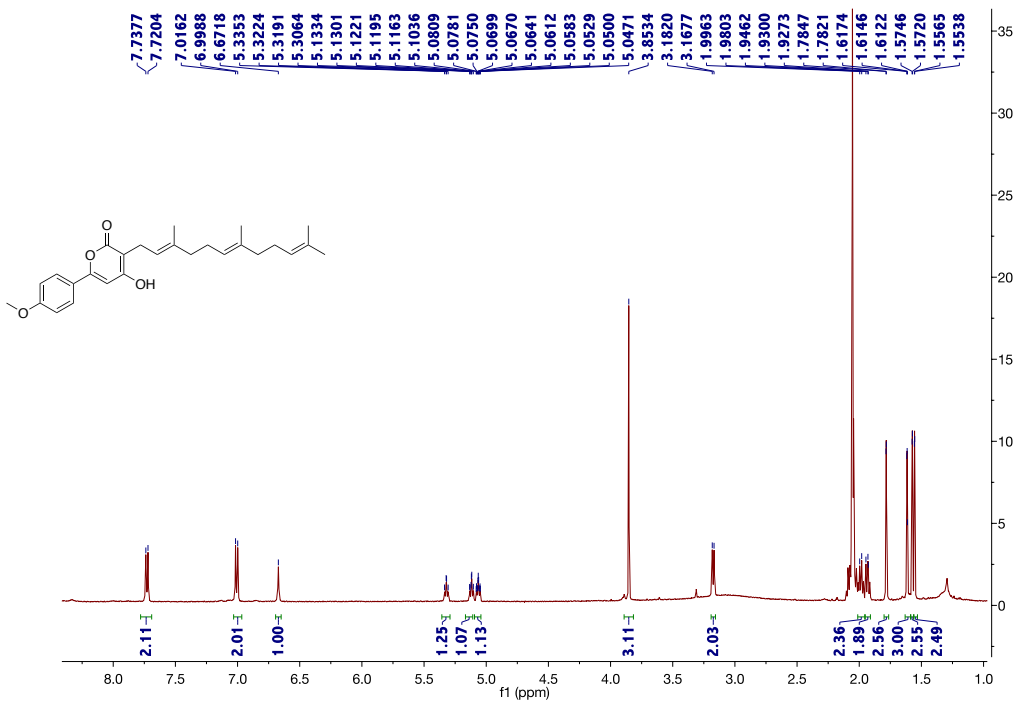


Figure C41. $^1\text{H-NMR}$ spectrum of compound **5.14** in $\text{Acetone-}d_6$ (500 MHz).

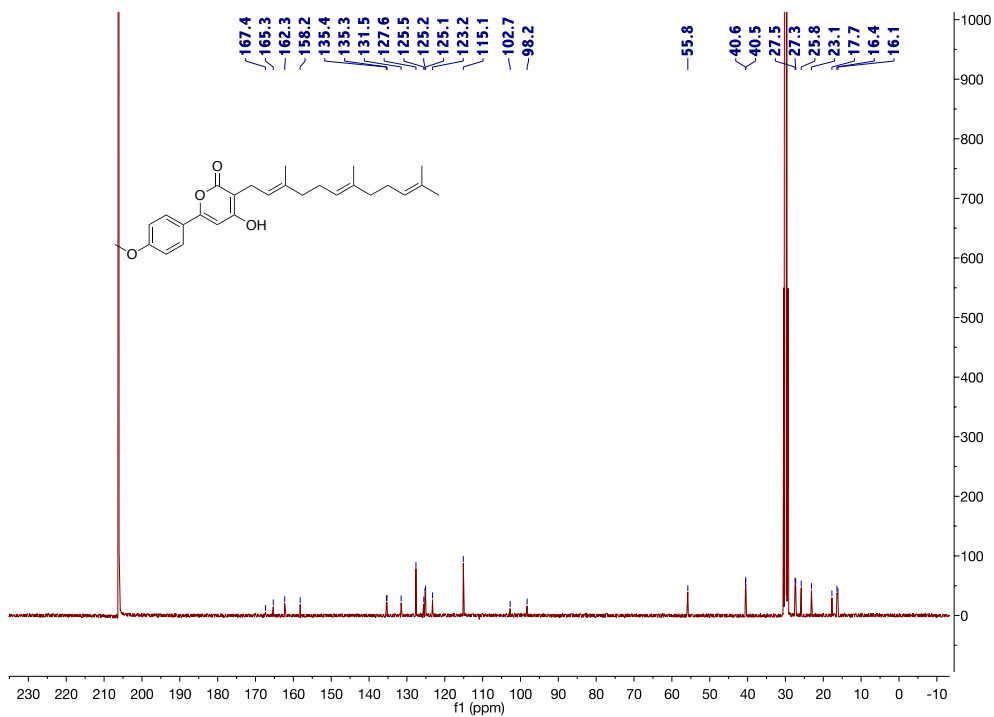


Figure C42. $^{13}\text{C-NMR}$ spectrum of compound **5.14** in $\text{Acetone-}d_6$ (100 MHz).

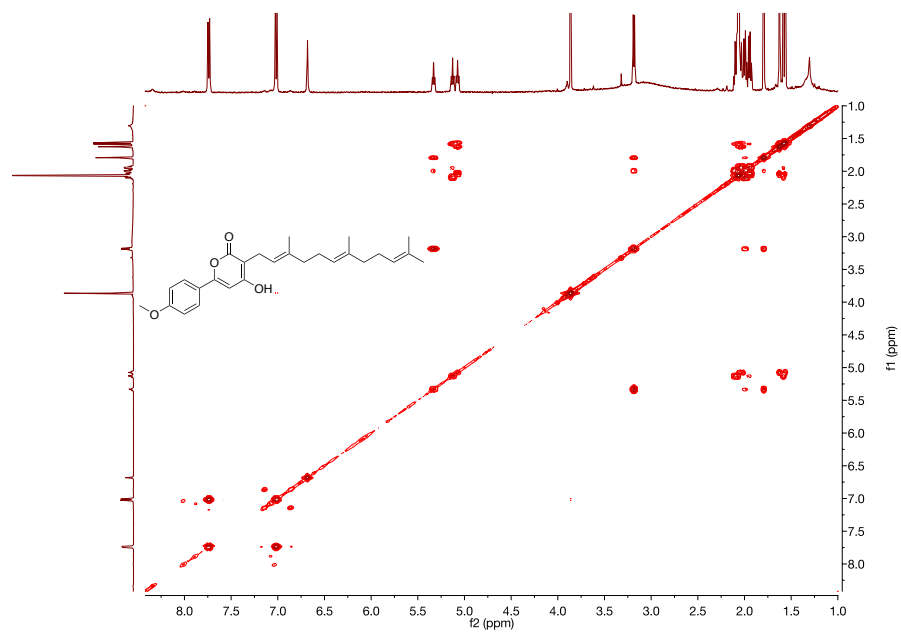


Figure C43. ^1H - ^1H spectrum of compound **5.14** in Acetone- d_6 (500 MHz).

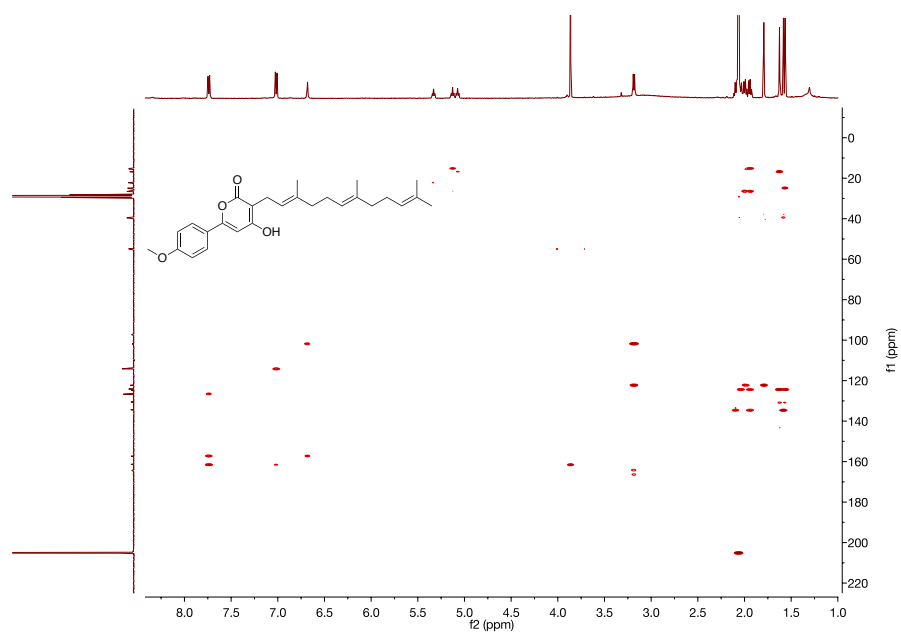


Figure C44. HSQC spectrum of compound **5.14** in Acetone- d_6 (500 MHz).

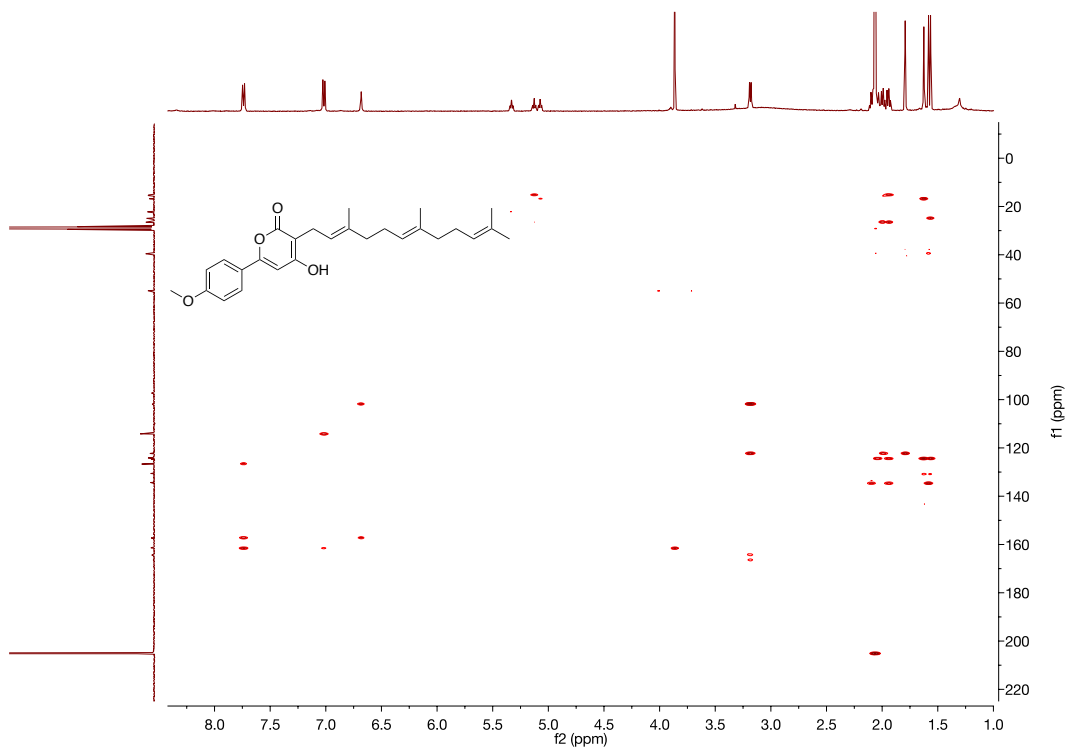


Figure C45. HMBC spectrum of compound **5.14** in Acetone- d_6 (500 MHz).

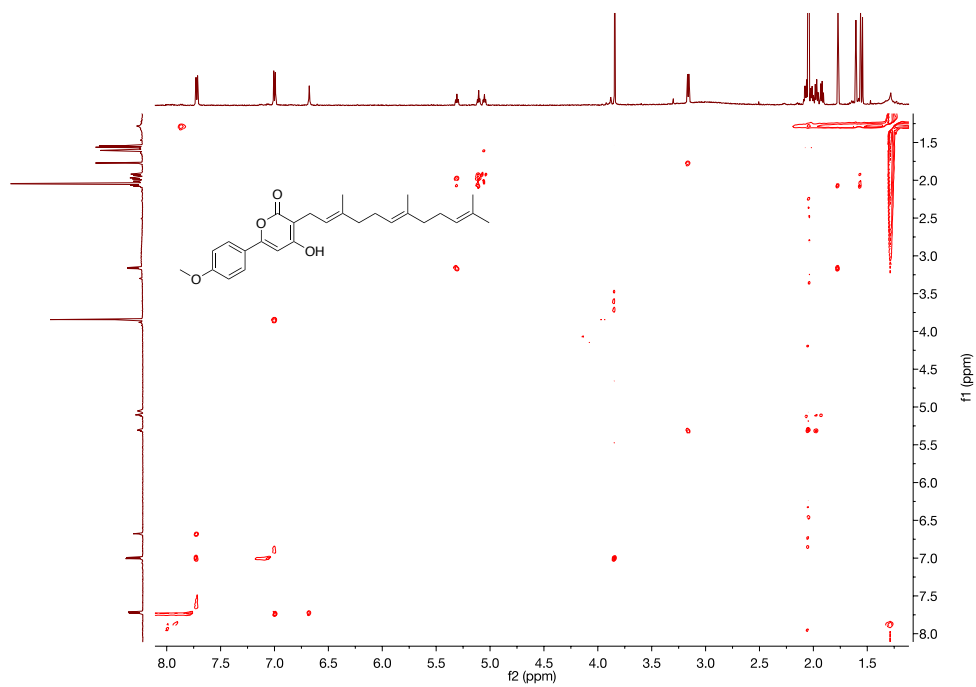


Figure C46. ROESY spectrum of compound **5.14** in Acetone- d_6 (500 MHz).

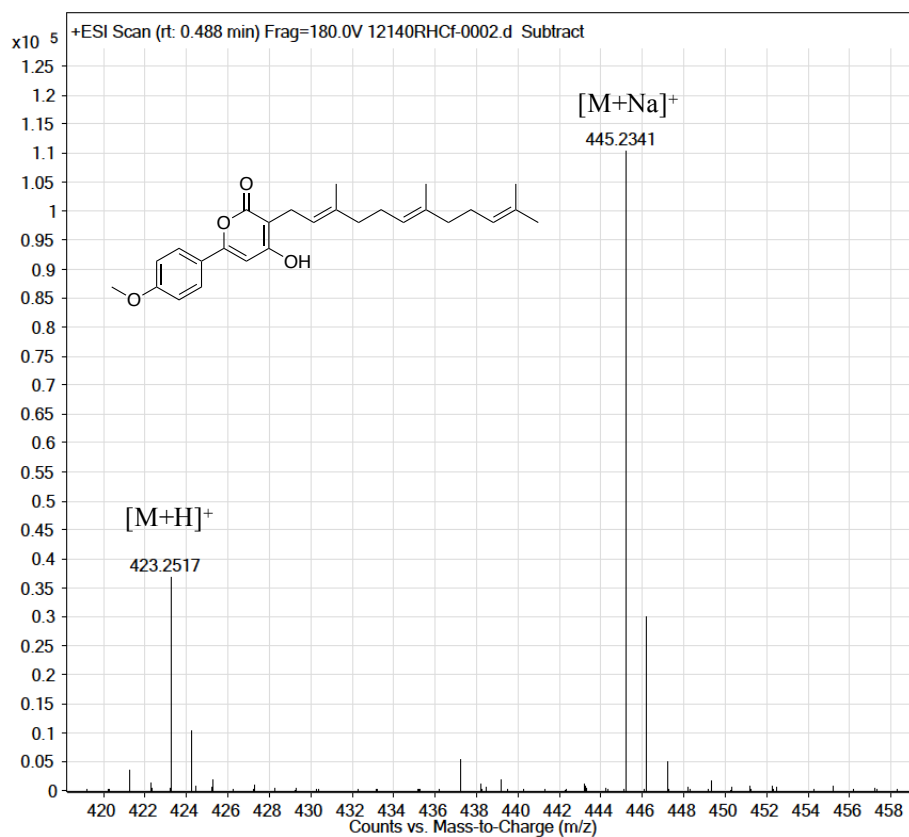


Figure C47. HRESIMS of compound **5.14**.

Abbreviations

ITS	internal transcribed spacer
RPB1	largest subunit of RNA polymerase
RPB2	second largest subunit of RNA polymerase
tub2/BenA	β -tubulin
tef1	translation elongation factor 1- α
MCM7	mini-chromosome maintenance protein
CaM	partial calmodulin
BLAST	basic local alignment search tool
CZI	Czapek Ivermectin Agar
PCR	polymerase chain reaction
SI	selectivity index
VLC	vacuum liquid chromatography
MTPA	α -methoxy- α -trifluoromethylphenylacetyl
FDAA	1-Fluoro-2-4-Dinitrophenyl-5- L-Alanine Amide
ATCC	the American Type Culture Collection
ACh	acetylcholine
AChE	acetylcholinesterase
BuChE	butyrylcholinesterase
CNS	central nervous system
AZM	azinphos-methyl
iso-OMPA	tetraisopropyl-pyrophosphoramidate
xirp2a	xin actin binding repeat containing 2a